



Finite element modeling and experimental approach of gas transport in polymer-based multimaterials and complex systems

Sarra Zid

► To cite this version:

Sarra Zid. Finite element modeling and experimental approach of gas transport in polymer-based multimaterials and complex systems. Polymers. Université de Lyon, 2019. English. NNT : 2019LYSE1268 . tel-03288847

HAL Id: tel-03288847

<https://theses.hal.science/tel-03288847>

Submitted on 16 Jul 2021

HAL is a multi-disciplinary open access archive for the deposit and dissemination of scientific research documents, whether they are published or not. The documents may come from teaching and research institutions in France or abroad, or from public or private research centers.

L'archive ouverte pluridisciplinaire **HAL**, est destinée au dépôt et à la diffusion de documents scientifiques de niveau recherche, publiés ou non, émanant des établissements d'enseignement et de recherche français ou étrangers, des laboratoires publics ou privés.



N°d'ordre NNT : 2019LYSE1268

THESE de DOCTORAT DE L'UNIVERSITE DE LYON

opérée au sein de
l'Université Claude Bernard Lyon 1

Ecole Doctorale N° accréditation
Matériaux ED34

Spécialité de doctorat : Matériaux Polymères et Composites
Discipline : Physique-Chimie

Soutenue publiquement le 13/12/2019, par :

Sarra Zid

Modélisation par éléments finis et approche expérimentale du transport de gaz dans les multimatériaux et systèmes complexes à base de polymères

Devant le jury composé de :

Mr. Eric Favre	Professeur	Université de Lorraine	Rapporteur
Mme. Valérie Guillard	Maitre de conférences	Université de Montpellier	Rapporteuse
Mme Nadège Follain	Maitre de conférences	Université de Rouen	Examinatrice
Mr. René Fulchiron	Professeur	Université Lyon 1	Examineur
Mme. Eliane Espuche	Professeur	Université Lyon 1	Directrice de thèse
Mr. Matthieu Zinet	Maitre de conférences	Université Lyon 1	Co-directeur de thèse

UNIVERSITE CLAUDE BERNARD - LYON 1

Président de l'Université

Président du Conseil Académique

Vice-président du Conseil d'Administration

Vice-président du Conseil des Etudes et de la Vie Universitaire

Vice-président de la Commission Recherche

Directeur Général des Services

M. Frédéric FLEURY

M. Hamda BEN HADID

M. Didier REVEL

M. Philippe CHEVALIER

M. Fabrice VALLÉE

M. Damien VERHAEGHE

COMPOSANTES SANTE

Faculté de Médecine Lyon Est – Claude Bernard

Faculté de Médecine et de Maïeutique Lyon Sud – Charles Mérieux

UFR d'Odontologie

Institut des Sciences Pharmaceutiques et Biologiques

Institut des Sciences et Techniques de la Réadaptation

Département de formation et Centre de Recherche en Biologie Humaine

Doyen : M. Gilles RODE

Doyenne : Mme Carole BURILLON

Doyenne : Mme Dominique SEUX

Directrice : Mme Christine VINCIGUERRA

Directeur : M. Xavier PERROT

Directrice : Mme Anne-Marie SCHOTT

COMPOSANTES ET DEPARTEMENTS DE SCIENCES ET TECHNOLOGIE

UFR Biosciences

Département Génie Electrique et des Procédés (GEP)

Département Informatique

Département Mécanique

UFR – Faculté des Sciences

UFR (STAPS)

Observatoire de Lyon

Ecole Polytechnique Universitaire Lyon 1

Ecole Supérieure de Chimie, Physique, Electronique (CPE Lyon)

Institut Universitaire de Technologie de Lyon 1

Institut de Science Financière et d'Assurances

ESPE

Directrice : Mme Kathrin GIESELER

Directrice : Mme Rosaria FERRIGNO

Directeur : M. Behzad. SHARIAT

Directeur : M. Marc BUFFAT

Administrateur provisoire: M. Bruno ANDRIOLETTI

Directeur : M. Yannick VANPOULLE

Directrice : Mme Isabelle DANIEL

Directeur : M. Emmanuel PERRIN

Directeur : M. Bernard BIGOT

Directeur : M. Christophe VITON

Directeur : M. Nicolas LEBOISNE

Administrateur Provisoire : M. Pierre CHAREYRON

Abstract

Controlling gas transport properties through polymeric membranes remains today an important parameter for different applications including barrier and gas separation applications. The optimization of such properties requires the addition of nano-fillers in the polymer matrix. Their presence is either an obstacle or a preferential path for the diffusing molecules. These systems have been studied in the literature experimentally as well as by modeling, most often considering ideal two-dimensional systems. In this thesis, we seek to develop a 3-dimensional numerical model in order to predict and analyze the barrier and separation properties of multiphase polymer-based systems taking into account various parameters, as well as to evidence the most important factors governing these properties. Gas diffusion in nanocomposites (polymer matrix phase with the dispersion of impermeable fillers) and the influence of fillers structural parameters on the final properties of the system were studied in the first part of this thesis through a numerical approach based on the Finite Element Method. The obtained model is valid for a wide range of fillers volume fraction values as well as aspect ratios, which makes it possible to consider diluted regimes as well as concentrated regimes. Furthermore, relationships between the system structure (presence of interphase layer/ aggregates, filler size polydispersity and spatial distribution) and the desired properties are investigated. As a second step of this work, gas separation properties of different multiphase polymer-based systems are studied. We considered two- and three-component systems composed essentially of polymer, ionic liquid and permeable fillers. The specificity of this work consists in the investigation of gas separation properties of such systems experimentally and numerically using the model developed in the first part and considering permeable fillers.

Keywords: multiphase; diffusion; separation; barrier; modeling; FEM

Résumé

Le contrôle des propriétés de transport du gaz à travers les membranes polymères constitue aujourd'hui un paramètre important pour différentes applications, y compris les propriétés barrière et la séparation des gaz. L'optimisation de telles propriétés nécessite l'ajout de nano-charges dans la matrice polymère. Leur présence constitue soit un obstacle soit un chemin préférentiel pour les molécules diffusantes. Ces systèmes ont été étudiés dans la littérature expérimentalement ainsi que par la modélisation en considérant le plus souvent des systèmes idéaux à deux dimensions. Dans les études menées dans le cadre de cette thèse, nous cherchons à développer un modèle numérique en 3 dimensions afin de prédire et analyser les propriétés de transport des systèmes multiphasés à base de polymères en fonction de divers paramètres ainsi qu'à déterminer les principaux facteurs qui régissent ces propriétés. La diffusion des gaz dans les nanocomposites (matrice polymère avec dispersion de charges imperméables) et l'influence des paramètres structuraux des charges sur les propriétés finales du système ont été étudiées dans la première partie de cette thèse par une approche numérique basée sur la méthode des éléments finis. Le modèle obtenu est valable sur une large gamme de valeurs de fractions volumiques de charges ainsi que des facteurs de forme, ce qui permet de considérer des régimes dilués aussi bien que des régimes concentrés. En outre, les relations entre la structure du système (présence d'interphase/ agrégats, hétérogénéité de la taille des charges et leur distribution spatiale) et les propriétés souhaitées sont élucidées. Dans un deuxième temps, les propriétés de séparation des gaz de différents systèmes multiphasés à base de polymères sont étudiées. Nous avons considéré des systèmes à deux et trois composants constitués d'une phase polymère, de liquide ionique et de charges perméables. La spécificité de ce travail réside dans l'étude des propriétés de séparation des gaz de tels systèmes expérimentalement, mais aussi numériquement en utilisant le modèle développé dans la première partie et en considérant des charges perméables.

Mots-clés: multiphase; diffusion; séparation; barrière; modélisation; FEM

Acknowledgement

First of all, I'm grateful to God and thankful for everything He gave to me.

I would like to thank my supervisor Eliane Espuche for her support, motivation and immense knowledge. She guided me in every little detail of my researches and I'm really grateful. I would like to tell you that it was a honor for me to work with you and I wish that I did a work that deserves your appreciation. Second, I would like to thank Matthieu Zinet, my second supervisor who was inspiring me through his excellent competences in simulation and modeling. I'm very happy that I worked with you and I think I will never be able to find more kind, patient and enthusiast supervisor as you. Thank you, both were amazing and the scientific and "non-scientific" discussions we had together are meaningful to me. I would like to thank Mr Eric Favre, Ms Valérie Guillard, Ms Nadège Follain and Mr René Fulchiron for accepting to assess this work.

I would like to acknowledge all the members of the IMP laboratory starting with Pierre Alcouffe for his help in SEM and EDX measurements. Thank you for your availability and pertinent remarks. Special thanks to Olivier and Valentin for their technical support in the heat treatment analysis. Thank you Fabrice, Nadia, Sabine, Ali, Sylvie, Florian, Thierry, Gisele and the permanent and non-permanent staff of the lab in general, with whom it was always pleasant to work, talk or even share some delights.

I would like now to thank all the PhD students, trainees and post-doc in the lab that I met during the past three years. Special thanks to my office colleagues Dimitri, Jimmy, Luisa, Cyrielle, Injee, Christophe, Guillaume and Luibov with whom I no longer count the laughter, the breaks, the scientific conversations or not ... thank you for your presence and your sense of humor. I will never forget the precious moments we spent together (Dim, your footages are the best :D)

I would like to thank my friends Riheb, Lily, Safa, Sabrine, Rimen, Amira^{1,2}, Oussama, Ahmed, Amine, Oumaima^{1,2}... Thank you Sana, Thouaiba and Marwa, you know girls I left the best for the last, "نح دكم ب رشا" is sufficient I think (or may be not!). I would like to thank my friends in Tunisia especially Soumaya, Lynda and Aida for their encouragements and love.

Finally, I would like to thank my family: starting with my beloved father who left us very early... I really wish that you were here to see your little daughter being a doctor; I love you

and miss you. I would like to thank my mamma, for her unconditional love and support. She always believed in me and I think I would never be able to be in such position without her presence: I love you.

Thank you Hayfa, Hajer, Moghlia, Zied, Faouzi, Sarah, Malika and my nephews for being by my side. I hope that I made you proud.

For you my new shining star A.

مَنْ سَلَكَ طَرِيقًا يَلْتَمِسُ فِيهِ عِلْمًا سَهَّلَ اللَّهُ لَهُ بِهِ طَرِيقًا إِلَى الْجَنَّةِ

***I've learned that anything in life worth having
comes from patience and hard work.***

Greg Behrendt

To my beloved parents

Table of content

Acknowledgement	vii
Table of content	ix
List of figures	xiv
List of tables	xix
Nomenclature.....	xx
General Introduction	1
Objectives of the thesis.....	5
PhD work plan	7
Part A Multiphase polymer-based systems for improved barrier applications.....	11
<i>Chapter 1 Modeling Diffusion Mass Transport in Multiphase Polymer Systems for Gas Barrier Applications: A Review</i>	<i>12</i>
1.1 Introduction.....	13
1.2 Background: transport mechanism in dense polymer materials	14
1.3 Modeling approaches.....	17
1.3.1 Analytical approaches.....	17
1.3.1.1 Influence of the filler shape and location/distribution	17
1.3.1.2 Influence of the filler size distribution.....	21
1.3.1.3 Influence of the filler orientation and stacking	22
1.3.2 Confrontation of the models with experimental data	26
1.4 Numerical approaches	31
1.4.1 Regular array	32
1.4.1.1 2D systems	33
1.4.1.2 3D systems	36
1.4.2 Random array	39
1.4.2.1 Homogeneous filler orientation/size	39
1.4.2.2 Heterogeneous filler orientation/size	44

1.5 Conclusion	49
<i>Chapter 2 3D Mass Diffusion in Ordered Nanocomposite Systems: Finite Element Simulation and Phenomenological Modeling</i>	51
2.1 Introduction.....	52
2.2 Finite Element Simulations	53
2.2.1 Geometrical model	53
2.2.2 Governing equation and boundary conditions.....	55
2.2.3 Numerical solution and effective diffusivity evaluation	56
2.3 Results and discussion	57
2.3.1 The projected area ratio as a governing parameter.....	61
2.3.2 Phenomenological modeling	66
2.3.2.1 Model derivation.....	66
2.3.2.2 Model validation	69
2.4 Conclusion	72
<i>Chapter 3 Numerical Analysis of 3D Mass Diffusion in Random Nanocomposite Systems: Effects of Polydispersity and Intercalation on Barrier Properties</i>	73
3.1 Introduction.....	74
3.2 Modelling Methodology.....	75
3.2.1 Geometry	75
3.2.2 Physical equations	76
3.2.3 Numerical analysis	77
3.3 Results and Discussion.....	78
3.3.1 Effect of filler aspect ratio polydispersity on the overall diffusivity.....	78
3.3.1.1 Monodisperse distribution	78
3.3.1.2 Polydisperse distributions	78
3.3.1.2.1 Polydisperse uniform distribution.....	79
3.3.1.2.2 Polydisperse Gaussian distribution	79

3.3.1.2.3 Polydisperse “specific” distribution (derived from Gaussian distribution with large standard deviation)	80
3.3.1.3 Comparison of barrier properties	82
3.3.2 Effects of intercalation on the effective diffusivity	85
3.3.2.1 Effects of stacking and polydispersity	85
3.3.2.2 Influence of the interplatelet space characteristics (spacing, diffusivity) ...	87
3.3.2.2.1 Analysis of interplatelet space contribution to overall diffusion for $D_{inter} = D_0$	88
3.3.2.2.2 Influence of interplatelet diffusivity ($D_{inter} \neq D_0$).....	92
3.4 Conclusion	94
Chapter 4 3D Numerical Analysis of Mass Diffusion in Nanocomposites: the Effect of the Filler-Matrix Interphase on Barrier Properties	95
4.1 Introduction.....	96
4.2 Modeling Methodology	98
4.2.1 Geometry	98
4.2.1.1 Ordered distribution	98
4.2.1.2 Random distribution.....	99
4.2.1.3 Interphase overlapping.....	100
4.2.2 Mass diffusion equation and boundary conditions	101
4.2.3 Numerical solution and effective diffusivity evaluation	103
4.3 Results and Discussion.....	104
4.3.1 Ordered filler distribution	104
4.3.1.1 Case A: No continuous diffusion path through interphases.....	104
4.3.1.1.1 1 st Domain: low values of D_{int}/D_0	105
4.3.1.1.2 2 nd Domain: D_{int}/D_0 within the range $[10^{-1}-10^4]$	107
4.3.1.1.3 3 rd domain: high values of D_{int}/D_0 ($>10^4$).....	108
4.3.1.2 Case B: Continuous path through interphases	109
4.3.2 Random filler distribution	110

4.3.2.1	Case A: No continuous diffusion path through interphases.....	111
4.3.2.2	Case B: Continuous diffusion path through interphases.....	112
4.4	Conclusion	114
Part B	Multiphase polymer systems for improved gas separation properties	115
Chapter 1	<i>Bibliographical study of multiphase polymer systems for improved gas separation properties</i>	<i>116</i>
1.1	Background and general description of gas separation membranes	117
1.1.1	Mixed Matrix membranes	122
1.1.1.1	Zeolites.....	123
1.1.1.2	Carbon molecular sieves (CMS).....	123
1.1.1.3	Metal Organic Frameworks (MOFs).....	124
1.1.2	Polymer/Ionic Liquids membranes.....	126
1.1.3	MMMs/IL membranes.....	132
1.2	Modeling of gas transport properties.....	134
1.2.1	Analytical modeling	134
1.2.1.1	Models for gas transport in MMMs	134
1.2.1.1.1	<i>Models for gas transport in ideal MMMs</i>	<i>134</i>
1.2.1.1.2	<i>Models for gas transport in non-ideal MMMs</i>	<i>136</i>
1.2.1.2	Models for gas transport in Polymer/IL membranes	137
1.2.1.3	Models for gas transport in MMMs/IL membranes.....	138
1.2.2	Numerical modeling	139
1.3	Conclusion	142
Chapter 2	<i>Gas transport properties of membranes based on polyetherimide, metal organic framework and ionic liquid: Influence of the composition and morphology</i>	<i>144</i>
2.1	Introduction.....	145
2.2	Experimental	147
2.2.1	Materials	147
2.2.2	Membranes preparation	147

2.2.2.1	PEI/IL membranes	147
2.2.2.2	PEI/ZIF-8 membranes	148
2.2.2.3	PEI/ZIF-8/IL membranes	148
2.2.3	Membrane characterization	148
2.2.4	Gas permeation analysis	149
2.3	Results	150
2.3.1	PEI/IL membranes	150
2.3.1.1	Membrane bulk and surface characterization	150
2.3.1.2	Gas transport properties	154
2.3.2	Polymer/ZIF-8 membranes	154
2.3.2.1	Membranes bulk and surface properties	154
2.3.2.2	Gas transport properties	157
2.3.3	PEI/IL/ZIF-8 membranes	160
2.3.3.1	Membrane bulk and surface characterization	161
2.3.3.2	Gas transport properties	163
2.3.4	Numerical modeling of gas diffusion in 2- and 3-component systems	165
2.4	Conclusion	169
	Conclusion and perspectives	170
	References	176

List of figures

Figure 1.1 The worldwide use of polymers (Geyer, Jambeck, & Law, 2017)	1
Figure 1.2 Gas transport process through nanocomposites showing the tortuous path	2
Figure A.1.1 Distance travelled by a penetrant in the neat polymer (d_s) and in the filled polymer (d_t)	16
Figure A.1.2 Filler configuration studied by Nazarenko et al. (Nazarenko et al., 2007)	24
Figure A.1.3 Filler distribution studied in 3D models (Aris, 1985, 1986; Cussler et al., 1988; Falla et al., 1996; Lape et al., 2004; Moggridge et al., 2003)	24
Figure A.1.4 Filler regular distribution in 2D systems.....	33
Figure A.1.5 Comparison of Swannack's 2D numerical results with Aris's model.....	34
Figure A.1.6 Unit cell and results of Statler et al. (Jr & Gupta, 2007) model.....	36
Figure A.1.7 Comparison of 3D Swannack numerical results and Aris equation.....	37
Figure A.1.8 Example of geometry studied by Goodyer et al. (Goodyer & Bunge, 2007) (the dashed red box is the unit cell).....	37
Figure A.1.9 Example of geometry adopted in Minelli's model	38
Figure A.1.10 3D numerical results for ordered fillers of various shapes (Minelli et al., 2011)	39
Figure A.1.11 Fillers random dispersion in 2D systems. BC indicate boundary conditions imposed at the upper and lower faces of the system. Arrows indicate mass flux direction. (A): filler mid-plane perpendicular to mass flux direction; (B): filler mid-plane angled with respect to mass flux direction.	39
Figure A.1.12 Angle of orientation defined in the cited models	40
Figure A.1.13 3D dispersion of homogeneous disks in the matrix	42
Figure A.1.14 Effect of structural parameters on diffusivity for the 3D random model proposed by Minelli et al. (Minelli et al., 2011).....	43
Figure A.1.15 Fillers randomly distributed in 2D: (A) random orientation; (B) polydisperse fillers; (C) stacks of fillers (intercalated system) with diffusive flux lines. Bold red lines correspond to the inlet and outlet boundaries for mass diffusion.....	44
Figure A.1.16 Geometry proposed by Greco et al. (Greco & Maffezzoli, 2015a).....	46
Figure A.2.1 Geometrical model of the ordered nanocomposite and definition of the unit cell (thickness-wise and plane-wise projections).....	54
Figure A.2.2 - Tridimensional representation of the unit cell showing the boundary conditions	56

Figure A.2.3 - Tetrahedral mesh used to discretize the computational domain	57
Figure A.2.4 – FEM-calculated relative effective diffusivity versus filler volume fraction in ordered nanocomposite systems for different filler aspect ratio values	58
Figure A.2.5 The effect of the number of unit cells on the overall diffusivity for different filler volume fraction and aspect ratio values	59
Figure A.2.6 Comparison of numerical results to Cussler, Fredrickson and Gusev models for different values of disks aspect ratio a) $\alpha=20$, b) $\alpha=50$ and c) $\alpha=100$) and d) to literature experimental results (Dal Pont, 2011; Dal Pont et al., 2013; Gain et al., 2005; Jacquelot et al., 2006; Kato, Okamoto, Hasegawa, Tsukigase, & Usuki, 2003; Meneghetti, Shaikh, Qutubuddin, & Nazarenko, 2008)	60
Figure A.2.7 - Definition of the total projected area S_{tot} and matrix projected area S_{matrix} on a plane normal to the diffusion direction (<i>i.e.</i> x - y plane) for a unit cell.....	62
Figure A.2.8 - Relative effective diffusivity versus the projected area ratio k for several values of parameter β (centered position of the middle-layer disk).....	64
Figure A.2.9 - Relative effective diffusivity versus the projected area ratio k for different β values.....	65
Figure A.2.10 - Exponential variation of the slope parameter a versus β	67
Figure A.2.11 - Relative effective diffusivity versus projected area ratio predicted by the linear and nonlinear analytical models and by FEM simulations	69
Figure A.2.12 Relative effective diffusivity versus filler volume fraction predicted by the analytical model (Eq. (A.2.30)) and by FEM simulations for several filler aspect ratio values	70
Figure A.2.13 – Relative effective diffusivity versus filler volume fraction predicted by the analytical model (Eq. (A.2.30)), FEM simulations and existing models in literature	72
Figure A.3.1 Comparison of the obtained results considering (a) symmetry and (b) impermeable boundary conditions	78
Figure A.3.2 Geometrical model of monodisperse system	78
Figure A.3.3 Disk size distribution for three different polydisperse uniform dispersions ($\alpha = 30$); resulting averaged distribution	79
Figure A.3.4 Disk size distribution actually generated for target values of Gaussian parameters $\alpha = 30$ and $\sigma = 1$	81
Figure A.3.5 Disk size distribution actually generated for target values of Gaussian parameters $\alpha = 30$ and $\sigma = 10$	81

Figure A.3.6 Disk size distribution actually generated for target values of Gaussian parameters $\alpha = 30$ and $\sigma = 20$	82
Figure A.3.7 Relative effective diffusivity vs. filler volume fraction for monodisperse and polydisperse Gaussian systems ($\sigma = 1$ (a) and $\sigma = 10$ (b)): FEM predictions and Lape et al. model (Lape et al., 2004)	83
Figure A.3.8 Relative effective diffusivity vs. filler volume fraction for monodisperse, polydisperse uniform and polydisperse Gaussian systems: FEM predictions	84
Figure A.3.9 Representative volume element (z -direction view) of three types of filler dispersion for similar filler volume fraction	85
Figure A.3.10 Example of 3D simulation domain of intercalated nanocomposites; (a) Monodisperse stacks (b) Polydisperse stacks (uniform distribution)	86
Figure A.3.11 Comparison of effective relative diffusivity predicted by FEM for exfoliated and intercalated systems as a function of filler volume fraction.....	87
Figure A.3.12 Geometrical model of intercalated non-oriented monodisperse system	88
Figure A.3.13 (a) Geometry of the actual stack and (b) corresponding fully impermeable stack.....	89
Figure A.3.14 (a) Relative effective diffusivity variation versus parameters R and e_{inter} for systems with permeable stacks (empty symbols) and corresponding fully impermeable stacks (full symbols), for several disk diameter values; (b) Diffusive flux lines in system with fully impermeable stacks (left) and permeable stacks (right), $D = 20$ nm, $e_{inter}=7$ nm; (c) Diffusive flux lines in system with fully impermeable stacks (left) and permeable stacks (right), $D = 100$ nm, $e_{inter}=7$ nm.....	90
Figure A.3.15 Relative effective diffusivity variation versus filler volume fraction for several values of interplatelet spacing	91
Figure A.3.16 Relative effective diffusivity variation versus D_{inter}/D_0 for several diameter values.....	93
Figure A.4.1 Thickness-wise and plane-wise views of the 3D geometrical model of the ordered distributions.....	99
Figure A.4.2 Two examples of generated RVE in the case of random filler distribution.....	100
Figure A.4.3 Molecular diffusion path (red lines) for different cases: (a) a continuous path formed by overlapping of interphase layers for random distribution ($e_{int} = 1$ nm); (b) a continuous path formed by overlapping of interphase layers (blue regions) for ordered distribution ($e_{int} = 1.75$ nm); (c) the absence of the continuous path for random distribution	

($e_{int} = 0.25$ nm); (d) the absence of continuous path for ordered distribution ($e_{int} = 0.25$ nm);	100
Figure A.4.4 Representation of the RVE showing the boundary conditions: (a) ordered distribution; (b) random distribution	102
Figure A.4.5 Discretization of the computational domain in the vicinity of a filler	103
Figure A.4.6 Relative effective diffusivity versus relative interphase diffusivity for several interphase thickness values and filler volume fractions in ordered filler distribution	105
Figure A.4.7 Comparison between the overall diffusivity for systems presenting low diffusivity interphase and fully impermeable interphase (a) $e_{int} = 0.25$ nm; (b) $e_{int} = 1$ nm	106
Figure A.4.8 Diffusive flux magnitude field ($\text{mol.m}^{-2}.\text{s}^{-1}$) and diffusive flux vector field in the vicinity of an impermeable filler surrounded by a low diffusivity interphase ($D_{int}/D_0 = 10^{-4}$) (left) and in the vicinity of the equivalent fully impermeable filler (right). Arrow length is proportional to the flux magnitude.	106
Figure A.4.9 D_{int}/D_0 values corresponding to $D_{eff}/D_0 = 1$ versus interphase thickness values	107
Figure A.4.10 Lower and upper asymptotic values of the relative effective diffusivity versus fillers volume fraction for several interphase thickness values	108
Figure A.4.11 (a) Relative effective diffusivity variation as a function of interphase thickness showing the presence of the continuous path (b) Zoom in the discontinuous pathway part showing differences in D_{eff}/D_0 values	110
Figure A.4.12 Relative effective diffusivity variation as a function of D_{int}/D_0 for two different interphase thickness values ($e_{int} = 0.25$ nm and 0.5 nm)	111
Figure A.4.13 Comparison between ordered and random distribution (a) D_{int}/D_0 variation versus filler volume fraction for $D_{eff}/D_0 = 1$ (b) D_{eff}/D_0 variation versus filler volume fraction in the plateau domains	112
Figure A.4.14 Comparison between random and ordered configurations for two different filler volume fraction and interphase thicknesses	113
Figure B.1.1 Background of membrane gas separations (S. Sridhar et al., 2014)	117
Figure B.1.2 O_2/N_2 upper-bound curve in polymeric membranes	119
Figure B.1.3 O_2/N_2 upper bound correlation for glassy and rubbery polymeric membranes as referred in (Robeson, 1991)	120
Figure B.1.4 Strategies to overcome challenges for MMMs fabrication as reported in Dong et al. work (Dong et al., 2013)	126

Figure B.1.5 Robeson plot for CO ₂ /N ₂ selectivity versus CO ₂ permeability as reported in literature (Close, Farmer, Moganty, & Baltus, 2012)	129
Figure B.1.6 The geometry used in Wang et al. work (a) fillers parallel to z-axis (mass flux direction) (b) fillers normal to z-axis (mass flux direction) (T. P. Wang & Kang, 2015)	140
Figure B.1.7 Schematic illustration of in-plane and out-of-plane diffusivity of the filler	141
Figure B.2.1 (a) TGA mass loss curves and (b) DSC thermograms for PEI/x IL (x=0; 2.5; 7)	150
Figure B.2.2 SEM images for the cross-section morphologies of (a) neat PEI (b) and (c) PEI/2.5 IL membranes (d) and (e) PEI/7 IL membranes	152
Figure B.2.3 EDX spectra of (a) PEI matrix and (b) IL.....	152
Figure B.2.4 (a) TGA mass loss curves and (b) DSC thermograms of the mixed matrix membranes	155
Figure B.2.5 SEM images of (a) PEI/10 wt% ZIF-8 (b) PEI/15 wt% ZIF-8 and (c) PEI/20 wt% ZIF-8	156
Figure B.2.6 EDX spectra of a filler aggregate in PEI/10 wt% ZIF-8	156
Figure B.2.7 Relative permeability variation as a function of ZIF-8 content for the three studied gases.....	158
Figure B.2.8 Comparison between Maxwell model and experimental CO ₂ permeability coefficients for the studied membranes.....	159
Figure B.2.9 Comparison of the experimental data of this work with several systems based on ZIF-8 from literature (Deniz, 2012; Eiras et al., 2016; Jusoh, Yeong, Lau, & Shariff, 2016; M. Li et al., 2017; Song et al., 2012)	160
Figure B.2.10 (a), (b) TGA and (c) DSC plots of the studied membranes	161
Figure B.2.11 SEM images of the prepared membranes (a) PEI/10 ZIF-8 (b) PEI/2.5 IL (c) PEI/2.5 IL/10 ZIF-8 (d) PEI/7 IL (e) PEI/7 IL/10 ZIF-8	162
Figure B.2.12 EDX spectra characterizing the different domains observed on SEM of PEI/7 IL/ 10 ZIF-8.....	163
Figure B.2.13 SEM image of the cross section of PEI/7 IL/10 ZIF-8	164
Figure B.2.14 H ₂ /CO ₂ selectivity of the prepared membranes versus H ₂ permeability compared to literature data (Deniz, 2012; E. Y. Kim et al., 2019)	165
Figure B.2.15 Simulation domain containing (a) discrete spherical filler aggregates (b) stacks composed of three aggregates	167
Figure B.2.16 Comparison of the experimental relative effective diffusivity.....	168

List of tables

Table A.1.1 - Summary of analytical models cited in the review.	29
Table A.1.2 : Sum-up of numerical models discussed in the review	48
Table B.1.1 Examples of the most used glassy and rubbery polymers in gas separation industrial applications (Bernardo et al., 2009)	120
Table B.1.2 Example of some couples Polymer/Filler used in mixed matrix membranes in the literature	122
Table B.1.3 Examples of anions and cations used for IL preparation.....	127
Table B.1.4 Examples of SILMs reported in literature	128
Table B.1.5 CO ₂ permeability and CO ₂ /N ₂ selectivity as reported in literature (Mahurin, Hillesheim, Yeary, Jiang, & Dai, 2012)	129
Table B.1.6 Mathematical models for permeability prediction in two component systems .	137
Table B.1.7 A sum-up of the theoretical models for gas transport properties in composite systems	138
Table B.2.1 Contact angle and surface energy measurements of the studied films	153
Table B.2.2 Gas transport properties of PEI/IL membranes (the uncertainty is about 5% for P and D_{CO_2} and 10% for S_{CO_2})	154
Table B.2.3 Gas transport properties of the prepared membranes	157
Table B.2.4 Gas permeability, diffusivity and selectivity of the prepared membranes.....	164

Nomenclature

$\overline{N_z}$: the average mass flux across a plane section normal to z-direction

\overline{D} : the average diameter

$\overline{\alpha}$: the average aspect ratio of fillers

γ^d : dispersive surface energy

γ^p : polar surface energy

ϵ_F : the slope of the plot defined by Falla and coworkers

a, b : the slope and the intercept

A : pre-exponential scaling parameter

a_0 : scaling constant of the exponential decay

A_s : surface area of the membrane

B : an exponential scaling decay constant

BC: Boundary Conditions

BEM: Boundary Element Method

C : the concentration of the gas

c_1, c_2 : the concentration at the upper and lower bounds of a membrane

CH_2Cl_2 : methylene chloride

D : disk diameter

D_{eff} : the effective diffusivity coefficient

d_i : distances between i disks in the same plane

D_{ij} : Fickian diffusivity coefficient

D_{int} : the coefficient of diffusion in the interphase

D_{inter} : the interplatelet space diffusivity coefficient

D_r : the relative effective diffusivity coefficient

d_s : the straight path length across the neat polymer

d_t : the diffusion path length in the filled matrix

e : disk thickness

e_{int} : the interphase thickness

e_{inter} : the interplatelet spacing

Emim-BF₄: 1-Ethyl-3-methylimidazolium Tetrafluoroborate

f : filler volume fraction

f_{bl} : blocked pores volume fraction

FEM: Finite Element Method

f_{IL} : ionic liquid filler volume fraction

f_m : maximum packing volume fraction of the fillers

f_{optim} : optimized filler volume fraction

f_v : voids volume fraction

FVM: Finite Volume Method

f_w : the welled dispersed phase volume fraction

g : size distribution function

h : geometric factor defined by Fredrickson and Bicerano

IL: Ionic Liquid

k : the projected area ratio

K_H: Higuchi empirical parameter

k_{lim} : a limiting value of k

L : filler length

l : the thickness of the polymeric membrane

L_{eff} : the average normalized path length

L_x, L_y, L_z : RVE dimensions in x, y and z directions

MC: Monte Carlo

MMMs: Mixed Matrix Membranes

MOF: Metal Organic Framework

n : the number of fillers

n_e : MWS factor

N_{ij} : the solute diffusive flux

N_L : the number of layers in one aggregate

O : orientational factor introduced by Bharadwaj

PBC: Periodic Boundary Conditions

P_d : the permeability in the dispersed phase

PDE: Partial Differential Equation

PDF: Probability Density Function

P_{eff} : the effective permeability coefficient

PEI: Polyetherimide

P_i : permeability coefficient of a specie i

P_{ij} : Fickian permeability coefficient

PIL: Polymeric Ionic Liquid

PIM: Polymer with Intrinsic Micro-porosity

p : the gas pressure

p_p : the isotropic in-plane spacing in x-y directions

P_r : the relative effective diffusivity coefficient

P_{trans} : trans-membrane pressure

p_x, p_y, p_z : the unit cell dimensions in x, y and z directions

r : A parameter defined by Minelli and coworkers

R : parameter defining the ratio between the interplatelet space volume and the total stack volume

RAM: Random Access memory

RSA: Random Sequential Adsorption

RTIL: Room Temperature Ionic Liquid

RVE: Representative Volume Element

S : plane section

s : the distance between two adjacent flakes

S_0 : the solubility in the neat polymer

S_{disk} : the projected area of a disk

S_{ij} : the solubility coefficient

SILM: Supported Ionic Liquid Membrane

S_L : the area of the filler lateral surface

S_{matrix} : the projected area of the matrix

$S_{n,M}$: the area corresponding to the cross section of the matrix region between adjacent layers

S_n : the cross-section area of filler

$S_{overlap}$: the overlapping projected area

S_{tot} : the projected area of the unit cell

s_x, s_y : shifts between two adjacent layers in x-y directions

t : the thickness of ribbons

T_g : glass transition temperature

T_G : thickness of the galleries as defined by Greco and coworkers

W : filler width

w : the width of ribbons

ZIF-8: Zeolitic Imidazolate Framework

α : filler aspect ratio

α_c : the corrected shape factor

α_{ij} : selectivity of species i and j

β : scaled space-step parameter

β_{eff} : model parameter for the effectiveness of fillers volume fraction

β_{min} : minimum value of β

γ : the mean free path travelled by a molecule

δ : supplementary term to be subtracted from the linear model

Δp : the pressure gradient

ε : the standard deviation between the numerical results

η : empirical coefficient defined by Dondero and coworkers

θ : the angle between the direction of penetrant flow and the normal vector

θ_c : contact angle

θ_{lg} : time lag

λ : an adjustable geometrical parameter defined by Tsiantis and coworkers

μ : geometric factor defined by Cussler and Aris

ρ : a factor introduced by Nielsen and coworkers

σ : the standard deviation

σ_s : the slit shape

τ : the tortuosity factor

v : Herman's orientation function

ϕ : the PDF function

χ : factor defined by Fredrickson and coworkers

ψ : selectivity of fillers

ω : the ratio between polymer and fillers diffusivities

ξ : factor defined by Cussler

General Introduction

Polymer materials came into prominence in the early twentieth century because of their interesting properties, low cost and easy processing allowing them to be used in various fields.

The industrial applications of these materials are being very diverse today: as it can be observed through the following chart, more than 1/3 of the mass of polymers produced in 2015 were used for packaging. Polymers are also widely exploited in other technological fields such as building, manufacturing of textiles, consumer goods and transportation equipment.

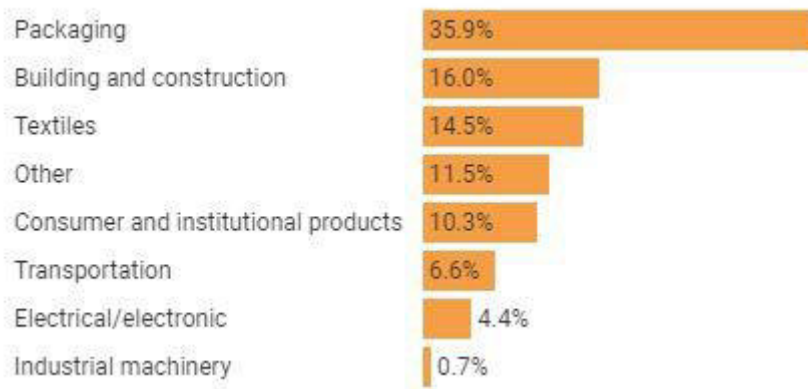


Figure 1.1 The worldwide use of polymers (Geyer, Jambeck, & Law, 2017)

In order to meet the ever-increasing requirements of engineering applications, polymers are often combined with inorganic fillers in order for enhancing their properties. Hence, in the last decades, new strategies have been proposed by material scientists in order to develop high-performance multiphase polymer systems. One immediately thinks about mechanical reinforcement, which in most cases comes down to increase the strength-to-weight ratio for structural applications. However, a substantial part of the research effort is devoted to the development of other material functions, which consists on “tailoring” the material physico-chemical properties in order to satisfy a particular technical need. Examples of common material functions, among others, are related to thermal properties (heat dissipation, thermal insulation, heat storage), electrical properties (electrical insulation / conduction, electromagnetic shielding), or mass transport properties (barrier effect, gas trapping, separation and filtration, etc.). This thesis will focus on two types of multiphase systems particularly appropriate and efficient for the development of material functionalities involving mass transport: polymer-based nanocomposites and mixed matrix membranes, respectively.

Polymer-based nanocomposite result from the dispersion of fillers showing at least one dimension in the nanometer range within a polymer matrix. These materials demonstrate a series of advantageous properties that are not found in higher (micrometric) scale composites (Camargo, Satyanarayana, & Wypych, 2009). As such, they are involved in an exceptionally extensive range of applications going from electronics to packaging and building. In the packaging field (food, sensitive products), where mass transport properties are key, nanocomposites based on impermeable lamellar nanofillers have become very popular due to their improved barrier properties, which reduces the gas flux through the packaging material (usually a film or membrane) without compromising optical transparency. This leads to an improved protection of the packaged product from the ambient atmosphere and allows the increasing of the product shelf life (Bhunia, Dhawan, & Sablani, 2012). Indeed, gas transport process through nanocomposites is based on a diffusion-solution mechanism in which diffusing molecules must follow a tortuous path because of the presence of impermeable fillers and thus enhanced barrier properties could be obtained (**Figure 1.2**).

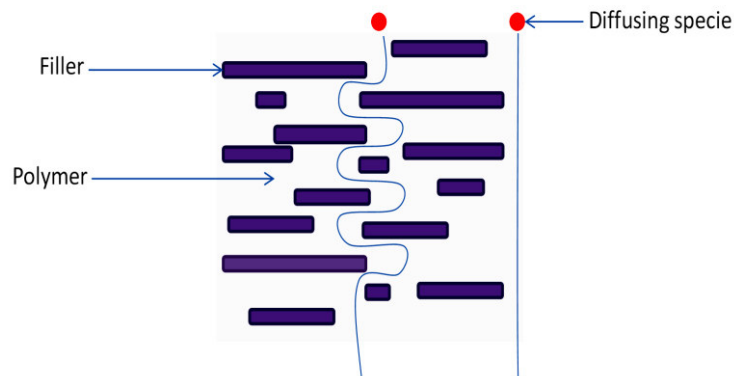


Figure 1.2 Gas transport process through nanocomposites showing the tortuous path

Increasing barrier (and mechanical) properties has thus gained a lot of attention for packaging applications but also for energy applications (protective coatings, gas tank, gas distribution, etc.). It has also to be noticed that transparency could be kept in these materials due to the low size of the dispersed objects and this represents an advantage for some applications. In this context, a lot of experimental work has been devoted to the study of the impact of adding inorganic fillers within various polymer matrices. Significant differences have generally been observed in the resulting properties, depending on the filler shape, content, and dispersion state. In particular, IMP laboratory has performed intensive work on nanocomposites based on natural and synthetic nanofillers during the last twenty years, focusing on the effect of structural parameters and also on interfacial parameters on the barrier properties (Cheviron,

Gouanvé, & Espuche, 2016; Gain, Espuche, Pollet, Alexandre, & Dubois, 2005; Jacquelot, Espuche, Gérard, Duchet, & Mazabraud, 2006; Masclaux, Gouanvé, & Espuche, 2010; Morel, Bounor-Legaré, Espuche, Persyn, & Lacroix, 2012; Picard, Espuche, & Fulchiron, 2011; Picard, Gérard, & Espuche, 2008; Picard, Vermogen, Gérard, & Espuche, 2007; Sabard, Gouanvé, Espuche, Fulchiron, Fillot, et al., 2014a; Sabard, Gouanvé, Espuche, Fulchiron, Seytre, et al., 2014).

On the other hand, while barrier nanocomposites are designed to block penetrant molecules, gas separation membranes are designed to permeate gases selectively. The gas separation field (e.g. air dehydration, ultrapure water production, CO₂ and other harmful gases removal from natural gas, etc.) has grown significantly since its beginnings in the early 1970's and it is expected to grow further in the coming years (Baker & Low, 2014). Compared to conventional technologies such as sorbents and scrubbing solutions which are generally energy-intensive, membrane technology has several advantages: low cost, small environmental footprint (such as carbon foot-print in water purification technology), easy processing, reliability and possibility to obtain highly pure products (Carreon, Dahe, Feng, & Venna, 2017).

The fundamental parameters characterizing membrane performance for gas separation applications are the permeability and the selectivity and the main goal is to optimize the trade-off relationship between these antagonistic parameters (Robeson, 2008). Hence, the development of new classes of membranes combining both high flux and selectivity is still a challenging issue. Different types of gas separation membranes were described in the literature, generally consisting of 2-components systems, the polymer acting as the continuous phase and the second component providing its high permeability and/or selectivity (Sanders et al., 2013). Mixed matrix membranes based on carbon molecular sieves have been deeply investigated and more recently a great attention has been paid on metal organic frameworks (MOFs) as functional fillers for association with polymer matrices. Another original bi-component membrane family that has been developed regarding CO₂ separation applications is Polymer/Ionic liquid membranes (H. B. Park, Kamcev, Robeson, Elimelech, & Freeman, 2017).

More recently, the development of three-component systems based on the addition of ionic liquid to mixed matrix membranes has been reported in literature as a way to achieve interesting separation properties thanks to the affinity of both fillers and IL towards diffusing gases (Monteiro et al., 2018).

In order to predict gas transport properties in both types of systems (i.e. nanocomposites for barrier properties and mixed matrix membranes for gas separation), the development of modeling approaches is essential. Several analytical models describing mass transfer through nanocomposite systems are available in the literature. These approaches are commonly based on geometrical analyses of the path traveled by diffusing molecules through the studied systems and have enabled approximate prediction of the gas transport properties of multicomponent polymer-based systems. Indeed, they necessarily assume (over)idealized systems, which can be insufficiently accurate to take into account the various effects induced by complexities and heterogeneities in the actual nanocomposite structure. (Wolf, Angellier-Coussy, Gontard, Doghieri, & Guillard, 2018).

In order to go further in the structure-properties relationships of these materials and to promote their optimization, advanced models able to describe mass transport in realistic systems are needed. Those models are generally too mathematically complex to yield explicit analytical equations, hence they have to be numerically solved using various techniques such as the Monte Carlo method (MC), the finite element method (FEM), the finite volume method (FVM) or the boundary element method (BEM). Several numerical studies of mass transport in multiphase polymer-based systems accounting for the influence of various structural parameters (filler size, orientation, dispersion, distribution) have been reported in the literature (Monsalve-Bravo & Bhatia, 2018).

It is noteworthy that most of these numerical models have considered two-dimensional systems and only few of them have taken into account the three-dimensional aspect of the actual materials. It has been shown that for a given filler loading content, 2D models generally overestimate the barrier properties compared to 3D models, due to the infinite extension assumption they imply for the dispersed phase (Swannack, Cox, Liakos, & Hirt, 2005).

Moreover, existing numerical models rarely considered the presence of imperfections in the system structure such as incomplete filler exfoliation (presence of stacks) or the existence of filler-matrix interphases which are known to have a non-negligible influence on the nanocomposite final properties.

Objectives of the thesis

The aim of this thesis project is to study gas transport properties of multiphase polymer-based systems considering two complementary aspects: numerical modeling and experimentation. As discussed above, we have focused on two types of systems: nanocomposites for barrier applications and mixed matrix membranes for gas separation applications.

1) Nanocomposite systems

During the last decades, several experimental works have been carried out in order to characterize mass diffusion through nanocomposite systems with various filler shapes for gas barrier applications. Useful analytical models predicting the gas transport properties of these systems have been derived and extensively reported in the literature. However, the complexity of the systems these models can describe is necessarily limited. In order to predict more accurately the behavior of actual nanocomposite materials (randomly distributed fillers with different shapes or sizes, presence of stacks, filler-matrix interphases), numerical approaches are indispensable.

In this context, our first objective is to develop a 3D finite element model of mass transfer through nanocomposite systems suitable for predicting their effective transport properties. Impermeable disk-shaped fillers embedded in a permeable matrix are considered. The influence of several structural parameters on the barrier properties will be investigated through parametric studies: filler aspect ratio distribution (assuming constant thickness and variable diameter), spatial distribution (ordered distributions / random distributions) and dispersion state (exfoliated fillers / intercalated systems).

The developed model will be extended to take into account and analyze the influence of a third phase, the interphase layer, on the gas barrier properties. The simulations will be validated by confronting them to existing numerical and analytical results as well as to existing experimental data.

2) Multi component polymer-based membranes

For gas separation applications, multi-component polymer-based membranes include mixing polymer materials with other additives such as zeolites, carbon molecular sieves or metal organic frameworks. In particular, the development of mixed matrix/ionic liquid membranes could further optimize the permeability/selectivity trade-off.

Hence, the second objective of this thesis is to prepare and characterize two-component and three-component membranes in order to obtain improved selectivity/permeability properties. Furthermore, numerical modeling will be used in order to develop a better understanding of the relationship between membrane's morphology and its diffusion properties.

PhD work plan

The PhD work plan is divided into two major parts: **Part A**, which aims at providing a numerical analysis of the gas barrier properties of nanocomposite systems based on polymer matrices and impermeable lamellar nanofillers and **Part B**, which is devoted to an experimental and numerical study of gas separation properties of multiphase systems based on a glassy polymer, MOFs and ionic liquid.

1) Part A

The first chapter of the thesis proposes a review of the existing knowledge and approaches available to model the gas barrier behavior of multiphase systems.

After a short reminder of the parameters governing the gas transport in polymers and a brief overview of the existing analytical approaches, a review of the numerical models available to predict the barrier properties of nanocomposite systems is presented. Moreover, the effects of parameters influencing diffusion such as fillers shape, orientation, dispersion and spatial distribution are discussed. A particular attention is paid to the recent developments and a critical comparative analysis of the different approaches is proposed.

- ❖ This chapter is the subject of a paper published in *Journal of Polymer Science Part B*, on January, 2 2018 and titled *Modeling Diffusion Mass Transport in Multiphase Polymer Systems for Gas Barrier Applications: A Review*.

The second chapter presents the general formulation of a 3D numerical model of mass transport in ordered nanocomposite systems, in the case of disk-shaped nanofillers. In a first step, the geometrical model is described and the variable parameters are specified. Then the mass transfer equation and the associated boundary conditions are formulated. After detailing the numerical analysis, the simulation results are presented and discussed with respect to the corresponding regimes (dilute, semi-dilute and concentrated regimes). Accordingly, a phenomenological analytical equation is derived and validated against the numerical results, allowing prediction of gas barrier properties of ordered nanocomposite systems with minimal computational effort.

- ❖ This chapter is the subject of a paper published in *Journal of Polymer Science Part B*, on November, 21 2018 and titled *3D Mass Diffusion in Ordered Nanocomposite Systems: Finite Element Simulation and Phenomenological Modeling*

The third chapter is devoted first to the analysis of the effect of fillers size polydispersity on gas barrier properties. We have developed for that purpose a step-by-step approach based on 3D finite element modeling, considering disk-shaped nanofillers randomly distributed in the polymer matrix. A comparison between monodisperse and polydisperse fillers is conducted and a study of the aggregation effect is presented. Moreover, in this chapter, the effect of interplatelet diffusion was assessed through a sensitivity study considering a wide range of diffusion coefficient values in the interplatelet area.

- ❖ This chapter is the subject of a paper published in *Journal of Membrane Science*, on July, 24 2019 and titled *Numerical analysis of 3D mass diffusion in random (nano) composite systems: Effects of polydispersity and intercalation on barrier properties*.

The fourth and last chapter of Part A is devoted to the numerical analysis of the effect of the filler-matrix interphase layer on the barrier properties of nanocomposites loaded with disk-shaped fillers. The 3D FEM models developed in chapters 2 and 3 are extended in order to take into account a third distinct phase in addition to the filler and matrix phases. Two types of filler distributions are investigated: ordered and random distributions. We have considered the possibility of interphase overlapping which could lead to the presence of continuous diffusion paths through the thickness of the nanocomposite and could affect significantly the barrier properties. Results are discussed considering a large range of interphase diffusivity values in order to understand and quantify the effect of such medium on the overall barrier properties.

- ❖ This chapter is the subject of a publication submitted to *Journal of Membrane Science*, titled *3D Numerical Analysis of Mass Diffusion in Nanocomposites: the Effect of the Filler-Matrix Interphase on Barrier Properties*.

2) Part B

The first chapter of this part provides a review of polymer-based membranes for gas separation: after presenting the background of existing membranes in literature, a description of their properties is given through examples of their gas separation performances. This analysis of the state of the art is followed by a presentation of the existing analytical and numerical models in literature for the prediction of membrane gas separation properties.

The second chapter of part B consists in an experimental and numerical study of gas separation properties of three different systems: polymer/ionic liquid membranes, mixed matrix membranes and mixed matrix membranes containing ionic liquid. Prepared membranes are characterized and their permeabilities and selectivities are determined. The relationships between the membrane structure and properties are established. The main objective concerning the three-component system is to identify an optimum area for permeability/selectivity trade-off. The experimental study is complemented by a numerical analysis using a 3D FEM model built in order to predict gas diffusion properties of the mixed matrix membranes. The simulation results are compared to the obtained experimental results.

Part A Multiphase polymer-based systems
for improved barrier applications

Chapter 1 Modeling Diffusion Mass Transport in Multiphase Polymer Systems for Gas Barrier Applications: A Review

An overview of the chapter

Polymer nanocomposites based on impermeable fillers (especially lamellar nanofillers) offer a great interest as gas barrier materials because of their much-enhanced properties arising from the nanoparticles shape, size and spatial arrangement within the matrix. However, optimization and further development of such materials requires fundamental understanding of the influence of the nanocomposite structure on the gas diffusion phenomena. This step can be greatly facilitated through modeling/simulation strategies used to establish relations between material microstructural parameters and the barrier properties. This chapter first presents the analytical models developed to estimate the effective diffusivity in polymer nanocomposites. The predictions of the models are analyzed in relation to experimental data reported in the literature and their ability to describe accurately the nanocomposite transport properties when the microstructure complexity increases is discussed. Then, modeling approaches based on numerical solution techniques (e.g. the finite element method) that allow simulating the diffusion processes and assessing the effect of filler shape, orientation, dispersion and spatial arrangement are reviewed and discussed. Finally, the importance of 3D simulation strategies for the understanding and prediction of gas transport in the most complex nanocomposite microstructures is addressed.

1.1 Introduction

The need for efficient gas barrier materials is of crucial importance for a large range of applications going from packaging to protective coatings. These applications are of major importance for a wide variety of domains (food preservation, biomedical applications, energy, building, etc.). In the last decades, a great attention has been paid to polymer materials due to their low cost, easy processing and interesting mechanical properties such as their high flexibility (A. Blanchard, Gouanvé, & Espuche, 2017; Mokwena & Tang, 2012; Vandewijngaarden et al., 2014). However, neat polymers cannot meet anymore the ever increasing barrier level required for these applications. Hence, they have been often combined with less permeable or totally impermeable components to improve their barrier properties (Charifou, Espuche, Gouanvé, Dubost, & Monaco, 2016; Ge & Popham, 2016; D. Kim & Kim, 2003; Mattioli et al., 2013; Mokwena, Tang, Dunne, Yang, & Chow, 2009). In this context, a lot of experimental work has been devoted to the study of the impact of adding inorganic fillers within various polymer matrices and significant differences have been experimentally observed in the resulting properties depending on the filler shapes, contents and dispersion states (Attaran, Hassan, & Wahit, 2017; Cui, Kumar, Rao Kona, & van Houcke, 2015; Cui, Kundalwal, & Kumar, 2016; Lizundia, Vilas, Sangroniz, & Etxeberria, 2017; Müller et al., 2017; Szymczyk et al., 2015). Although some trends have been drawn from these experimental works, notably showing the efficiency of lamellar type nanofillers (Espuche, 2011), the need for specific tools allowing better understanding and prediction of the effect of each parameter has become of paramount importance in order to design materials with targeted properties.

The aim of this work is to review the approaches developed to model the behavior of multiphase systems of interest for barrier applications. The earlier approaches are analytical, but recently, calculations based on numerical approaches such as finite element method (FEM) have been carried out to simulate the diffusion processes into such systems. The constant evolution in the modeling approach has allowed a progressive increase in the complexity of the described systems (e.g. tridimensional morphologies), enabling the models to become more realistic with respect to the actual materials. After a short reminder of the parameters governing the gas transport in polymers and a brief overview of the existing analytical approaches, this paper extensively reviews the numerical models available to predict the barrier properties of (nano) composites, assessing the effect of parameters influencing diffusion such as filler shape, orientation, quantity, dispersion and spatial

distribution. A particular attention will be paid to the recent developments and a critical comparative analysis of the different approaches will be proposed.

1.2 Background: transport mechanism in dense polymer materials

Basically, mass transport in a polymer is related to the ease with which gas molecules can penetrate and get through the material. It is described by a solution-diffusion mechanism. At a given temperature, the transport of a gas molecule through a homogeneous polymer matrix in a permeation mode is the result of a three-step process (Crank & Park, 1968): sorption of the component at the upstream face of the membrane, followed by diffusion/solution through the material cross- section under the influence of the applied driving force (pressure gradient which corresponds to a chemical potential gradient) and finally desorption at the downstream face of the film. In a Fickian transport mechanism, the time necessary to reach interfacial equilibrium is much shorter than the characteristic time of the diffusion process, which is then the governing process of the transport mechanism. Both the solubility and diffusion parameters are dependent on the nature of the membrane material and of the permeating gases.

In a Fickian mechanism, the permeability coefficient of specie i in a medium j , denoted by P_{ij} , is the product of the solubility coefficient S_{ij} and the diffusion coefficient D_{ij} :

$$P_{ij} = D_{ij} \cdot S_{ij} \quad (\text{A.1.1})$$

The solubility coefficient has a thermodynamic origin and depends on the molecule-polymer interactions, on the polymer free volume as well as on the ability of the gas to condense. It is related to the local concentration of the gas C dissolved in the polymer and to the gas pressure by the following relation:

$$C = S_{ij} \cdot p \quad (\text{A.1.2})$$

Diffusion is the process by which the small molecule is transferred in the system due to random molecular motions. Therefore, the diffusion coefficient D_{ij} is a kinetic term related to the free volume and the molecular mobility in the polymer phase; it is expressed in $\text{m}^2 \cdot \text{s}^{-1}$.

As mentioned, diffusion is often the dominant mechanism of the transport process. It is described by Fick's law, which assumes a proportionality relationship between the diffusive flux and the concentration gradient. By analogy to Fourier's law of heat conduction, the first Fick's law for one-dimensional diffusion reads:

$$N_{ij} = -D_{ij} \frac{\partial C}{\partial x} \quad (\text{A.1.3})$$

where N_{ij} is the solute diffusive flux and $\frac{\partial C}{\partial x}$ is the solute concentration gradient. Later, Fick developed the unsteady form of this equation that relates the rate of change of concentration to the diffusive flux:

$$\frac{\partial C}{\partial t} = D_{ij} \nabla^2 C \quad (\text{A.1.4})$$

In the case of one-dimensional diffusion, the previous equation could be written as follow:

$$\frac{\partial C}{\partial t} = D_{ij} \frac{\partial^2 C}{\partial x^2} \quad (\text{A.1.5})$$

If l is the thickness of the polymer membrane, under the assumptions of steady state and constant diffusion coefficient, the gas flux N is constant and equal to:

$$N_{ij} = -D_{ij} \frac{(C_1 - C_2)}{l} \quad (\text{A.1.6})$$

where C_1 and C_2 are respectively concentrations of gas dissolved at the downstream and upstream faces of the polymer membrane. N_{ij} can be related to the permeability:

$$P_{ij} = \frac{l N_{ij}}{\Delta p} \quad (\text{A.1.7})$$

where Δp is the pressure gradient applied to the membrane.

Adding a second dispersed phase (the fillers) to the continuous phase constituted by the polymer matrix can significantly influence the transport properties. Hence, several phenomenological models have been built in order to correlate diffusivity with various characteristic parameters for such systems. These models can either be based on analytical or numerical approaches. In the following sections of this paper, modeling works belonging to both categories will be presented with a special focus on the models devoted to the study of nanocomposite systems. It is noteworthy to precise that the various models/equations discussed in this review consider ideal binary systems. They do not take into account the potential effect of the filler/matrix interface (which can be considered as a third phase). This means that sufficiently strong interactions between the dispersed phase and the continuous phase are supposed to take place in order to have no defects at the interface. Moreover, it is assumed that these interactions are not strong enough to modify the properties at the

boundaries of each phase and that the presence of the dispersed phase does not modify the properties of the continuous phase.

In the case of ideal binary systems composed of impermeable fillers dispersed in a continuous permeable phase, the solubility S_{ij} can be expressed by:

$$S_{ij} = S_0(1 - f) \quad (\text{A.1.8})$$

where S_0 is the solubility in the neat polymer and f is the volume fraction of the fillers.

Due to the presence of those fillers, the diffusion path is lengthened, as defined by the tortuosity factor (Barrer, 1968):

$$\tau = \frac{d_t}{d_s} \quad (\text{A.1.9})$$

where d_t is the diffusion path length in the filled matrix and d_s is the straight path length across the neat polymer (**Figure A.1.1**).

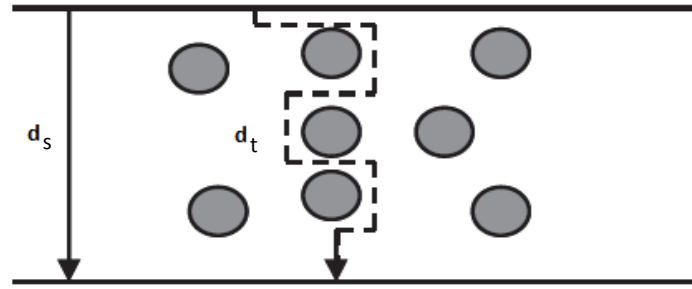


Figure A.1.1 Distance travelled by a penetrant in the neat polymer (d_s) and in the filled polymer (d_t)

Besides, the effective diffusivity in the nanocomposite can be expressed as follow:

$$D_{eff} = \frac{D_0}{\tau} \quad (\text{A.1.10})$$

where D_0 is the diffusivity in the neat polymer.

Considering a Fickian transport mechanism, the permeability coefficient of the composite material (or effective permeability) can be expressed as:

$$P_{eff} = P_0 \frac{(1 - f)}{\tau} \quad (\text{A.1.11})$$

where P_0 is the permeability of the neat polymer. The relative effective permeability can then be defined as:

$$P_r = \frac{P_{eff}}{P_0} = \frac{(1-f)}{\tau} \quad (\text{A.1.12})$$

and the relative effective diffusion coefficient as:

$$D_r = \frac{D_{eff}}{D_0} = \frac{P_r}{(1-f)} = \frac{1}{\tau} \quad (\text{A.1.13})$$

Throughout this paper, for comparison purposes, it has been chosen to represent the effect of nanofillers on the composite barrier properties by a unique parameter: the relative effective diffusivity $\frac{D_{eff}}{D_0}$, which relates to the effective relative permeability as given by equation (A.1.13).

1.3 Modeling approaches

1.3.1 Analytical approaches

The main analytical approaches developed to model gas transport properties in biphasic polymer based films are presented hereafter. We will show how different parameters (such as filler shape and content, filler location and distribution, filler size distribution, filler orientation or filler stacking) have been taken into account in these models and how the models have been exploited in combination with experimental data to bring a better understanding of the relations between the materials structure and their barrier properties.

1.3.1.1 Influence of the filler shape and location/distribution

Maxwell and Bruggemann (Barrer, 1968; Bouma, Checchetti, Chidichimo, & Drioli, 1997; Bruggeman, 1935; Maxwell, 1873) developed the first theoretically based models to predict the permeability properties of gases in biphasic systems, considering a spherical morphology for the dispersed phase. The general Maxwell law can be expressed as:

$$\frac{D_{eff}}{D_0} = \frac{1}{(1-f)} \cdot \frac{P_d + 2P_0 - 2f(P_0 - P_d)}{P_d + 2P_0 + f(P_0 - P_d)} \quad (\text{A.1.14})$$

where D_{eff} is the effective diffusivity in the composite system, P_0 and D_0 are the permeability and diffusivity of the continuous phase respectively, P_d is the permeability in the dispersed

phase and f is the volume fraction of the dispersed phase. In the case of impermeable dispersed spheres, Maxwell's model can be reduced to the following expression:

$$\frac{D_{eff}}{D_0} = \frac{1}{(1 + \frac{f}{2})} \quad (A.1.15)$$

According to this model, as expected, the effective diffusivity decreases as the volume fraction of impermeable nanoparticles increases.

Bruggemann also proposed an equation to describe the transport phenomenon in biphasic media composed of a continuous matrix with spherical dispersed fillers:

$$\frac{P_{eff}}{P_0} = \left(\frac{\frac{P_d}{P_0} - \frac{P_{eff}}{P_0}}{(1-f)(\frac{P_d}{P_0} - 1)} \right)^3 \quad (A.1.16)$$

where P_{eff} is the effective permeability in the nanocomposite.

Hence, the relative effective diffusivity is expressed as follow:

$$\frac{D_{eff}}{D_0} = \frac{1}{(1-f)} \cdot \left(\frac{\frac{P_d}{P_0} - \frac{P_{eff}}{P_0}}{(1-f)(\frac{P_d}{P_0} - 1)} \right)^3 \quad (A.1.17)$$

After the impermeable dispersed phase assumption ($P_d = 0$), Bruggemann equation could be reduced to:

$$\frac{D_{eff}}{D_0} = (1-f)^{1/2} \quad (A.1.18)$$

The Maxwell model showed a good accuracy with experimental permeability data for filler volume fraction up to 0.2 whereas Bruggeman model could consider heavier filling. However, in both Maxwell and Bruggeman models, neither the filler shape/size distribution nor the filler dispersion was considered.

The modified Maxwell-Wagner-Sillars model (Bouma et al., 1997; Rafiq, Maulud, Man, & Muhammad, 2014) was developed to consider these morphological parameters. For impermeable dispersed fillers, Maxwell-Wagner-Sillars equation can be written as:

$$\frac{D_{eff}}{D_0} = \frac{1}{(1-f)} \cdot \frac{(1-n_e) - (1-n_e)f}{(1-n_e) + n_e f} \quad (A.1.19)$$

where n_e accounts for the filler shape, size and dispersion state. n_e is defined as:

$$n_e = \alpha \frac{f}{f_m} \quad (\text{A.1.20})$$

α is the filler shape factor and f_m is the maximum packing volume fraction of the fillers, which depends on the filler shape, filler size and filler dispersion. For $n_e = 1/3$, the modified Maxwell-Wagner-Sillars model is equivalent to the Maxwell model.

Higuchi (Higuchi, 1958; Higuchi & Higuchi, 1960; Idris, Man, Maulud, & Ahmed, 2016; Sadeghi, Semsarzadeh, & Moadel, 2009; Semsarzadeh & Ghalei, 2013) studied the permeability of composites constituted of the dispersion of impermeable spheres within a permeable matrix and proposed a model that could be written as:

$$\frac{D_{eff}}{D_0} = \frac{1}{(1-f)} \cdot \left(1 - \frac{6f}{4+2f-K_H(1-f)}\right) \quad (\text{A.1.21})$$

In the Higuchi equation, the empirical parameter K_H is related to the filler dispersion state.

While a large number of studies initially focused on the dispersion of spherical fillers, a growing interest has been then paid to impermeable fillers of various shapes (disks, cylinders, ribbons, etc.). Most models considered dilute or semi-dilute regime, meaning that the fillers could not overlap. Moreover, the studies were primarily focused on systems in which the fillers were oriented perpendicularly to the gas flow. Nielsen (Nielsen, 1967) gave a mathematical solution that allowed the description of the molecular flux in a medium filled with circular and square platelets of infinite length, uniformly and completely dispersed in the polymer matrix. The general Nielsen law expression for effective diffusivity is:

$$D_{eff} = \frac{D_0}{1 + \frac{L}{2W}f} \quad (\text{A.1.22})$$

where L is the filler length and W its width. By this equation, Nielsen showed that the fillers shape (circular or square) had an effect on diffusivity: the higher the $\frac{L}{W}$ ratio, the lower the diffusion and the permeability.

In agreement with Nielsen law, Raleigh et al. (L. Rayleigh, 1892) showed that the relative diffusivity in a nanocomposite system, where the polymer membrane contains a periodic array of infinite cylinders perpendicular to the membrane surface, only depends on the filler volume fraction:

$$\frac{D_{eff}}{D_0} = \frac{1}{1+f} \quad (\text{A.1.23})$$

Fredrickson and Bicerano (Fredrickson & Bicerano, 1999) proposed the following equation to predict barrier properties of composites containing a random dispersion of impermeable disks in a dilute regime:

$$\frac{D_{eff}}{D_0} = 1 - h(\alpha f) + h^2(\alpha f)^2 + \dots \quad (\text{A.1.24})$$

where $h = \frac{\pi}{\ln \alpha}$ is a geometric factor and α is the disk aspect ratio defined as the ratio between the diameter D and the thickness e .

Cussler (Cussler, Hughes, Ward, & Aris, 1988; Lape, Nuxoll, & Cussler, 2004; Moggridge, Lape, Yang, & Cussler, 2003; C. Yang, Smyrl, & Cussler, 2004) increased the complexity of the studied systems by considering different arrays of the dispersed impermeable fillers (flakes or lamellae). Two types of arrays were studied: regular and random arrays of oriented plates. The model developed by Cussler and coworkers can be expressed as follow:

$$\frac{D_{eff}}{D_0} = \frac{1}{1 + \frac{\xi}{1-f} \left(\frac{\alpha f}{2}\right)^2} \quad (\text{A.1.25})$$

assuming that α is the filler aspect ratio defined as the quotient of the width of the dispersed ribbons w by its thickness t , f is their volume fraction and ξ is a factor that depends on the case studied:

- $\xi = 1$, when the ribbons are dispersed in a regular array (Cussler et al., 1988);
- $\xi = 1/2$, when flakes are dispersed into two sequences with alignment and misalignment occurring with equal probability (C. Yang et al., 2004);
- $\xi = 2/27$, when fillers are hexagons and randomly distributed within the matrix (C. Yang et al., 2004).

According to ξ values, regular array of ribbons is the most efficient configuration for improving barrier properties.

Equation (A.1.26) is derived from the one developed by Cussler et al. (Lape et al., 2004) in the case of a random distribution of ribbons within a polymer matrix:

$$\frac{D_{eff}}{D_0} = \frac{1}{\left(1 + \frac{2}{3}f\alpha\right)^2} \quad (\text{A.1.26})$$

Due to the limitation of the previous equations to describe the behavior at high filler content, some authors investigated the effect of more concentrated systems. Aris and Cussler (Cussler et al., 1988) developed a model for plate-like particles in the semi-dilute regime. In this case, the relative effective diffusivity could be expressed by:

$$\frac{D_{eff}}{D_0} = (1 + \mu\alpha^2 f^2)^{-1} \quad (\text{A.1.27})$$

where $\mu = \frac{\pi^2}{16\ln^2\alpha}$ is the geometric factor.

Fredrickson and coworkers (Fredrickson & Bicerano, 1999) also considered the semi-dilute regime where disks are randomly distributed. They derived a model resulting in the following equation:

$$\frac{D_{eff}}{D_0} = \left(\frac{4(1 + \chi + 0.1245\chi^2)}{2 + \chi} \right)^{-2} \quad (\text{A.1.28})$$

assuming that $\chi = (\pi\alpha f)/(2\ln(\alpha/2))$.

Lu and coworkers (Lu & Mai, 2007) proposed a 2D theoretical model where platelets of high aspect ratios are randomly distributed in the polymer matrix. The equation developed by the group for such geometry results in the following expression for (D_{eff}/D_0) :

$$\frac{D_{eff}}{D_0} = \frac{1,66}{\left(1 + \frac{\alpha f}{2}\right)^{5/3}} \quad (\text{A.1.29})$$

Through this model, it was shown that an increase in relative diffusivity at higher filler content could be due to a lack of exfoliation or a decrease in fillers aspect ratio. Hence nanocomposites properties (critical volume fraction and aspect ratios) have been estimated and compared to experimental results.

1.3.1.2 Influence of the filler size distribution

In the previously cited studies, it was assumed that all the dispersed fillers have the same dimensions. Lape et al. (Lape et al., 2004) investigated the effect of the dispersion of impermeable flakes having different size. They studied two cases: a discrete distribution of

polydisperse flakes and a continuous distribution of polydisperse flakes. In all cases, the flake thickness t was assumed to be constant.

In the first case, the relative diffusivity in a film filled with a discrete distribution of polydisperse flakes could be described by equation (A.1.30):

$$\frac{D_{eff}}{D_0} = \left(1 + \left(\frac{2}{3} \frac{f}{t \sum_i n_i w_i} \right) \sum_i n_i w_i^2 \right)^{-2} \quad (\text{A.1.30})$$

where n_i and w_i are respectively the number and the width of flakes in size category i .

In the second case (continuous distribution) the equation has been modified to obtain:

$$\frac{D_{eff}}{D_0} = \left(1 + \left(\frac{2}{3} \frac{f}{t \bar{w}} \right) \int_0^\infty w^2 g dw \right)^{-2} \quad (\text{A.1.31})$$

In this equation, g is the size distribution function of flakes i.e. $g dw$ is the fraction of flakes having a width w . In both cases, the authors found that an increase in polydispersity leads to a decrease in permeability. In other words, barrier properties of polydisperse flakes were predicted to be superior to those of monodisperse flakes.

1.3.1.3 Influence of the filler orientation and stacking

Bharadwaj (Bharadwaj, 2001) modified the Nielsen model by giving a correlation between parameters such as filler orientation, length, concentration and their state of aggregation in the matrix. This model was developed in order to describe diffusivity in filled polymers based on tortuosity considerations. He introduced a new orientational order factor O in the Nielsen equation:

$$O = \frac{1}{2} (3 \cos^2 \theta - 1) \quad (\text{A.1.32})$$

where θ is the angle between the direction of penetrant flow and the normal to the layers.

O values can range from 1 ($\theta = 0$), indicating perfect orientation of fillers with diffusing gas direction, to $-1/2$ ($\theta = \pi/2$) indicating perpendicular or orthogonal orientation. A value of 0 indicates random orientation of fillers. The resulting equation reads:

$$\frac{D_{eff}}{D_0} = \frac{1}{1 + \frac{L}{2} W f \left(\frac{2}{3} \right) \left(O + \frac{1}{2} \right)} \quad (\text{A.1.33})$$

The Bharadwaj model predicts that small platelets are more sensitive to orientational disorder than large ones. It shows, in agreement with previous models, that barrier properties are lower in the case of aggregates with smaller aspect ratio than an individual platelet aspect ratio, taking into account the absence of intra-platelet diffusion.

Sorrentino et al. (Sorrentino, Tortora, & Vittoria, 2006) built a new geometrical model in order to study barrier properties of nanocomposite systems as a function of fillers orientation, volume fraction and intercalation between them. According to their description, their model seems the most adequate one for analyzing diffusion behavior in systems in which fillers have a very high aspect ratio. From their work, two main equations can be derived for a system of regularly distributed ribbons:

- regularly oriented ribbons:

$$\frac{D_{eff}}{D_0} = \left((1 - f) + f \left(1 + \frac{\alpha}{2} \right)^2 \right)^{-1} \quad (\text{A.1.34})$$

- randomly oriented ribbons:

$$\frac{D_{eff}}{D_0} = \left((1 - f) + \frac{4f}{\pi} \left(1 + \frac{\alpha}{4} + \frac{1}{\alpha} \right) \right)^{-1} \quad (\text{A.1.35})$$

Another approach was developed recently by Nazarenko et al. (Nazarenko, Meneghetti, Julmon, Olson, & Qutubuddin, 2007), considering the effect of layers stacking on gas barrier properties. They modified the Nielsen model in order to obtain an accurate equation that represents this configuration. Their model was based on the substitution of the individual mineral layer by layer stacks as shown in **Figure A.1.2**:

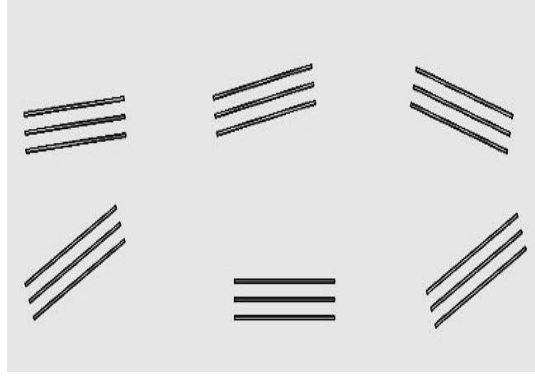


Figure A.1.2 Filler configuration studied by Nazarenko et al. (Nazarenko et al., 2007)

The Nazarenko model can be considered as an extension of the Bharadwaj model, in which the volume fraction and aspect ratio of the impermeable phase are taken into account. They supposed that diffusion inside the nanofillers, which are in this case homogenously dispersed and randomly oriented perpendicular to the diffusion direction, is neglected. Accordingly, the modified Nielsen equation is presented in the following form:

$$\frac{D_{eff}}{D_0} = \frac{1}{1 + \frac{1}{3} \left(\frac{fL}{2WN_L} \right)} \quad (\text{A.1.36})$$

assuming that L and W are respectively the length and the thickness of the fillers and N_L is the number of layers in each aggregate.

Some authors (Aris, 1985, 1986; Cussler et al., 1988; Falla, Mulski, & Cussler, 1996; Lape et al., 2004; Moggridge et al., 2003) attempted to model mass diffusion in tridimensional heterogeneous systems. A 3D analytical model based on a regular array as shown in **Figure A.1.3** was considered:

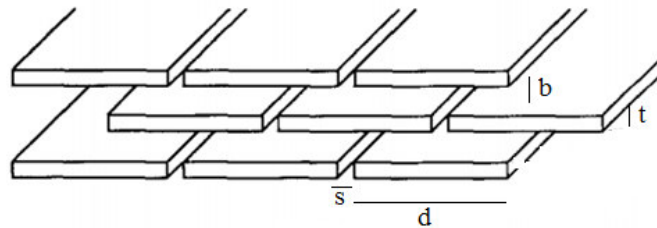


Figure A.1.3 Filler distribution studied in 3D models (Aris, 1985, 1986; Cussler et al., 1988; Falla et al., 1996; Lape et al., 2004; Moggridge et al., 2003)

It is worth to note that Aris built one of the first 3D analytical models (Aris, 1985, 1986). The well-known model he proposed to describe diffusion in such nanocomposite systems can be cast in the following form:

$$\frac{D_{eff}}{D_0} = \left(1 + \frac{\alpha^2 f^2}{1-f} + \frac{\alpha f}{\sigma_s} + \frac{4\alpha f}{\pi(1-f)} \ln \left(\frac{\pi \alpha^2 f}{\sigma_s(1-f)} \right) \right)^{-1} \quad (\text{A.1.37})$$

where σ_s is the slit shape i.e. the ratio of the distance between two adjacent flakes to its thickness (s/t) while the expression of f depends on the space surrounding the plates ($f = (d \cdot t) / ((\frac{d}{2} + s) \cdot (t + b))$) and the filler aspect ratio is $\alpha = d/(2t)$.

The first term in Eq. (A.1.37) is just unity. The relative diffusivity becomes 1 when the flake volume fraction f equals zero. The second term is attributed to the tortuous path around the flakes. The third term, involving σ_s , represents resistance to diffusion due to constriction between adjacent flakes. The last term corresponds to the resistance offered by the “necking” phenomenon faced by a diffusive molecule while circumventing the edges of the flakes at the entrance or exit of the slit. Wakeham and Mason (Wakeham & Mason, 1979) proposed a slightly different equation:

$$\frac{D_{eff}}{D_0} = \left(1 + \frac{\alpha^2 f^2}{1-f} + \frac{\alpha f}{\sigma_s} + 2(1-f) \ln \left(\frac{1-f}{2\sigma_s f} \right) \right)^{-1} \quad (\text{A.1.38})$$

The difference between equations (A.1.37) and (A.1.38) is the fourth term. It is assumed to be dependent of the aspect ratio for Aris and independent of this parameter for Wakeham and Mason. This fourth term is the most controversial of those in these equations. Cussler et al. (Cussler et al., 1988; Moggridge et al., 2003; C. Yang et al., 2004) argued that this resistance as well as the third term should be insignificant for nanocomposites with a large number of layers or flakes. They proposed then two simplified equations depending on the filler shape. For ribbon-like flakes, the simplified equation is:

$$\frac{D_{eff}}{D_0} = \left(1 + \frac{\alpha^2 f^2}{2(1-f)} \right)^{-1} \quad (\text{A.1.39})$$

For hexagonal flakes, it reads:

$$\frac{D_{eff}}{D_0} = \left(1 + \frac{2(\alpha^2 f^2)}{27(1-f)}\right)^{-1} \quad (A.1.40)$$

More recently, Dil and coworkers (Jalali Dil, Ben Dhieb, & Ajji, 2019) have developed a new analytical model in order to study the effect of fillers on nanocomposites barrier properties.

They have derived their model from Bharadwaj's analytical model where they have defined a new factor called "Herman's orientation function" v ($v = (3\cos^2\theta - 1)/2$).

Their derived equation is given by equation (A.1.41) :

$$\frac{D_{eff}}{D_0} = \left(\alpha f \left(1 - \sqrt{\frac{2}{3(1-v)}}\right)\right)^{-1} \quad (A.1.41)$$

The expressions of the relative diffusivity for the analytical models detailed in this review are summarized in **Table A.1.1**. In the next section it will be shown how these analytical models have been used to make comparison with experimental data to improve the understanding of gas barrier properties of biphasic systems in regards to their morphology.

1.3.2 Confrontation of the models with experimental data

Among the different models depicted in the previous part, Maxwell law is one of the most used models when focusing on polymer matrices loaded with spherical phases and considering f below 0.3 (Alix et al., 2012; Bitinis et al., 2012; Bugatti et al., 2010; Choudalakis & Gotsis, 2009; O. C. Compton, Kim, Pierre, Torkelson, & Nguyen, 2010; Crétois et al., 2014; Guan et al., 2016; Ha et al., 2016; Hotta & Paul, 2004, p. 200; Jacquelot et al., 2006; Kwon & Chang, 2015; Y. T. Park et al., 2013; Picard, Vermogen, et al., 2007; Shah, Krishnaswamy, Takahashi, & Paul, 2006; Takahashi et al., 2006; Thomas P & Thomas, 2012; Yano, Usuki, Okada, Kurauchi, & Kamigaito, 1993). Simplified Maxwell law (equation (A.1.15)) has been shown to accurately describe the transport properties of a wide range of polymers filled with spherical inorganic particles such as precipitated calcium carbonate fillers, metal nanofillers (Di Maio, Santaniello, Di Renzo, & Golemme, 2017; Morel et al., 2012; Morel, Espuche, Bounor-Legaré, Persynn, & Lacroix, 2016; Simon, Alcouffe, & Espuche, 2014; Su, Buss, McCloskey, & Urban, 2015). This law permits to describe the impact of dispersed domains with very different sizes (from a few tens of nanometers to a few hundred micrometers). However, it fails when defects (voids) or increase in free volume

produces at the polymer/filler interface leading to an unpredicted increase of permeability or when strong interactions are established at the polymer/filler interface inducing a slowdown of the diffusion rate in the interfacial area in comparison with the diffusion rate in the bulk matrix (J. Compton et al., 2006; Espuche et al., 2005; Morel et al., 2012; Shen & Lua, 2012; Takahashi et al., 2006). Only few authors have focused on comparing different models concerned with the dispersion of spherical domains to the same experimental data. Shen et al. (Shen & Lua, 2012) showed that the following order was obtained for prediction of permeability results of polyvinylidene fluoride/SiO₂ membranes: Maxwell model > Bruggeman model > Higuchi model.

During the last decades, a great attention has been paid to lamellar nanofillers (such as montmorillonite, vermiculite, double hydroxide layers, graphene...) due to the significant reinforcement of barrier properties expected from their high aspect ratio (Alix et al., 2012; Bitinis et al., 2012; Bugatti et al., 2010; Choudalakis & Gotsis, 2009; J. Compton et al., 2006; Crétois et al., 2014; Cui et al., 2016; Guan et al., 2016; Ha et al., 2016; Hotta & Paul, 2004; Jacquelot et al., 2006; Kwon & Chang, 2015; Y. T. Park et al., 2013; Picard, Vermogen, et al., 2007; Shah et al., 2006; Takahashi et al., 2006; Thomas P & Thomas, 2012; Yano et al., 1993). For platelets lying in the plane of the film, experimental results have been often analyzed thanks to Nielsen equation. In most studies, the methodology consists in using the chosen model (Nielsen, Cussler or Fredrickson & Bicerano...) to calculate the filler mean aspect ratio that allows fitting with a good accuracy the experimental relative permeability values of the nanocomposites prepared for increasing filler volume contents. The calculated mean aspect ratio is finally compared with the theoretical aspect ratio of the individual platelet or more often with the mean aspect ratio measured thanks to morphological analyses performed by transmission electron microscopy. A rather good agreement is obtained between experimental and theoretical values when a high degree of platelet exfoliation is achieved (E. Picard, Vermogen, et al. 2007; Y. T. Park et al. 2013; Shah et al. 2006; Hotta et Paul 2004). Moreover, although some differences are observed between the aforementioned models, it is generally difficult to decide which of the various theories provide the best prediction because the theoretical aspect ratio values are often within the range of aspect ratios determined by experimental observations (Picard, Vermogen, et al., 2007; Takahashi et al., 2006). However, for many systems, the morphology obtained is significantly different from the ideal morphology (e.g. fully exfoliated structures lying in the plane of the film). Very often, all the dispersed objects are not perfectly lying perpendicular to the gas flow (Jacquelot et al., 2006; Van Rooyen, Bissett, Khoathane, & Karger-Kocsis, 2016). Furthermore, in many cases, the

dispersed objects do not have the same size due to the coexistence of exfoliated and intercalated structures (Hotta & Paul, 2004; Mittal, 2008; Picard, Vermogen, et al., 2007; Shah et al., 2006). For these non-ideal morphologies, the barrier properties calculated by the previous models do not agree with experimental results. Therefore, Bharadwaj equation has been used to model systems with a random orientation of exfoliated platelets (Bharadwaj, 2001). For that morphology, the value of O parameter in Bharadwaj equation is fixed to 0 and the methodology consists here again in determining the filler mean aspect ratio value that allows the best fitting of the experimental results obtained for increasing volume fractions of dispersed fillers. The calculated value is then discussed with respect to the experimental one estimated thanks to the morphological observations performed on the samples. When the dispersed structures are intercalated, the platelet stacks are usually considered as impermeable domains for modeling. A reduced filler aspect ratio value is taken into account due to the increase of the considered thickness. A reduction of barrier properties is generally evidenced through experimental data in agreement with theoretical analysis. However, it is to highlight that some authors have experimentally shown that platelet stacks could not always be considered as impermeable phases. Indeed, an increase of gas solubility was evidenced in some nanocomposites based on intercalated structures in comparison with nanocomposites based on exfoliated structures (Jacquelot et al., 2006). However, it appears that this does not significantly impact the barrier properties at low filler volume fraction. One explanation could be that the volume fraction concerned by this phenomenon (related to the volume between the platelets in the stacks) is too small to play a significant role in the transport phenomenon. For a significant number of nanocomposite systems, the morphology is not as simple as that depicted in the previous discussed cases. A coexistence of exfoliated and intercalated structures can be observed. Moreover, all intercalated structures do not always contain the same platelet number. This complex morphology is often favored as the filler volume fraction increases in the material. Some experimental results (Picard, Vermogen, et al., 2007) have shown that contrary to what was commonly expected, some interesting gas barrier properties could be obtained in agreement with Lape et al. work (Lape et al., 2004). To explain such results, Picard et al. assigned different density values to exfoliated and intercalated structures due to the presence of organic species in the last structures (Picard, Vermogen, et al., 2007). Taking into account these different density values and based on a detailed quantitative analysis of the dispersed objects resulting from transmission electron microscopy and scanning electron microscopy observations, they have proposed a modified expression of the classical models (Nielsen, Cussler). In their modified models, a discretization of the aspect

ratio values of the different dispersed phases is considered in relation with the morphological data obtained from a detailed TEM and SEM analysis of the samples. A good agreement between experimental and calculated permeability values was observed. The fact that the intercalated structures haven't a detrimental effect on gas barrier properties is explained in this case by the limited number of platelets forming the stacks and also the relatively low amount of stacks. By this example, it can be clearly seen that the analysis and understanding of barrier properties in non-ideal systems can become very complex, needing both detailed morphological analyses and more complex models. Among the analytical models described in the previous part of this review, Aris model is one of the most detailed and complex models (Aris, 1985, 1986). According to our knowledge, unfortunately, the Aris model was not confronted with nanocomposites experimental results probably due to a general lack of detailed quantitative morphological analyses performed on materials.

Table A.1.1 - Summary of analytical models cited in the review.

Model	Filler type	Array/Orientation	Model dimension	Aspect ratio	Relative diffusivity
Maxwell (Maxwell, 1873)	Spherical form	Homogeneous dispersion of impermeable spheres	2D	1	$\frac{D_{eff}}{D_0} = \frac{1}{1 + f/2}$
Bruggeman (Bruggeman, 1935)	Spherical form	Homogeneous dispersion of impermeable spheres	2D	1	$\frac{D_{eff}}{D_0} = (1 - f)^{1/2}$
Maxwell-Wagner-Sillars (Bouma et al., 1997; Rafiq et al., 2014)	Spherical form	Homogeneous dispersion of impermeable spheres	2D	1	$\frac{D_{eff}}{D_0} = \frac{(1 - n_e) - (1 - n_e)f}{(1 - f)((1 - n_e) + n_e f)}$ $n_e = \alpha \frac{f}{f_m}$
Higuchi (Higuchi, 1958; Higuchi & Higuchi, 1960)	Spherical form	Homogeneous dispersion of impermeable spheres	2D	1	$\frac{D_{eff}}{D_0} = \left(1 - \frac{6f}{4 + 2f - K_H(1 - f)}\right) (1 - f)^{-1}$
Nielsen (Nielsen, 1967)	Ribbons of infinite length with a width w and thickness t	Regular array, oriented	2D	w/t	$\frac{D_{eff}}{D_0} = \frac{1}{1 + \frac{\alpha f}{2}}$

Cussler (Cussler et al., 1988)	Ribbons of infinite length with a width w and thickness t	Regular array, oriented	2D	w/t	$\frac{D_{eff}}{D_0} = \frac{1}{1 + \frac{\xi}{1-f} \left(\frac{\alpha f}{2}\right)^2}$ $\xi=1$
Cussler (C. Yang et al., 2004)	Ribbons of infinite length with a width w and thickness t	Two courses of ribbons with alignment and misalignment occurring with equal probability	2D	w/t	$\frac{D_{eff}}{D_0} = \frac{1}{1 + \frac{\xi}{1-f} \left(\frac{\alpha f}{2}\right)^2}$ $\xi=1/2$
Cussler (C. Yang et al., 2004)	Hexagons with a width w and thickness t	Random array, oriented	2D	w/t	$\frac{D_{eff}}{D_0} = \frac{1}{1 + \frac{\xi}{1-f} \left(\frac{\alpha f}{2}\right)^2}$ $\xi=2/27$
Raleigh(Lord Rayleigh, 1892)	Cylindrical form	Regular array, oriented	2D	1	$\frac{D_{eff}}{D_0} = \frac{1}{1+f}$
Lape-Cussler (Lape et al., 2004)	Ribbons of infinite length with a width w and thickness t	Random array, oriented	2D	w/t	$\frac{D_{eff}}{D_0} = \frac{1}{(1 + \frac{2}{3} f \alpha)^2}$
Lu (Lu & Mai, 2007)	Platelets of infinite length with a width w and thickness t	Random array, non-oriented	2D	w/t	$\frac{D_{eff}}{D_0} = \frac{1,66}{\left(1 + \frac{\alpha f}{2}\right)^{5/3}}$
Bharadwaj (Bharadwaj, 2001)	Ribbons of infinite length with a width w and thickness t	Random array, non-oriented	2D	w/t	$\frac{D_{eff}}{D_0} = \frac{1}{1 + \frac{Lf}{2W} \left(\frac{2}{3}\right) \left(O + \frac{1}{2}\right)}$ $O = \frac{1}{2} (3\cos^2\theta - 1)$
Sorrentino (Sorrentino et al., 2006)	Ribbons of infinite length with a width w and thickness t	Regular array, non-oriented	2D	w/t	$\frac{D_{eff}}{D_0} = \frac{1}{(1-f) + f \left(\frac{\frac{\alpha+1}{2}}{\frac{\alpha}{2\sin\theta + \cos\theta}}\right)^2}$
Nazarenko (Nazarenko et al., 2007)	Stacks of disks with a diameter D and thickness e	Random array, non-oriented	2D	d/t	$\frac{D_{eff}}{D_0} = \frac{1}{1 + 1/3 \left(\frac{fD}{2 \cdot e \cdot N}\right)}$

Aris (Aris, 1986)	Flakes of d wide and t thick, separated by distance b , and extending infinitely	Regular array, oriented	3D	$d/2t$	$\frac{D_{eff}}{D_0} = \left(1 + \frac{\alpha^2 f^2}{1-f} + \frac{\alpha f}{\sigma_s} + \frac{4\alpha f}{\pi(1-f)} \ln \left(\frac{\pi \alpha^2 f}{\sigma_s(1-f)} \right) \right)^{-1}$
Fredrickson-Bicerano (Fredrickson & Bicerano, 1999)	Disk with a diameter D and thickness e	Random array, oriented	3D	d/t	$\frac{D_{eff}}{D_0} = \left(\frac{4(1+\chi+0.1245\chi^2)}{2+\chi} \right)^{-2}$ $\chi = \pi \alpha / f (2 \ln(\alpha/2))$
Dil et al (Jalali Dil et al., 2019)	Ribbons of infinite length with a width w and thickness t	Random array, non-oriented	2D	$d/2t$	$\frac{D_{eff}}{D_0} = \left(\alpha f \left(1 - \sqrt{\frac{2}{3(1-v)}} \right) \right)^{-1}$ $v = \frac{3 \cos^2 \theta - 1}{2}$

The vast majority of models cited in this first part of the review cover cases that range from simple 2D / 3D systems, where particles of rectangular shape such as platelets or ribbons are regularly or randomly distributed in the polymer matrix. In these approaches, the effects of several parameters (volume fraction, aspect ratio, orientation, dispersion, distribution) on barrier properties have been investigated. According to most authors, the modification of the expression of the tortuosity factor is sufficient to account for the main effects of those parameters on barrier properties. Furthermore, those analytical models are often experimentally supported for the most simple nanocomposite structures. However, in order to go further in the understanding of actual materials and their barrier properties, the need for new models allowing simulation of 2D and 3D complex systems is clearly evidenced. New models have been built in order to simulate 2D and 3D complex systems where fillers are symmetrical disks or flakes of different shapes instead of infinite ribbons. Those models are too complex to yield a simple analytical equation for the relative diffusivity, so they need to be solved numerically using various numerical methods and tools.

1.4 Numerical approaches

In order to overcome the limitations of the previous approaches, more geometrically complex models have been proposed to predict the enhancement in barrier properties of 2D and 3D systems containing different nanofiller types. Generally, as these models cannot be solved

through analytical calculations, various numerical methods can be used to obtain approximate solutions. This paper discusses several works based on the Monte Carlo (MC) method, the boundary element method (BEM), the finite volume method (FVM) and the finite element method (FEM) (Bhunia et al., 2012). The Monte Carlo (MC) method relies on a repeated random sampling of a large number of single events in order to provide an approximate averaged solution. Schematically, MC simulations provide numerical solutions of a deterministic problem through a microscopic and probabilistic approach (Eitzman, Melkote, & Cussler, 1996; Swannack et al., 2005). Contrary to the MC method, the BEM, FVM and FEM are based on the solution of partial differential equations (PDE), meaning that the problem formulation is cast in a macroscopic and deterministic way. The BEM distinguishes itself as a “boundary” method, meaning that the numerical discretization is conducted at reduced spatial dimension, leading to smaller linear equation systems and less computer memory requirements (Wrobel, 2002). The FVM is conservative in essence and based on flux evaluation at cell boundaries (Versteeg & Malalasekera, 2007). Its main strengths are accuracy and rapidity on regular meshes. However, when the studied geometry becomes more irregular and complex, these advantages turn out to be less remarkable. The FEM is also a method of choice for simulating diffusion problems. One of its main benefits is that it offers great freedom in the selection of discretization: shape and dimension of elements that can be used to discretize the space domain as well as basis interpolation functions. Furthermore, in order to describe the diffusion process in nanocomposites and to analyze the influence of the structural parameters such as aspect ratio, orientation angle, volume fraction, intercalation level, etc., the FEM was found to be the most suitable because it is consistently robust for representing various structures. It is also flexible enough to incorporate a 3D structuration of the nanofillers (Bhunia et al., 2012). As aforementioned, the complexity of the structure of the systems (polymer matrix + fillers) is the main reason why numerical models have been developed. Hence, in the following, several modeling approaches (from simple, regular 2D systems to more complex, randomly distributed 3D morphologies) will be presented and discussed.

1.4.1 Regular array

This type of dispersion, for which fillers are placed perpendicularly to the gas flow, has often been considered because it is supposed to lead to better barrier performance. It has been analyzed in the case of two-dimensional systems as well as three-dimensional systems.

1.4.1.1 2D systems

Similarly to analytical models, the earlier numerical approaches have been conducted for a regular distribution of fillers in the polymer matrix because those systems are the simplest ones and can be considered as ideal systems. The studied geometries are often distributed as shown in **Figure A.1.4**.

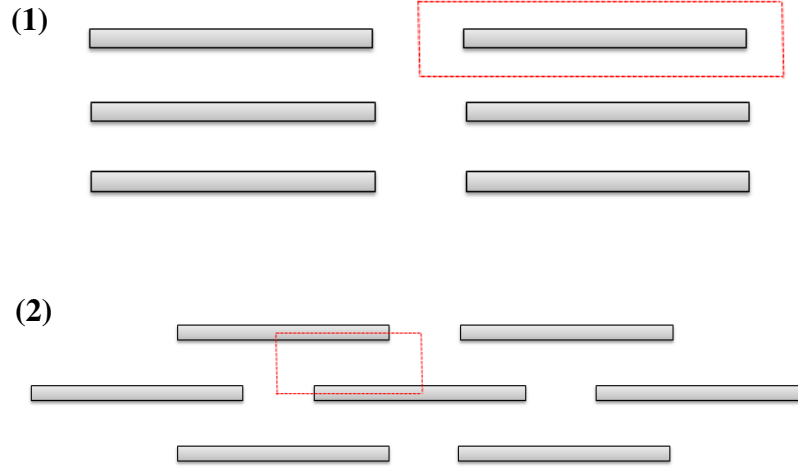


Figure A.1.4 Filler regular distribution in 2D systems

Falla et al. (Falla et al., 1996) used Monte Carlo approaches to simulate transport across membranes containing oriented fillers. The method adopted by the authors consists in calculating the molecular mean square displacement as a function of time to estimate the relative effective diffusivity:

$$\frac{D_{eff}}{D_0} = \frac{3 * \varepsilon_F}{\gamma} \quad (\text{A.1.42})$$

where ε is the slope of the plot of the mean square displacement versus time and γ is the mean free path travelled by the molecule. Their model is one of the oldest ones, but it was efficient to predict barrier properties of nanocomposites in which fillers were organized as shown in the work of Cussler et al. (**Figure A.1.3**), except in the present case the system is 2D. The considered fillers were ribbons of infinite length, regularly spaced and oriented perpendicularly to the diffusion path. The volume fraction of the fillers, their aspect ratio α and the slit shape σ_s were varied. As a result, it has been found that diffusivity is less affected when α is small and σ_s is large, while it is more affected when α is large with small values of σ_s . These results are in good agreement with Aris's equation (A.1.37).

Chen et al. (X. Chen & Papathanasiou, 2007) focused their study on the barrier properties of flake-filled polymer membranes. They built a numerical model where flakes were aligned parallel to the membrane surfaces and diffusion has been set to be perpendicular to the membrane surface. They used the boundary element method to solve diffusion equations. Two cases of arrays for a periodic arrangement of aligned monodisperse flakes were analyzed: quadratic array (**Figure A.1.4 (1)**) and staggered array (**Figure A.1.4 (2)**). The red boxes shown in **Figure A.1.4** are the unit cells chosen for each distribution. The authors found that the results yielded by their numerical model are in good agreement with the Aris model which predict barrier properties of high aspect ratio, monodisperse flakes in a staggered array. This conclusion is similar to that of Falla's study.

Swannack et al. (Swannack et al., 2005) have conducted Monte Carlo simulations of a polymer-clay nanocomposite system in order to study its barrier properties. They built a 2D model where impermeable rectangular platelets were regularly dispersed in the polymer matrix as shown in **Figure A.1.4 (2)**. They also proved that their 2D Monte Carlo simulation results are in accordance with Aris equation. **Figure A.1.5** shows this agreement for a slit shape value of 0.1 (the slit shape is defined as the ratio of the horizontal gap between fillers to their thickness).

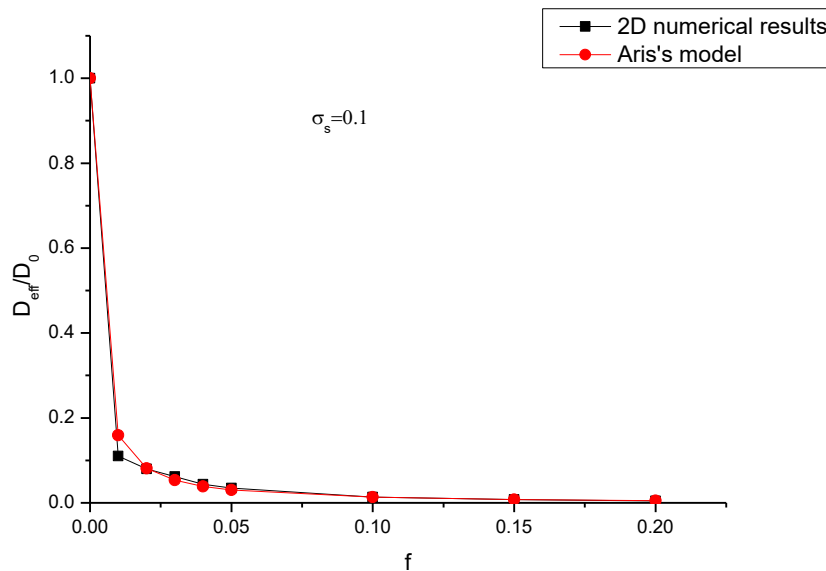


Figure A.1.5 Comparison of Swannack's 2D numerical results with Aris's model

Minelli et al. (Minelli, Baschetti, et Doghieri 2009) focused on impermeable fillers inserted regularly in the polymer matrix perpendicularly to gas diffusion, in a staggered array. As well as in Chen's work, they considered a repeating unit cell to simplify the diffusion problem (**Figure A.1.4 (2)**). They used a finite volume method to build and solve a numerical model

which could take into account parameters such as filler shape, distribution and volume fraction. They compared their numerical results to an analytical model derived from a modification of Aris's equation:

$$\begin{aligned} \frac{D_0}{D_{eff}} = & \frac{\alpha f}{\sigma_s} \left(1 + \frac{\sigma}{\alpha}\right)^2 + \frac{(\alpha f)^2 (1 + \sigma_s/\alpha)^4}{1 - f(1 + \sigma_s/\alpha)} \\ & + \frac{\alpha f}{\pi/4} \left(1 + \frac{\sigma_s}{\alpha}\right)^2 \ln \left[\frac{1 - f(1 + \sigma_s/\alpha)}{f \sigma_s (1 + \sigma_s/\alpha) (\pi/2)} \right] \end{aligned} \quad (\text{A.1.43})$$

In this equation, the overall resistance to mass transport is subdivided into two resistances: the resistance of the neat matrix and the resistance due to the tortuous path. They have found a good agreement. Moreover, their results have been compared to previous empirical models developed for the same purpose (X. Chen & Papathanasiou, 2007; Falla et al., 1996; Swannack et al., 2005). They concluded that the increase in barrier properties is predicted for low slit shape values.

According to their results, the smaller the ratio α/σ_s , the lower the enhancement of barrier properties. Sridhar et al. (L. N. Sridhar, Gupta, & Bhardwaj, 2006) attempted to evaluate the transport properties in 2D heterogeneous system containing aligned flakes. Again, the studied configuration can be represented by **Figure A.1.4**. They considered a computational method based on a network of series/parallel resistances associated with a finite difference method. They could assess the decrease in relative diffusivity as a function of filler aspect ratio, volume fraction, orientation and their structural parameters. Numerical results matched with experimental data for a gap between fillers value equal to 6 nm.

Later, in the same context, Statler et al. (Jr & Gupta, 2007) used a finite element method to evaluate the reduction of the diffusivity in nanocomposites systems. The impermeable fillers have been considered as uniformly dispersed platelets with perpendicular orientation to the mass transfer direction similarly to previously cited works (**Figure A.1.6**). In the computational procedure, a unit cell has been chosen and boundary conditions were set (a ratio of concentration (C/C_0) was set between 0 and 1 at the left and right boundaries of the unit cell). It was found that the numerical results are in good agreement with the Cussler analytical model for a slightly important filler volume fraction (beyond 8%). In addition, the Nielsen model over-predicts relative diffusivity in the same region (**Figure A.1.6**). Indeed, the Nielsen theory does not take into account the reduction of the area for diffusion whereas Cussler's model does.

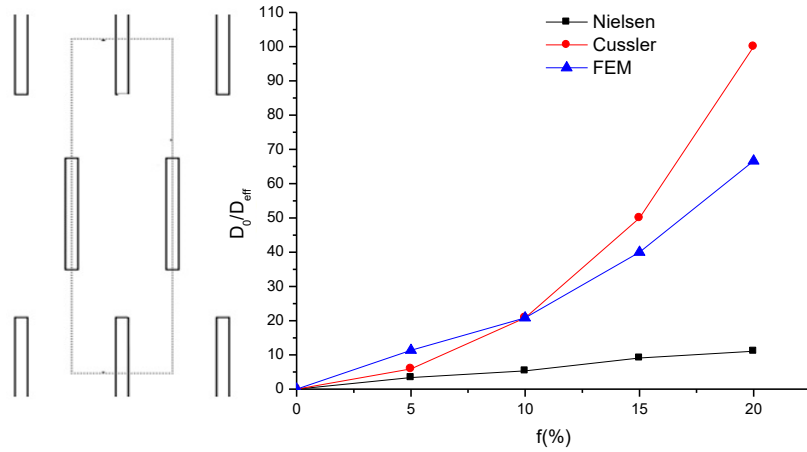


Figure A.1.6 Unit cell and results of Statler et al. (Jr & Gupta, 2007) model

1.4.1.2 3D systems

Most of the earlier numerical approaches developed to model gas diffusion properties of nanocomposite materials only considered bi-dimensional systems. However, new approaches allowing the description of the composite material in 3 dimensions have been used increasingly.

Swannack et al. (Swannack et al., 2005) built a 3D model in which the fillers are regularly spaced parallelepiped platelets. Similarly to the 2D part of their work, they used a Monte Carlo approach in order to calculate the values of the ratio D_0/D_{eff} for several ranges of structural parameters. The results were compared to their 2D model and Aris's equation. They obtained a reasonable agreement with Aris's equation for low values of filler volume fraction but in the majority of cases, Aris's equation under-predicts the effective diffusivity values, contrary to what has been obtained with the 2D geometry (**Figure A.1.7**). Actually, the 2D simulations predict a lower effective diffusivity than the 3D simulations. The authors explained these discrepancies by pointing out that for a given filler volume fraction, a truly 3D geometry (platelets with finite extension) allows more permeation than a 2D geometry (platelets with infinite extension) and thus leads to a higher effective diffusivity value.

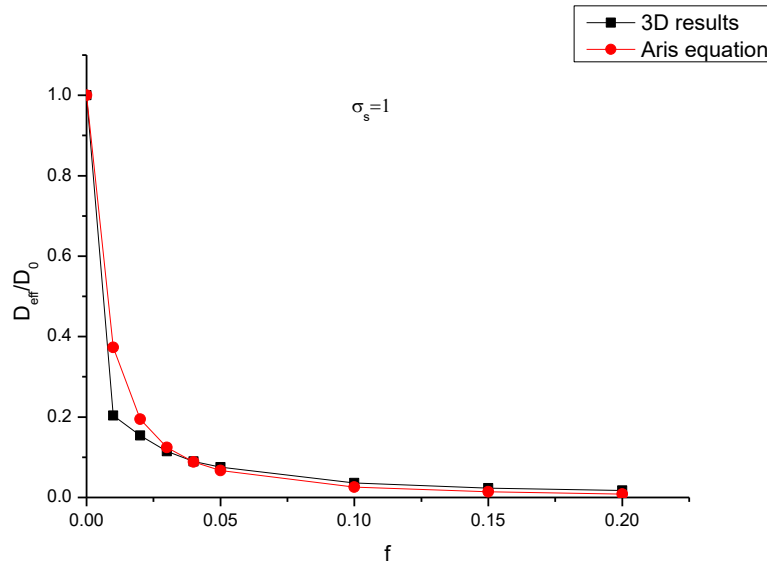


Figure A.1.7 Comparison of 3D Swannack numerical results and Aris equation

Goodyer and Bunge (Goodyer & Bunge, 2007) later developed a finite element model based on the resolution of Fick's law in 3D geometries with different filler shape (ribbons, squares, hexagons). The main objective of their work was to compare numerical simulation results to the experimental work of Cussler and Liu (Q. Liu & Cussler, 2006). The unit cell, shown by a dotted red line in **Figure A.1.8**, extends down through the transversal direction of the domain. Besides, the chosen unit cell depends on the repeated unit in the considered geometry. They considered in their model the so-called necking effect of molecules diffusing into and out of the slits between fillers. They could show that for one layer of flakes, whatever the filler geometry, the numerical results were in agreement with previous models. Furthermore, for multiple layers of fillers, the numerical results over-estimated the barrier effect experimentally achieved by Cussler and Liu.

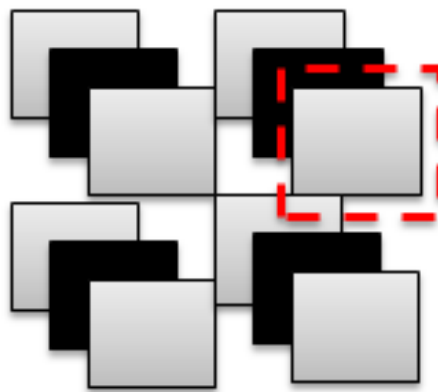


Figure A.1.8 Example of geometry studied by Goodyer et al. (Goodyer & Bunge, 2007) (the dashed red box is the unit cell)

In order to gain a better understanding of the relationship between morphological characteristics and effective permeability in nanocomposites systems, Minelli et al. (Minelli, Baschetti, & Doghieri, 2011) built a 3D finite volume model of ordered dispersed flakes which presented various (but homogeneous) shapes (**Figure A.1.9**).

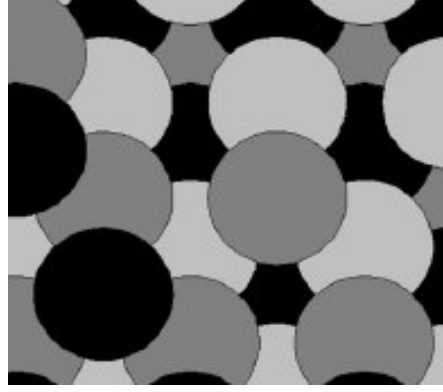


Figure A.1.9 Example of geometry adopted in Minelli's model

They considered hexagonal tablets, square tablets, octagonal tablets and circular disks. In this work, the authors introduced the following expressions of filler aspect ratio and slit shape:

$$\alpha = \frac{S_n}{S_L} \quad (\text{A.1.44})$$

$$\sigma_s = \frac{S_{nM}}{S_L} \quad (\text{A.1.45})$$

where S_L is the area of the filler lateral surface, S_n is the cross section area of filler (normal to the flux direction) and S_{nM} is the area corresponding to cross section of the matrix region between adjacent fillers, in the filler plane. Several ranges of fillers aspect ratio values, volume fractions and slit shapes have been considered in order to study their effect on the composite transport properties. For both 2D and 3D geometries, the authors compared their simulation results to Aris's equation (A.1.37). The good agreement obtained means that Aris's equation could be directly applied to the 3D ordered geometries if the definitions they proposed for the fillers aspect ratio and slit shape (Eqs. (A.1.44) and (A.1.45)) were used. **Figure A.1.10** shows the variation of diffusivity as a function of the filler shape and volume fraction for fixed values of slit shape $\sigma_s = 0.5$ and aspect ratio $\alpha = 5$.

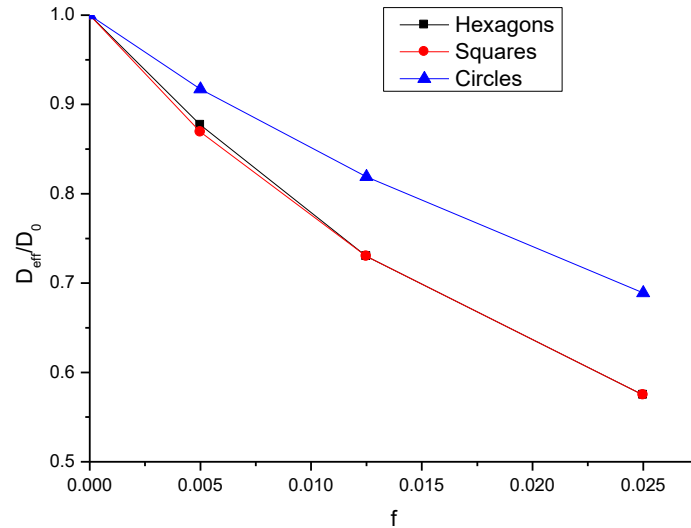


Figure A.1.10 3D numerical results for ordered fillers of various shapes (Minelli et al., 2011)

It is interesting to note through **Figure A.1.10** that relative diffusivity actually depends on the filler shape. Indeed, for a given volume fraction, a dispersion of circular flakes affects less diffusivity than a dispersion of hexagonal or square flakes does.

1.4.2 Random array

1.4.2.1 Homogeneous filler orientation/size

2D systems

Several efforts have been carried out to numerically evaluate the enhancement in barrier properties brought by random dispersion of impermeable flakes in a dense matrix. Geometries studied in the next works are presented in **Figure A.1.11**.

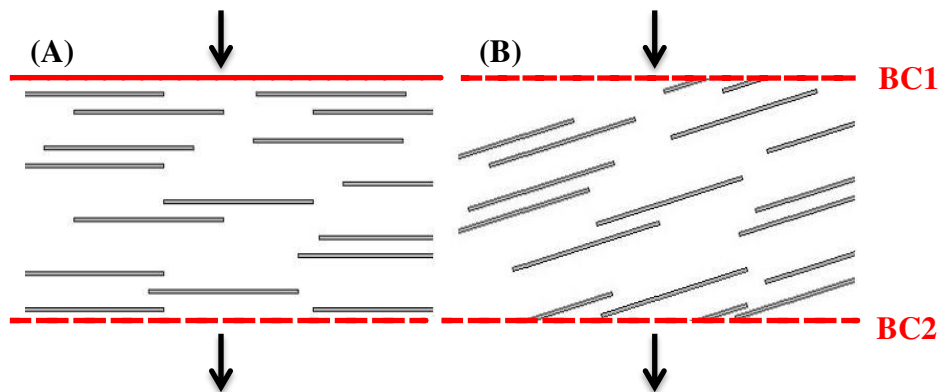


Figure A.1.11 Fillers random dispersion in 2D systems. BC indicate boundary conditions imposed at the upper and lower faces of the system. Arrows indicate mass flux direction. (A): filler mid-plane perpendicular to mass flux direction; (B): filler mid-plane angled with respect to mass flux direction.

Using the fast multipole accelerated boundary element method, Chen and coworkers (X. Chen & Papathanasiou, 2007) have built a 2D model where simulations were based on models of random arrays of monodisperse flakes (**Figure A.1.11(A)**). While the dispersion of fillers seemed complex and non-uniform, the authors have adopted a non-periodic representative volume element (RVE) to solve the problem. The concentration boundary conditions were applied on the upper and lower faces of the unit cell as shown in **Figure A.1.11**. They found that their model over-predicted the results of the theoretical model proposed by Lape et al. (Lape et al., 2004) because the latter induced too much simplification of the influence of the flake-flake interactions on the diffusion path tortuosity.

In order to study a random array with homogeneous filler size and orientation, Minelli (Minelli et al., 2011) built a 2D geometry through an algorithm that randomly distributes platelets of fixed structural parameters in the computational domain. They concluded that the barrier enhancement effect increases as filler aspect ratio or volume fraction increases. Furthermore, their numerical results showed an agreement with previous numerical models such as Chen's model. Bhunia et al. (Bhunia et al., 2012) developed a computer simulation model using the FEM method in order to analyze the changes in barrier nanocomposites properties when the structural parameters are modified. Fillers were chosen to be platelets of rectangular cross section, either perpendicular to the diffusion path or showing an orientation angle θ between the direction of diffusion and the average orientation of the flakes as shown in **Figure A.1.12**.

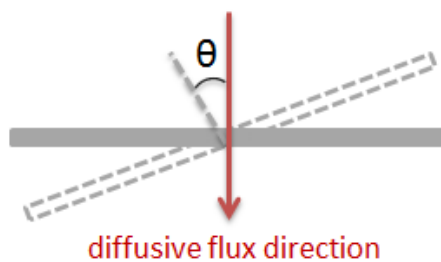


Figure A.1.12 Angle of orientation defined in the cited models

Their results indicated that for a filler volume fraction f ranging from 1% to 7% and a filler aspect ratio α ranging from 50 to 1000, the best barrier property for an exfoliated system could be obtained for the optimum structural parameter couple ($f = 5\%$, $\alpha = 500$). Moreover, they showed that an exfoliated system could improve barrier properties much more efficiently than an intercalated one. Finally, the gas barrier properties could be greatly reduced if the

orientation angle increases (θ ranges from 0 to 85 i.e. from perpendicular to quasi parallel direction with respect to the diffusion flux).

Another recent model has been built by Tsiantis and Papathanasiou (Tsiantis & Papathanasiou, 2017), which treated the barrier properties of flake filled composites as a function of fillers orientation. For that purpose, they used a Random Sequential Adsorption (RSA) algorithm in order to build a representative volume element of the geometry. The unit cell adopted was quite similar to the one presented in **Figure A.1.11** (B). They used the OpenFOAM software in order to generate the adequate mesh to solve the steady-state diffusion equation. Their computational results have shown that the effective diffusivity for a system of randomly placed flakes oriented with an angle $(\pi/2 - \theta)$ with respect to the direction of the diffusive flux is:

$$\frac{D_{eff}}{D_0} = \frac{1-f}{(1+\alpha f/\lambda)^2} \cos^2 \theta + \frac{1-f}{1+f/2\alpha} \sin^2 \theta \quad (A.1.46)$$

where θ is the angle formed between the direction of the diffusion and the outward normal vector on the flake surface and λ is an adjustable geometrical parameter.

The same authors (Tsiantis & Papathanasiou, 2019) derived numerical solutions for barrier properties of flake filled composites where fillers were randomly placed and oriented ($0 < \theta < \pi/2$).

They have shown through their work that 1D representation of the studied systems is suitable for very high aspect ratio flakes. Their numerical results were in adequacy with the harmonic and the arithmetic averages based on Nielsen and Lape's models.

3D systems

Various 3D models have been built taking into account the random dispersion of fillers in a homogenous system as shown in **Figure A.1.13**.

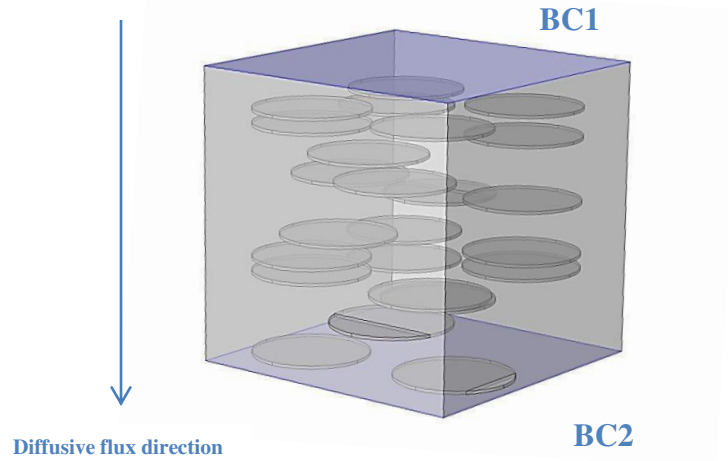


Figure A.1.13 3D dispersion of homogeneous disks in the matrix

Gusev and Lusti (Gusev & Lusti, 2001) have used a direct finite element method to solve a three dimensional periodic model comprised of a random dispersion of perfectly parallel impermeable disks in an isotropic matrix (**Figure A.1.13**) by solving Laplace's equation. Concentration boundary conditions have been applied on the upper and lower faces of the box and periodic boundary conditions on the lateral faces of the box. As results, they have shown that permeability in such a system was reduced by a factor defined as the product of the filler aspect ratio α and its volume fraction f . Furthermore, Gusev and coworkers derived an empirical equation from these numerical predictions:

$$\frac{D_{eff}}{D_0} = \exp\left(-\left(\frac{\alpha f}{3.47}\right)^{-0.71}\right) \quad (\text{A.1.47})$$

Through this study, they also showed that the presence of high-aspect-ratio atomic-thickness nanofillers could lead to changes in the local gas properties especially around fillers.

A similar work has been performed by Nagy et al. (Nagy & Duxbury, 2002) to study the effect of the tortuous path on the overall diffusivity in a 3D flake-filled system. They adopted a resistor representation and showed that the enhancement of barrier properties is a function of the factor αf through the sum of linear and quadratic contributions.

Minelli et al. (Minelli et al., 2011) also developed a 3D finite element model to analyze a similar configuration (**Figure A.1.13**). Their work resulted in the following equations which could be applied for either 2D or 3D systems:

$$\frac{D_{eff}}{D_0} = \frac{f}{2\alpha} (\alpha + 2)^2 + \frac{f^2(\alpha + 2)^4}{4(\alpha^2 - \alpha f(\alpha + 2))} + \frac{2}{\pi} (\alpha + 2)^2 \ln \left[\frac{2}{\pi} \left(\frac{\alpha}{f(\alpha + 2)} - 1 \right) \right] \quad (\text{A.1.48})$$

if $r \leq 1$

$$\frac{D_{eff}}{D_0} = 1 + \frac{f}{2} (\alpha + 2) + \frac{2f}{\alpha\pi} (\alpha + 2)^2 \ln \left[\frac{1}{\pi} (\alpha + 2) \right] \quad (\text{A.1.49})$$

if $r \geq 1$

where

$$r = \frac{2(\alpha - f(\alpha + 2))}{f(\alpha + 2)^2} \quad (\text{A.1.50})$$

and α is the filler aspect ratio as defined in equation (A.1.44). Like previous works, they have concluded that in the case of 3D random systems, the barrier enhancement effect increases as α or f increases. **Figure A.1.14** shows that the shape of the filler cross section (circles or squares) has no significant effect on the overall barrier properties of the nanocomposite.

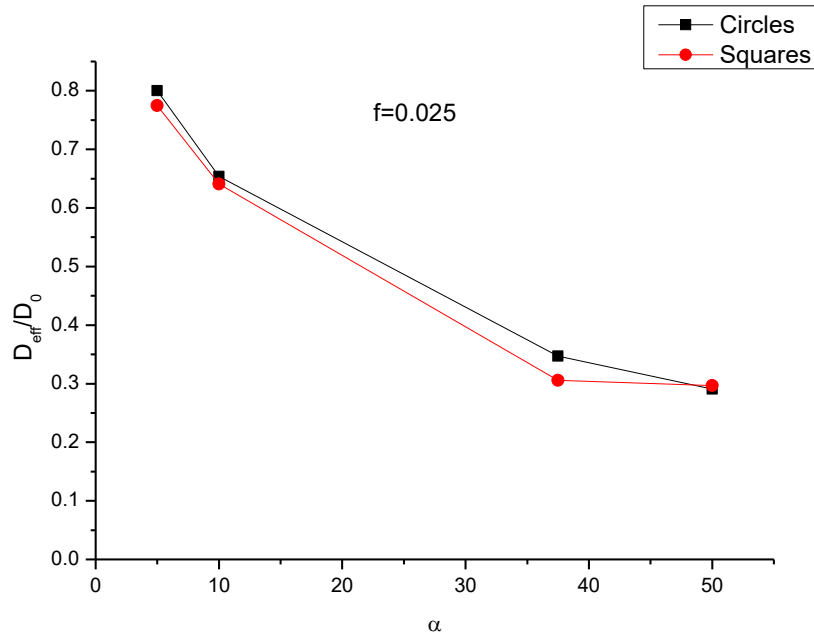


Figure A.1.14 Effect of structural parameters on diffusivity for the 3D random model proposed by Minelli et al. (Minelli et al., 2011)

1.4.2.2 Heterogeneous filler orientation/size

2D systems

In this class of systems, the fillers are randomly positioned in the matrix as in the previously described works, but in addition, they do not all have the same size or orientation. Several configurations have been considered in 2D systems and some of them are summed up in **Figure A.1.15**.

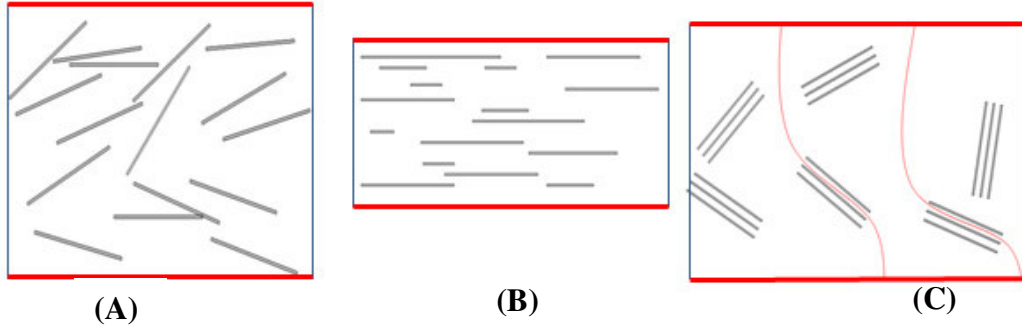


Figure A.1.15 Fillers randomly distributed in 2D: (A) random orientation; (B) polydisperse fillers; (C) stacks of fillers (intercalated system) with diffusive flux lines. Bold red lines correspond to the inlet and outlet boundaries for mass diffusion.

Greco (Greco, 2014a) used the finite element method in order to build a 2D model that describes barrier properties of randomly oriented nanocomposites (**Figure A.1.15** (A)). In this study, the ‘normalized’ diffusivity coefficient was defined as:

$$D_{eff} = (L_{eff})^{-4} \quad (\text{A.1.51})$$

L_{eff} being the average normalized length which depends on structural parameters such as fillers aspect ratio, volume fraction and orientation angle. The relation proposed by Greco in 2D is given by equation (A.1.52) :

$$D_{eff} = (1 - f) \left(1 + \sqrt{2} \left(1 - \frac{\sqrt{2}}{2} \right) f \alpha (\cos \theta)^2 \right)^{-4} \quad (\text{A.1.52})$$

θ is the angle formed between the direction of diffusion and the normal vector to the platelet surface. Later, Greco (Greco, 2014b) expanded his previous work to intercalated nanocomposites by introducing the notion of galleries, i.e. matrix layers between stacked nanofillers. He considered that diffusing moieties could follow trajectories corresponding to the flux lines shown in **Figure A.1.15** (C). He introduced a new equation of diffusivity taking into account the orientation angles of fillers as well as the presence of galleries:

$$D_{eff} = \left(1 + 0.5 \frac{f\alpha}{n} \cos\theta(1 - \sin\theta) + f \left(1 + \left(1 - \frac{1}{n} \right) \frac{T_G}{t} \right) \sin\theta(1 - \sin\theta) \right)^{-4} \quad (\text{A.1.53})$$

where G subscript refers to galleries. n is the number of platelets while T_G and t are the thickness of the galleries and platelets respectively. Since the numerical model built by Greco was able to simulate diffusion between platelets, it was concluded that the coefficient of diffusion decreases as the following parameters increase: the degree of intercalation, the lamellar galleries thickness, and the degree of dispersion. It also decreases as the number of lamellar sheets in each stack decreases.

Dondero and coworkers (Dondero, Tomba, & Cisilino, 2016) built a model in which impermeable fillers of rectangular shapes are randomly dispersed in a homogenous and isotropic matrix and focused on the effect of the orientation angle. The configuration is represented by **Figure A.1.15** (A). The boundary element method (BEM) was used to simulate the diffusion process governed by Fick's law. The authors considered that the membrane becomes anisotropic in terms of diffusion due to the presence of fillers. Hence, the expression of the diffusion coefficient was associated to a flux in i -direction due to a concentration gradient in j -direction. They have adopted also the RVE strategy which consisted in determining the number of flakes, the aspect ratio and the width of excluded boundary strips. A new equation was introduced for the prediction of the diffusivity tensor which extends Lape's model (Lape et al., 2004) by using Bharadwaj's approach (Bharadwaj, 2001):

$$\frac{D_{eff}}{D_0} = \frac{1 - f}{\left[1 + \eta \frac{2}{3} \alpha f \frac{2}{3} \left(O + \frac{1}{2} \right) \right]^2} \quad (\text{A.1.54})$$

assuming that O is the orientational order introduced by Bharadwaj and η is an empirical coefficient which was introduced by Dondero et al. in order to improve the performance of their analytical model compared to the numerical results. Dondero's analytical model showed that the disorder in flake orientation had a significant impact on diffusivity in the direction parallel to the flakes orientation.

Chen (X. Chen & Papathanasiou, 2007) also studied the barrier performances of nanocomposites in which polydisperse fillers were randomly dispersed. The configuration adopted is represented in **Figure A.1.15** (B). The main results obtained for this configuration is that polydisperse flakes could have a greater impact on the relative effective diffusivity than

monodisperse flakes i.e. barrier properties are more enhanced in the polydisperse case. This conclusion validates Lape's and Cussler's analytical approaches.

A new work has been developed recently by Papathanasiou et al. (Tsiantis & Papathanasiou, 2019) studying the barrier properties in 2D nanocomposite systems of randomly oriented high aspect ratio fillers. Fillers geometry considered in their work is flakes having a very long length in the out-of-plane direction. Moreover, they have considered three different predictions of effective diffusivity expressions (arithmetic, harmonic and geometric averages) and associated for each a corresponding equation. They showed that, for fillers parallel to diffusion direction, the harmonic average is the most close to their computational work and relative effective diffusivity follows an asymptotic behavior when (αf) is high. Moreover, their model is in agreement in existing models in literature for different misalignment states going from unidirectional to random.

3D systems

Although 3D models are computationally intensive, the ability to analyze quite realistic configurations incited authors to build such models in order to study diffusion in randomly dispersed and oriented nanocomposites. To this purpose, Greco and Maffezzoli (Greco & Maffezzoli, 2015a) used the FEM approach and a geometrical representation based on the random distribution of small stacks composed of regularly spaced lamellae (**Figure A.1.16**). All stacks comprised the same number of lamellae. This work is a continuity of Greco's previous work in 2D.

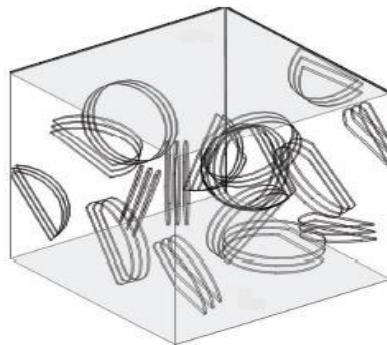


Figure A.1.16 Geometry proposed by Greco et al. (Greco & Maffezzoli, 2015a)

In addition to the effect of the structural parameters on diffusivity, the authors integrated in their model the effect of galleries thickness and orientation parameter, taking into account diffusion between stacks and around them. This work seems to be the first 3D approach to study diffusion inside galleries. The comparison of the results to those obtained from an analytical model such as Nazarenko and coworkers (Nazarenko et al., 2007) showed a good agreement. They introduced an alternative equation to express the normalized diffusivity:

$$D_{eff} = (1 - f) \cdot \left(1 + \left(\frac{4}{3\pi} \right) \left(\frac{1}{\sqrt{3}} \right) \left(1 - \frac{\sqrt{2}}{\sqrt{3}} \right) \left(\frac{f\alpha}{n} \right) \left(1 + \frac{6\sqrt{2}}{\pi} \right) \left(\frac{1}{\alpha_s} \right) \right)^{-4} \quad (\text{A.1.55})$$

where α_s is the stack aspect ratio, α the platelet aspect ratio, n is the number of platelets and f is the volume fraction of fillers.

Another step towards the improvement of the representativeness of numerical models consists in building a 3D geometry directly from the morphological and filler dispersion data obtained by TEM images. For instance, using this approach, Cerisuelo et al. (Cerisuelo, Gavara, & Hernández-Muñoz, 2015) have shown through FEM simulations a reduction in the effective diffusivity which was in agreement with previous works. They also studied the effect of the tortuosity and necking effects on diffusivity in nanocomposite materials. Cerisuelo and coworkers showed that in spite of possible size effect of diffusing molecules, which wasn't considered in their model, the results obtained seem to agree with previous analytical models and with experimental data. As well, they showed that filler particles are responsible for the reduction in the solute diffusivity, since they increase the distance of the diffusion path, reduce the crossing area, and, as a result, increase the resistance undergone by the solute when it is displaced through the spacing between adjacent particles in the same horizontal plane.

Table A.1.2 gives a concise overview of the numerical models discussed in this part, with respect to the considered filler shape, orientation, array, the model dimension and the simulation method they use. It also clarifies which type of methodology is related to each model as it specifies for each case if an analytical equation has been derived from numerical results, if an equation has been used to formulate the numerical model or if an analytical equation has been used to validate the numerical model, the details being discussed previously.

Table A.1.2 : Sum-up of numerical models discussed in the review

a) Equation derived from numerical results, **b)** Equation used to formulate the numerical model, **c)** Analytical equation used to validate the numerical model

Model	Filler type	Array/Orientation	Model dimension	Method	Equation
Minelli (Minelli, Baschetti, & Doghieri, 2009)	Platelets	regular array// homogeneous distribution	2D	FVM	a)
Falla (Falla et al., 1996)	Platelets	regular array// homogeneous distribution	2D	Monte Carlo	c)
Chen (X. Chen & Papathanasiou, 2007)	Rectangular flakes	regular array// homogeneous distribution	2D	BEM	c)
		Random array// homogeneous distribution			
		regular array// heterogeneous distribution			
Swannack (Swannack et al., 2005)	Rectangular flakes	Regular array// homogeneous distribution	2D	Monte Carlo	c)
Sridhar (L. N. Sridhar et al., 2006)	Platelets	Regular array// homogenous distribution	2D	FDM	b)
Statler (Jr & Gupta, 2007)	Platelets	Regular array// homogenous distribution	2D	FEM	b)
Minelli (Minelli et al., 2011)	Hexagonal, square, octagonal tablets and circular disks	Random array// homogenous distribution	2D	FVM	a)
Bhunja (Bhunja et al., 2012)	Platelets	Random array// homogeneous distribution	2D	FEM	c)
Tsiantis (Tsiantis & Papathanasiou, 2017)	Rectangular flakes	Random array// homogeneous distribution	2D	RSA algorithm	a)

Tsiantis (Tsiantis & Papathanasiou, 2019)	Rectangular flakes	Random array// homogeneous distribution	2D	RSA algorithm	a) c)
Greco (Greco, 2014a)	Rectangular platelets	Random array// heterogeneous distribution	2D	FEM	a)
Dondero (Dondero et al., 2016)	Rectangular flakes	Random array// heterogeneous distribution	2D	BEM	a)
Greco (Greco, 2014b)	Rectangular platelets with presence of galleries	Random array// heterogeneous distribution	2D	FEM	a)
Minelli (Minelli et al., 2011)	Hexagonal, squares, octagonal tablets and circular disks	regular array// homogeneous distribution	3D	FVM	c)
		Random array// homogeneous distribution			a)
Swannack (Swannack et al., 2005)	Rectangular flakes	regular array// homogeneous distribution	3D	Monte Carlo	c)
Goodyer (Goodyer & Bunge, 2007)	Ribbons, squares and hexagons	regular array// homogeneous distribution	3D	FEM	a)
Gusev (Gusev & Lusti, 2001)	Disks	Random array// homogeneous distribution	3D	FEM	b)
Greco (Greco & Maffezzoli, 2015a)	Permeable disks with presence of galleries	Random array// heterogeneous distribution	3D	FEM	a)
Cerisuelo (Cerisuelo et al., 2015)	TEM micrographs	Random array// heterogeneous distribution	3D	FEM	c)

1.5 Conclusion

The development of polymer-based nanocomposites for barrier applications requires a comprehensive understanding of the impact of their structure on gas diffusion. In the past

decades, this need has significantly stimulated the development of analytical and numerical modeling, either as complementary or alternative approaches to experimental ones. Analytical approaches led to the first models. They have been widely used and have permitted to establish the first relationships between gas barrier properties and the size, shape, content, dispersion and array of nanofillers. Although these approaches have undoubtedly enhanced the understanding of gas barrier properties and agree rather well with experimental data, they suffer from some limitations when considering complex structures. In this context, various numerical approaches using the most common and proven computational methods (the Monte Carlo method, the boundary element method, the finite volume method and the finite element method) have been developed. The finite element method has made possible to study more complex nanocomposite structures ranging from simple, regular 2D systems to randomly distributed 3D morphologies. It has also allowed to evidence and to discuss the effect of additional parameters in comparison with the analytical models such as necking effects, flake-flake interactions, possibility for the gas to diffuse in the interspace gallery between platelets in filler stacks as some examples. Some recent developments have shown the definite potential of the FEM-based approach in modeling the behavior of a real sample on the basis of representing the actual sample morphology acquired by transmission electron microscopy.

Chapter 2 3D Mass Diffusion in Ordered Nanocomposite Systems: Finite Element Simulation and Phenomenological Modeling

An overview of the chapter

It has been shown through the extensive state of art presented in 0that barrier properties of nanocomposite systems are strongly related to the structural parameters of fillers, their dispersion and distribution in the polymer matrix. Indeed; various nanofiller natures, shapes and loading fractions have been experimentally considered and a wide range of barrier materials has been obtained. Concurrently, several numerical approaches have been developed to model gas diffusion properties of nanocomposite materials. However, these approaches often considered bi-dimensional systems, which can be inaccurate for certain filler. The aim of the present chapter is to develop a 3D finite element model in order to predict to predict the gas barrier properties of ordered nanocomposites with disk-shaped nano-fillers, valid in diluted, semi-diluted and concentrated regimes. An analytical equation describing barrier properties of such systems has been also derived from phenomenological considerations and numerical simulation results.

2.1 Introduction

Problems involving gas diffusion arise today in a large range of fields such as food preservation, medicinal products packaging (X. Li et al., 2016), solar cell protective coatings (Kausar, 2018; Yu, Yang, Chen, Tao, & Liu, 2016), fuel cell membranes (Magana et al., 2015; Makinouchi, Tanaka, & Kawakami, 2017; Yamazaki & Kawakami, 2010), fuel and gas transportation (Deveci, Oksuz, Birtane, & Oner, 2016; Klopffer, Berne, & Espuche, 2015), as a few. Most of these domains need materials that combine low cost, easy processing, long-term flexibility and barrier properties. Although polymers exhibit appropriate cost, processing and mechanical properties, they cannot meet alone the ever increasing level of barrier properties required by the applications. Impermeable fillers are then dispersed within the host polymer matrix to increase the gas diffusion path length by a tortuosity effect (Barrer, 1968; Bruggeman, 1935; Cussler et al., 1988; Nielsen, 1967). Among the wide range of available impermeable fillers, nanometer thick lamellar fillers such as montmorillonite, graphene, double hydroxide layer, zirconium phosphate platelets, etc. are chosen due to their high aspect ratio (Dal Pont, Gérard, & Espuche, 2013; Follain et al., 2016; Jia, Ma, Gao, & Lv, 2018; X. Li, Bandyopadhyay, Nguyen, Park, & Lee, 2018; Picard, Vermogen, et al., 2007; Sun, Boo, Clearfield, Sue, & Pham, 2008; Wolf et al., 2018). Most of the experimental studies and analytical modeling approaches based on nanocomposites agree with the fact that lamellar fillers have to be placed perpendicular to the gas flow to maximize the tortuosity effect and therefore increase the barrier properties (Bharadwaj, 2001; Cussler et al., 1988; Gusev & Lusti, 2001; Nielsen, 1967; Picard, Vermogen, et al., 2007). In this context, analytical modeling approaches have investigated the effects of filler content (f) and aspect ratio (α) (Bouma et al., 1997; Nielsen, 1967). The fillers are most often represented as regularly dispersed ribbons of infinite length. Moreover, the penetrant trajectory is considered as a one dimensional path in a dilute regime ($\alpha f \ll 1$) (Fredrickson & Bicerano, 1999). With the development of high performance numerical tools such as finite element modeling (FEM) (Crisuolo et al., 2015; Gusev & Lusti, 2001) or boundary element method (BEM) (X. Chen & Papathanasiou, 2007; Dondero et al., 2016), detailed modeling of more realistic nanocomposite structures has become possible and several numerical approaches have focused on diffusion in nanocomposites with homogeneous distribution of nanofillers oriented perpendicular to the diffusion direction (Goodyer & Bunge, 2007; Minelli et al., 2009, 2011; Swannack et al., 2005). It is noteworthy that although most of these numerical models have considered the studied systems as two-dimensional ones, only few of them have taken into

account the three-dimensional aspect of the studied materials. The main objective of these 3D models has been to investigate the effects of different filler shapes (hexagonal tablets, square tablets, octagonal tablets and circular disks) and to compare the obtained results with those derived by 2D or analytical approaches. It has been shown that 2D simulations generally predict a lower effective diffusivity than the 3D simulations (Swannack et al., 2005). Indeed, for a given filler volume fraction, a truly 3D geometry (platelets with finite extension) allows a more important permeation than a 2D geometry (platelets with infinite extension) and thus leads to a higher effective diffusivity value. One interest of the numerical modeling approach is that it permits quite easily to extent the studies to semi-diluted regimes.

Specifically, the aim of this work is to build a 3D numerical model using the finite element method in order to predict gas barrier properties in nanocomposite systems where fillers, considered as disks, are distributed regularly and uniformly in a unit cell. The specificity of the model is its validity for a wide range of fillers volume fractions and aspect ratios, allowing to go from diluted regime ($\alpha f < 1$) to semi-diluted and concentrated regime as α values up to 25 were considered. Moreover, the analysis of the numerical simulation results obtained for all the systems considered in this work allowed to clearly evidence the governing role of a particular geometrical parameter. Accordingly, a phenomenological analytical model was derived, aiming to predict gas barrier properties of nanocomposites as a function of the parameters describing the fillers shape and their spatial distribution. Comparison with FEM simulation results showed an excellently good agreement.

2.2 Finite Element Simulations

2.2.1 Geometrical model

The nanocomposite systems considered in this work consist in a polymer matrix homogeneously filled with disk-shaped impermeable nanofillers (**Figure A.2.1**). This simple filler shape can be considered as representative of platelet-like fillers and has already been used by several authors to investigate the gas transport properties of nanocomposites from analytical or numerical approaches. The volume fraction of nanofillers f , chosen in the range 0 – 10%, is a parameter of the geometrical model. The disk thickness values e have been chosen in the range 0.6 nm - 2 nm to match the typical thickness values of the elementary platelets for the most common lamellar nanofiller types (Charifou, Gouanvé, Fulchiron, & Espuche, 2015; Dal Pont et al., 2013). The disk diameter D was varied between 100 nm and 500 nm. Finally, couples of (e, D) values were considered to cover filler aspect ratio values $\alpha = D/e$ ranging from 50 to 250. All disks are oriented perpendicular to the overall diffusion direction z . The

fillers are dispersed in the matrix in an ordered arrangement consisting in a superposition of odd and even layers. Though the even layers are identical (in nature and arrangement) to the odd layers, they are shifted by distances s_x and s_y , in the x and y directions respectively, with respect to the odd layers. Within a given layer, the fillers are arranged according to an orthogonal grid. The distances separating the centers of two adjacent fillers (or in-plane space steps) in the x and y directions are respectively p_x and p_y . The in-plane distribution of the fillers is assumed to be isotropic, *i.e.* $p_x = p_y$. The space step in the diffusion direction (or thickness-wise direction) p_z is defined as the interlayer distance from center to center (as specified for p_x and p_y). In order to further analyze the results in terms of dimensionless parameters, a scaled space-step $\beta = p_z/D$ is defined. The representative volume element (RVE) of such a two-phase ordered periodic system is the simplest repeating unit in the system, as shown on **Figure A.2.1**. It consists of a parallelepipedic volume whose vertices coincide with the centers of the eight nearest neighboring odd layer disks. The middle layer corresponds to the even disks. It should be noted that this unit cell contains one net odd layer disk ($8 \times 1/8$ disk) and one net even layer disk. By definition, the unit cell is invariant by translation along x , y and z by a distance equal to any integer multiple of p_x , p_y and p_z respectively.

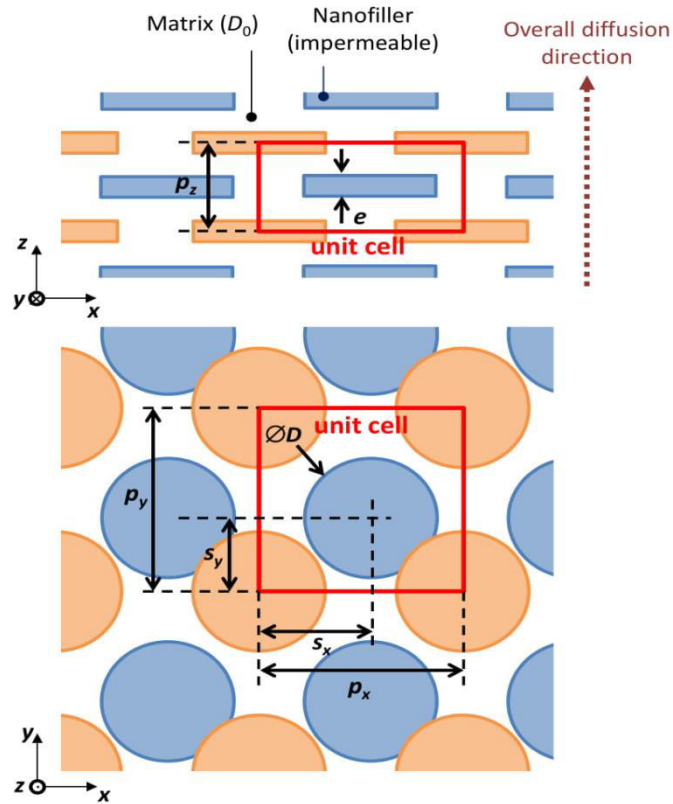


Figure A.2.1 Geometrical model of the ordered nanocomposite and definition of the unit cell (thickness-wise and plane-wise projections)

Considering the unit cell, the filler volume fraction is the ratio of the volume occupied by fillers (two net disks) to the total volume of the unit cell, which reads:

$$f = \frac{\pi D^2 e}{2p_x p_y p_z} \quad (\text{A.2.1})$$

Hence, the in-plane space step p_x can be expressed solely as a function of the geometrical parameters of the system:

$$p_x = \left(\frac{\pi D^2 e}{2f p_z} \right)^{1/2} \quad (\text{A.2.2})$$

In other words, the in-plane dimensions p_x and p_y of the unit cell are completely determined by the given filler dimensions D and e , volume fraction f and thickness-wise space step p_z . Using appropriate boundary conditions, the unit cell constitutes a relevant computational domain for solving the governing equation of the diffusion mass transfer process in the repeating structure.

2.2.2 Governing equation and boundary conditions

Mass transfer in the nanocomposite is assumed to follow Fick's second law of diffusion, which can be expressed, in the absence of mass source and in stationary regime, by the partial differential equation:

$$\nabla \cdot (-D_{ij} \vec{\nabla} c_i) = 0 \quad (\text{A.2.3})$$

where c_i is the molar concentration of the permeating specie i and D_{ij} is the mass diffusion coefficient (or diffusivity) of permeating specie i in medium j . In the present case, diffusion is assumed to occur only in the matrix phase and the diffusivity of the considered specie in the matrix phase is denoted by D_0 . In the numerical simulation, a constant value $D_0 = 10^{-12} \text{ m}^2 \cdot \text{s}^{-1}$ has been used. It is a representative value of the diffusion of gases in polymers. In the following, the variable associated with the molar concentration of the permeating specie at any point of the computational domain (*i.e.* the concentration field) is denoted by $c(x, y, z)$.

In order to obtain a well-posed boundary value problem, Fick's PDE was solved together with the following boundary conditions:

- concentration boundary conditions were imposed on the lower ($z = 0$) and upper ($z = p_z$) faces of the unit cell, respectively $c(x, y, 0) = c_1 = 1000 \text{ mol} \cdot \text{m}^{-3}$ and $c(x, y, p_z) =$

$c_2 = 500 \text{ mol.m}^{-3}$. In this work, the matrix diffusivity is assumed constant and not concentration-dependent, meaning that the concentration values chosen as boundary conditions for the upper and lower faces have rigorously no influence on the effective diffusivity calculated in this work;

- periodic boundary conditions were imposed on the side boundaries of the unit cell in order to set up a constraint that makes any quantity equal on the so-called “source” and “destination” boundaries. Thus, the periodic boundary condition allows simulating an infinite repetitive structure based on the explicit modeling of the unit cell representing this structure;
- no-flux boundary conditions were imposed on all filler-matrix interfaces in order to model the impermeability of the fillers.

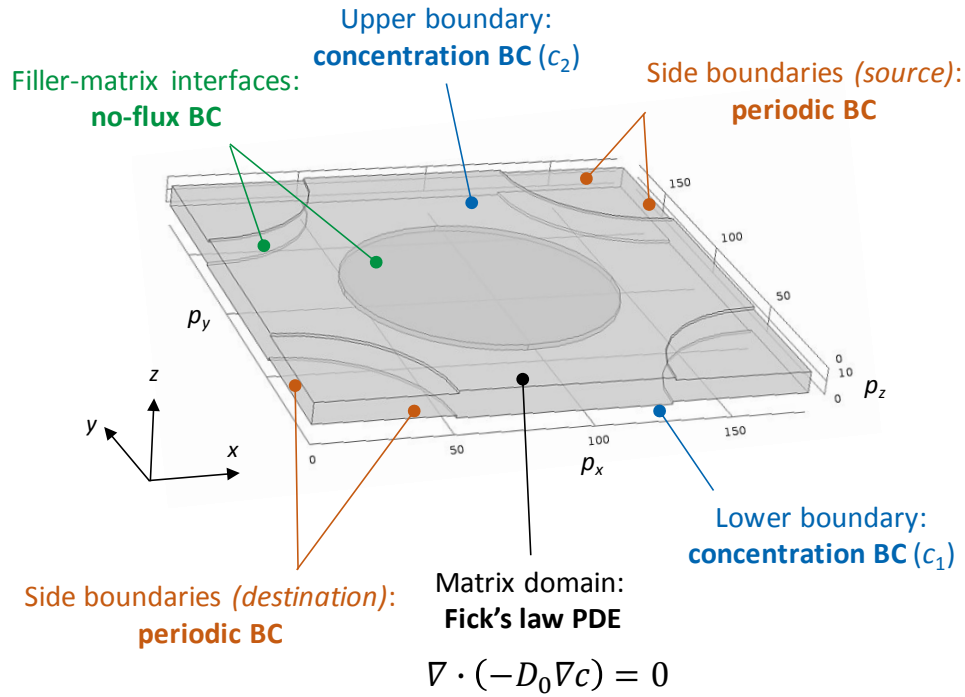


Figure A.2.2 - Tridimensional representation of the unit cell showing the boundary conditions

2.2.3 Numerical solution and effective diffusivity evaluation

The boundary value problem is solved by the finite element method using the commercial package COMSOL Multiphysics. The FEM requires proper discretization (or meshing) of the computational domain in order for the numerical solver to provide accurate and stable results. Since the fillers are assumed impermeable, only the matrix phase domain needs to be meshed. An unstructured mesh consisting in tetrahedral elements was generated (**Figure A.2.3**) and

refined sufficiently to ensure obtaining a mesh-independent solution, meaning that the results are not affected by any numerical artifact arising from the discretization method.

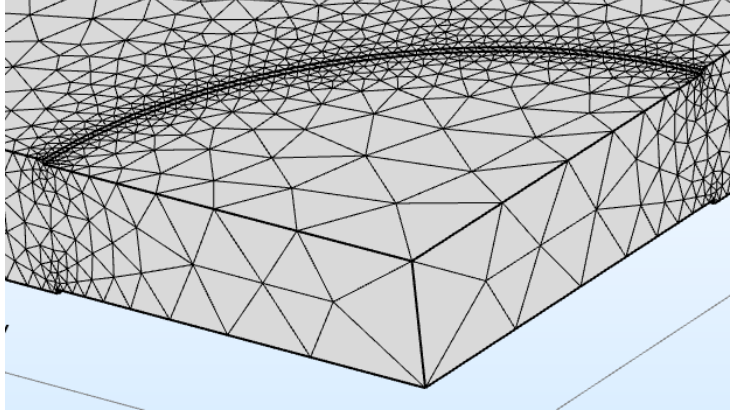


Figure A.2.3 - Tetrahedral mesh used to discretize the computational domain

The solution of the boundary value problem yields the molar concentration field of the permeating specie $c(x, y, z)$. Then, the mass flux vector field of the permeating specie can be calculated from the concentration field:

$$\vec{N}(x, y, z) = -D_0 \vec{\nabla} c(x, y, z) \quad (\text{A.2.4})$$

The effective diffusivity of the nanocomposite is finally given by:

$$D_{eff} = \frac{\overline{N_z} p_z}{c_1 - c_2} \quad (\text{A.2.5})$$

where $\overline{N_z}$ is the average mass flux of the permeating specie across a plane section S normal to z -direction and located at $z = z_0$ within the unit cell:

$$\overline{N_z} = \frac{1}{p_x p_y} \iint_S N_z(x, y, z_0) dx dy \quad (\text{A.2.6})$$

with N_z the z -component of the mass flux vector. It should be noted the mass conservation principle and the periodic boundary conditions ensure that the average mass flux is the same in any plane section. Hence, z_0 could be indifferently any value chosen between 0 and p_z . In the present work, the mass flux surface integral was evaluated on the upper face of the unit cell (*i.e.* $z_0 = p_z$).

2.3 Results and discussion

Previous analytical models (Cussler et al., 1988; Nielsen, 1967) and experimental results (O. C. Compton et al., 2010; Hotta & Paul, 2004; Thomas P & Thomas, 2012) showed that

diffusivity in nanocomposites is highly dependent on nanofillers aspect ratio and volume fraction values. The effect of these parameters on the relative effective diffusivity was investigated by varying the parameter β between 0.00585 and 0.1, for several filler aspect ratios ranging from $\alpha = 50$ ($D = 100$ nm, $e = 2$ nm) to $\alpha = 250$ ($D = 171$ nm, $e = 0.684$ nm). The middle layer filler is assumed to be centered within the unit cell ($s_x = p_x/2$, $s_y = p_y/2$), as shown on **Figure A.2.4**. Hence, the filler volume fraction f varied in the range 0 - 10% for each aspect ratio value. The most convenient quantity to characterize and compare the enhancement of barrier properties in different filled systems is the relative effective diffusivity, defined as the ratio of the nanocomposite effective diffusivity to the neat matrix diffusivity: D_{eff}/D_0 . As expected, improvement of barrier properties is observed when the filler volume fraction increases for a given value of filler aspect ratio. Likewise, for a given volume fraction, the higher the filler aspect ratio, the better the barrier effect. Similar trends were observed by Minelli and coworkers (Minelli et al., 2009) who built a two-dimensional model using an algorithm based on the finite volume method.

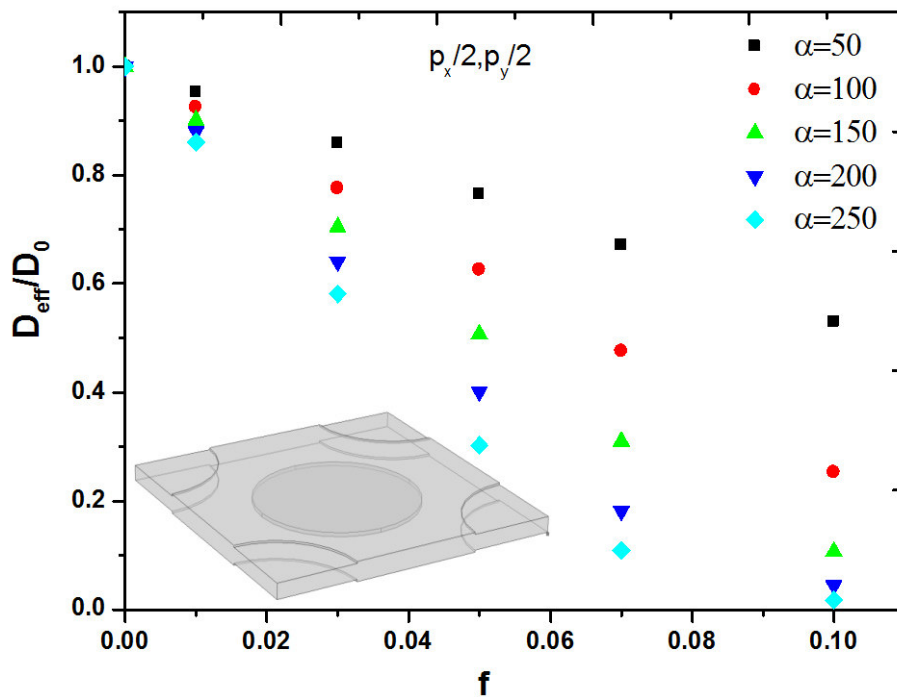


Figure A.2.4 – FEM-calculated relative effective diffusivity versus filler volume fraction in ordered nanocomposite systems for different filler aspect ratio values

As a further analysis of the obtained results, the effect of the number of unit cells on the overall diffusivity has been investigated and the obtained results are presented in **Figure A.2.5**.

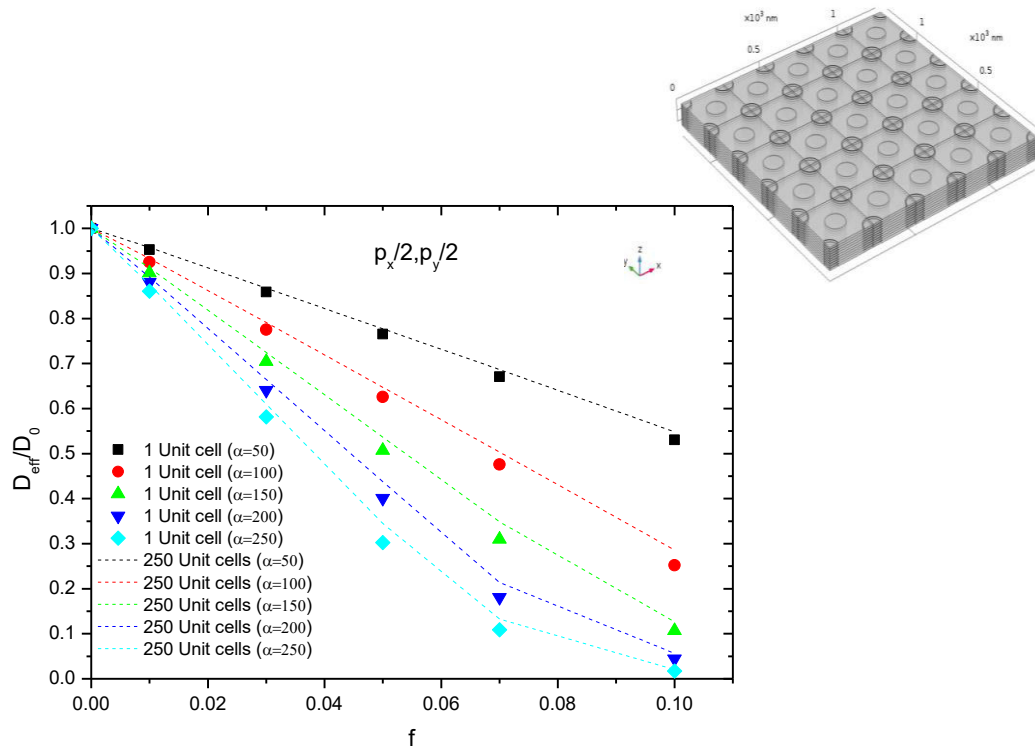


Figure A.2.5 The effect of the number of unit cells on the overall diffusivity for different filler volume fraction and aspect ratio values

As it can be observed, 250 unit cells have been considered and the corresponding numerical results were compared to those corresponding to a unique unit cell. The results show that the size of the simulation domain (the number of unit cells) doesn't have a significant effect on the overall diffusivity of the considered system.

The decrease of diffusivity in nanocomposites constituted of impermeable fillers has been explained by a tortuosity effect that is enhanced as the aspect ratio and volume content of fillers increase (Espuche, 2011). Several analytical models such as the Gusev and Lusti model (Gusev & Lusti, 2001), the Fredrickson and Bicerano model (Fredrickson & Bicerano, 1999) and the modified-Cussler model (Cussler et al., 1988) already investigated the effect of impermeable disks on the diffusion properties of a polymer nanocomposite system. In these approaches, a random dispersion of nanofillers was considered. **Figure A.2.6** (a to c) compares the predictions of the different models with the present FEM simulation results for three values of α : 20, 50 and 100.

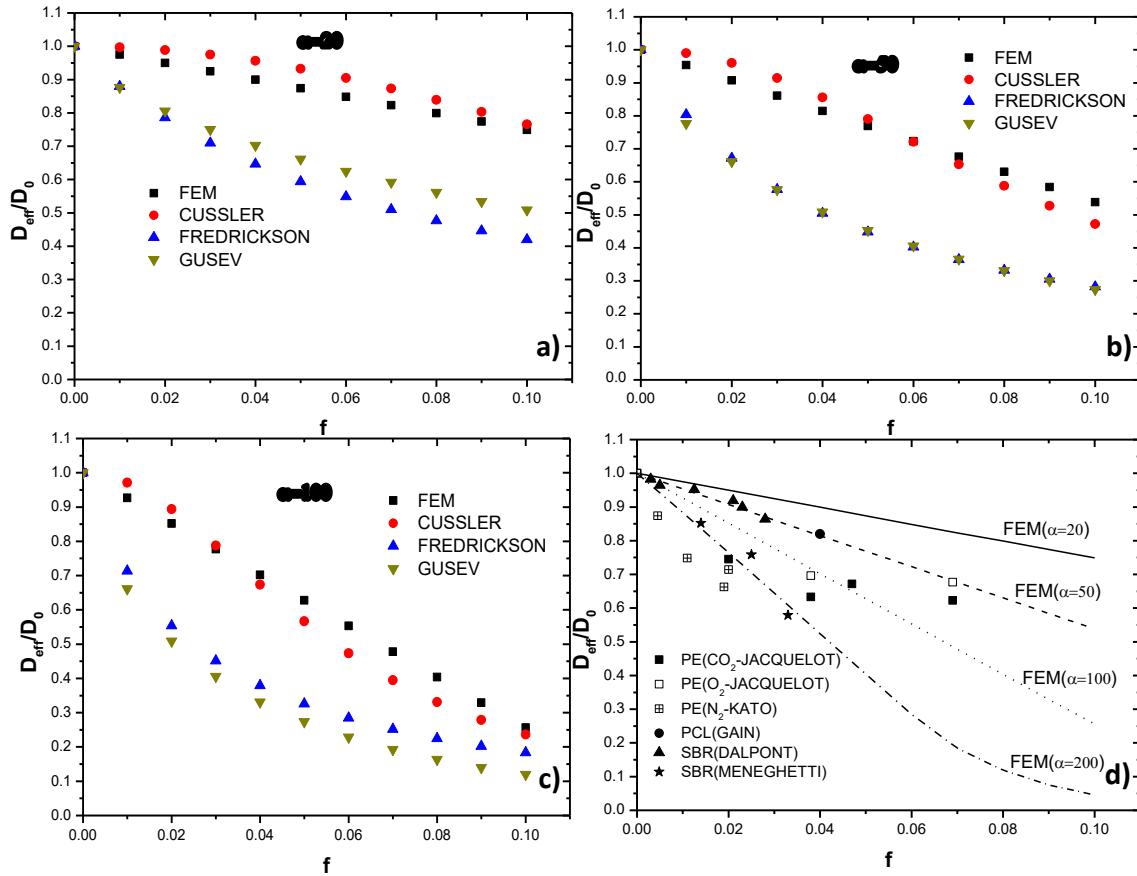


Figure A.2.6 Comparison of numerical results to Cussler, Fredrickson and Gusev models for different values of disks aspect ratio **a)** $\alpha=20$, **b)** $\alpha=50$ and **c)** $\alpha=100$ and **d)** to literature experimental results (Dal Pont, 2011; Dal Pont et al., 2013; Gain et al., 2005; Jacquelot et al., 2006; Kato, Okamoto, Hasegawa, Tsukigase, & Usuki, 2003; Meneghetti, Shaikh, Qutubuddin, & Nazarenko, 2008)

The FEM results show good agreement with Cussler's predictions for different values of disks aspect ratio and for disks volume fraction ranging between 1% and 10%. Nevertheless, a slight deviation is observable and may be related to different filler distributions. Furthermore, the Fredrickson model and the Gusev models yield similar trends for the decrease of the relative effective diffusivity values. One should remember that those models were derived based on some approximations (dilute and semi-dilute regime in the Fredrickson model for example) which could explain the observed deviations. The difference between the four models is slightly reduced for high values of disk volume fraction and aspect ratio. Moreover, our numerical results were compared in **Figure A.2.6 d)** to experimental data covering a wide range of nanocomposite materials (going from PE to PCL and rubber matrices and montmorillonite to ZrP nanofillers) (Dal Pont, 2011; Dal Pont et al., 2013; Gain et al., 2005; Jacquelot et al., 2006; Kato et al., 2003; Meneghetti et al., 2008). It should be noticed that

FEM results are fitting well with Dal Pont et al. results (Dal Pont et al., 2013) for fillers aspect ratio 50. The experimental results obtained by Meneghetti et al. (Meneghetti et al., 2008) and Kato et al. (Kato et al., 2003) can be accurately described by our FEM approach considering a filler aspect ratio close to 200. Finally the comparison between the experimental results obtained by Jacquelot et al. (Jacquelot et al., 2006) and our FEM approach suggests that filler stacks are formed as the filler amount increases, this trend being largely observed in the literature (Picard, Vermogen, et al., 2007). Indeed, a filler aspect ratio value near to 100 allows to describe the experimental data for a filler volume fraction around 0.04 whereas it decreases down to 50 when the filler volume amount increases up to 0.07.

2.3.1 The projected area ratio as a governing parameter

The simulation results presented in **Figure A.2.6** have shown that in addition to the filler volume fraction, the filler aspect ratio has quite a significant effect on the diffusion properties of the nanocomposite. Hence, it can be suggested that a single parameter encompassing the effects of both geometrical quantities may govern the relationship between the structural arrangement of the ordered nanocomposite and its diffusion properties. More specifically, in this work, it is postulated that the relative effective diffusivity of the nanocomposite is strongly correlated to the probability that a molecule entering the unit cell at the lower boundary can diffuse to the upper boundary according to a path strictly parallel to the z direction, without being deflected by the presence of impermeable filler. This probability can be related to the projected area ratio k , defined as:

$$k = \frac{S_{matrix}}{S_{tot}} \quad (\text{A.2.7})$$

where S_{tot} is the total projected area of the unit cell on a plane normal to the diffusion direction z :

$$S_{tot} = p_x p_y \quad (\text{A.2.8})$$

and S_{matrix} is the projected area of the matrix phase on a plane normal to the diffusion direction z , as shown on **Figure A.2.7**. Indeed, a molecule entering the unit cell inside the contour of the S_{matrix} area has a non-zero probability of diffusing strictly parallel to the z direction, and the farther from the contour the molecule enters, the closer to 1 this probability.

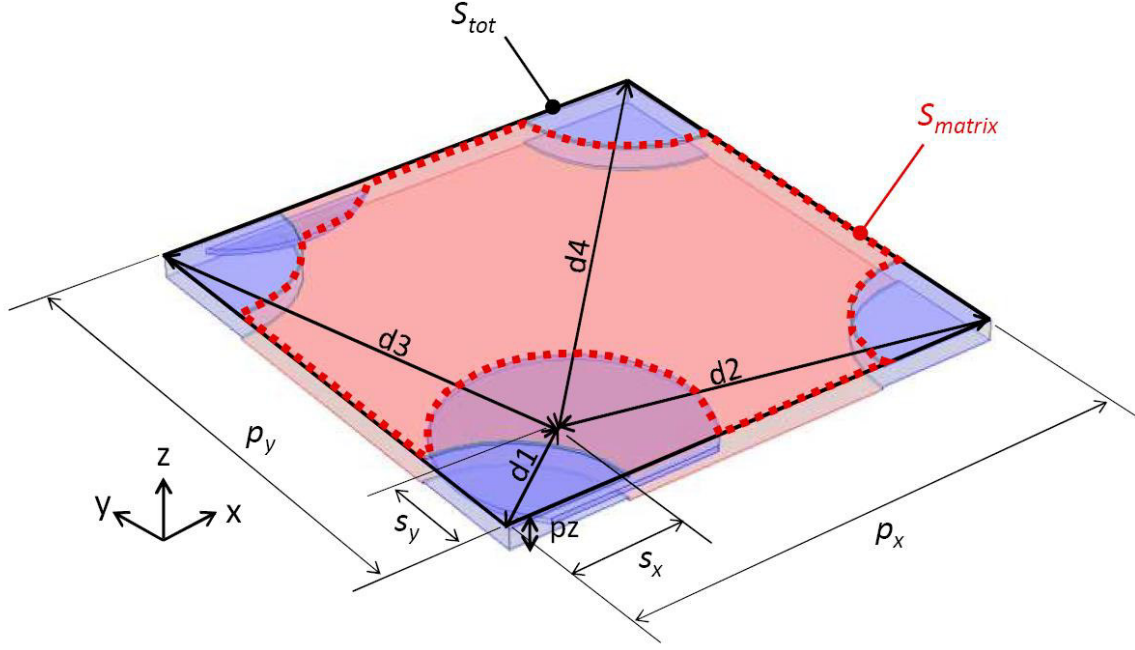


Figure A.2.7 - Definition of the total projected area S_{tot} and matrix projected area S_{matrix} on a plane normal to the diffusion direction (*i.e.* x - y plane) for a unit cell

S_{matrix} is equal to the total projected area of the unit cell, from which is subtracted the projected area of the fillers (area of two net disks in a unit cell) minus the overlapping projected area:

$$S_{matrix} = S_{tot} - (2S_{disk} - S_{overlap}) \quad (\text{A.2.9})$$

where

$$S_{disk} = \frac{\pi D^2}{4} \quad (\text{A.2.10})$$

The overlapping projected area is composed of the individual overlapping areas S_i of the middle layer disk with each one of the four disks located in the corners of the unit cell:

$$S_{overlap} = \sum_{i=1}^4 S_i \quad (\text{A.2.11})$$

The intersection area S_i of two disks of same diameter D whose centers are located at a distance d_i from each other is given by:

$$\begin{cases} S_i = \frac{1}{2} \left[D^2 \cos^{-1} \left(\frac{d_i}{D} \right) - d_i \sqrt{D^2 - d_i^2} \right] & \text{if } d_i < D \\ S_i = 0 & \text{if } d_i \geq D \end{cases} \quad (\text{A.2.12})$$

where the distances d_i (represented on **Figure A.2.7**) are calculated as:

$$\left\{ \begin{array}{l} d_1 = \sqrt{s_x^2 + s_y^2} \\ d_2 = \sqrt{(p_x - s_x)^2 + s_y^2} \\ d_3 = \sqrt{s_x^2 + (p_y - s_y)^2} \\ d_4 = \sqrt{(p_x - s_x)^2 + (p_y - s_y)^2} \end{array} \right. \quad (\text{A.2.13})$$

Assuming that $p_x = p_y = p_p$ (*i.e.* the filler spacing in each nanocomposite layer is isotropic in both in-plane directions x and y), the projected area ratio is expressed as:

$$k = \frac{p_p^2 - \frac{\pi D^2}{2} + \sum_{i=1}^4 S_i}{p_p^2} \quad (\text{A.2.14})$$

Recalling the expression of the filler volume fraction f (Eq. (A.2.1)), the in-plane dimension of the unit cell p_p can be written as:

$$p_p = D \sqrt{\frac{\pi e}{2f p_z}} \quad (\text{A.2.15})$$

Inserting Eq. (A.2.15) into Eq. (A.2.14), the k ratio finally reads:

$$k = 1 - \alpha \beta f \left(1 - \frac{2}{\pi D^2} \sum_{i=1}^4 S_i \right) \quad (\text{A.2.16})$$

One should note that if there is no overlapping of the filler layers, Eq. (A.2.16) reduces to:

$$k = 1 - \alpha \beta f \quad (\text{A.2.17})$$

The effect of the k ratio on the effective relative diffusivity was investigated at first on a unit cell configuration with a centered position of the middle layer disk (*i.e.* $s_x = s_y = p_p/2$). In order to allow matching a volume fraction range of 1% to 10%, the dimensionless space step β was varied between 0.05 and 1. For each β value, the k ratio was then changed by modifying the filler volume fraction f . For each studied configuration, the relative effective diffusivity D_{eff}/D_0 was evaluated from the FEM calculation results (Eq. (A.2.5)) and plotted against the corresponding k ratio value (**Figure A.2.8**).

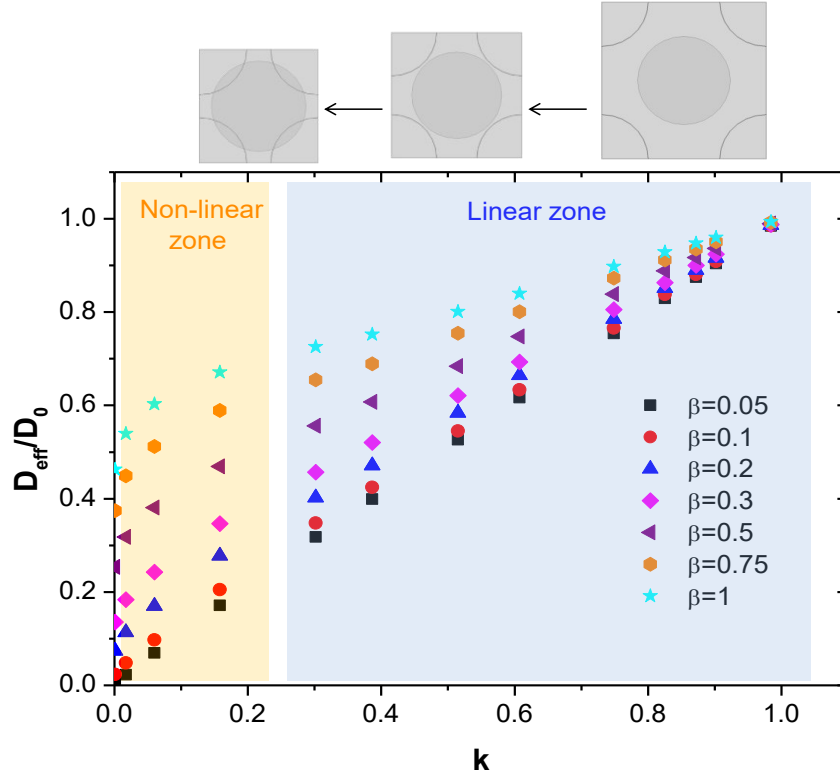


Figure A.2.8 - Relative effective diffusivity versus the projected area ratio k for several values of parameter β (centered position of the middle-layer disk)

As the k ratio decreases from 1 to 0, the obtained plots exhibit two distinct sections, or regimes. First, for k ratio values over around 0.25, the relative effective diffusivity decreases linearly with decreasing k . Since there is no overlapping of the fillers, the effect of the free diffusion section (quantified by the projected area of the matrix phase) governs the effective diffusivity, whereas tortuosity effects are not predominant. However, the smaller the parameter β , the faster the effective diffusivity decrease, meaning that tortuosity effects are more sensitive for closely superposed filler layers. Then, for k values below around 0.25, the correlation is no longer linear, but a concave-shaped curvature is evidenced in the lower end of the k range. In other words, the effective diffusivity decreases faster and faster as the free diffusion section reduces and overlapping increases (as shown on the unit cell representations on top of **Figure A.2.8**). In this case, the presence of overlapping disks forces more molecules to deflect their diffusion path, inducing more significant second order tortuosity effects. In the present configuration of the unit cell (centered middle layer), it can be shown that overlapping occurs for disk diameter values superior to $p_p/\sqrt{2}$, hence for k ratio values inferior to:

$$k_{lim} = 1 - \frac{\pi}{4} \cong 0.215 \quad (\text{A.2.18})$$

This theoretical value is quite consistent with the value discriminating the two regimes observed on the plot of **Figure A.2.8**.

As expected, as the k ratio tends to unity (*i.e.* unfilled matrix), the relative effective diffusivity also tends to unity. On the other hand, as the k ratio approaches zero, (*i.e.* maximum overlapping) the relative effective diffusivity reaches a minimum value. Besides, for a fixed disk diameter value, the smaller the parameter β , the closer to zero that minimum value, which can be explained by the increasing tortuosity and the decreasing diffusion section as the filler layers are positioned closer to one another. One should note that in the limiting case of contacting filler layers (minimum β value), the relative effective diffusivity is rigorously equal to the k ratio: the diffusing molecules cannot circumvent the fillers, they can only diffuse in the matrix zones where there is no overlapping. These observations are of major importance since the correlation equation developed further in this work must be consistent with these limiting cases.

The effect of the k ratio on effective diffusivity can also be investigated in the case of a unit cell with an off-centered (or shifted) middle layer. Using a similar simulation methodology, the evolution of the relative effective diffusivity values versus k has been plotted for comparison in **Figure A.2.9**, for three different positions of the middle-layer disk and three β values (0.2, 0.5 and 1).

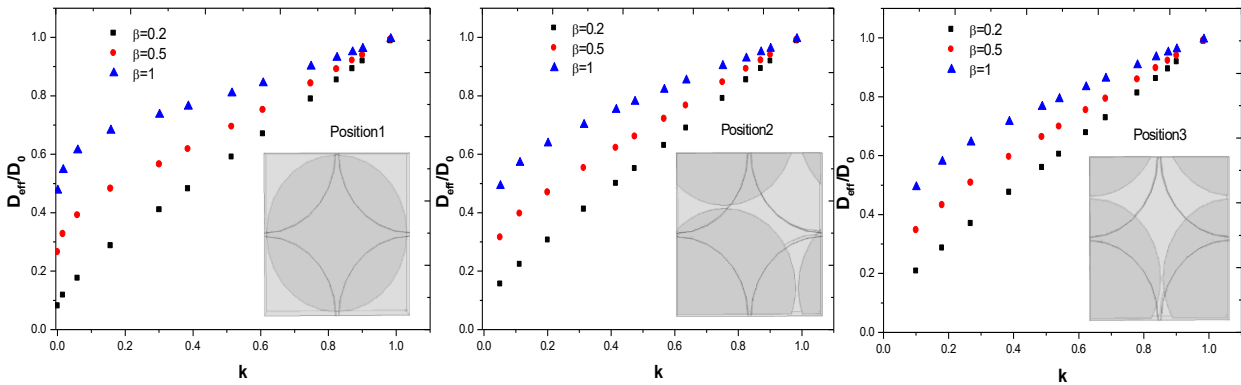


Figure A.2.9 - Relative effective diffusivity versus the projected area ratio k for different β values

In these example configurations, the middle-layer disk position was changed by modifying the values of the shift parameters in the x and y directions, s_x and s_y . The first position corresponds to the previously discussed “centered” configuration: $s_x = s_y = p_p/2$. The second position is obtained with $s_x = p_p/3$ and $s_y = p_p/6$ and the third position with $s_x = p_p/50$ and $s_y =$

$p_p/4$. It should be mentioned here that for the sake of simplicity, the disks dimensions were kept constant and the various k values were obtained by varying the in-plane space step size p_p values. However, the same study could be carried out for different disk dimensions without fundamentally changing the conclusions.

These plots exhibit the same curve shape: almost linear for small β values, linear to nonlinear regime transition for larger β values, the nonlinearity being all the more pronounced as the β value is larger. One can note that the more the middle layer position deviates from the so-called centered position, the more the regime transition is shifted towards larger k values (approximately $k = 0.3$ for position 2 and $k = 0.45$ for position 3). Indeed, overlapping is likely to occur for smaller filler volume fraction, *i.e.* larger k ratio, when the middle layer disk is significantly off-center.

Eventually, the plots presented in **Figure A.2.8** and **Figure A.2.9** clearly show that diffusivity reduction is affected by the increasing values of β and predominantly governed by the k ratio. Based on these numerical simulation results, the following section is devoted to the development and identification of an analytical equation correlating the relative effective diffusivity variation to the full range of k values. Then, the obtained model will be validated against FEM simulation results on a broader range of unit cell configurations.

2.3.2 Phenomenological modeling

2.3.2.1 Model derivation

At the first order, as shown by the plots of the numerical simulation results, the relationship between the relative effective diffusivity and the k ratio is assumed to follow a linear regime. Hence, it can be represented by the affine equation:

$$\frac{D_{eff}}{D_0} = ak + b \quad (\text{A.2.19})$$

where a and b are respectively the slope and the intercept (*i.e.* the limit value of the relative effective diffusivity as k tends to zero) of the affine line. However, as demonstrated by **Figure A.2.8** the relative effective diffusivity also depends on the thickness-wise space step parameter β . Plotting the values of the obtained slope a against the corresponding β values (**Figure A.2.10**) leads to a decreasing exponential relationship, which can be expressed in the following way:

$$a = a_0 \exp(-\beta) \quad (\text{A.2.20})$$

where a_0 is the scaling constant of the exponential decay. Inserting Eq. (A.2.20) into Eq. (A.2.19):

$$\frac{D_{eff}}{D_0} = a_0 \exp(-\beta) k + b \quad (\text{A.2.21})$$

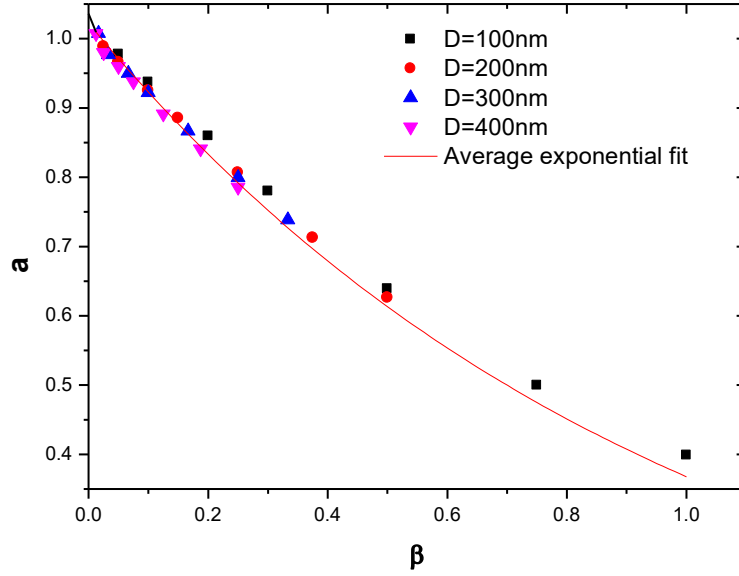


Figure A.2.10 - Exponential variation of the slope parameter a versus β

In order to find the b constant, the limiting case $k = 1$ (*i.e.* unfilled matrix) has to be considered. Obviously, in this case, the effective diffusivity is that of the matrix: $D_{eff}/D_0 = 1$. Hence,

$$b = 1 - a_0 \exp(-\beta) \quad (\text{A.2.22})$$

which leads to:

$$\frac{D_{eff}}{D_0} = 1 - (1 - k) a_0 \exp(-\beta) \quad (\text{A.2.23})$$

The opposite limiting case is $k \rightarrow 0$ (*i.e.* maximum overlapping, the matrix phase projected area is zero). If in addition the filler layers are in contact ($\beta = \beta_{min} = 2/\alpha$), then no diffusion is possible and $D_{eff}/D_0 = 0$. This yields:

$$0 = 1 - a_0 \exp\left(-\frac{2}{\alpha}\right) \quad (\text{A.2.24})$$

then a_0 can be written as:

$$a_0 = \exp\left(\frac{2}{\alpha}\right) \quad (\text{A.2.25})$$

Inserting Eq. (A.2.25) into Eq. (A.2.23), the expression of the relative effective diffusivity finally reads:

$$\frac{D_{eff}}{D_0} = 1 - (1 - k) \exp\left(-\left(\beta - \frac{2}{\alpha}\right)\right) \quad (\text{A.2.26})$$

One should note that the present linear model does not contain any adjustable parameter and has a clear physical meaning:

- the diffusion barrier effect induced by the increase of the filler projected area (represented by the quantity $(1 - k)$) decays exponentially with the distance between the successive layers in the z -direction, as this corresponds to a decrease in tortuosity;
- the diffusion barrier effect induced by the increase of the filler projected area is enhanced for larger filler diameters, as this leads to a longer diffusion path and an increase in tortuosity.

Moreover, for the limiting case $\beta = 2/\alpha$ (contacting layers), the equation indeed yields a proportionality relationship:

$$\frac{D_{eff}}{D_0} = k \quad (\text{A.2.27})$$

which is consistent with the behavior observed in **Figure A.2.8**.

However, the linear model becomes less accurate as the k values get lower, due to the overlapping effects increasing the tortuosity of the system: in the low k range, the linear model tends to overestimate the effective diffusivity. Hence, a supplementary term δ has to be subtracted from Eq. (A.2.27) in order to correct the D_{eff}/D_0 values in the low k range:

$$\delta = \left[1 - \exp\left(-\left(\beta - \frac{2}{\alpha}\right)\right)\right] \cdot A \cdot \exp\left(-\frac{k}{B}\right) \quad (\text{A.2.28})$$

The first factor $1 - \exp\left(-\left(\beta - \frac{2}{\alpha}\right)\right)$ ensures that δ vanishes if $\beta = \beta_{min} = 2/\alpha$ and that δ is maximum if β is very large. Indeed, as shown by **Figure A.2.9**, the deviation between the linear regime and the non-linear regime increases with β . A is a pre-exponential scaling parameter to be determined by fitting the numerical simulation results. The value $A = 0.27$ has been found to provide good agreement with the numerical data. Finally, the second

exponential factor $\exp\left(-\frac{k}{B}\right)$ ensures that the value of δ asymptotically tends to zero as k tends to unity. Hence, B is an exponential decay constant that can be approximated as:

$$B \approx \frac{k_{lim}}{5} \quad (\text{A.2.29})$$

recalling that any quantity undergoing exponential decay virtually vanishes when the dependent variable reaches a value approximately equal to 5 times the decay constant. Indeed, in the present case, the δ term is supposed to vanish when overlapping disappears, *i.e.* for $k \geq k_{lim}$. Considering that $k_{lim} = 0.215$ (for the centered middle layer disk case), a value $B = 0.04$ has been assumed and proved to yield good agreement.

In summary, based on equations (A.2.26) and (A.2.28), the complete expression of the analytical model correlating the relative effective diffusivity to the k ratio by taking into account linear and non-linear effects reads:

$$\frac{D_{eff}}{D_0} = 1 - (1 - k) \exp\left(-\left(\beta - \frac{2}{\alpha}\right)\right) - \left[1 - \exp\left(-\left(\beta - \frac{2}{\alpha}\right)\right)\right] \cdot A \cdot \exp\left(-\frac{k}{B}\right) \quad (\text{A.2.30})$$

with $A = 0.27$ and $B = 0.04$.

2.3.2.2 Model validation

Both analytical equations (A.2.26) and (A.2.30) have been compared to the FEM simulation results and the plots are shown on **Figure A.2.11**, for several β values ranging from 0.05 to 1.

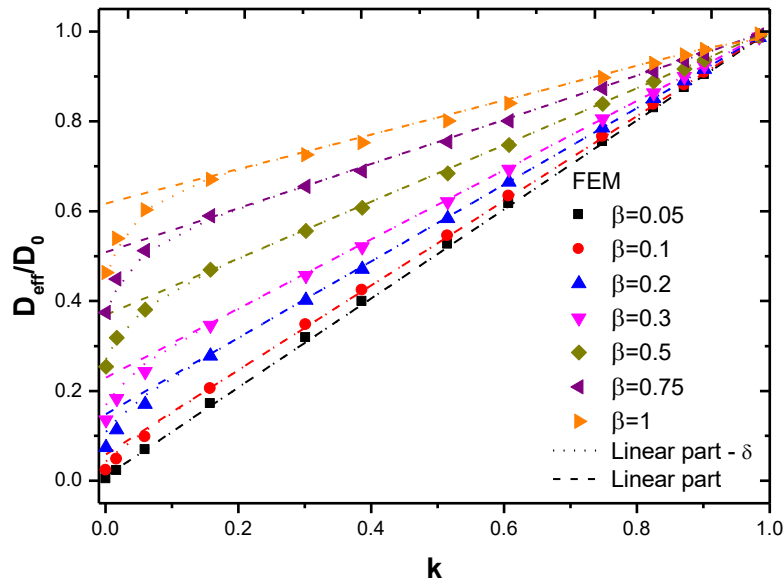


Figure A.2.11 - Relative effective diffusivity versus projected area ratio predicted by the linear and nonlinear analytical models and by FEM simulations

The linear model Eq. (A.2.26) is quite accurate on the full k range for small p_z values only, as well as on the non-overlapping k range $[0.2 - 1]$ for the larger β values. The nonlinear model (including the δ correction term) Eq. (A.2.30) leads to very good overall prediction of the effective diffusivity, even in the low k range (where overlapping occurs) for large β values.

In order to assess the accuracy of the developed analytical model on a larger filler aspect ratio range, the values yielded by Eq. (A.2.30) were compared to the results of the finite element analysis. Relative effective diffusivity values obtained from the numerical simulation and predicted by the analytical equation were plotted against filler volume fraction f for values of the aspect ratio α ranging between 50 and 250 (**Figure A.2.12**). A p_z value of 10 nm has been fixed in order to allow reaching significant filler volume fractions compatible with the chosen aspect ratio range. The obtained plot shows that the simulation results and the analytical equation are in very good agreement for disk aspect ratio values below 200. Beyond this value and especially for filler volume fractions greater than 7% (leading to a quasi-total barrier effect), a slight deviation can be observed. This could be due to the fixed values of the adjustable parameters A and B , which were identified for the case $\alpha = 50$. Nevertheless, the analytical model proves to be quite robust and accurate on a relatively broad range of configurations using only a single set of two adjustable parameters. One should note that for this small p_z value, the linear model Eq. (A.2.26) would give quasi-similar predictions to those of Eq. (A.2.30).

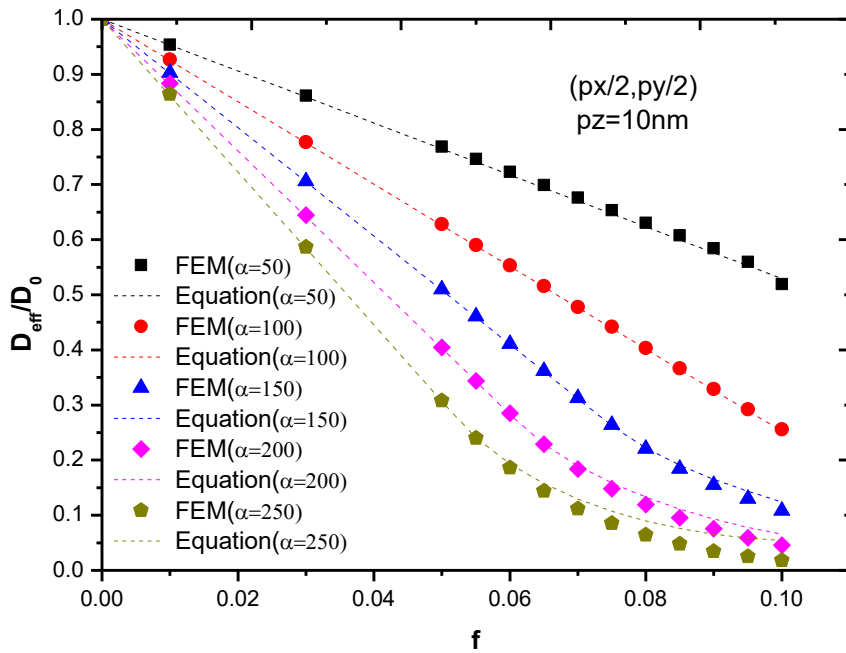


Figure A.2.12 Relative effective diffusivity versus filler volume fraction predicted by the analytical model (Eq. (A.2.30)) and by FEM simulations for several filler aspect ratio values

Furthermore, results obtained from FEM calculations and from the developed equation were compared to Minelli (Minelli et al., 2011) and Aris (Aris, 1986) works. It should be mentioned here that Minelli and coworkers proposed an analytical model depending on the r factor defined as:

$$r = \frac{\alpha - f(\alpha + \sigma_s)}{f(\alpha + \sigma_s)^2} \quad (\text{A.2.31})$$

where σ_s is the so-called slit shape *i.e.* the parameter quantifying the aspect ratio of the matrix phase region located between adjacent fillers. For the unit cell geometry used in the present work, the slit shape could be expressed as follows:

$$\sigma_s = \frac{p_x p_y - \frac{\pi D^2}{4}}{\pi D e} \quad (\text{A.2.32})$$

Minelli's model consists of two equations:

$$\begin{aligned} r \leq 1 \quad \frac{D_{eff}}{D_0} = & \left(\left(\frac{\alpha f}{\sigma_s} \right) \left(1 + \frac{\sigma_s}{\alpha} \right)^2 + \frac{(\alpha f)^2 \left(1 + \frac{\sigma_s}{\alpha} \right)^4}{1 - f \left(1 + \frac{\sigma_s}{\alpha} \right)} \right. \\ & \left. + \frac{\alpha f}{\frac{\pi}{4}} \left(1 + \frac{\sigma_s}{\alpha} \right)^2 \ln \left(\frac{1 - f \left(1 + \frac{\sigma_s}{\alpha} \right)}{f \sigma_s \left(1 + \frac{\sigma_s}{\alpha} \right) \left(\frac{\pi}{2} \right)} \right) \right)^{-1} \end{aligned} \quad (\text{A.2.33})$$

and

$$r > 1 \quad \frac{D_{eff}}{D_0} = \left(1 + \left(\frac{\alpha f}{\sigma_s} \right) \left(1 + \frac{\sigma_s}{\alpha} \right) + \frac{\alpha f}{\frac{\pi}{4}} \left(1 + \frac{\sigma_s}{\alpha} \right)^2 \ln \left(\frac{\alpha \left(1 + \frac{\sigma_s}{\alpha} \right)}{\sigma_s \left(\frac{\pi}{2} \right)} \right) \right)^{-1} \quad (\text{A.2.34})$$

It should be mentioned that fillers aspect ratio in Minelli's model is defined in a slightly different way with respect to the current work.

Aris's equation is recalled hereinafter:

$$\frac{D_{eff}}{D_0} = \left(1 + \frac{\alpha^2 f^2}{1 - f} + \frac{\alpha f}{\sigma_s} + \frac{4 f \alpha}{\pi(1 - f)} \ln \left(\frac{\pi \alpha^2 f}{\sigma_s(1 - f)} \right) \right)^{-1} \quad (\text{A.2.35})$$

The results are compared for a fixed value of $\sigma_s = 5$ and $\alpha = 40$ and for fillers volume fraction ranging between 0.5% and 10% (**Figure A.2.13**).

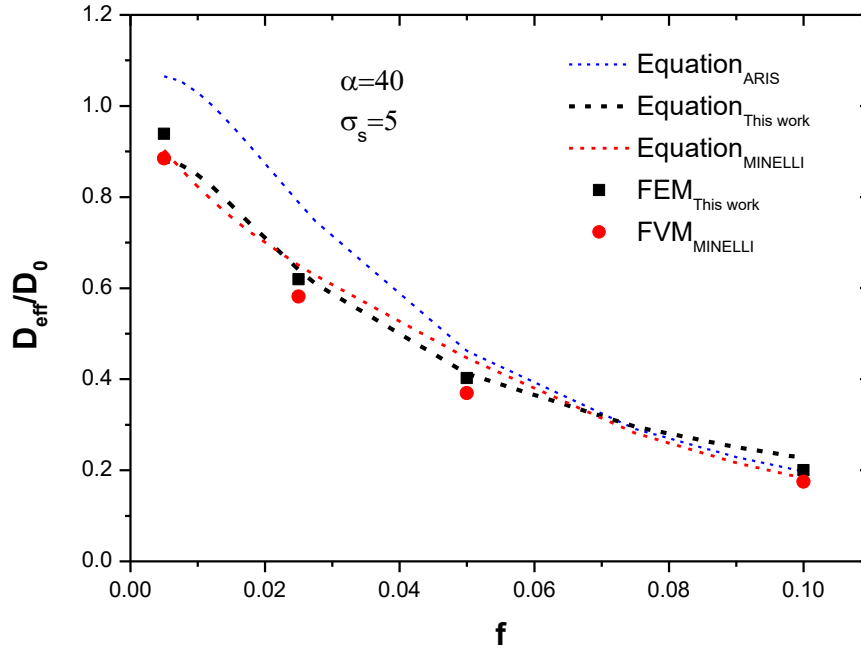


Figure A.2.13 – Relative effective diffusivity versus filler volume fraction predicted by the analytical model (Eq. (A.2.30)), FEM simulations and existing models in literature

As demonstrated in **Figure A.2.13**, the FEM numerical simulation results as well as the analytical equation developed in this work are in good agreement with Minelli's FVM results and analytical equation. However, some discrepancies with the predictions of Aris equation can be noted, which could be due to differences in the geometrical shape of the fillers (flake-shaped fillers in Aris model).

2.4 Conclusion

In this paper, a 3D FEM model was developed in order to study gas diffusion in nanocomposites for barrier applications. The adopted geometry was the disk shape. Thus, different disk volume fraction, aspect ratio and positions were investigated here. The results raise several observations that merit discussion, the first being that increasing fillers volume fraction and aspect ratio had a great effect on improving barrier properties of nanocomposite systems. Furthermore, it was shown that relative diffusivity is strongly governed by a remarkable parameter, the projected area ratio, reflecting the area available for straight path diffusion of the molecules. Calculation results show that the greater this parameter, the higher the relative effective diffusivity. Through these results, a new analytical equation was developed, taking into consideration the filler aspect ratio, the thickness-wise spacing between fillers and the projected area ratio. The equation was validated against FEM calculations and showed good agreement with other existing models.

Chapter 3 Numerical Analysis of 3D Mass Diffusion in Random Nanocomposite Systems: Effects of Polydispersity and Intercalation on Barrier Properties

An overview of the chapter

The previous chapter was focused on the effect of fillers structure parameters on the overall diffusivity of “idealized” nanocomposite systems assuming full exfoliation (i.e. individual fillers) and ordered spatial dispersion in the matrix. However, in actual systems, the fillers are generally randomly distributed in the polymer matrix and individual fillers can coexist with filler stacks, making the morphology much more complex. Besides, filler size polydispersity can also be observed and could affect barrier properties. It appears essential to elucidate the influence of such parameters on the effective diffusivity of nanocomposites. The first objective of the present chapter is to analyze and discuss the effect of filler size polydispersity on the gas barrier properties of nanocomposites using three-dimensional finite element modeling. Secondly, systems composed of monodisperse and polydisperse stacks are considered and the effect of interplatelet diffusion effect on the overall diffusivity is quantified through a parametric study. The analysis is carried out for large ranges of fillers dimensions and diffusion coefficient values in the interplatelet area.

3.1 Introduction

In the past decades, there has been specific interest in nanocomposite materials because of their applications in various fields, especially for gas barrier application. An increase of the barrier properties is expected from the addition of impermeable lamellar nanofillers to the polymer matrix thanks to an increase of the gas diffusion path. Different experimental, analytical and numerical studies have been carried out to investigate the dependency of this tortuous effect and resulting barrier properties on morphological factors such as the filler content or aspect ratio (Greco, 2014a; Greco & Maffezzoli, 2013; H. D. Huang et al., 2014; Minelli et al., 2009, 2011; Nielsen, 1967; Yano et al., 1993). In these studies, it is usually considered that all dispersed objects have the same dimensions (Greco, 2014a; Greco & Maffezzoli, 2013). However, the nanocomposite morphology is often more complex. Several studies have underlined the coexistence of dispersed objects with different aspect ratios in nanocomposites prepared from a single nanofiller type due to the difficulty to achieve complete exfoliation of the platelets (Alexandre et al. 2009; Masclaux, Gouanvé, et Espuche 2010; Picard, Gérard, et Espuche 2008; Kim, Abdala, et Macosko 2010). Picard et al. (Picard, Gauthier, Gérard, & Espuche, 2007) showed that in PA6/montmorillonite nanocomposites the coexistence of exfoliated structures and small filler stacks (less than 5 sheets per stack) was not detrimental to barrier properties. This result, that could appear surprising with respect to commonly used Nielsen law (Nielsen, 1967), was explained by the low amount and low width of the stacks. Thus, the small decrease of mean filler aspect ratio was compensated by the increase of the impermeable volume fraction, the volume occupied by the stacks being considered as impermeable.

The effect of the polydispersity of the filler aspect ratios on barrier properties has been modeled in several works (X. Chen & Papathanasiou, 2007; Lape et al., 2004). In these studies, the considered fillers have the same thickness but generally differ by their length. The analytical model developed by Lape et al. (Lape et al., 2004) evidenced that the barrier properties are better improved when fillers are larger. Moreover, Chen et al. (X. Chen & Papathanasiou, 2007) developed a 2D numerical model based on the Boundary Element Method (BEM) through which they confirmed the interest of filler size polydispersity for improved barrier properties. As already mentioned, in all these studies, the dispersed objects consisted of individual fillers with the same thickness but different lengths. On the other hand, some works focused on the effect of filler stacks on gas transport (Bharadwaj, 2001; Paul & Robeson, 2008). The stacks dispersed in the matrix had the same size and they were usually

considered as impermeable phases. Only few authors investigated the influence of possible gas diffusion in the interplatelet space on the overall gas transport properties. By considering the gas diffusion rate in the interplatelet space similar to that in the matrix, Nazarenko (Nazarenko et al., 2007) found that the contribution of the interplatelet diffusion on the overall transport was negligible. An extension of the model proposed by Nazarenko was derived by Greco and coworkers (Greco, Corcione, & Maffezzoli, 2016; Greco & Maffezzoli, 2015a) with the aim to discuss the impact of different diffusion rates in the interplatelet space. Through their numerical approach, Greco et al. showed that diffusion in the interplatelet space is quite relevant especially for high values of the space inside stacks. It is noteworthy that in all these previous works the platelet stacks dispersed in the matrix were all of the same sizes. According to our knowledge, no modeling study investigated the impact of stacks with polydisperse sizes on the gas transport properties.

The aim of the present study is to discuss the effect of the filler size polydispersity on gas barrier properties through a step-by-step approach based on three-dimensional finite element modeling (FEM). In the first part, systems filled with polydisperse single platelets (*i.e.* same thickness but different diameter distributions) are compared with monodisperse systems. In the second part, dispersions of monodisperse stacks and polydisperse stacks are investigated. In order to assess the effect of interplatelet diffusion, a sensitivity study is carried out considering a wide range of diffusion coefficient values in the interplatelet area. It should be kept in mind that throughout this study, random spatial dispersion of the fillers (or stacks) has been assumed in order to be as representative of the actual systems as possible.

3.2 Modelling Methodology

3.2.1 Geometry

The geometric modeling of the nanocomposite systems is based on a three-dimensional representative volume element (RVE) approach. The parallelepipedic simulation domain representing the RVE has dimensions L_x , L_y and L_z in a Cartesian coordinate system (x,y,z) , with z the overall diffusion direction. As in the previous section 2.2, fillers are modeled as three-dimensional disks (diameter D , thickness e). The choice of the discoidal filler shape was based on literature as detailed in the first chapter because of its representativeness of platelet-like nanofillers. Two types of geometric configurations have been considered:

- the first type of configuration consisted of dispersions of single impermeable disks randomly positioned in the matrix and oriented normally to the overall flux direction z .

The disk size can be either monodisperse or polydisperse. The random positioning of disks in the computational domain was generated using a JAVA algorithm coupled with the commercial finite element package COMSOL Multiphysics. This algorithm contains conditions that ensure non-overlapping of the generated disks.

- the second type of configuration consisted in dispersions of stacks of three impermeable disks, randomly positioned and oriented in the polymer matrix using the same generation algorithm. As in the first type of configuration, the disk size can be either monodisperse or polydisperse.

In the whole study, the disk thickness was assumed to be 2 nm and the mean diameter value \bar{D} was targeted to 60 nm. The filler aspect ratio α was defined as the ratio between the diameter and the thickness. A target value of the filler volume fraction was specified as an input parameter of the distribution generation algorithm. However, the actual volume fraction f of the generated distribution was calculated through a volume integration of the matrix domain after generating the geometry and was varied between 1% and 14%. The computational domain contains a sufficient number of fillers through which well-aimed results could be obtained (200 - 264 dispersed fillers with and without stacks).

3.2.2 Physical equations

The mass diffusion process in stationary regime was modeled according to Fick's second law without mass source (2.2.2 :

$$\nabla \cdot (-D_{ij} \nabla c_i) = 0 \quad (\text{A.3.1})$$

where c_i is the molar concentration of the permeating specie i (mol.m^{-3}) and D_{ij} is the mass diffusion coefficient of permeating specie i in medium j . In the present study, the diffusion coefficient of permeating specie in the neat matrix was chosen as $D_0 = 10^{-12} \text{ m}^2/\text{s}$.

The finite element method is used to solve the mass diffusion equation in the matrix domain with the following boundary conditions:

- concentration boundary conditions were imposed on the upper and lower faces of the simulation domain: $c_1 = 1000 \text{ mol.m}^{-3}$; $c_2 = 500 \text{ mol.m}^{-3}$. The matrix diffusivity is considered constant and not concentration-dependent, meaning that concentration values chosen as BCs for the upper and lower faces have rigorously no effect on the effective diffusivity calculated in this study;

- since disks are impermeable to mass diffusion, no-flux boundary condition was imposed on all filler-matrix interfaces;
- for symmetry reasons, no-flux boundary conditions were applied on the lateral faces of the simulation domain.

3.2.3 Numerical analysis

An unstructured mesh consisting of tetrahedral linear elements in order to provide accurate results was adopted in the previous chapter 2.2.3 . It has been verified that the number of mesh elements is sufficiently high not to affect the obtained results (*e.g.* for 200 disks generated in the RVE, the number of mesh elements is about 126360). The solution of the boundary value problem yields the molar concentration field of the permeating specie $c(x,y,z)$. Finite element solutions were obtained using the commercial package Comsol Multiphysics (version 5.4, DELL computer with i3 processor and 8 Go of RAM). The computational time was between 1 and 5 min. Then, the mass flux vector field of the permeating specie can be calculated from the concentration field:

$$\vec{N}(x, y, z) = -D_0 \vec{\nabla} c(x, y, z) \quad (\text{A.3.2})$$

and the overall effective diffusivity is given as follow:

$$D_{eff} = \frac{\overline{N_z} L_z}{c_1 - c_2} \quad (\text{A.3.3})$$

where $\overline{N_z}$ is the average mass flux of the permeating specie across a plane section S normal to z -direction and located at $z = z_0$ within the unit cell:

$$\overline{N_z} = \frac{1}{L_x L_y} \iint_S N_z(x, y, z_0) dx dy \quad (\text{A.3.4})$$

assuming that N_z is the z -component of the mass flux vector.

In the current work, relative effective diffusivity, defined as the ratio D_{eff}/D_0 , is considered the most convenient parameter to characterize and compare the enhancement of barrier properties in the various studied systems. It has been shown through the previous chapter 2.2.3 that it does not depend on the neat matrix diffusivity value D_0 .

Since the systems under consideration are composed of disks randomly placed in the RVE, we show hereinafter that the use of impermeable boundary condition on the sides of the RVE is similar in terms of results to the use of symmetry boundary conditions (**Figure A.3.1**).

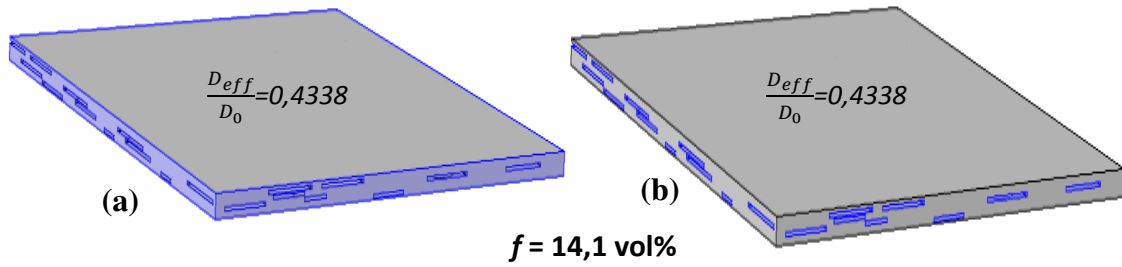


Figure A.3.1 Comparison of the obtained results considering (a) symmetry and (b) impermeable boundary conditions

3.3 Results and Discussion

3.3.1 Effect of filler aspect ratio polydispersity on the overall diffusivity

This section focuses on the effect of filler aspect ratio polydispersity on nanocomposite barrier properties. For this purpose, simulations were conducted for different generated distributions in order to compare their effect on the overall diffusivity. For the sake of clarity, the generated distributions are described first, then the obtained results are discussed and compared to existing models from literature.

3.3.1.1 Monodisperse distribution

Monodisperse distributions have been generated according to the following method: single disks having a fixed diameter value $D = 60 \text{ nm}$ corresponding to an aspect ratio value $\alpha = 30$ were positioned randomly on 4 layers separated by 1 nm of the polymer matrix, each. The developed generation algorithm ensured that disks did not overlap in a given layer (**Figure A.3.2**).

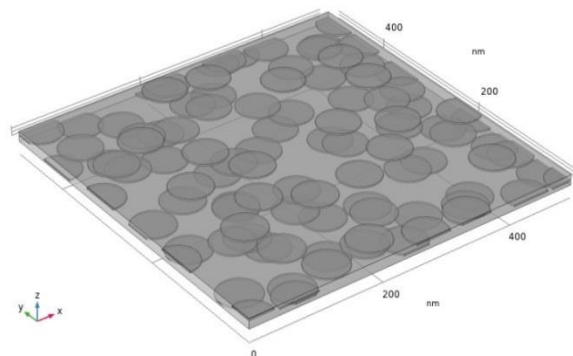


Figure A.3.2 Geometrical model of monodisperse system

3.3.1.2 Polydisperse distributions

Nanocomposite systems could have various filler size distributions. In this section, three different types of distributions are presented where the polydispersity was controlled. For

each type of distribution, three dispersions were randomly generated in order to verify the repeatability of the method.

3.3.1.2.1 Polydisperse uniform distribution

In order to generate a polydisperse system with uniform size repartition in a given range, the generation algorithm randomly picks an equiprobable random value of the disk diameter in the specified range (20 – 100 nm in the present case) and attempts to position the disk at a randomly chosen position. If no overlapping occurs, the disk is actually inserted. Otherwise, the disk is discarded and a new disk with new random diameter and position is generated. The process is repeated as many times as needed to attain the desired number of disks in the RVE. Due to this process, it is expected that the actual diameter distribution slightly deviate from the ideal uniform distribution, since small disks are generally easier to position than large disks. For a total number of 200 generated disks in the RVE, the actually obtained distributions of disk size for an average disk aspect ratio $\bar{\alpha} = 30$ (corresponding to an average diameter $\bar{D} = 60$ nm) is presented in **Figure A.3.3**.

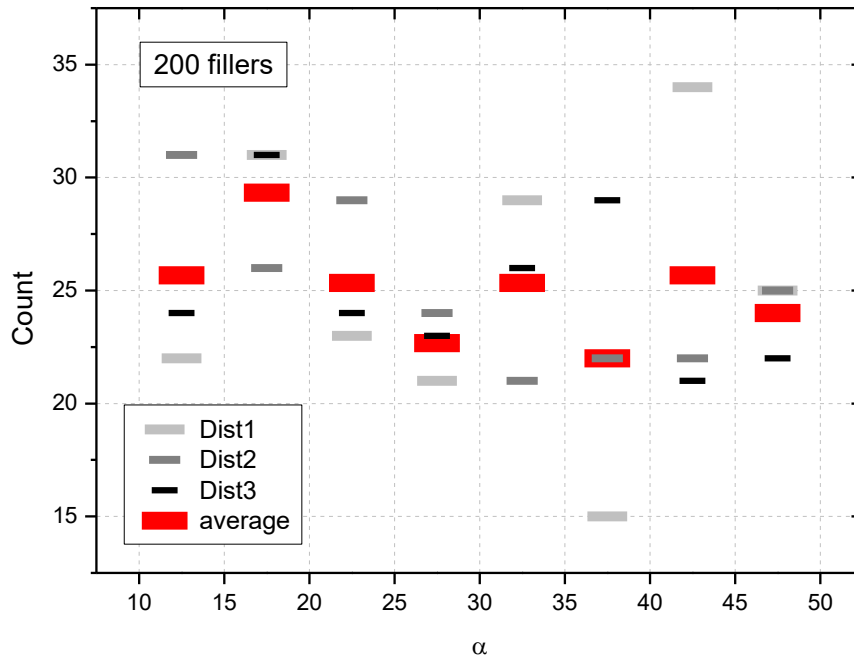


Figure A.3.3 Disk size distribution for three different polydisperse uniform dispersions ($\bar{\alpha} = 30$); resulting averaged distribution

3.3.1.2.2 Polydisperse Gaussian distribution

Polydisperse systems with Gaussian size distribution were generated. This type of distribution has the following probability density function (PDF):

$$\phi = \frac{1}{\sqrt{2\pi}\sigma} e^{-\frac{(D-\bar{D})^2}{2\sigma^2}} \quad (\text{A.3.5})$$

where \bar{D} is the diameter mean value and σ the diameter standard deviation. Two different standard deviation values $\sigma = 1$ (narrow distribution) and $\sigma = 10$ (wide distribution) were chosen, in order to stay in the same range of individual D values as for the uniform distribution. For each σ value, three different dispersions were generated. The obtained diameter distributions are plotted and compared to Gaussian fits of these distributions on **Figure A.3.4** and **Figure A.3.5** for $\sigma = 1$ and $\sigma = 10$, respectively. It appears clearly that for both σ values, the actually obtained distributions (represented by the histograms) were quite close to Gaussian distributions.

3.3.1.2.3 Polydisperse “specific” distribution (derived from Gaussian distribution with large standard deviation)

The aim was to generate target Gaussian distributions with a mean aspect ratio value $\bar{\alpha} = 30$ and a larger standard deviation value $\sigma = 20$. However, due to the overlapping management process described earlier, the generation algorithm tends to discard the larger disks (whose diameters belong to the upper tail of the Gaussian) more frequently and thus to favor the smaller disks. Consequently, the mean aspect ratio values of the actually obtained distributions ($\bar{\alpha}_1 = 22.3$; $\bar{\alpha}_2 = 22.4$ and $\bar{\alpha}_3 = 21.7$) are significantly smaller than the target value $\bar{\alpha} = 30$. Moreover, the obtained distributions clearly deviate from true Gaussian distributions and present a truncated aspect in the lower tail (**Figure A.3.6**).

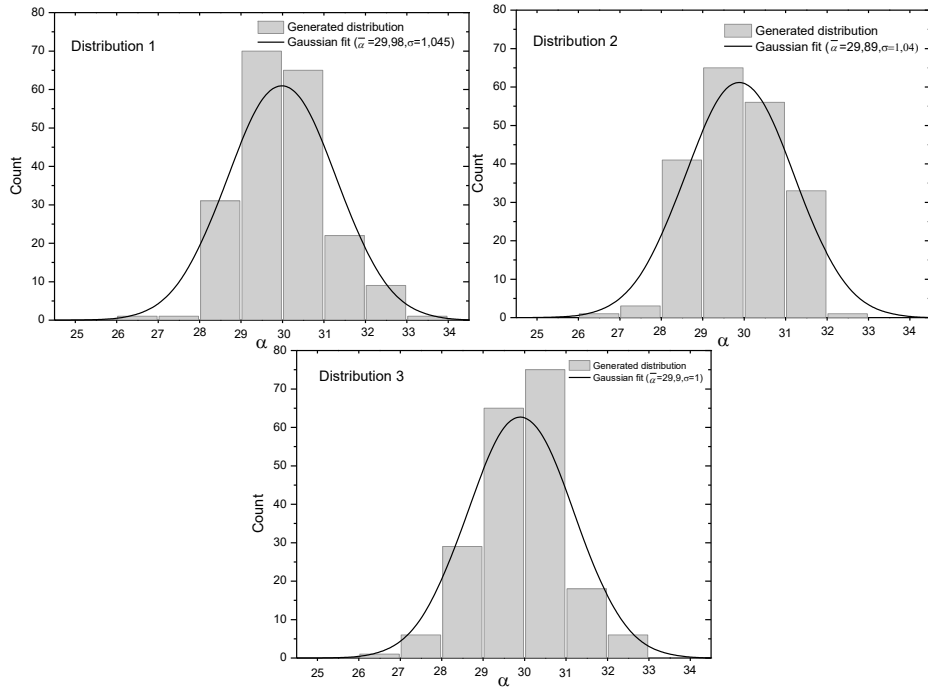


Figure A.3.4 Disk size distribution actually generated for target values of Gaussian parameters $\bar{\alpha} = 30$ and $\sigma = 1$

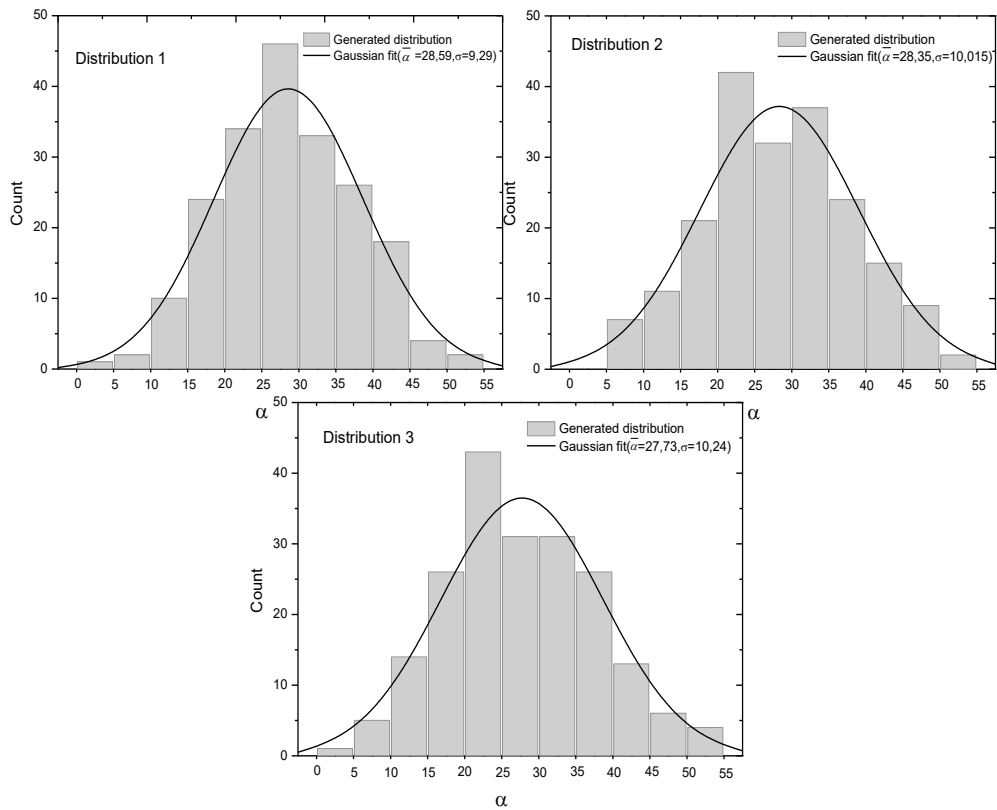


Figure A.3.5 Disk size distribution actually generated for target values of Gaussian parameters $\bar{\alpha} = 30$ and $\sigma = 10$

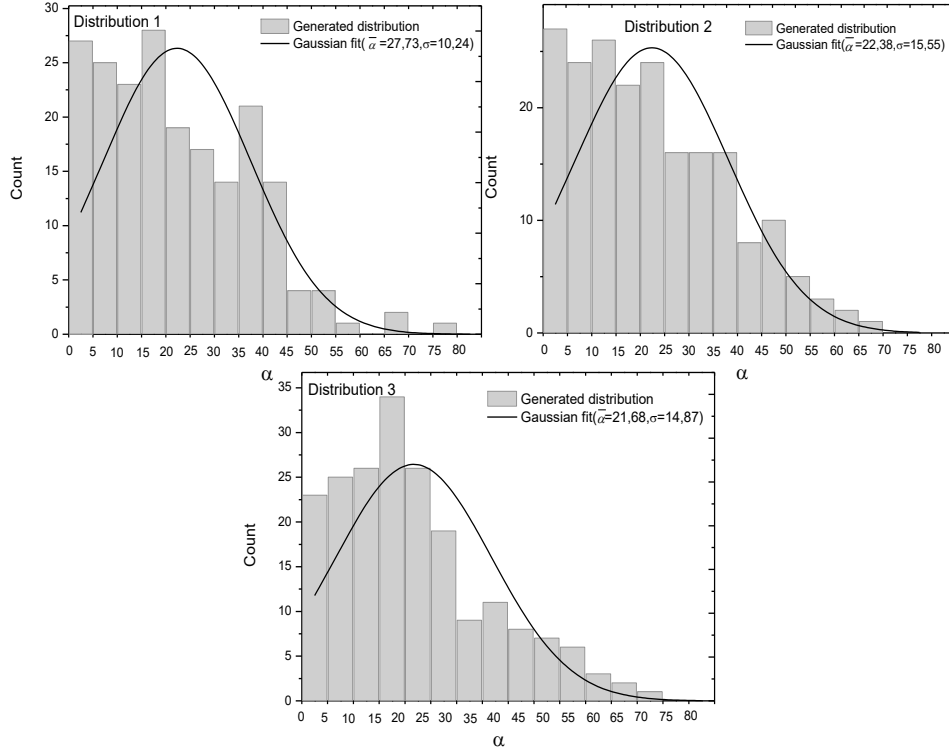


Figure A.3.6 Disk size distribution actually generated for target values of Gaussian parameters $\bar{\alpha} = 30$ and $\sigma = 20$

3.3.1.3 Comparison of barrier properties

An objective of this study is to clarify which type of filler dispersion is the most efficient in the enhancement of nanocomposite barrier properties. Hence, in this section, relative effective diffusivity (D_{eff}/D_0) results from finite element simulations of the different studied configurations are compared. Moreover, the numerical results are compared to Lape et al. (Lape et al., 2004) analytical equation, for which filler size also follows a Gaussian distribution:

$$\frac{D_{eff}}{D_0} = \frac{1 - f}{\left(1 + \left(\frac{f}{3e\bar{D}}\right)\left(\frac{\bar{D}^2}{4} + \sigma^2\right)\right)^2} \quad (\text{A.3.6})$$

where f is the filler volume fraction, e the disk thickness, \bar{D} the disk average diameter and σ the diameter standard deviation. **Figure A.3.7** plots the relative diffusivity predicted by FEM for the monodisperse and Gaussian polydisperse systems, as well as Lape analytical model's predictions for the Gaussian polydisperse systems ($\sigma=1$ and 10). It must be noted here that ε is the standard deviation between the obtained results.

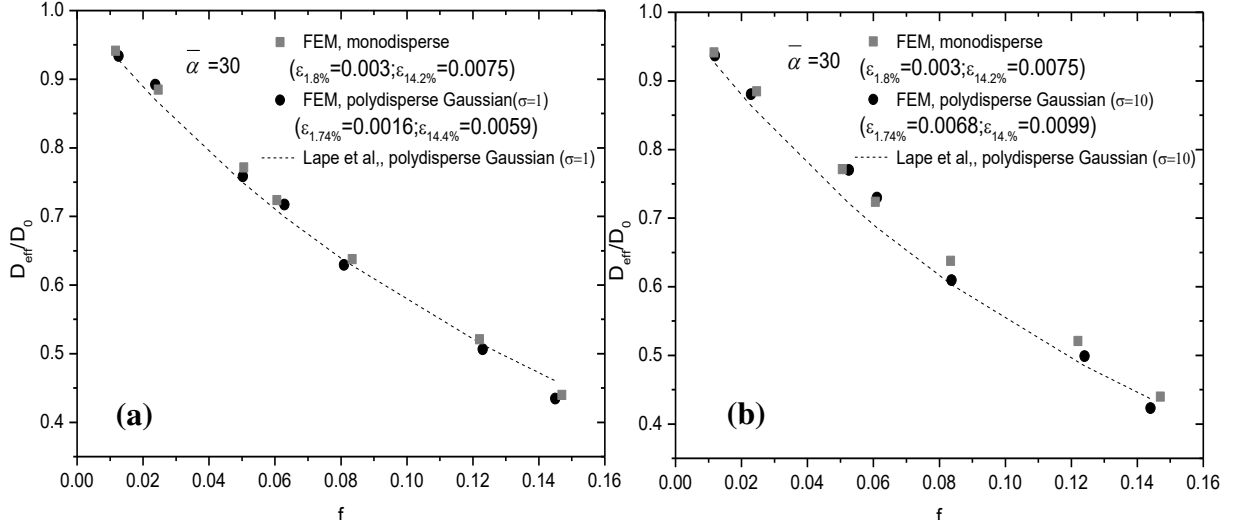


Figure A.3.7 Relative effective diffusivity vs. filler volume fraction for monodisperse and polydisperse Gaussian systems ($\sigma = 1$ (a) and $\sigma = 10$ (b)): FEM predictions and Lape et al. model (Lape et al., 2004)

It can be noticed that in both cases, results from the present simulations are in good agreement with Lape's model predictions. Moreover, when σ is increasing, the deviation between polydisperse and monodisperse systems is slightly increasing too. Lape et al. (Lape et al., 2004) showed that an increase in polydispersity (i.e. an increase in σ) implies a decrease in diffusivity, which is consistent with our calculations. Moreover, the statistical analysis made through calculating ε shows that small differences between the obtained results can be considered as insignificant.

In a next step, the comparison has been extended by taking into account the polydisperse uniform distribution and the polydisperse specific distribution described previously (**Figure A.3.8**).

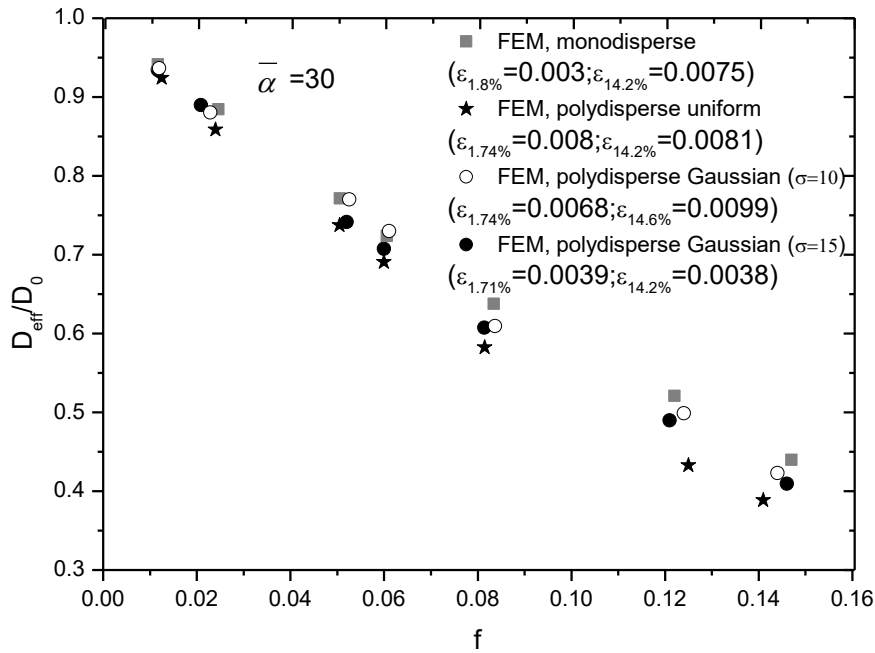


Figure A.3.8 Relative effective diffusivity vs. filler volume fraction for monodisperse, polydisperse uniform and polydisperse Gaussian systems: FEM predictions

It appears clearly that although relative effective diffusivity always decreases as fillers volume fraction increases, the type of distribution does have a significant effect. Indeed, the lowest diffusivity values were obtained in the case of uniform polydispersity. It has been shown in 2.3.1 that barrier properties enhancement is correlated to the projected area ratio for penetrating molecules which was defined as the ratio of the projected area of the matrix phase on a plane normal to the diffusion direction z and the total projected area of the RVE. In this case, this factor, denoted k_i , was calculated for three different cases of size distributions (monodisperse (k_1), polydisperse uniform (k_2), and Gaussian $\sigma = 10$ (k_3)). The values of k_i reported in **Figure A.3.9** are the average values calculated from 3 different dispersions for each size distribution. As it can be observed, the lowest value of the projected area ratio is obtained for the polydisperse uniform configuration which is in adequacy with the obtained numerical diffusivity results.

Furthermore, a comparison of the results for the Gaussian distribution shows a slightly better decrease in relative effective values in the case where $\sigma = 15$ compared to $\sigma = 10$. One should remember that, when the standard deviation is targeted to $\sigma = 20$, the generated distribution is not perfectly Gaussian and the actual standard deviation is about $\sigma = 15$. Thus, In all cases, relative effective diffusivity values are smaller than the monodisperse case; this is consistent with Chen et al.'s 2D simulation results (X. Chen & Papathanasiou, 2007).

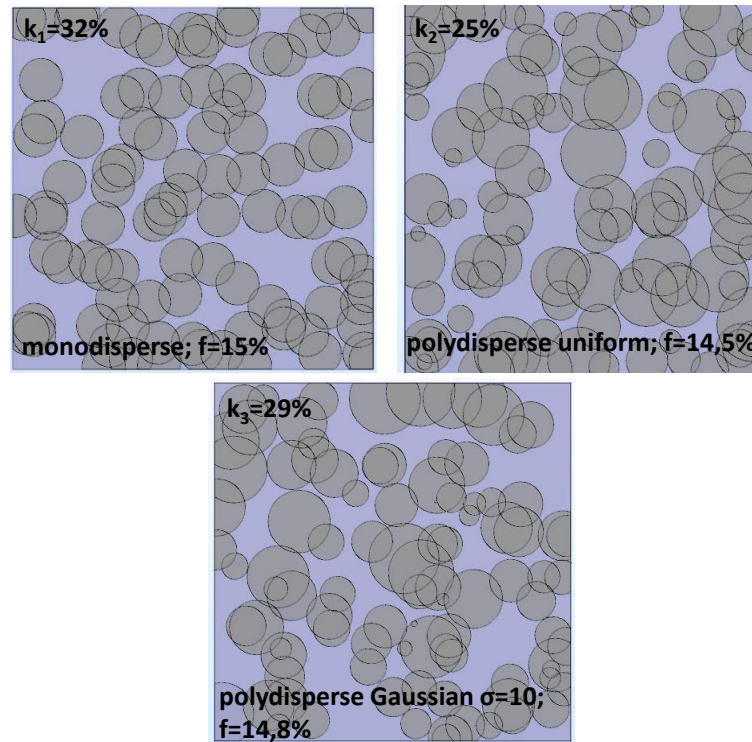


Figure A.3.9 Representative volume element (z -direction view) of three types of filler dispersion for similar filler volume fraction

3.3.2 Effects of intercalation on the effective diffusivity

Fillers present in nanocomposites (graphene, montmorillonite) often have an intercalated structure (Corcione, Freuli, & Maffezzoli, 2013; H. Kim et al., 2010; Masclaux et al., 2010; Picard et al., 2008; Picard, Vermogen, et al., 2007). Hence, investigating the effects of filler stacking on diffusion mass transfer is an indispensable step to understand the barrier properties of such nanocomposite films. In the previous section, the size polydispersity of the dispersed objects (single fillers) was taken into account by the variation of the disk diameter. In the case of nanocomposites prepared from lamellar nanofillers, the size polydispersity is related to the presence of nanofiller stacks (Picard, Vermogen, et al., 2007). In this section, a step-by-step analysis is presented, covering monodisperse and polydisperse stacks and considering the most efficient size distributions evidenced previously.

3.3.2.1 Effects of stacking and polydispersity

First, an analysis has been conducted in order to examine to what extent the presence of stacked fillers affects the barrier properties in comparison to an exfoliated system with a similar volume fraction. Each stack was modeled as a superposition of three identical disks (diameter D , thickness e). The interplatelet spacing, *i.e.* the gap between two adjacent disks in

a stack, e_{inter} , was assumed identical ($e_{inter} = 1$ nm) for all stacks. The stacks were randomly positioned in the simulation domain and oriented perpendicularly to the gas flow. The z -dimension of the simulation domain corresponds to four layers of stacks. Two examples of generated stacks dispersions are shown in **Figure A.3.10**. In all cases, the generation algorithm ensured non-overlapping of stacks. The following distributions have been generated and diffusion mass transfer has been numerically simulated for various volume fractions using the methodology presented in 3.2 :

- monodisperse distribution: identical stacks ($D = 60$ nm, $e = 2$ nm, $e_{inter} = 1$ nm);
- polydisperse uniform distribution (diameter range : 20-80 nm, $\bar{D} = 60$ nm, $e = 2$ nm, $e_{inter} = 1$ nm);
- polydisperse Gaussian distribution (average diameter $\bar{D} = 60$ nm with a standard deviation $\sigma = 10$, $e = 2$ nm, $e_{inter} = 1$ nm);

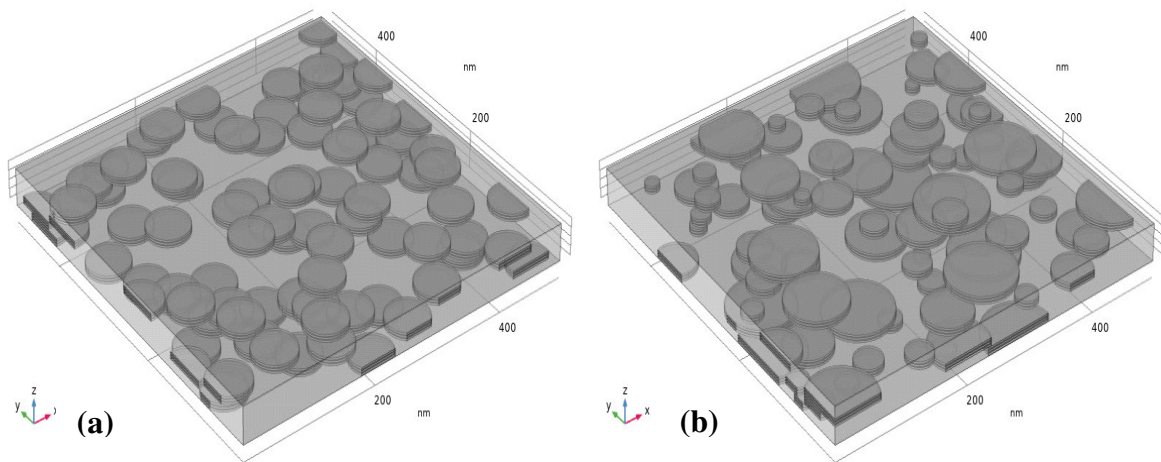


Figure A.3.10 Example of 3D simulation domain of intercalated nanocomposites; **(a)** Monodisperse stacks **(b)** Polydisperse stacks (uniform distribution)

The effective relative diffusivity values predicted for the three types of intercalated dispersions have been reported in **Figure A.3.11** and compared to the results obtained in section 3.3.1.3 for the exfoliated structures. As expected, the relative effective diffusivity is a decreasing function of fillers volume fraction. It is noteworthy that whatever the filler volume fraction, the relative diffusivity is lower for the exfoliated dispersions than for intercalated ones. This observation can be assigned to the tortuosity effect. Indeed, for a given value of the filler volume fraction, the total projected area of the impermeable phase is larger in the case of single disks than in the case of stacks. According to the results obtained in the previous chapter 2.3.1 , this factor can be related to the tortuous path a diffusing molecule

has to follow due to the presence of the impermeable phase. More specifically, for the intercalated systems, it can be noticed that the highest relative diffusivity values are obtained for monodisperse stacks while the lowest relative diffusivity values are recorded for the polydisperse uniform distribution of stacks. Thus, the trends observed for exfoliated dispersion are also valid for intercalated dispersion.

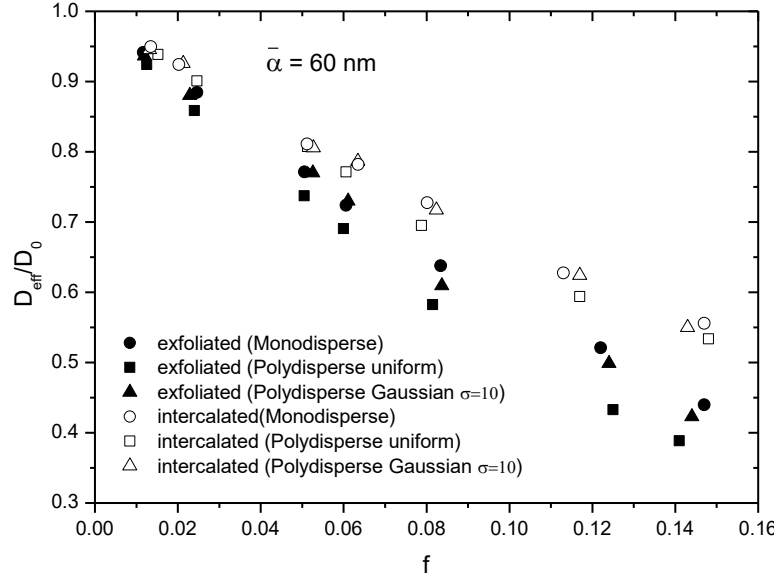


Figure A.3.11 Comparison of effective relative diffusivity predicted by FEM for exfoliated and intercalated systems as a function of filler volume fraction

3.3.2.2 Influence of the interplatelet space characteristics (spacing, diffusivity)

In order to investigate the potential contribution of the interplatelet space to overall diffusion, monodisperse systems composed of 3-disks stacks with a fixed diameter were considered. The stacks were randomly positioned in the polymer matrix. Moreover, they were randomly tilted with angles ranging between 0° and 30° around both x and y axes, as shown in **Figure A.3.12**. The disk thickness was fixed to $e = 2$ nm whereas the disk diameter could be chosen in the range [20 nm - 100 nm]. The interplatelet spacing e_{inter} was varied between 1 nm and 10 nm. This range of values is representative of the interplatelet distance measured on several organo-modified lamellar nanofillers (Dal Pont, Gérard, & Espuche, 2012; Mariano, Freitas, Mendes, Carvalho, & Ramos, 2019). The matrix diffusivity was fixed to $D_0 = 10^{-12}$ m²/s while in a second step, the diffusivity in the interplatelet space, denoted by D_{inter} , could be varied in the range [$10^{-4} D_0 - 10^5 D_0$]. Indeed, some experimental works have shown that the interplatelet space within stacks could not always be considered as impermeable (Aitken, Koros, & Paul, 1992; Dal Pont, 2011; Jacquolot et al., 2006). It could then be interesting to consider through

a parametric analysis a wide range of interplatelet behavior going from very low permeability to high permeability.

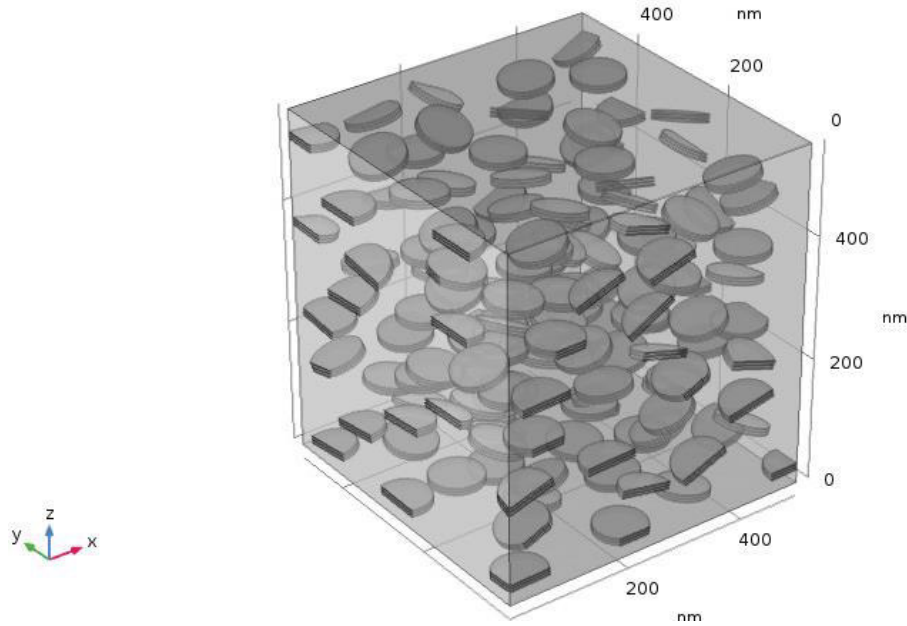


Figure A.3.12 Geometrical model of intercalated non-oriented monodisperse system

3.3.2.2.1 Analysis of interplatelet space contribution to overall diffusion for $D_{inter} = D_0$

Several experimental studies available in literature describe intercalated nanocomposite as systems for which interplatelet diffusion inside stacks is considered similar to diffusion in the polymer matrix (Bharadwaj et al., 2002; Nazarenko et al., 2007; Wolf et al., 2018). Indeed, Nazarenko et al. (Nazarenko et al., 2007) showed that for low values of e_{inter} (about 5 nm), intra-stack diffusion can be considered as negligible compared to the overall diffusion. In addition, different analytical and numerical models (Greco et al., 2016; Greco & Maffezzoli, 2015a, 2015b) investigated the effect of stacks on the barrier properties of intercalated nanocomposite systems. However, the structural parameters appearing in some works were considered over a limited range of values, for example, in Greco et al. work (Greco & Maffezzoli, 2015a), the filler aspect ratio was fixed to 50 however interplatelet space did not exceed 4 nm). Since it was shown in previous works (Cussler et al., 1988) and in the previous chapter that the effective diffusivity in nanocomposite systems strongly depends on fillers structural parameters, it appears necessary to extend those analyses to different values.

In order to assess the importance of interplatelet diffusion, a suitable approach consists in comparing the predicted effective diffusivity in identical systems in which the interplatelet space is assumed either permeable ($D_{inter} = D_0$) or impermeable. In the latter case, the stacks

can be modeled by the corresponding fully impermeable cylindrical volume, as shown in **Figure A.3.13**. Note that in both cases, stacks positions are kept strictly identical in order to cancel all variability effects due to random positioning.

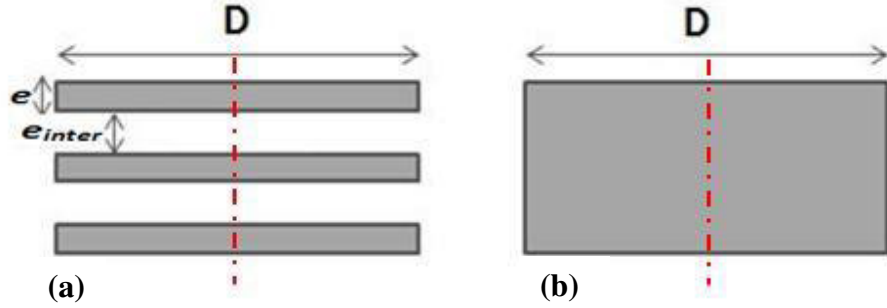


Figure A.3.13 (a) Geometry of the actual stack and (b) corresponding fully impermeable stack

The relative effective diffusivity values predicted by the FEM simulations (for a monodisperse size distribution case; D ranging between 20 and 100 nm, $e=2\text{nm}$ and f between 0.11 and 2.7%) have been plotted on **Figure A.3.14** as a function of the interlayer thickness e_{inter} and of the parameter R which was defined as the ratio of the interplatelet space volume to the total stack volume:

$$R = \frac{2e_{inter}}{3e + 2e_{inter}} \quad (\text{A.3.7})$$

As shown by equation (A.3.7), the parameter R increases with increasing intra-stacks spacing e_{inter} .

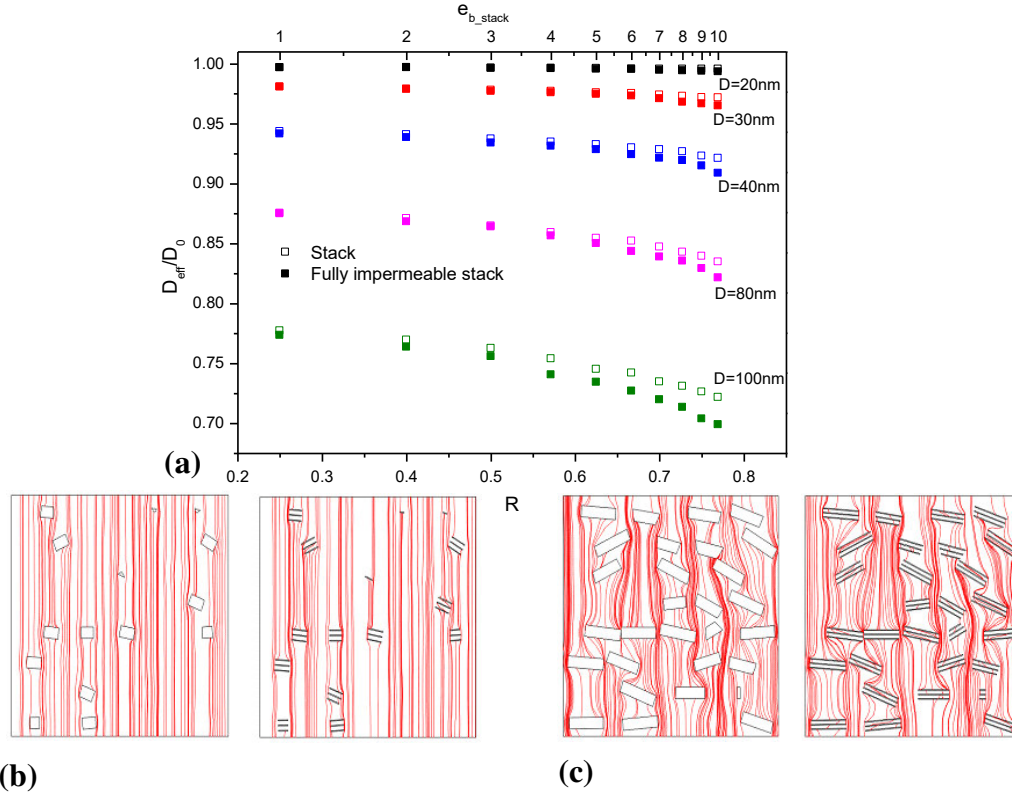


Figure A.3.14 (a) Relative effective diffusivity variation versus parameters R and e_{inter} for systems with permeable stacks (empty symbols) and corresponding fully impermeable stacks (full symbols), for several disk diameter values; (b) Diffusive flux lines in system with fully impermeable stacks (left) and permeable stacks (right), $D = 20\text{ nm}$, $e_{inter}=7\text{nm}$; (c) Diffusive flux lines in system with fully impermeable stacks (left) and permeable stacks (right), $D = 100\text{ nm}$, $e_{inter}=7\text{nm}$

Figure A.3.14 shows that for a given volume fraction, the barrier effect is enhanced when R (*i.e.* e_{inter}) is increased. Moreover, the enhancement is more pronounced as the diameter of stacks increases. This result could be explained by the following mechanism: since spacing between stacked fillers increases, the stacks occupy more space in the matrix, which is correlated to a reduction of the free volume and then a decrease in effective diffusivity. Comparing the results for permeable stacks and impermeable stacks leads to the conclusion that interplatelet flux could be neglected if the filler diameter or the interplatelet gap are small. Indeed, the relative effective diffusivity values predicted in the cases of permeable stacks and impermeable stacks remain very close (*e.g.* for $R = 0.75$ and $D = 20\text{ nm}$, the deviation in relative effective diffusivity values is only 0.18 %). This result is in adequacy with the observations of Nazarenko et al. (Nazarenko et al., 2007). The minor contribution of the diffusion in interplatelet spaces to the overall diffusion was confirmed through the

analysis of the diffusive flux lines shown in **Figure A.3.14** (b). However, for large and loosely stacked fillers, intra-stack diffusion can become slightly significant (*e.g.* for $R = 0.75$ and $D = 100$ nm, the effective diffusivity increases by 3.3 % if the interplatelet space is permeable). However, this contribution remains low as evidenced by the diffusive lines shown in **Figure A.3.14** (c) for $D=100$ nm and $e_{inter}=7$ nm. In order to go deeper in the analysis of the influence of e_{inter} on the overall diffusivity, the impact of filler volume fraction has been investigated, for a filler diameter $D = 100$ nm (**Figure A.3.15**). Indeed, it has to be noticed from **Figure A.3.14** (a) that this filler diameter leads to the highest barrier properties.

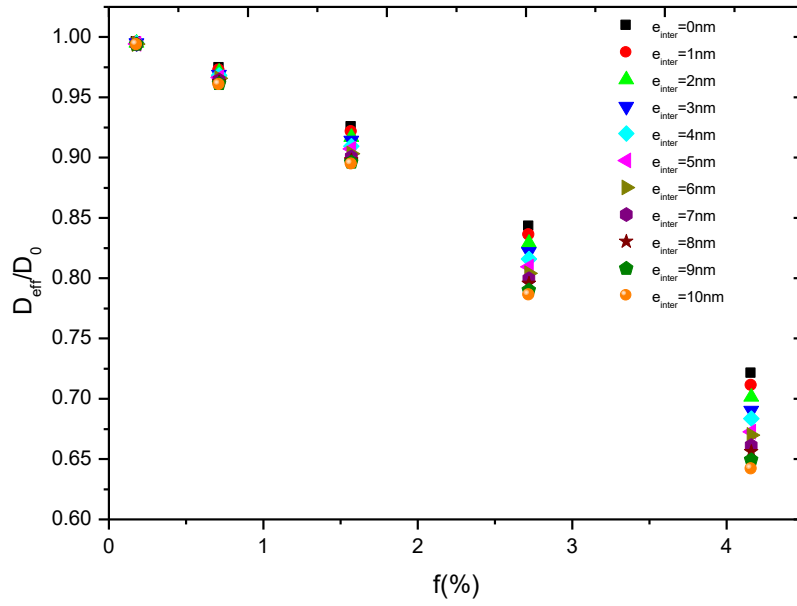


Figure A.3.15 Relative effective diffusivity variation versus filler volume fraction for several values of interplatelet spacing

The obtained results clearly show that relative effective diffusivity is decreasing when the spacing between fillers in one stack increases, which confirms that diffusion, occurs preferentially in the vicinity of the stacks and not through them. This effect is accentuated for higher fillers volume fractions, since this parameter is known to promote tortuosity in the system. In agreement with previous works (Greco et al., 2016; Greco & Maffezzoli, 2015a; Lape et al., 2004; Nazarenko et al., 2007; Picard, Vermogen, et al., 2007) these observations confirm, for larger ranges of fillers size and interplatelet spacing values, that the contribution of interplatelet spaces to overall diffusion in intercalated systems is actually very limited.

3.3.2.2.2 Influence of interplatelet diffusivity ($D_{inter} \neq D_0$)

The effect of diffusion inside stacks has been little studied in literature. For instance, Greco et al. (Greco et al., 2016; Greco & Maffezzoli, 2015a) showed that relative effective diffusivity is increasing linearly in function of D_{inter}/D_0 for values ranging between 0.2 and 1.8. We aim to expand D_{inter}/D_0 range to go from nearly impermeable to highly diffusive interplatelet areas. The methodology is similar to that described in section 3.3.2.2. Fillers volume fraction was varied in the range [0.11% - 2.6%] whereas the intra-stack relative diffusivity D_{inter}/D_0 was varied between 10^{-3} and 10^5 . Disks diameter was varied between 20 and 100 nm. The predicted evolution of the nanocomposites relative effective diffusivity is represented on **Figure A.3.16** versus D_{inter}/D_0 .

First, one should notice that relative effective diffusivity values are decreasing when stacks diameter is increasing which is in agreement with the results discussed in **Figure A.3.14** (a). In addition, three distinct regions are clearly visible in the plots:

- low values of $\frac{D_{inter}}{D_0}$: this region corresponds to the case of nearly impermeable interplatelet spaces, for which the effective diffusivity of the system decreases when spacing between fillers in one stack increases. For each disk diameter (D), filler volume fraction (f) and interplatelet (e_{inter}), the relative effective diffusivity values define a plateau showing that there is no significant effect of intra-stack diffusivity on the simulated coefficient of diffusion in that region;
- $0.1 < \frac{D_{inter}}{D_0} < 10$: this region corresponds to an interplatelet diffusivity of the same order of magnitude as that of the matrix. The relative effective diffusivity increases as D_{inter}/D_0 increases. Its evolution shows an inflection point which is converging towards lower values when disks diameter and volume fraction increase. This region reveals the significant effect of the interplatelet diffusivity on the nanocomposite effective diffusivity and one must conclude that the barrier effect caused by increasing interplatelet spacing is compensated and even largely exceeded by the intra-stack diffusion effect;
- high values of $\frac{D_{inter}}{D_0}$: this region corresponds to highly diffusing interplatelet spaces, for which the effective diffusivity of the system increases with the interplatelet spacing. In this case, the contribution of interplatelet diffusion becomes very

significant. One must see here that all curves are converging to constant values showing that intra-stack diffusivity has, as expected, a local effect and then doesn't affect the overall diffusivity. At last, it can be observed that for $D_{inter}/D_0 \sim 10$, low disks diameters ($D=20$ nm and $D=40$ nm) and disks volume fraction values (0.11% and 0.44%), the nanocomposite system is being more permeable than the polymer matrix for large e_{inter} values. This result underlines that in some cases, the presence of stacks can be totally detrimental to barrier properties.

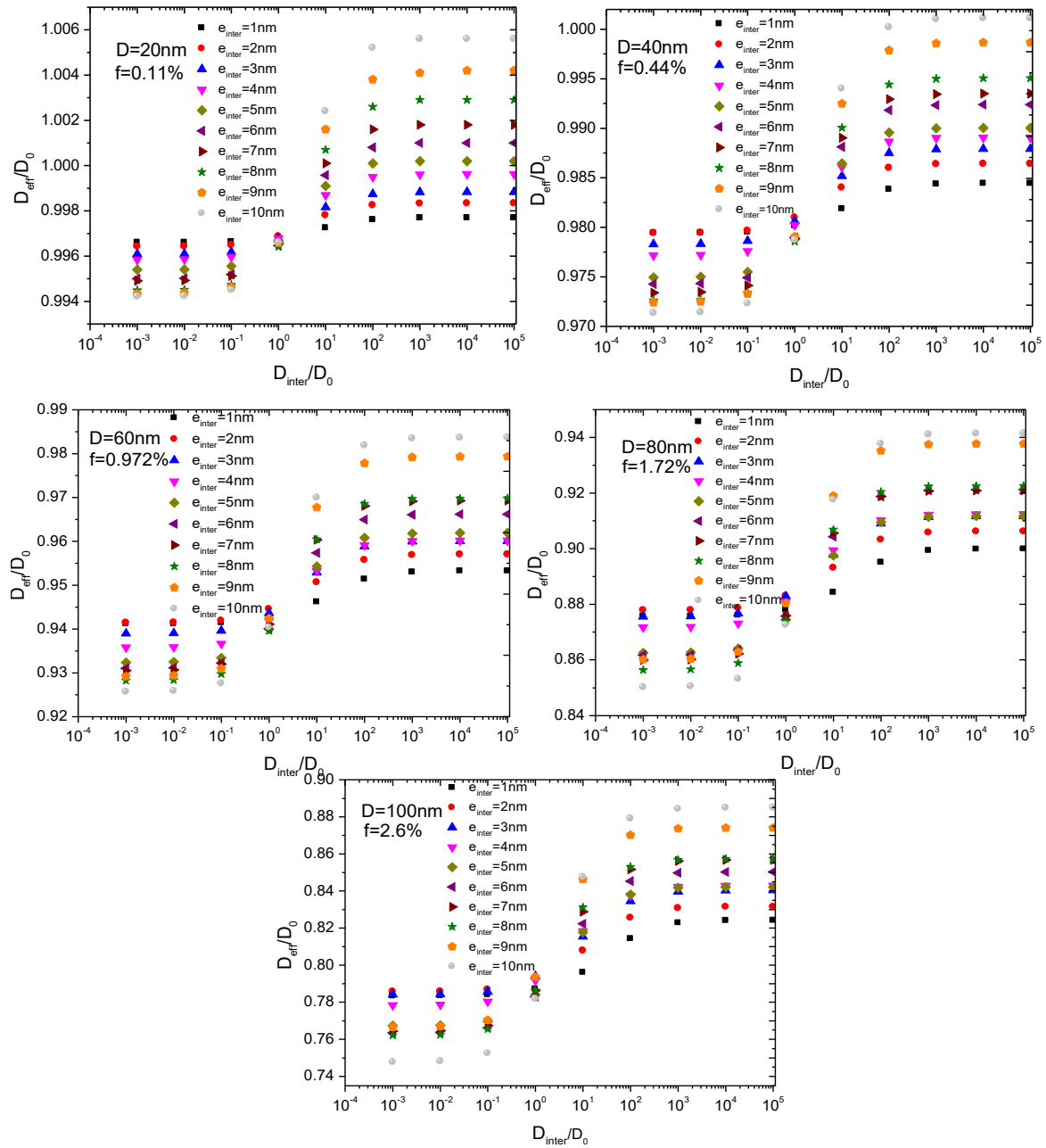


Figure A.3.16 Relative effective diffusivity variation versus D_{inter}/D_0 for several diameter values

3.4 Conclusion

In this study, a 3D numerical model of mass diffusion in nanocomposites, based on the Finite Element Method, was built in order to investigate the effects of several key morphological parameters on barrier properties. Different types of disk-shaped fillers, spatial distribution and size dispersion were taken into account in the model. Polydisperse fillers were found to be more efficient than monodisperse fillers for the enhancement of nanocomposites barrier properties, which is more apparent when the size polydispersity is large (Gaussian distribution). Furthermore, the simulations showed that on a given range of filler diameter, uniform (equiprobable) polydispersity is more effective than Gaussian polydispersity. These results were extended and validated in the case of intercalated nanocomposite systems. Accordingly, the developed model predicts that these systems are less efficient than exfoliated systems in the enhancement of barrier properties for an equivalent volume fraction value. Moreover, effective diffusivity was predicted to be strongly dependent on interplatelet spacing within stacks. The results were compared to fully impermeable stack for a large range of parameter values i.e. for large ranges of fillers size and interplatelet spacing values; the contribution of interplatelet spaces to overall diffusion in intercalated systems can be considered as limited when the intra-stack diffusion value is equal or below the matrix diffusivity value. However, it can be detrimental to barrier properties, especially when the platelet diameter is low, the interplatelet distance is important and its diffusivity exceeds that of the matrix by an order of magnitude.

Chapter 4 3D Numerical Analysis of Mass Diffusion in Nanocomposites: the Effect of the Filler-Matrix Interphase on Barrier Properties

An overview of the chapter

The first three chapters of Part A have focused on establishing the relationship between several key morphological parameters and the barrier properties of nanocomposite systems, assuming that such systems can be described by 2-phase models (a continuous phase: the matrix and a dispersed phase: the fillers). However, when synthesizing polymer-based nanocomposites, the adhesion between both phases can be insufficient to guarantee the absence of interfacial voids or defects, which results in the existence of an interfacial area, the “interphase”, having different diffusion properties from that of the matrix. Experimental studies have clearly demonstrated that the presence of interphases can significantly affect (positively or negatively) the barrier properties. Nevertheless, attempts to investigate the interphase effect through modeling have been scarce and to the best of our knowledge, the only numerical study reported in the literature considers 2D systems. In Chapter 4, the 3D finite element model developed in the previous chapters is expanded to include a third phase representing the filler-matrix interphase. The effect of the properties of the interphase (thickness, diffusivity) on the overall diffusivity of nanocomposites containing various contents of disk-shaped fillers is analyzed and discussed. Ideal ordered spatial distributions as well as random distributions are considered. Moreover, the effect of continuous diffusion paths, which may occur between overlapping interphases, is investigated.

4.1 Introduction

Organic or inorganic nanofillers are often introduced within polymer matrices to bring specific properties. Impermeable fillers with high aspect ratio such as montmorillonite, graphene, hydroxide double layers, zirconium-phosphate nanofillers... are widely used for barrier properties reinforcement (Cui et al., 2016; Follain et al., 2016; H. Kim et al., 2010; Wolf et al., 2018) whereas molecular sieves such as zeolites, metal organic frameworks, cyclodextrins... are exploited for their separation abilities (Bae et al., 2010; Goh, Ismail, Sanip, Ng, & Aziz, 2011; Grossi, Espuche, & Escoubes, 2001). Although nanocomposite systems have been most often considered as 2-phase systems composed of a continuous phase (the polymer matrix) and a dispersed phase (the nanofillers), several experimental studies showed that the matrix region located in the vicinity of the filler surface could be considered to form a third distinct phase with specific properties: the interphase. For example, Liang et al. (C. Y. Liang et al., 2012) showed that the interphase in their nanocomposite system (polyether sulfone (PES)/montmorillonite) included voids due to poor adhesion between hydrophobic polymers and hydrophilic particles, leading to high gas permeability values. Such behavior was also observed by Clémenson et al. in polyvinyl alcohol (PVA)/Ag nanocomposite systems (Clémenson, Léonard, Sage, David, & Espuche, 2008). Koros described the different possible behaviors of the interfacial regions in the case of mixed matrix membranes as a function of the polymer chain packing density and mobility near the sieves (Mahajan & Koros, 2000, 2002a, 2002b; Moore & Koros, 2005; Moore, Mahajan, Vu, & Koros, 2004). In order to ensure a homogeneous dispersion of the nanofillers within the polymer matrix and to avoid the presence of defects such as voids in the interphase domain that lead to totally uncontrollable transport properties, filler surface modification is often performed. Depending on the filler type, it can be based on ionic exchange or on grafting organic species of different chain lengths and mobilities (Dal Pont et al., 2012, 2013; Giannelis, 1996; Morel et al., 2012, 2016; Okada & Usuki, 1995; Picard, Gauthier, et al., 2007; Pinnavaia, 1983). The nanocomposites based on such modified fillers cannot be considered as binary systems and a clear contribution of the interphase has been experimentally evidenced by several authors working on nanocomposites for barrier applications. In some cases, the interphase led to reinforced barrier effects (Espuche et al., 2005; Gain et al., 2005; Picard, Gérard, & Espuche, 2015) through strong filler/matrix interfacial interactions whereas a loss of barrier properties was clearly observed in other cases where increased mobility or lack of packing density were evidenced in the region surrounded

the nanofillers (C. Y. Liang et al., 2012; Sabard, Gouanvé, Espuche, Fulchiron, Fillot, et al., 2014b; Suzuki & Yamada, 2005; Waché, 2004; Waché, Klopffer, & Gonzalez, 2015).

Several models have been proposed in literature to describe the interphase effects on nanocomposites for barrier properties (Cornelius & Marand, 2002; Nielsen, 1967; Osman, Mittal, Morbidelli, & Suter, 2003; Tenn et al., 2013; Waché, 2004; Waché et al., 2015). Most of the existing models were based on geometrical/analytical approaches (Nielsen, 1967). Nielsen proposed a theoretical model where the total permeability in the nanocomposite system is composed of two parts: the permeability of the filled polymer and the permeability of the interphase layer, which has been defined as a volume between the filler and the polymer matrix where a non-negligible fraction of liquid can be trapped. Considering interfacial effects, Waché and coworkers defined the interphase layer as a domain surrounding the fillers through which diffusing species can either easily penetrate or not. The volume fraction assigned to the interphase is negligible compared to the filler volume fraction meaning that the diffusion rate in the interphase is considered to be the main parameter. Their model is applied to liquid permeation in polyethylene based nanocomposites for either strong (higher density) or weak (higher mobility) interphase regions (Waché, 2004; Waché et al., 2015). Recently, a numerical approach has been developed by Minelli (Minelli, 2009). He conducted finite volume simulations in order to study the effect of the interphase layer on the overall diffusivity of polymer layered silicates. He showed that the barrier effect is in a lesser extent enhanced when the interphase layer is very diffusive for different interphase thickness values (0.5, 1 and 10 times the thickness of the filler) and filler volume fraction values (5 and 10 vol %). However, Minelli's model is based on two-dimensional geometries, which is relevant in the case of elongated fillers such as ribbons, but constitutes a significant approximation in the case of short platelets or flakes. In addition, the considered set of filler volume fraction values (5 and 10 vol %) is somewhat limited.

The aim of the present paper is to analyze, through finite element modeling, the effect of the interphase layer on the barrier properties of nanocomposites loaded with disk-like fillers. In order to simulate mass diffusion in such systems, three-dimensional representative geometries will be considered. Moreover, two types of filler spatial distributions will be investigated: ideal ordered distributions and random distributions, which are a more realistic way of describing actual materials. For both cases, the possibility of interphase overlapping (depending on the distance between filler layers in the overall diffusion direction) will be taken into account. Indeed, interphase overlapping may lead to the occurrence of continuous

diffusion paths through the whole thickness of the nanocomposite and then significantly influence the effective transport properties. According to our knowledge, it is the first time that such configurations are investigated through numerical modeling. Thus a parametric study considering a large range of interphase diffusivity values will allow understanding and quantifying these effects over a wide spectrum of cases ranging from virtually impermeable interphase to highly diffusive interphase and from diluted (low filler volume fraction) to concentrated (high filler volume fraction) regimes.

4.2 Modeling Methodology

4.2.1 Geometry

As described in the second chapter of this part 3.2.1, the geometric modeling of the nanocomposite system is based on a three-dimensional representative volume element (RVE) approach. The simulation domain representing the RVE is parallelepipedic in a Cartesian coordinate system (x, y, z) , with z the overall diffusion direction (**Figure A.4.1**). In the present work, fillers are modeled as impermeable disks (diameter D , thickness e , aspect ratio $\alpha = D/e = 50$) oriented normally to the overall flux direction z . The discoidal shape of nanofillers was adopted because it is widely used and convenient to model platelet-like nanofillers (Espuche et al., 2005; Gain et al., 2005; Morel et al., 2016; Picard et al., 2015). The interphase surrounding the filler is modeled as an intermediate layer with homogeneous thickness (e_{int}). Two types of spatial filler distributions are investigated in this work: ordered distributions and random distributions. In all cases, the range of filler volume fraction f is within 0 - 20% and the interphase thickness e_{int} ranges between 0.25 nm and 1 nm. This interphase thickness range has been chosen according to data from literature (Minelli, 2009).

4.2.1.1 Ordered distribution

In order to model diffusion in ordered nanocomposites, nanofillers were positioned in the polymer matrix following an ordered and periodic distribution. This configuration has been derived from the previous chapter and it is depicted in **Figure A.4.1**. The unit cell has dimensions p_x and p_y in the x - y plane, which are the distances separating the centers of two adjacent fillers in the x and y directions. The space step in the diffusion direction (thickness-wise direction) p_z is defined as the distance between two identical layers (from filler mid-plane to filler mid-plane) and was fixed to 10 nm. Assuming that $p_x = p_y$, the in-plane unit cell dimension p_x is given as a function of the filler volume fraction as:

$$p_x = \left(\frac{\pi D^2 e}{2f p_z} \right)^{1/2} \quad (\text{A.4.1})$$

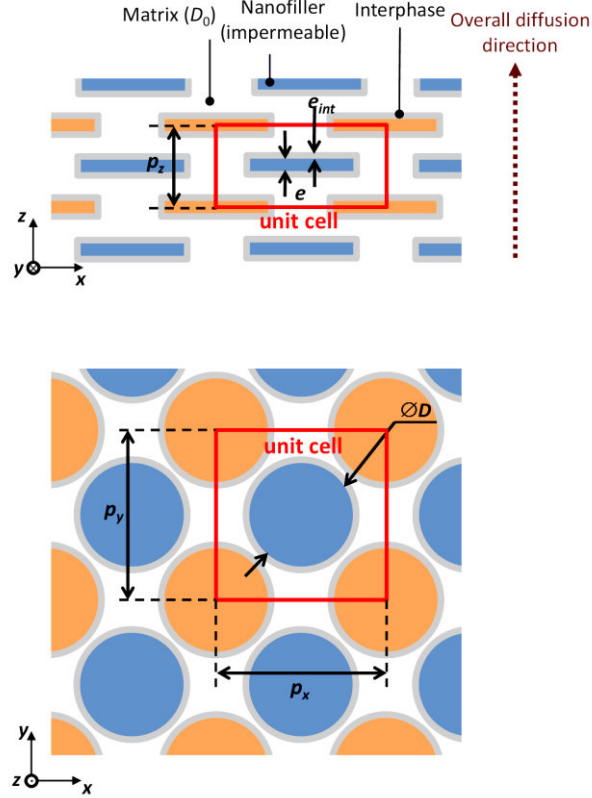


Figure A.4.1 Thickness-wise and plane-wise views of the 3D geometrical model of the ordered distributions

4.2.1.2 *Random distribution*

In this type of configuration, the disks are also oriented perpendicular to the overall diffusion direction. The random positioning of fillers in the computational domain was generated using a JAVA algorithm coupled with the commercial finite element package COMSOL Multiphysics. This algorithm contains conditions that ensure non-overlapping of the generated disks (fillers cannot overlap, but interphases can). The built RVE has dimensions 500 nm x 500 nm x 10 nm and contains three layers of fillers (**Figure A.4.2**).

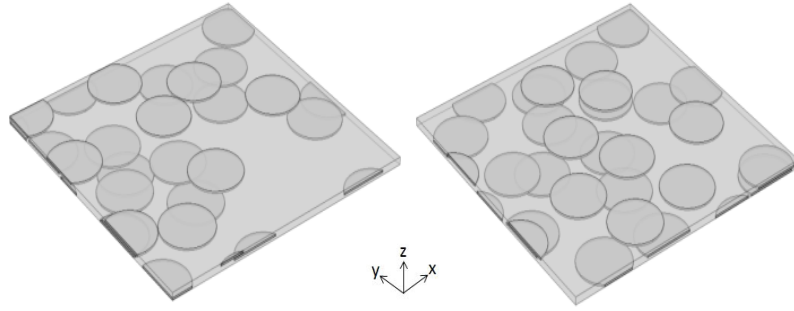


Figure A.4.2 Two examples of generated RVE in the case of random filler distribution

4.2.1.3 Interphase overlapping

It is noteworthy that for both types of studied configurations, an overlapping of the interphases may occur, leading to the formation of continuous diffusion pathways that could affect nanocomposite barrier properties. **Figure A.4.3** illustrates several examples of configurations leading or not to the formation of a thickness-wise continuous path through interphases.

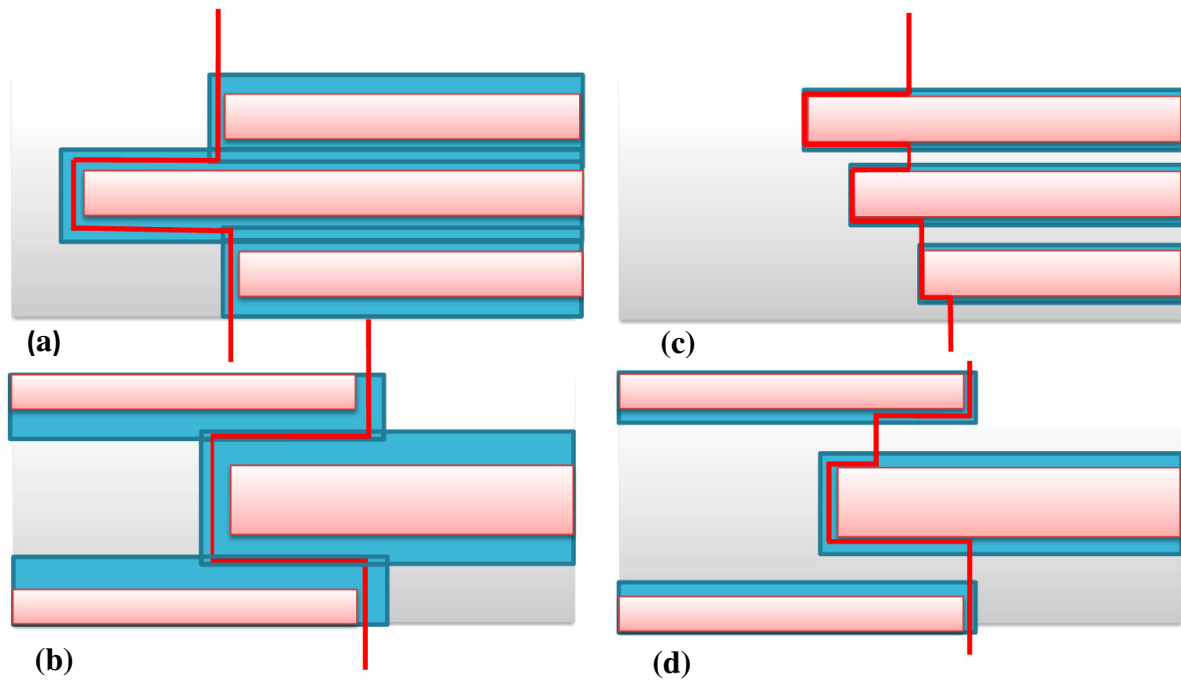


Figure A.4.3 Molecular diffusion path (red lines) for different cases: **(a)** a continuous path formed by overlapping of interphase layers for random distribution ($e_{int} = 1$ nm); **(b)** a continuous path formed by overlapping of interphase layers (blue regions) for ordered distribution ($e_{int} = 1.75$ nm); **(c)** the absence of the continuous path for random distribution ($e_{int} = 0.25$ nm); **(d)** the absence of continuous path for ordered distribution ($e_{int} = 0.25$ nm)

In ordered distributions, a continuous path in z direction is obtained for the following geometrical conditions expressing interphase contiguity: $4e_{int} + 2e \geq p_z$ (thickness-wise) and $\frac{p_x\sqrt{2}}{2} \leq D + 2e_{int}$ (plane-wise). These inequalities respectively lead to: $e_{int} \geq \frac{p_z - 2e}{4}$ and $f \geq \frac{\pi D^2 e}{4p_z(D + 2e_{int})^2}$.

Thus, considering a p_z value equal to 10 nm and a disk thickness equal to 2 nm, the interphase layer should be at least 1.5 nm and the filler volume fraction should be at least 14.8 % in order to obtain interphase overlapping (**Figure A.4.3 (b)**).

For randomly distributed fillers, the continuous path in z direction can potentially occur for $6e_{int} + 3e \geq p_z$, which means that the interphase layer should be thicker than 0.66 nm (**Figure A.4.3 (a)**). This condition is necessary but not sufficient, but as opposed to the case of ordered systems, a threshold volume fraction value cannot be inferred: the randomness of the positioning does not guarantee that a given interphase belonging to layer i is contiguous with an interphase belonging to layer $i + 1$. However, the higher the filler volume fraction, the higher the probability of occurrence of interphase overlapping.

4.2.2 Mass diffusion equation and boundary conditions

The mass diffusion process in the defined computational domains is described according to Fick's second law, which is expressed, in the absence of mass source and in stationary regime, by the following partial differential equation (PDE):

$$\nabla \cdot (-D_{ij} \vec{\nabla} c_i) = 0 \quad (\text{A.4.2})$$

where c_i (mol.m⁻³) is the molar concentration of the permeating specie i and D_{ij} is the mass diffusion coefficient (or diffusivity) of permeating specie i in medium j . In the present case, it is assumed that diffusion can occur in the matrix phase and in the interphase layer. The diffusivity of the considered specie in the matrix phase and the interphase layer is denoted as D_0 and D_{int} respectively. In the numerical simulations, a constant value $D_0 = 10^{-12}$ m².s⁻¹ has been adopted (a representative value of gas diffusion in polymers as reported in section 2.2.3 and 3.2.3). The interphase diffusion coefficient was defined relative to the matrix diffusion coefficient in order to account for various types of interphase behavior: diffusion resistant interphase (low D_{int}/D_0 values, in the range $[10^{-4} - 10^{-1}]$), iso-diffusive interphase ($D_{int}/D_0 = 1$) and highly diffusive interphases (D_{int}/D_0 values beyond 10). In the following, the variable

associated with the molar concentration of the permeating specie at any point of the computational domain (*i.e.* the concentration field) is denoted by $c(x, y, z)$.

In order to obtain a well-posed boundary value problem, the mass diffusion equation was solved considering the following boundary conditions:

- concentration boundary conditions were imposed on the lower ($z = 0$) and upper ($z = p_z$) faces of the unit cell, respectively $c(x, y, 0) = c_1 = 1000 \text{ mol.m}^{-3}$ and $c(x, y, p_z) = c_2 = 500 \text{ mol.m}^{-3}$. Since the matrix diffusivity is assumed constant and not concentration-dependent, the concentration values chosen as boundary conditions for the upper and lower faces have rigorously no influence on the calculated effective diffusivity;
- periodic boundary conditions (PBC) were the same as those applied in the first chapter for ordered distribution of disks in the matrix. However, in the case of random distribution there is no periodicity of the RVE, thus no-flux boundary conditions (mimicking symmetry) were applied instead of PBC;
- no-flux boundary conditions were imposed on all filler-interphase boundaries in order to model the impermeability of the fillers;
- concentration continuity and flux continuity were assumed at the interphase-matrix boundaries.

Figure A.4.4 summarizes the main boundary conditions applied on the studied geometries.

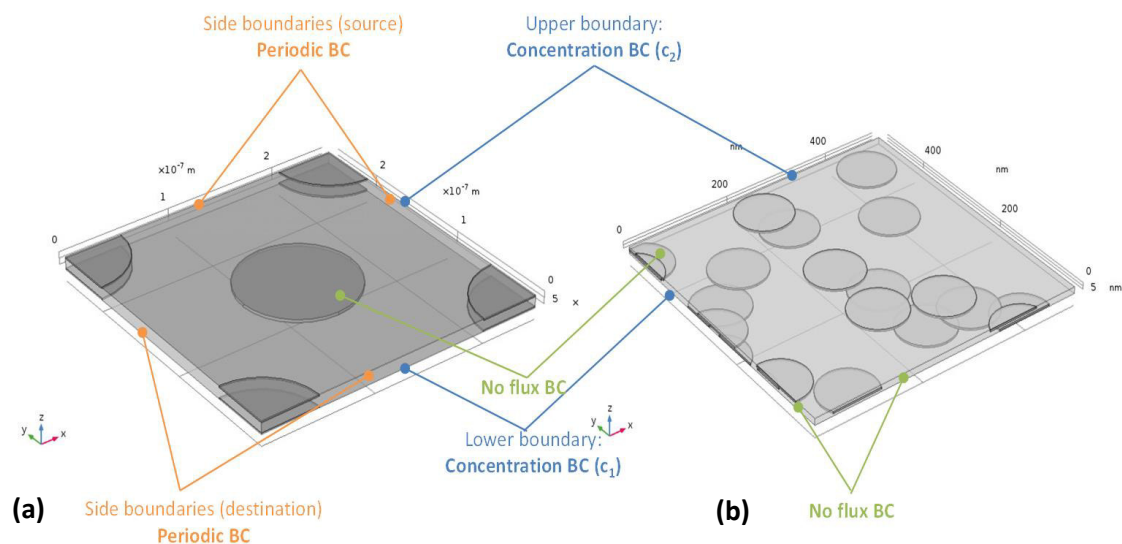


Figure A.4.4 Representation of the RVE showing the boundary conditions: **(a)** ordered distribution; **(b)** random distribution

4.2.3 Numerical solution and effective diffusivity evaluation

The FEM requires proper discretization (or meshing) of the computational domain in order for the numerical solver to provide accurate and stable results. Since the fillers are assumed impermeable, only the matrix and interphase domains must be meshed. An unstructured mesh consisting of tetrahedral elements was generated and refined sufficiently to ensure obtaining a mesh-independent solution, meaning that the results are not affected by any numerical artifact arising from the discretization method (**Figure A.4.5**).

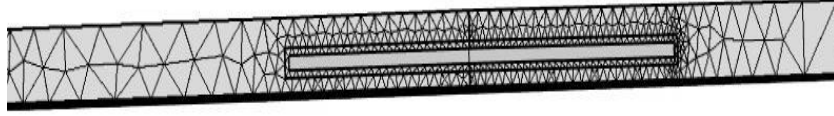


Figure A.4.5 Discretization of the computational domain in the vicinity of a filler

The solution of the boundary value problem yields the molar concentration field of the permeating species $c(x, y, z)$. The used machine for the calculations is a DELL computer with i3 processor and 8 Go of RAM. The computational time was between 1 and 5 min for ordered distributions with low interphase thickness values and between 5 and 30 min for the other configurations. Then, the mass flux vector field of the permeating species can be calculated from the concentration field:

$$\vec{N}(x, y, z) = -D_0 \vec{\nabla} c(x, y, z) \quad (\text{A.4.3})$$

The effective diffusivity of the nanocomposite is finally given by:

$$D_{eff} = \frac{\overline{N_z} p_z}{c_1 - c_2} \quad (\text{A.4.4})$$

where $\overline{N_z}$ is the average mass flux of the permeating species across a plane section S normal to z -direction and located at $z = z_0$ within the unit cell:

$$\overline{N_z} = \frac{1}{p_x p_y} \iint_S N_z(x, y, z_0) dx dy \quad (\text{A.4.5})$$

with N_z the z -component of the mass flux vector. It should be noted that the mass conservation principle and the periodic boundary conditions ensure that the average mass flux is the same in any plane section. Hence, z_0 could be indifferently any value chosen between 0 and p_z . In the present work, the mass flux surface integral was evaluated on the upper face of the unit

cell (*i.e.* $z_0 = p_z$). The most convenient parameter for characterizing and comparing the barrier effect obtained in the different simulated nanocomposite systems is the relative effective diffusivity, defined as the ratio D_{eff}/D_0 . One should note that this dimensionless quantity is not dependent on the neat matrix diffusivity D_0 , as shown in the previous chapters.

4.3 Results and Discussion

In this section, results will be presented and discussed for both types of filler arrangement (ordered and random) in the polymer matrix, considering two complementary cases:

- case A: interphases are thin enough and filler volume fraction is low enough to prevent overlapping in z -direction and the formation of a continuous diffusion path;
- case B: interphases are thick enough and filler volume fraction is high enough to overlap and a continuous diffusion path may be formed through the whole domain thickness.

4.3.1 Ordered filler distribution

4.3.1.1 Case A: No continuous diffusion path through interphases

Diffusion in systems composed of regularly distributed fillers surrounded by interphase layers with thickness varying from 0.25 to 1 nm was simulated using the RVE presented in **Figure A.4.4** (a). The calculated relative effective diffusivity versus relative interphase diffusivity values are shown in **Figure A.4.6** for fillers volume fractions ranging between 1 % and 9 %.

All curves exhibit a similar sigmoidal shape where three distinct domains can be easily discriminated: the first one corresponds to low values of D_{int}/D_0 (between 10^{-4} and 10^{-1}), the second one to D_{int}/D_0 values ranging between 10^{-1} and 10^4 and the third one corresponds to high values of D_{int}/D_0 (beyond 10^4).

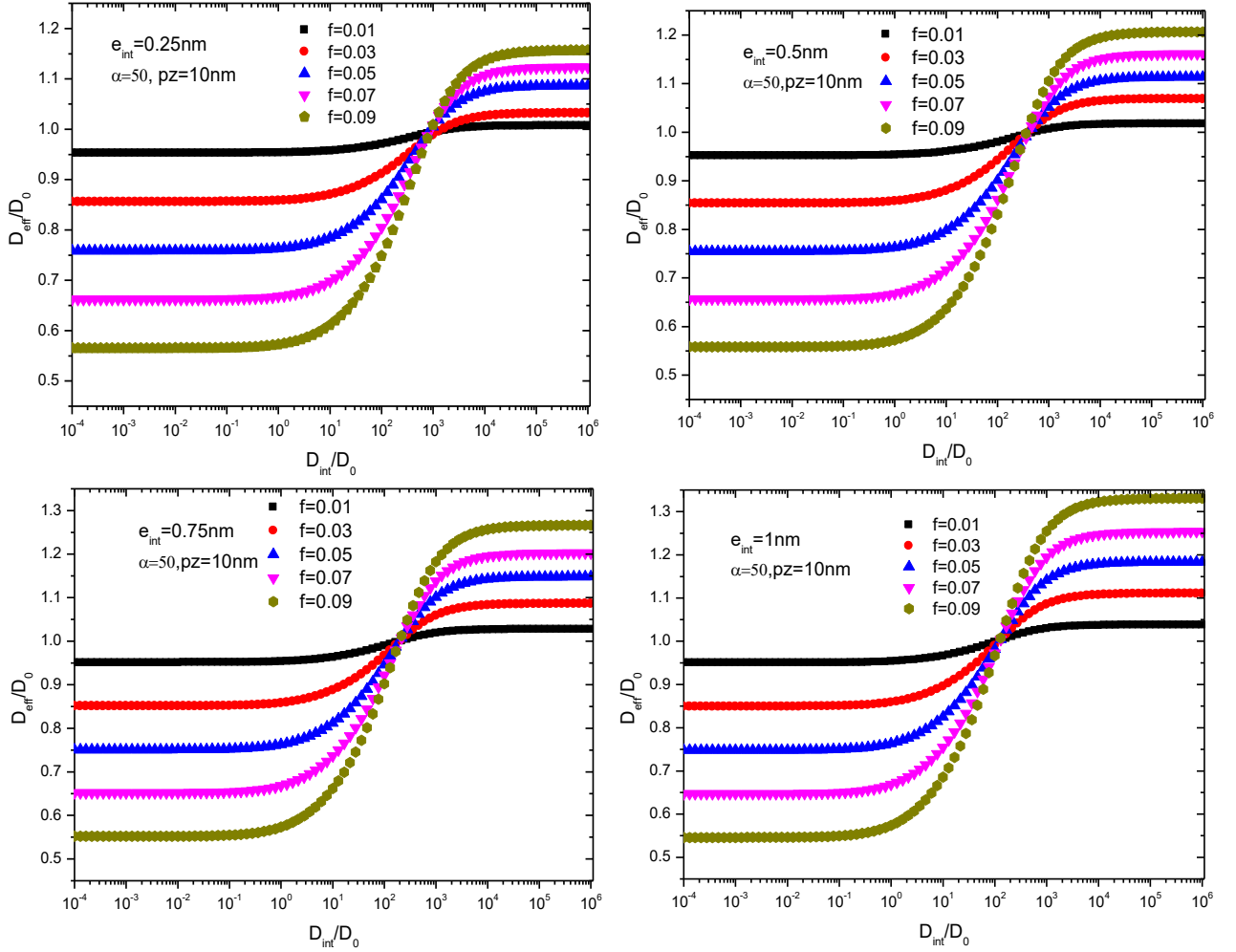


Figure A.4.6 Relative effective diffusivity versus relative interphase diffusivity for several interphase thickness values and filler volume fractions in ordered filler distribution

4.3.1.1.1 1st Domain: low values of D_{int}/D_0

In this domain ($D_{int}/D_0 < 10^{-1}$), the relative effective diffusivity is almost constant for a given interphase thickness and filler volume fraction. Moreover, for a fixed value of e_{int} , the overall diffusivity decreases when filler volume fraction increases. In addition, for a fixed filler volume fraction, the relative effective diffusivity decreases as e_{int} increases (e.g. for $f = 9\%$ a decrease of 2.94% is observed when e_{int} goes from 0.25 to 1 nm). In all cases, the plateau shape defined by the curves in this domain suggests that the contribution of the interphase to the overall diffusivity could be considered as negligible. To confirm this hypothesis, the relative effective diffusivity values obtained for a system in which $D_{int}/D_0 = 10^{-4}$ were compared with those calculated for a system containing equivalent fully impermeable disks (diameter $D + 2e_{int}$; thickness $e + 2e_{int}$). **Figure A.4.7** reports the results obtained for two different interphase thickness values 0.25 and 1 nm, respectively.

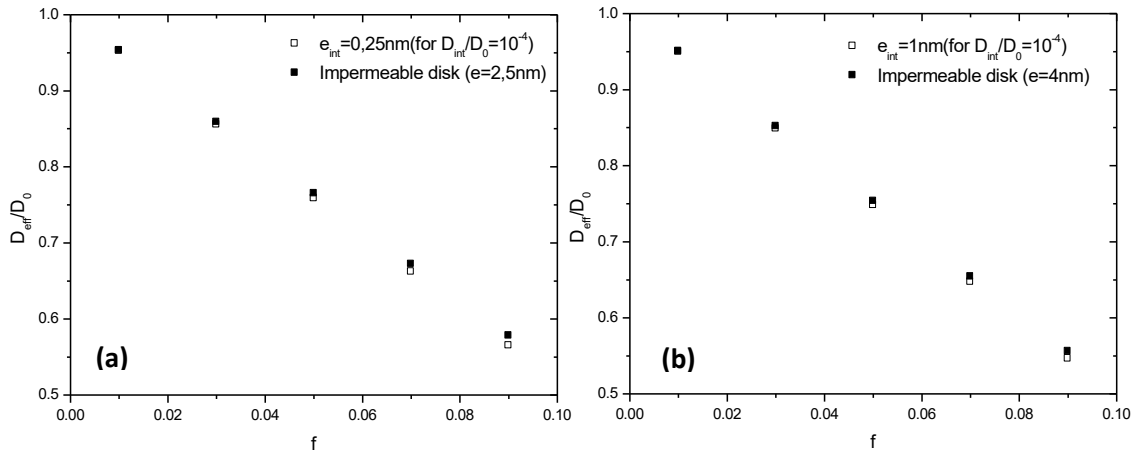


Figure A.4.7 Comparison between the overall diffusivity for systems presenting low diffusivity interphase and fully impermeable interphase (a) $e_{int} = 0.25 \text{ nm}$; (b) $e_{int} = 1 \text{ nm}$

The difference between both configurations is very small (less than 2.25% for $e_{int} = 0.25 \text{ nm}$ (Figure A.4.7 a) and less than 1.7% for $e_{int} = 1 \text{ nm}$ (Figure A.4.7 b) considering the filler volume range up to 9%). This result shows that fillers surrounded by a weakly diffusive interphase layer can be assimilated to impermeable fillers dispersed in the polymer matrix. To consolidate this result, diffusive flux lines were analyzed in the vicinity of the impermeable fillers surrounded by a low diffusive interphase ($D_{int}/D_0 = 10^{-4}$) and in the vicinity of the corresponding fully impermeable filler (Figure A.4.8).

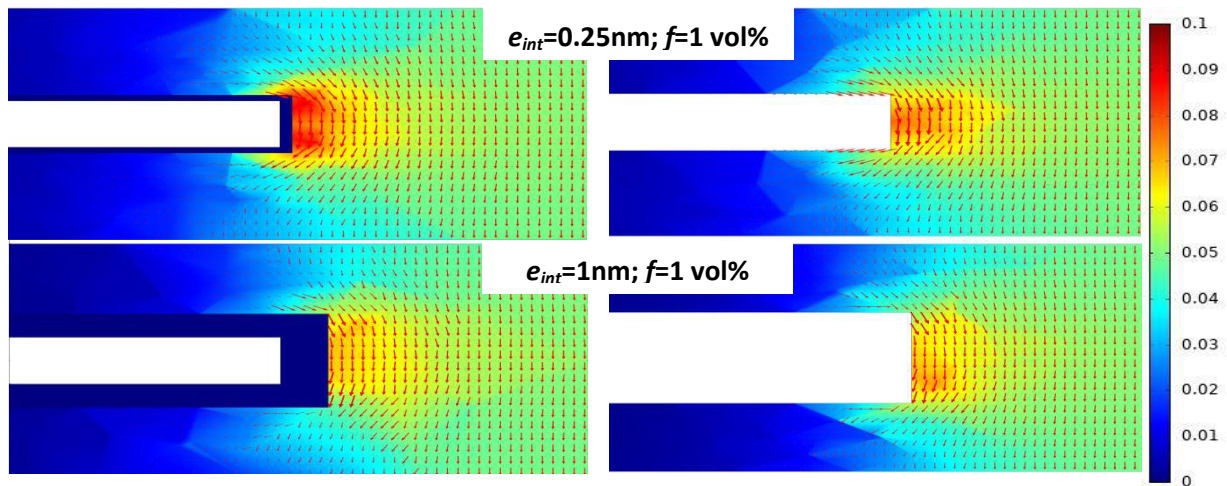


Figure A.4.8 Diffusive flux magnitude field ($\text{mol.m}^{-2}.\text{s}^{-1}$) and diffusive flux vector field in the vicinity of an impermeable filler surrounded by a low diffusivity interphase ($D_{int}/D_0 = 10^{-4}$) (left) and in the vicinity of the equivalent fully impermeable filler (right). Arrow length is proportional to the flux magnitude.

The quasi-zero flux value and the absence of flux vector of significant magnitude in the interphase domain confirm the negligible contribution of the interphase to diffusion.

Moreover, for a fixed interphase thickness, it can be observed that the diffusive flux field in the polymer matrix surrounding the fillers is almost the same in the system modeling explicitly the filler and the interphase and in the system based on the equivalent fully impermeable filler, which supports the assumption that considers both systems equivalent. Indeed, the observable local discrepancies in field values between the 3-phase model and the 2-phase model can be mainly attributed to a slightly different meshing due to the absence of interphase in the case of the 2-phase model.

4.3.1.1.2 2nd Domain: D_{int}/D_0 within the range $[10^{-1}-10^4]$

This domain corresponds to D_{int}/D_0 values between 10^{-1} and 10^4 . In fact, as the interphase diffusivity reaches that of the neat polymer, the interphase plays a more significant role in the transport process. As it can be observed in **Figure A.4.6**, for all filler volume fraction values, the relative effective diffusivity is increasing with D_{int}/D_0 in this domain. It is noteworthy that for a given interphase layer thickness, all curves intersect at a common point corresponding to $D_{eff}/D_0 = 1$. At this specific point, the tortuosity effect is exactly compensated by a higher diffusion rate in the interfacial region than in the neat matrix. In order to better analyze this behavior, the D_{int}/D_0 values corresponding to $D_{eff}/D_0 = 1$ were plotted in **Figure A.4.9** for several values of the interphase thickness.

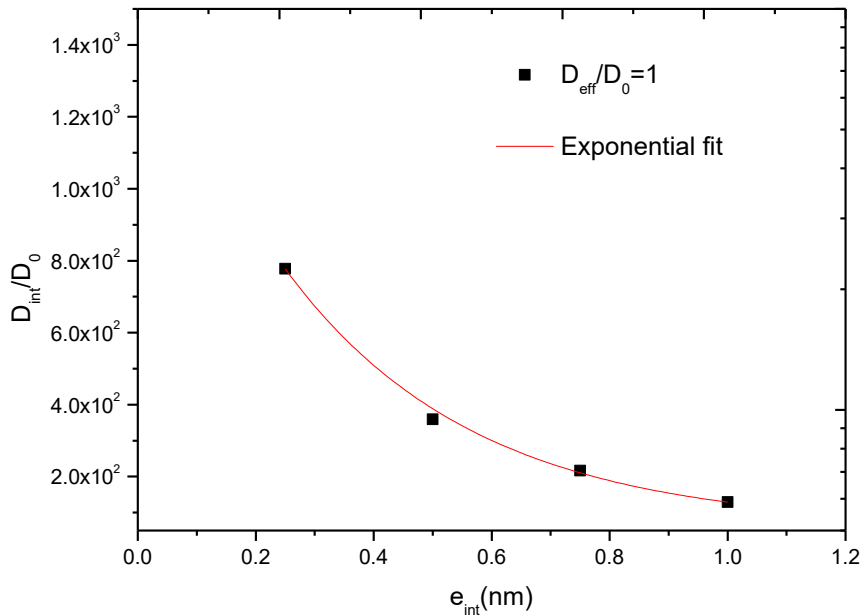


Figure A.4.9 D_{int}/D_0 values corresponding to $D_{eff}/D_0 = 1$ versus interphase thickness values

One must see through **Figure A.4.9** that the D_{int}/D_0 values leading to $D_{eff} = D_0$ are much higher than 1. In addition, as the interphase thickness increases, D_{int}/D_0 follows an exponential decrease. This means that for thin and highly diffusive (respectively thick and

weakly diffusive) interphases, the overall diffusivity could be equal to the neat matrix diffusivity, cancelling the barrier effect induced by the fillers themselves.

4.3.1.1.3 3rd domain: high values of D_{int}/D_0 ($>10^4$)

In this region corresponding to highly diffusive interphases, the effective diffusivity of the system stops increasing and reaches a plateau. **Figure A.4.10** shows that the D_{eff}/D_0 plateau values increase as the diffusion rate in the interphase layers increases. Moreover, increasing the filler content also leads to increased values of D_{eff}/D_0 . This result can be explained by the fact that as the filler content increases, the volume fraction of interphases in the system also increases.

In order to have a complete overview of the effect of both kinds of interphases (highly diffusive or weakly diffusive) on effective diffusivity, the lower and upper asymptotic relative effective diffusivity values determined in each plateau domain have been reported in **Figure A.4.10** as a function of filler volume fraction for the different investigated interphase thickness values.

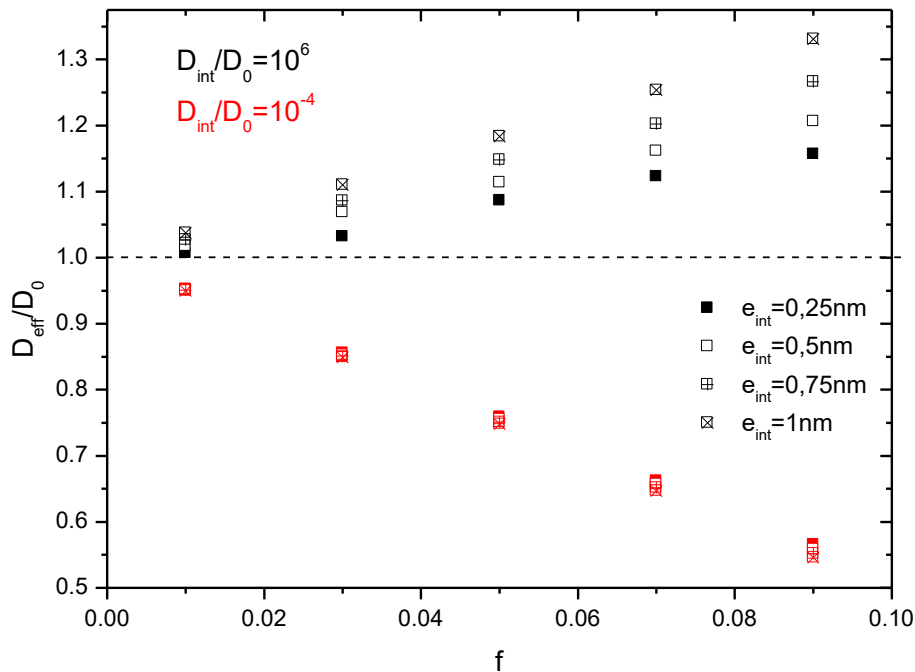


Figure A.4.10 Lower and upper asymptotic values of the relative effective diffusivity versus fillers volume fraction for several interphase thickness values

On one hand, when the diffusivity in the interphase layer is low, relative effective diffusivity decreases as the filler volume fraction increases. Moreover, the discrepancies between the relative effective diffusivity values obtained for the different interphase thickness values are

very small. As previously discussed, the filler + interphase domain can be regarded as fully impermeable filler, meaning that the transport properties are mainly governed by the tortuosity effect. As the tortuosity directly depends on the filler aspect ratio and as the interphase thickness remains low in comparison to the filler dimensions, one can consider that the tortuosity does not vary significantly. On the other hand, in the case of highly diffusive interphases, the overall diffusion increases with filler volume fraction, especially for high interphase thickness values. It can be observed that the more the interphase thickness and filler volume fraction f are high, the more the deviation between simulation results is significant (for $f = 1$ %, the difference observed between relative effective diffusivity values for $e_{int} = 0.25$ nm and $e_{int} = 1$ nm is 3.07 %, whereas it is about 17.4 % for $f = 9$ %). This confirms the major effect of the interphase on the transport properties especially when it is highly diffusive.

4.3.1.2 Case B: Continuous path through interphases

It has been shown that discrete interphases could play a relevant role in changing the transport properties of nanocomposite systems depending on their size and intrinsic properties. Thus, it is of great interest to know whether this effect can be emphasized by combining sufficiently high values of filler volume fraction and interphase layer thickness. For ordered filler distributions and considering the range of filler volume fraction and interphase layers thickness investigated ($f < 20$ % and $e_{int} < 2$ nm), this configuration can only occur in concentrate regime *i.e.* for $f > 14.8\%$ and $e_{int} > 1.5$ nm. Two different values of filler volume fraction (15% and 20%, respectively) were considered in order to obtain geometries featuring a continuous diffusion path through interphase layers. The simulations yielded the evolution of D_{eff}/D_0 as a function of interphase thickness as represented in **Figure A.4.11** for two values of D_{int}/D_0 : 10^{-3} and 10^4 . These values were chosen to be representative of a weakly diffusive interphase and a highly diffusive interphase, respectively.

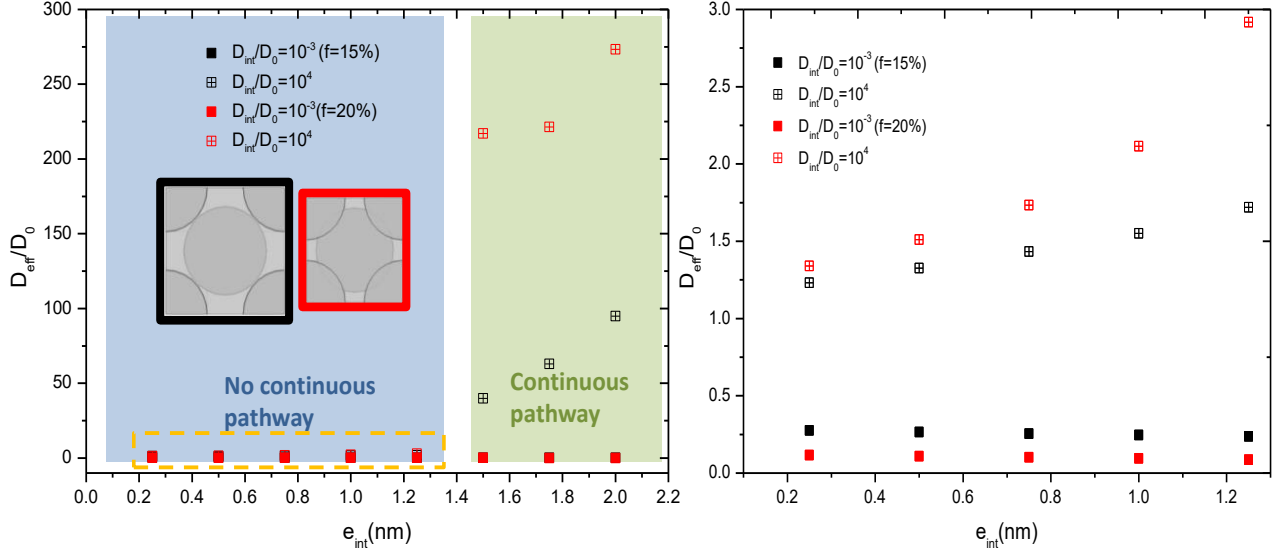


Figure A.4.11 (a) Relative effective diffusivity variation as a function of interphase thickness showing the presence of the continuous path **(b)** Zoom in the discontinuous pathway part showing differences in D_{eff}/D_0 values

It can be noticed that when interphase layer thickness is ranging between 0.25 and 1 nm, all D_{eff}/D_0 values are below 1 for $D_{int}/D_0 = 10^{-3}$ and they are comprised between 1.2 and 2.15 for $D_{int}/D_0 = 10^4$. Moreover, the diffusivity variation appears as limited for a given filler volume fraction. This trend is in agreement with the results discussed previously which refer to discontinuous interphases paths. For interphases thicknesses higher than 1.4 nm, a totally different behavior is observed. For $D_{int}/D_0 = 10^{-3}$, D_{eff}/D_0 values rises from 0.0775 to 0.2 when the interphase thickness increases from 1.5 to 2. For D_{int}/D_0 value equal to 10^4 , a large increase of D_{eff}/D_0 values is evidenced reaching 272.5. For the considered filler volume fractions (15 and 20 vol %) and e_{int} values higher than 1.55 nm, interphase layers are being interconnected. The continuous paths that are formed through the sample thickness represent easy diffusion paths for penetrant molecules especially when D_{int}/D_0 values are higher than 1 and these paths highly contribute to the overall transport phenomenon. For low D_{int}/D_0 values, the continuous paths still represent resistant diffusion paths in comparison with the matrix so that the tortuosity effect is predominant in this case.

4.3.2 Random filler distribution

For this type of distributions, disks positions were randomly determined by the generation algorithm. The actual filler volume fractions were calculated through a volume integration of the generated simulation domains and were varied between 1.09% and 9.56%.

4.3.2.1 Case A: No continuous diffusion path through interphases

It has been mentioned before that formation of continuous interphase paths for a random distribution of disk-shaped fillers in the polymer matrix could be obtained for an interphase thickness value beyond 0.66 nm. Thus, e_{int} values equal to 0.25 nm and 0.5 nm were considered at first to avoid the creation of these continuous paths. The calculated relative effective diffusivity variation as a function of D_{int}/D_0 for several filler volume fractions f is reported in **Figure A.4.12**.

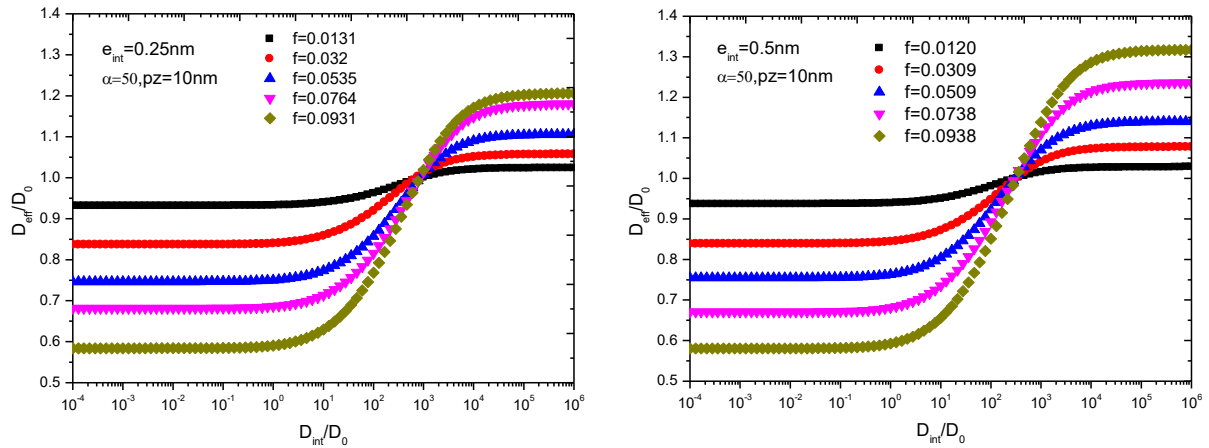


Figure A.4.12 Relative effective diffusivity variation as a function of D_{int}/D_0 for two different interphase thickness values ($e_{int} = 0.25$ nm and 0.5 nm)

The sigmoidal shape of the curves is very similar to that obtained in the case of ordered distributions of disks. Three main domains can be distinguished:

- the first domain (low D_{int}/D_0 value) is characterized by a plateau (lower asymptote) where relative effective diffusivity is almost constant for given filler volume fraction and interphase thickness. As in the ordered distribution case, the interphase layer can be considered as impermeable;
- the second domain features an increase of D_{eff}/D_0 values with D_{int}/D_0 and a characteristic point corresponding to iso-diffusivity ($D_{eff}/D_0 = 1$) for which all the curves intersect. **Figure A.4.13** reports the D_{int}/D_0 values that allow reaching $D_{eff}/D_0 = 1$ for the two interphase thickness values considered in these simulations. The results are compared to those obtained in the case of ordered disk distribution. Similar trends are evidenced in both cases, confirming the assumption that the presence of thin and highly diffusive interphases (and inversely, weakly diffusive and thick interphases) can counterbalance the tortuosity effect;

- the third domain observed at high values of D_{int}/D_0 (beyond 10^4) corresponds to a second plateau (upper asymptote) where relative effective diffusivity is higher than 1.

Figure A.4.13 b allows comparing the influence of the filler distribution type (ordered or random) on the relative effective diffusivity determined for the plateau at low and high D_{int}/D_0 values, respectively.

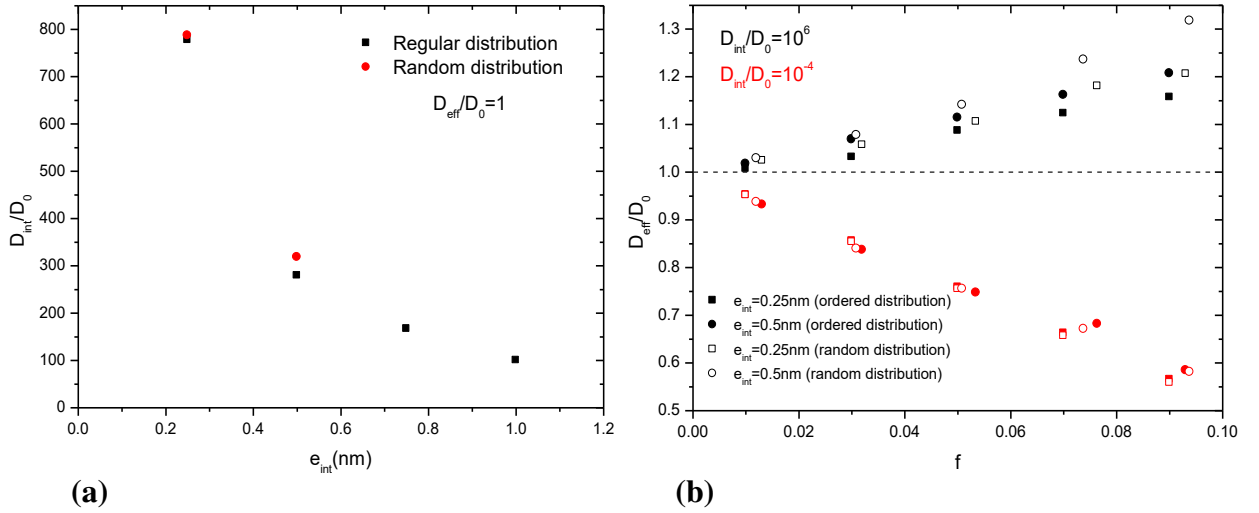


Figure A.4.13 Comparison between ordered and random distribution (a) D_{eff}/D_0 variation versus filler volume fraction for $D_{eff}/D_0 = 1$ (b) D_{eff}/D_0 variation versus filler volume fraction in the plateau domains

Similar trends are observed independently of the type of filler distribution with increasing D_{eff}/D_0 plateau values as a function of the filler volume fraction for highly diffusive interphases and decreasing D_{eff}/D_0 plateau values as a function of the filler volume fraction for low diffusive interphases. It is noteworthy that the random distribution of fillers leads to slightly higher D_{eff}/D_0 values for high D_{int}/D_0 value whereas it has no significant effect for low D_{int}/D_0 values. The differences observed for high D_{int}/D_0 values seem to increase as the filler volume fraction increases. Both high filler content and random filler distribution can thus favor filler neighboring leading to enhanced effective diffusivity when fillers are surrounded by diffusive interphases.

4.3.2.2 Case B: Continuous diffusion path through interphases

When fillers are randomly positioned in the RVE, the probability that interphase layers interconnect is very high in comparison with the ordered case. In the present work, we have investigated systems based on ordered filler distribution and random distribution for 7 and 9 vol% fillers. The interphase layer thickness values considered are 0.75 and 1 nm, respectively.

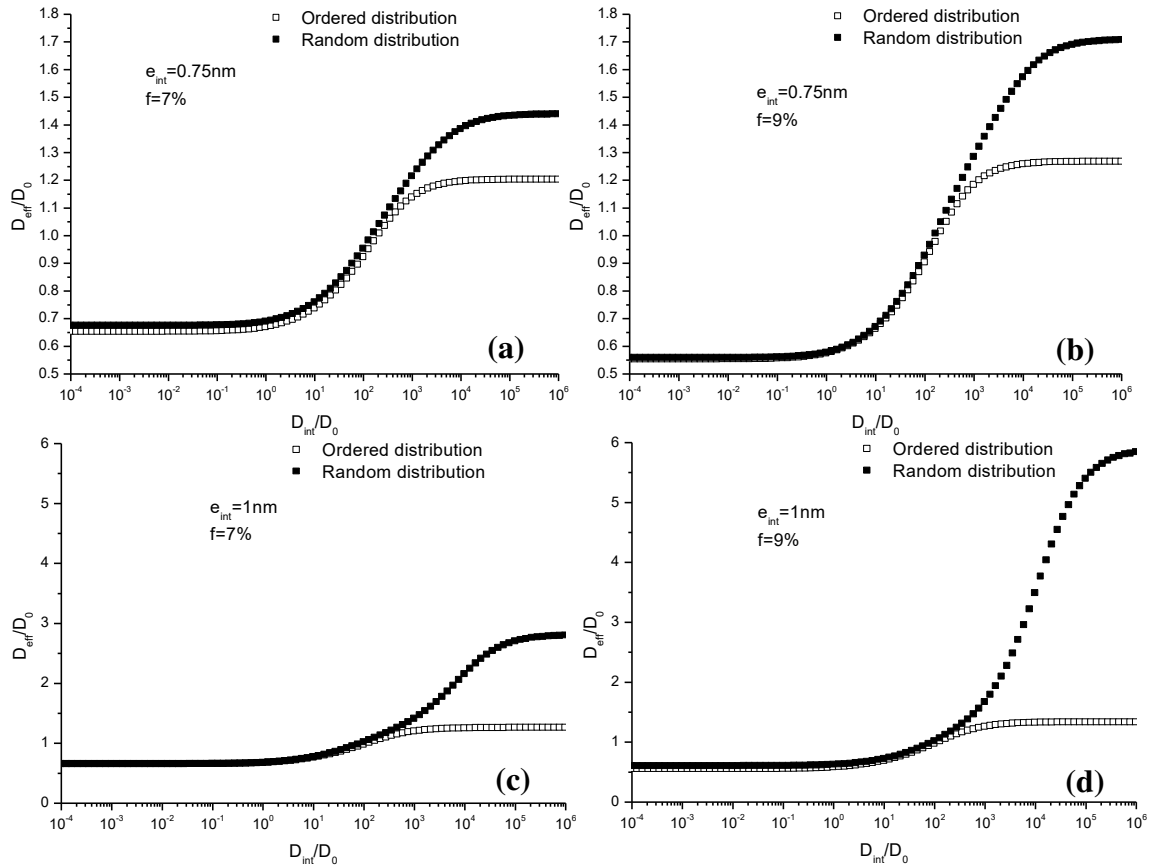


Figure A.4.14 Comparison between random and ordered configurations for two different filler volume fraction and interphase thicknesses

For low D_{int}/D_0 values, difference between ordered and random distributions of fillers in the system is not very important. In fact, in this range of values, the contribution of the interphase to the overall diffusivity is not significant regardless if there is a continuous path or not.

It can be seen through **Figure A.4.14** that difference between ordered and random distributions is clearly visible for highly diffusive interphases. In the random case, the conditions to form a continuous pathway between interphases are reached whereas the continuous path cannot be obtained for similar interphase thicknesses and filler volume fractions in the ordered case. Moreover, as explained before, the more filler volume fraction is increasing, the more D_{eff}/D_0 values are drastically increasing because interphase layers are being more interconnected. This effect can be confirmed by comparing **Figure A.4.14** (a) and (b) (D_{eff}/D_0 increases from 1.44 to 1.77) or **Figure A.4.14** (c) and (d) (D_{eff}/D_0 increases from 2.79 to 5.82) respectively. Additionally, increasing interphase layer thickness is also an important factor for the interconnection of interphases and thus increasing D_{eff}/D_0 values.

4.4 Conclusion

The current work is a numerical investigation of the interphase effect on the overall nanocomposite barrier properties. It has been shown through the developed FEM model that relative effective diffusivity is widely affected by the presence of the interphase for different values of filler volume fraction values. Depending on its quality (less or high diffusive), it can be beneficial or totally detrimental to the nanocomposite barrier properties. The results in the current work showed that the continuous path –caused by the interconnection between interphase layers- is particularly critical for barrier properties in the case of highly diffusive interphases. Indeed, in that case, it can promote the diffusion of the penetrating species, totally counterbalance the tortuosity effect and then leads to effective diffusivity values significantly higher than the diffusivity value of the pure matrix. Moreover, it has been shown that the continuous path effect may occur more easily (e.g. for lower filler volume fractions and thinner interphases) in the random distribution case compared to the regular one.

Part B Multiphase polymer systems for
improved gas separation properties

Chapter 1 Bibliographical study of multiphase polymer systems for improved gas separation properties

An overview of the chapter

After having presented in Part A of this thesis an in-depth analysis of the role of the parameters governing the barrier properties of nanocomposites based on polymer matrices and impermeable fillers, Part B is devoted to another subject of interest in the field of mass transport: the development of membranes for gas separation and especially CO₂ separation, which represents a real challenge nowadays.

Our work is focused on polymer-based membranes containing specific fillers in order improve the functional properties. These membranes are known as Mixed Matrix Membranes (MMMs). We have chosen to work with a promising type of filler that belongs to the metal organic framework (MOFs) family. The idea was to take advantage of the porous structure of the filler to improve the gas transport properties.

As in the case of nanocomposites for barrier properties, several bottlenecks must be addressed to obtain MMMs with interesting functional properties. The control of the filler dispersion state as well as the adaptation of the filler/matrix interface represents crucial parameters for obtaining optimized properties. Indeed the creation of defects at the filler/matrix interface is totally detrimental to the selectivity. On the other hand, a lack of accessibility of the porous structure of the filler by the gas is also detrimental to the membrane functional properties. We propose an original route to optimize the morphology and interfacial properties in our systems: the use of an ionic liquid. Finally a numerical simulation approach based on finite element modeling has been developed to confirm the role played by the ionic liquid in our systems.

Before describing more thoroughly these experimental developments, we will first define in this chapter the parameters of interest for the field of gas separation membranes. An overview of the different routes used to improve gas separation properties of polymer-based membranes will be presented from the analysis of literature data. We will also propose a summary of the existing analytical and numerical models related to gas separation properties.

1.1 Background and general description of gas separation membranes

Development of gas separation membranes is one of the fastest expanding technologies in polymer engineering today. In fact, the increasing interest paid on such membranes is due to the potential energy savings compared to conventional separation techniques (distillation, absorption,...) (Monsalve-Bravo & Bhatia, 2018). The separation process through membranes is based on the differential permeation of the components in one mixture. The first experiments on gas permeation membranes were conducted by Graham who studied the use of polymeric membranes and gave the first description of the “solution-diffusion mechanism” (Graham, 1866; Pandey & Chauhan, 2001).

Later, Fick studied gas diffusion through polymeric membranes and developed his own concept of diffusion known as “Fick’s laws” that describe quantitatively mass transport through boundary layers (S. Sridhar, Bee, & Bhargava, 2014). The background of gas separation membranes history is presented in **Figure B.1.1**.

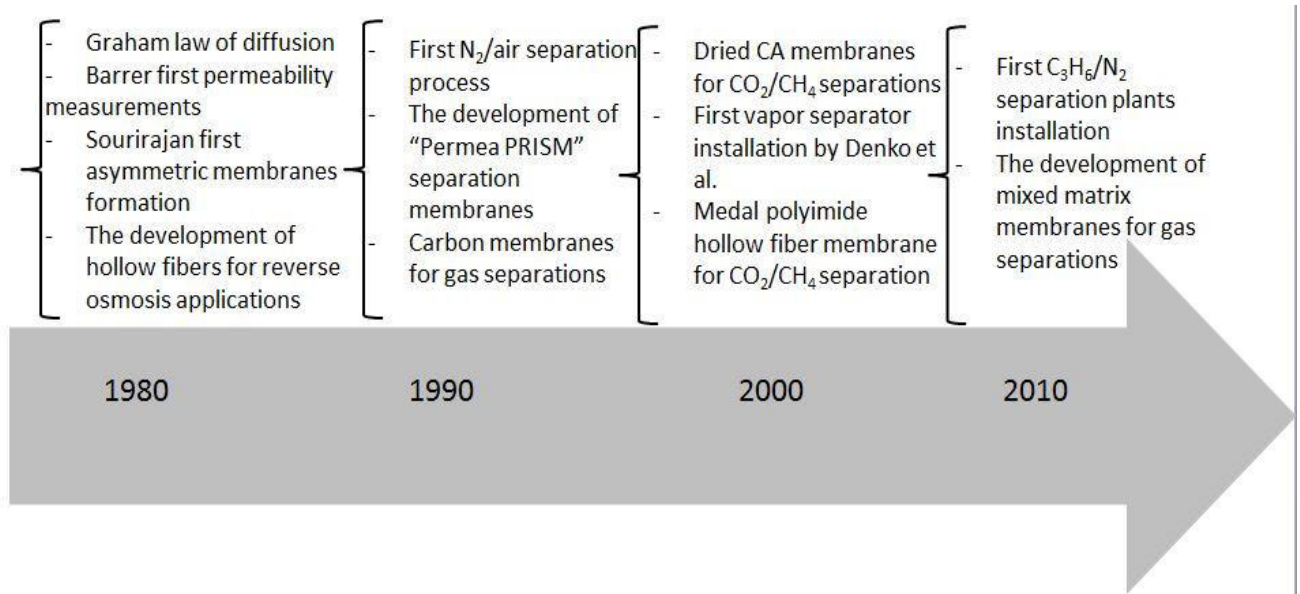


Figure B.1.1 Background of membrane gas separations (S. Sridhar et al., 2014)

Conventionally, the efficiency of gas separation membrane can be estimated through the determination of its permeability and selectivity.

The permeability has already been defined in the first part of the manuscript (1.2

The selectivity α_{ij} is defined as the ratio of the permeability of the penetrant “i” to the permeability of the penetrant “j”:

$$\alpha_{ij} = \frac{P_i}{P_j} \quad (\text{B.1.1})$$

This ratio provides a useful measure of the so-called “perm-selectivity” of a given membrane for a gas mixture (Hellums, Koros, Husk, & Paul, 1989).

For gas separation, the most common way used to investigate the functional properties of polymer-based membranes is to work at first on dense membrane and to determine the ideal selectivity.

Assuming that the transport mechanism is governed by a Fickian process, it can be considered that the permeability is equal to the product of the solubility (S_{ij}) and diffusion (D_{ij}) coefficients. Thus, the perm-selectivity can be written as:

$$\alpha_{ij} = \frac{P_i}{P_j} = \frac{S_i}{S_j} \cdot \frac{D_i}{D_j} \quad (\text{B.1.2})$$

The perm-selectivity is indeed the product of the solubility selectivity and the diffusion selectivity. Diffusion often plays a governing role in the case of glassy polymers for the separation of gases that present a low solubility and significantly different kinetic diameters (for example H_2/N_2). In the case of gas pairs implying CO_2 , the solubility can also play a significant role in the separation properties.

For the most interesting materials, real selectivity can then be studied. The real selectivity is indeed not always equal to the ideal selectivity, which can be due for example to plasticization or gas competition effects (Galizia et al., 2017).

Finally asymmetric or composite membranes can also be prepared from the same material in the first case or from the association of different materials in the second case (Le & Nunes, 2016). Thanks to their specific morphology, consisting in a dense and thin layer supported by a porous structure, these membranes allow to reach a high permeability level while still exhibiting good separation and mechanical properties.

Thus, it appears that in the whole membrane design process, the first step consisting in the selection or development of the polymer-based material with appropriate permeability and selectivity is crucial.

As stated above, permeability and selectivity are the main parameters describing the performance of a membrane: an ideal membrane is very permeable and highly selective.

Unfortunately, polymeric membranes showing high selectivity are generally lowly permeable and vice versa (Robeson, 1999).

It is important to mention here that Robeson et al. showed that for a specific gas pair, polymeric membranes are lying on or below a curve defined as the upper bound tradeoff curve (Aroon, Ismail, Matsuura, & Montazer-Rahmati, 2010) (**Figure B.1.2**).

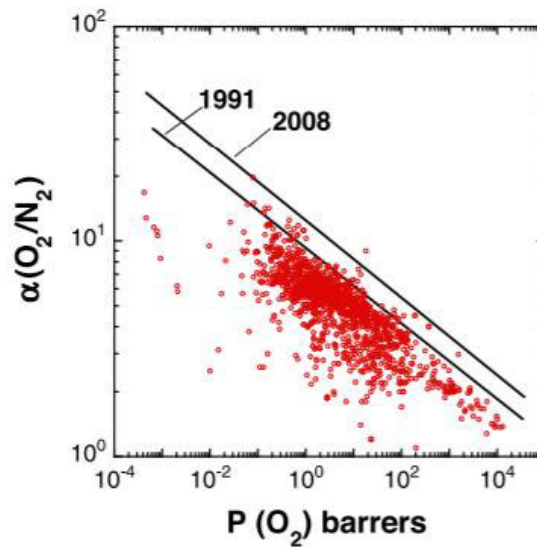


Figure B.1.2 O₂/N₂ upper-bound curve in polymeric membranes

It was shown that glassy polymers were preferred over rubbery polymers in industries, first because of their durability (H. B. Park et al., 2017; Shindo & Nagai, 2013) and secondly, because they are located nearer to the upper-bound trade-off curve (occupying the left part of the plot) (Ismail, Khulbe, & Matsuura, 2015) (**Figure B.1.3**).

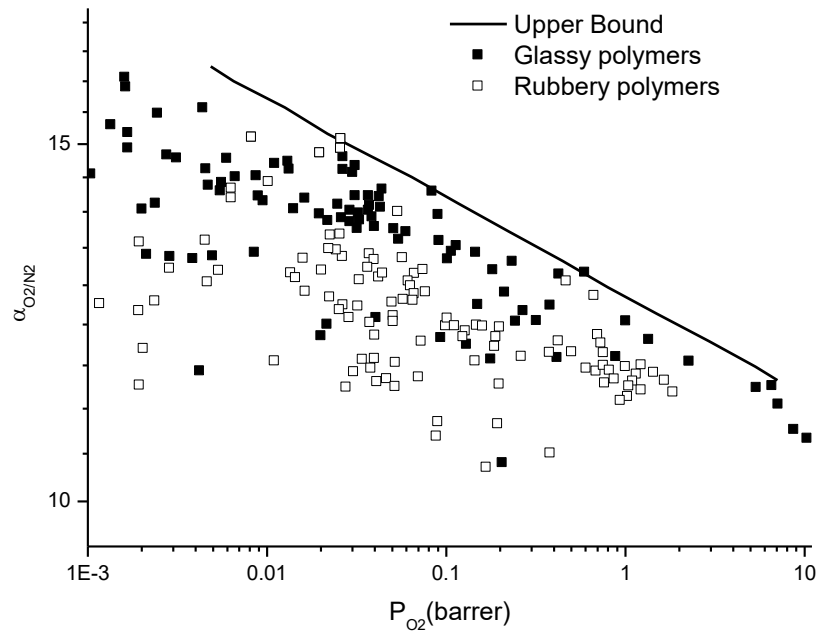


Figure B.1.3 O_2/N_2 upper bound correlation for glassy and rubbery polymeric membranes as referred in (Robeson, 1991)

Table B.1.1 presents examples of the major glassy and rubbery polymers used in the gas separation industries (Bernardo, Drioli, & Golemme, 2009).

Table B.1.1 Examples of the most used glassy and rubbery polymers in gas separation industrial applications (Bernardo et al., 2009)

Glassy polymers	Rubbery polymer
Polyimides Polysulfone Poly(phenylene oxide) Polyperfluorodioxoles Cellulose acetate Polycarbonate	Poly (dimethylsiloxane) Copolymer families (e.g. Ethylene oxide/propylene oxide-amide)

Polyimides have been one of the most widely used polymers for gas separation applications. They are rigid and stable, thanks to their high glass transition temperatures. They are obtained by polycondensation reactions of dianhydrides with diamines and it is easy to tune the free volume in this membranes by the appropriate choice of the monomers (Tanaka & Okamoto,

2006). Although they are permeable, polysulfones are used for some gas separation applications (such as hydrogen recovery). Hollow fibers are prepared from PSF which is the most commercially used polymer (Fried, 2006). A series of substituted polycarbonates of bisphenol-A have also been shown to have an attractive combination of permeability and perm-selectivity properties depending on the size and number of the groups that are grafted on the aromatic ring of the polymer (Hellums et al., 1989).

In addition to the aforementioned polymers, a new class of polymeric membranes having high permeability has been developed consisting in PIMs (Polymers with Intrinsic Micro-porosity). These materials have shown good separation properties for different gas pairs such as CO₂/CH₄ (C. Liu, Greer, & O'Leary, 2016). Their behavior is assigned to their rigid molecular structure and very high free volume. Unfortunately, membranes from PIMs are cost effective and remain complicated to implement in the form of membranes.

In parallel with the development of organic membranes, an evolution has also been observed concerning inorganic membranes. The main interests of these membranes are their thermal and chemical stability and their high plasticization resistance to condensable gases (C. Liu et al., 2016).

Inorganic molecular sieve membranes (molecular sieve, carbon molecular sieves ...) and zeolitic imidazolate frameworks have shown excellent separation properties (C. Liu et al., 2016).

Carbon molecular sieves are considered as very high free-volume materials containing slit-shaped pores (Bernardo et al., 2009). They have been prepared in both supported and unsupported forms. Interesting gas separations were reported for these membranes especially for O₂/N₂ separation. However, despite these interesting properties, they present several drawbacks such as their brittleness (Koresh & Soffer, 1987; Koros & Mahajan, 2000; Saufi & Ismail, 2004) and the presence of defects. Moreover, the gas transport mechanism is very complex depending on the temperature and upstream pressure. In addition, compared to polymeric membranes, those membranes are very costly and difficult to be transformed into a high surface area module (Vu, Koros, et Miller 2003). However, the species used to prepare inorganic membranes have inspired new developments in connection with polymers: the so-called mixed matrix membranes.

1.1.1 Mixed Matrix membranes

Since polymeric membranes have low separation performance characteristics compared to inorganic materials, various alternatives have been developed to find a compromise between the needs of the industry and actual membranes properties (S. Sridhar et al., 2014). The multiphase approach consisting in the dispersion of inorganic porous fillers within polymer matrix seems to be a good solution. The obtained membranes are called mixed matrix membranes (MMMs) where a combination of the high gas separation properties of molecular sieves materials and the desirable mechanical properties of polymers is sought (Moore et al., 2004). The properties of mixed matrix membranes depend on the selection of the inorganic dispersed phase. Several studies have reported the use of zeolite (Breck, 1974; Van Rooyen et al., 2016), carbon molecular sieves (Bertelle, Gupta, Roizard, Vallières, & Favre, 2006; Chung, Jiang, Li, & Kulprathipanja, 2007; Espuche, 2011) and more recently Metal Organic Framework (Espuche, 2011; C. Liu et al., 2016; Vu, Koros, & Miller, 2003) as fillers.

Table B.1.2 shows examples of filler/matrix couples reported in literature for gas separation enhancement.

Table B.1.2 Example of some couples Polymer/Filler used in mixed matrix membranes in the literature

Polymer	Filler	Reference
Ultem1000 and Matrimid5218	Zeolite/Carbon molecular sieves	(Husain & Koros, 2007; J. Liu et al., 2009; Vu et al., 2003; C. Zhang, Dai, Johnson, Karvan, & Koros, 2012)
PDMS and polysulfone	Cu-BTC	(Car, Stropnik, & Peinemann, 2006)
Pebax	UiO-66; ZIF-7; ZIF-8	(Sánchez-Laínez, Gracia-Guillén, Zornoza, Téllez, & Coronas, 2018)
Poly(vinyl acetate)	Zeolite 4A	(Adams et al., 2011; J. Ahmad & Hägg, 2013b, 2013a)
Polyethersulfone (PES)	Zeolite 5A	(Y. Li, Chung, Cao, & Kulprathipanja, 2005)
Rubber	Zeolite 4A	(Amnuaypanich, Naowanon, Wongthep, & Phinyocheep, 2012)

We can observe that all fillers types have been used in combination with glassy as well as rubbery polymer matrix. In the following part, we will more particularly focus on MMMs based on glassy polymers because our experimental work involves polyetherimide matrix. The aim will be first to give some examples of the performances that can be reached with MMMs. Then we will discuss the problems to face during the MMM preparation in order to obtain optimized properties.

Functional properties of glassy polymer-based MMMs

1.1.1.1 Zeolites

Zeolites are characterized by their high surface area and the regularity of their pores structure (Darrin & O’Leary, 2009). Incorporating those materials in polymer matrix offers the opportunity to get excellent separation properties. The most promising zeolites used for gas separation applications are zeolite-L ($M_9[Al_9Si_{27}O_{72}] \cdot 21 H_2O$ ($M = K^+$ or Na^+)) and zeolite-4A ($Na_{12}[Al_{12}Si_{12}O_{48}]27H_2O$) (Süer, Baç, & Yilmaz, 1994). It has been reported by Chung et al. (Chung et al., 2007; He, 2018) that the morphology and the separation properties of the mixed matrix membranes based on zeolites are related to the properties of both polymer and inorganic fillers. For example, zeolite-4A was incorporated in PES matrix by Süer and coworkers and an improvement in CO_2 permeability by a factor around 4 was observed (Süer et al., 1994). The same system exhibited an increase of CO_2/N_2 selectivity by a factor of 2. Zeolite-4A and Matrimid mixed matrix films showed an important increasing of O_2 permeability from 1.32 to 4 Barrer (Mahajan, Burns, Schaeffer, & Koros, 2002). Other mixed matrix membranes have been developed combining zeolite-L with the copolymer composed of the glassy polyimide (6FDA-6FPDA) and the polymer polydimethylsiloxane (PDMS) leading to a significant increasing of O_2 permeability from 4 to 44 Barrer (Pechar et al., 2006).

1.1.1.2 Carbon molecular sieves (CMS)

Those materials are characterized by their high porosity which justifies their use in the fabrication of MMMs. Vu and coworkers prepared mixed matrix membranes of Matrimid and CMS and showed that CO_2/CH_4 selectivity has increased of about 45% (Vu et al., 2003). In the same work, CMS particles (35 vol%) have been incorporated into Ultem matrix and the gas permeation tests showed an enhancement of more than 40% in CO_2/CH_4 selectivity over the corresponding selectivity of the pure Ultem matrix.

1.1.1.3 Metal Organic Frameworks (MOFs)

This type of materials has recently attracted the attention of researchers for the enhancement of gas separation properties of the mixed matrix membranes thanks to their controlled porosity and their affinity towards certain gases (CO₂, CH₄) (Dong, Li, & Chen, 2013). Two of the most commonly used MOFs for MMMs preparation in literature are: MOF-5 (Perez, Balkus, Ferraris, & Musselman, 2009), ZIF-8 (Eiras, Labreche, & Pessan, 2016; Hao, Li, Yang, & Chung, 2013; D. Liu, Ma, Xi, & Lin, 2014). MOF-5 is a Metal-organic framework compound with the formula Zn₄O(BDC)₃ while ZIF-8 formula is C₈H₁₀N₄Zn.

Yaghi and coworkers, have shown that MOF-5 present high H₂ storage capacity which is attributed to their high surface area and also to H₂/MOF-5 interactions (Rosi et al., 2003). Moreover, the addition of 30 wt% MOF-5 particles to Matrimid matrix has increased the permeability of H₂ from 24.4 to 53.8 Barrer, that of O₂ from 1.90 to 4.1 Barrer and CO₂ permeability from 9.0 to 20.2 Barrer, respectively (Jeazet, Staudt, & Janiak, 2012).

Adding ZIF-8 (40 wt%) to Matrimid matrix led to an increase of permeability up to 271% for CH₄, 239% for N₂ and 170% for CO₂. According to the authors, this high permeability value suggests that the addition of ZIF-8 particles to Matrimid matrix increased the distance between polymer chains creating more polymer free volume (Ordonez, Balkus Jr, Ferraris, & Musselman, 2010).

In addition, hybrid fibers have been prepared using Ultem matrix with ZIF-8 particles. A significant enhancement of the perm-selectivity (as high as 20% compared to the neat polymer matrix) has been obtained (Dai, Johnson, Karvan, Sholl, & Koros, 2012). Perm-selectivity value equal to 32 has been obtained for the gas pair CO₂/N₂ with the membrane containing 17 vol% ZIF-8.

Several studies have focused on the addition of ZIF-8 particles to PPEES polymer matrix (poly-(1, 4-phenylene ether-ether-sulfone)) with different loadings ranging between 10 and 30 wt%. An increase of CO₂ diffusion coefficient has been recorded from 2.1×10^{-8} cm² /s to 9.3×10^{-8} cm² /s for membranes containing 30 wt% of ZIF-8 (Díaz, Garrido, López-González, Del Castillo, & Riande, 2009).

However, to reach optimized functional properties, some problems have to be overcome during the membrane preparation. This will be detailed hereinafter.

Factors influencing the membrane preparation

The addition of fillers to the polymer matrix must be done considering the adhesion between both phases. Some experimental works have faced difficulties in the preparation of MMMs because of the formation of some voids at the interface between glassy polymers and zeolites (Duval et al., 1994). In this work, different strategies have been developed to solve this problem consisting in modifying the external surface of zeolites or even adding some plasticizers to increase polymers flexibility (Mahajan et al., 2002; Mahajan & Koros, 2002a; Yong, Park, Kang, Won, & Kim, 2001).

Going into more details, the fabrication of MMMs depends on two main factors in order to be efficient for gas separation applications:

- Interfacial morphology

Several experimental works have shown that the low adhesion between both components could be due to the formation of some voids at the interface which is the result of the de-wetting of polymer chains at the external surface of fillers (this is currently observed in the case of glassy polymers) (Car et al., 2006; Duval, Folkers, Mulder, Desgrandchamps, & Smolders, 1993; Husain & Koros, 2007). To overcome those issues, thermal annealing and liquid addition (such as the poly(RTILs)) to wet the polymer matrix and the particle have been proposed by Hudiono et al. (Hudiono, Carlisle, LaFrate, Gin, & Noble, 2011).

A partial blockage of the particles pores by polymer chains may also occur in some systems leading to a decrease of gas permeability with respect to that expected by considering an ideal binary system.

In some other systems, deviations of gas transport properties with respect to ideal binary systems have been assigned to polymer rigidification in the vicinity of the fillers.

Thus, it appears that interfacial phenomena can play a major role in MMMs' gas transport properties.

- Dispersion of fillers

The development of membranes with enhanced gas transport properties generally requires the incorporation of a high amount of fillers in the polymer matrix. The idea is to promote the formation of continuous diffusion path through the porous fillers and then to achieve good separation properties could be obtained. However, as in the case of nanocomposite systems (Part A of this thesis), increasing filler volume fraction can lead to undesired morphologies

such as the dispersion of high sized filler agglomerates within the matrix, which can constitute a main cause of the reduction of membrane selectivity (Dong et al., 2013). The so-called “prime” protocol has been proposed by Mahajan et al. (Mahajan et al., 2002; Mahajan & Koros, 2000) which aims to avoid the agglomeration of fillers. It consists in adding a portion of the polymer solution to the particles suspension and then a decantation will take place.

Another alternative to achieve a good dispersion of the fillers consists in incorporating the inorganic fillers in the solvent rather than in the polymer solution before mixing both solutions. According to several authors (Das, Perry, et Koros 2010; Kong, Shintani, et Tsuru 2010), this process reduces filler agglomeration in the final solution. Examples of the different strategies for preparing gas separation mixed matrix membranes reported in literature are presented in the following figure (**Figure B.1.4**).

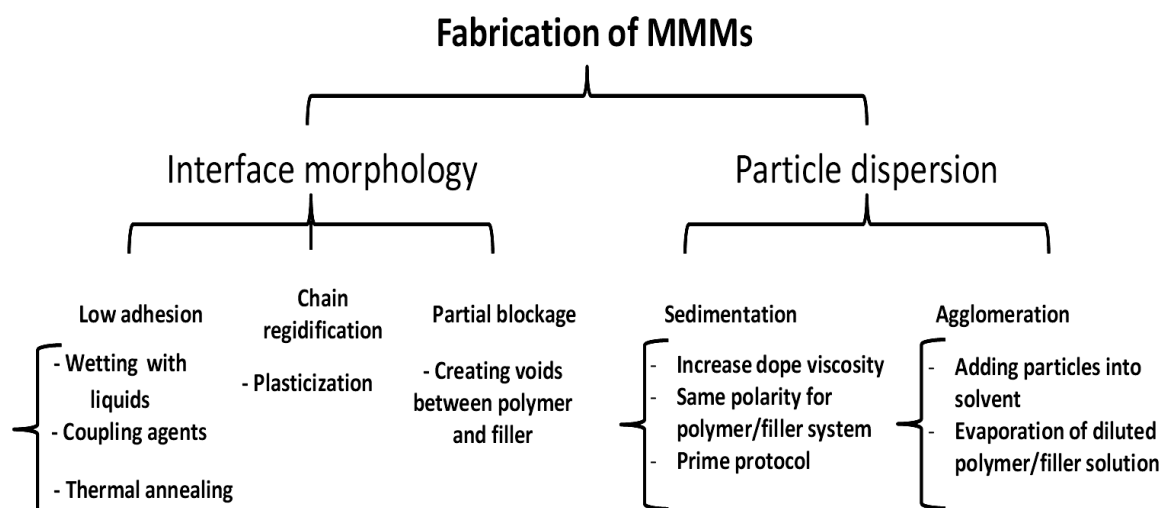


Figure B.1.4 Strategies to overcome challenges for MMMs fabrication as reported in Dong et al. work (Dong et al., 2013)

To sum up, MMMs are considered as a promising route for gas separation membranes. Obtaining interesting properties basically requires the use of large quantity of fillers and the control of both fillers dispersion and filler-matrix interfaces.

1.1.2 Polymer/Ionic Liquids membranes


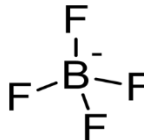
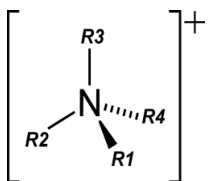
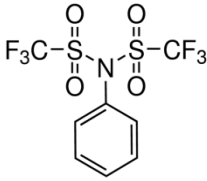
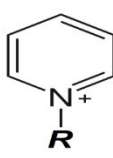
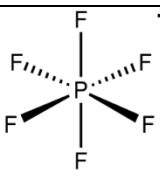
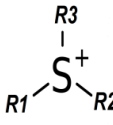
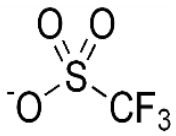
Despite the huge success of polymeric membranes and MMMs in gas separation applications, the CO₂ concern requires today the development of novel materials with enhanced performances. In this context, Favre and coworkers for example developed hollow fiber micro-porous membranes combined with amine based absorption mechanism (Boucif, Favre,

& Roizard, 2008). In this section, we will focus on the use of ionic liquids as a new alternative to fabricate highly effective membranes for gas separation applications (Magana, Gain, Gouanvé, & Espuche, 2016).

Ionic liquids (ILs) have gained an important growth and interest thanks to their various properties (Tomé, 2014). Those salts have melting points below 100°C caused by the low intermolecular interactions of their asymmetrical ions and the delocalization of their charges (V. Plechkova et R. Seddon 2008). Apart from their melting point, the utility of the ionic liquids can be determined through their viscosity which is ranging between 15 cP and 3000 cP (Hojniak, 2014). Moreover, they are always referred to as “green solvents” thanks to their non-volatility and recyclability.

Table B.1.3 summarizes some examples of cations and anions used to form ionic liquids:

Table B.1.3 Examples of anions and cations used for IL preparation

<i>Cations</i>	<i>Anions</i>
Imidazolium [im] 	Tetrafluoroborate [BF ₄] 
Ammonium [N] 	Bis(Triflimide) [Tf ₂ N] 
Pyridinium [py] 	Hexafluorophosphate [PF ₆] 
Sulfonium [S] 	Triflate [OTf] 

Ionic liquids can be used for gas separation applications according to various ways. The most cited approach in literature is the supported ionic liquid membranes (SILMs) (Tomé, 2014), where IL is occluded in the pores of a polymeric membrane by capillary forces (Morgan, Ferguson, & Scovazzo, 2005). Those membranes make the best use of the properties of ILs,

such as their thermal stability and non-volatility, in CO₂ separation applications (Hojniak, 2014). The gas separation process through SILMs is governed by the solution-diffusion mechanism (Hojniak, 2014). Moreover, compared to non-supported liquid membranes, SILMs increase the efficiency and selectivity in the separation processes because of the higher contact area between the ILs and the gases.

Hereinafter is a summary of some of the SILMs that have been cited in literature:

Table B.1.4 Examples of SILMs reported in literature

<i>Selective separation studied</i>	<i>IL/polymer support</i>	<i>References</i>
CO ₂ /CH ₄	[Bmim] [BF ₄]/PVDF	(Lee, Kim, Lee, Park, & Lee, 2006; Martínez-Palou, Likhanova, & Olivares-Xometl, 2014)
	[Bmim] [Tf ₂ N]/PP [Bmim] [Tf ₂ N]/PA	(de los Ríos, Irabien, Hollmann, & Fernández, 2013)
	[Bmim] [OTf]/PVDF	(de los Ríos et al., 2013)
	[Emim] [Tf ₂ N]/PES	(Scovazzo et al., 2002)
CO ₂ /N ₂	[Emim] [Tf ₂ N]/PES	(Scovazzo et al., 2004)
	[Bmim] [PF ₆]/PTEE	(Jindaratamee, Shimoyama, Morizaki, & Ito, 2011)
CO ₂ /H ₂ S	[Bmim] [PF ₆]/PVDF	(X. Zhang et al., 2017)

The way used to prepare Supported Ionic Liquids Membranes plays an important role in the membrane performance. Three main methods are mainly cited in literature, which are direct immersion, immersion under vacuum and immersion under pressure (Fortunato et al., 2005; Hernández-Fernández, de los Ríos, Tomás-Alonso, Palacios, & Villora, 2009; Santos, Albo, & Irabien, 2014).

Room Temperature Ionic Liquids (RTILs) (Scovazzo et al., 2002) were used for acid gas separations such as CO₂/N₂ and CO₂/CH₄ separations. For the gas pair CO₂/CH₄ a selectivity of 120 was reported while CO₂ permeability increased from 149 to 1720 Barrer.

On the other hand, it has been concluded through the work of Ilconich et al. (Ilconich, Myers, Pennline, & Luebke, 2007) that the nature of the anion of the ionic liquid could have a major

role to control the CO₂ solubility. Hereinafter are reported some experimental values of CO₂ permeability and CO₂/N₂ selectivity for different IL having different anions with the same cation.

Table B.1.5 CO₂ permeability and CO₂/N₂ selectivity as reported in literature (Mahurin, Hillesheim, Yeary, Jiang, & Dai, 2012)

<i>Ionic Liquid</i>	<i>CO₂ permeability (Barrer)</i>	<i>CO₂/N₂ selectivity</i>
[Emim] [Tf2N]	1702	23
[Emim] [OTf]	1171.4	40.5
[Emim] [BF ₄]	968.5	44.5

Other researchers tried to compare SILMs to polymeric membranes and have concluded that the former showed better performance with permeabilities/selectivities that were close to the Robeson plot upper bound (**Figure B.1.5**) (Cserjési, Nemestóthy, & Bélafi-Bakó, 2010; Robeson, 2008; Scovazzo, Havard, McShea, Mixon, & Morgan, 2009).

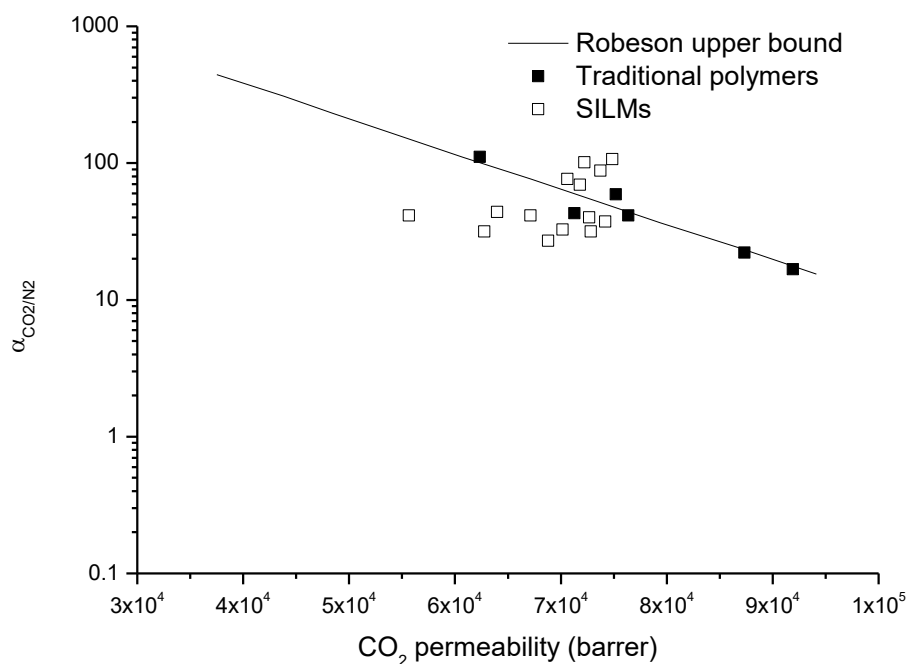


Figure B.1.5 Robeson plot for CO₂/N₂ selectivity versus CO₂ permeability as reported in literature (Close, Farmer, Moganty, & Baltus, 2012)

The same result has been obtained recently in the work of Close et al. for the couple of gas CO₂/N₂ (Close et al., 2012). The CO₂ permeability of their prepared membranes was greater than 1000 Barrer while the ideal CO₂/N₂ selectivity was ranging between 12 and 21 lying close to the Robeson upper bound.

Since SILMs separation performance is strongly dependent on the used IL, hereinafter are cited some of the important criteria to take into account in order to obtain promising IL-based membranes for CO₂/N₂ or CO₂/CH₄ separations (Hojniak, 2014) :

- melting point
- viscosity
- resistance to gas stream impurities
- N₂ or CH₄ solubility
- toxicity
- price
- CO₂ solubility

Nevertheless, SILMs stability is still a major issue for gas separation applications due to the high pressure differential across the membranes (Tomé, 2014).

To overcome the drawbacks of SILMs, the incorporation of IL into a polymer matrix seems to be a good alternative to promote their use in gas separation applications. Polymer/ionic liquid membranes are usually prepared by the dispersion of the IL in polymer solution prior to the membrane formation.

Hong and coworkers (Hong, Park, Ko, & Baek, 2009) have incorporated different amounts of [c2mim] [BF₄] in PVDF-HFP copolymer (RTIL : polymer ratio ranging between 0.5:1 and 2:1) and obtained interesting gas separation properties. CO₂ permeability increased from 45 to 400 Barrer and N₂ permeability from 0.9 to 6.7 Barrer. Similarly, CO₂/N₂ selectivity increased with gas permeability to reach 60. Those results are similar to those obtained for SILMs with the advantage of having more stable membranes in this case. Consequently, this approach was adopted by several researchers for different polymer/IL membranes (e.g. p(VDF-HFP)/[Emim] [TFSI]; Pebax/[bmim] [CF₃SO₃], etc.) in order to improve the gas separation of different mixtures such as CO₂/N₂ (H. Z. Chen, Li, & Chung, 2012; Erdni-Goryaev et al., 2012; Friess et al., 2012), CO₂/H₂ (L. Liang, Gan, & Nancarrow, 2014; Rabiee, Ghadimi, & Mohammadi, 2015) and CO₂/CH₄ (Jansen, Friess, Clarizia, Schauer, & Izak, 2010; Uchytel, Schauer, Petrychkovych, Setnickova, & Suen, 2011). Pebax copolymers have been used in the same context by Bernardo et al. High CO₂/N₂ selectivity values (ranging between 40 and 50) were obtained (Bernardo et al., 2012). Magana and coworkers developed Pebax-IL membranes to study the water sorption and diffusion properties of the prepared membranes (Magana et al., 2016). An enhancement of diffusion rate was evidenced below 30 wt% IL. For

membranes prepared from polymer/IL mixtures, the migration of IL at the film surface can occur. This migration phenomenon prevents the incorporation of high filler rates and is detrimental to the stability of the membranes.

Thus another approach to use IL for gas separation applications was developed: the PILs (Polymeric Ionic Liquids) approach. PILs are a subclass of polyelectrolytes that contains IL species connected through a polymeric backbone to form a macromolecular architecture (Green, Grubjesic, Lee, & Firestone, 2009; Jourdain, Antoniuk, Serghei, Espuche, & Drockenmuller, 2017; Mecerreyes, 2011; Yuan & Antonietti, 2011; Yuan, Mecerreyes, & Antonietti, 2013). The development of such materials is based on the free radical polymerization of ionic liquid monomers or via chemical modification of the polymers (Marcilla et al., 2006). The importance of this material family in gas separation applications can be attributed to the development of new original PIL chemical structures and also to the introduction of new types of cations and anions in the IL structure. PIL-based membranes are characterized by their good stability (Tomé, 2014; Tomé & Marrucho, 2015). Consequently, they have been considered as alternative solid sorbents for CO₂ capture. It has been shown by Tang and coworkers that imidazolium-based PILs exhibit higher CO₂ absorption capacity than the corresponding ILs (Tang, Sun, Tang, Radosz, & Shen, 2005). In the same context, new series of PILs based on polyurethane which were considered as low cost materials, have been developed and showed excellent CO₂ sorption performance compared to other PILs (75.7 mol% at 20 bar) (Magalhães et al., 2014).

Since an ideal membrane should combine adequate permeability and perm-selectivity properties, a new concept combining PIL and IL appears as a good way to achieve membranes with higher gas permeabilities while maintaining their mechanical stability. Bara et al. (Bara, Hatakeyama, Gin, & Noble, 2008) were the first to prepare such membranes by the polymerization of an IL monomer in the presence of a non-polymerizable IL (free IL). Their prepared membranes recorded very large gas permeability improvements (CO₂ permeability was around 44 Barrer while N₂ and CH₄ permeability values were 1.1 and 1.6 Barrer respectively; CO₂/N₂ and CO₂/CH₄ selectivities were 39 and 27 respectively) which inspired other researchers to pursue their approach.

Li and coworkers (P. Li, Pramoda, & Chung, 2011) synthesized different PIL/IL composite membranes and showed that the incorporation of the ionic liquid caused an increase in the free volume of the membranes and thus an enhancement of the CO₂ and N₂ permeability,

solubility and diffusivity coefficients. N₂ permeability has increased from 4.55 to 21.6 Barrer and CO₂ permeability increased from 101.4 to 559.5 Barrer.

Unfortunately, this approach did not have a significant effect on CO₂/N₂ perm-selectivities (P. Li et al., 2011). To overcome this problem, the same authors have investigated PIL/IL composites based on alkyl functionalized vinylimidazolium PILs which were blended with different ILs such as [C2mim] [N(CN)₂]. The result of such choice led to an increase in CO₂ permeability values and also an enhancement of CO₂/N₂ perm-selectivity.

Other studies dealt with this subject using the same strategy (Carlisle, Nicodemus, Gin, & Noble, 2012) and confirmed that the enhancement of gas separation properties could be achieved through the addition of free IL. Moreover, it has been shown through those works that the choice of the appropriate IL is crucial in the tailoring of the PIL-IL membrane properties for improving their CO₂ separation performance (Tomé, 2014).

Thus, an increasing interest was paid to IL during the last years with the aim to obtain membranes with improved selectivity while keeping a good stability. Hereinafter, we will describe another original way to use IL that has caught our attention.

1.1.3 MMMs/IL membranes

We have seen that researchers encountered different challenges when preparing two-component membranes for gas separation applications. For example, for MMMs, the interfacial defects and poor adhesion between inorganic fillers and polymer matrix was identified as a major problem in the preparation of the membranes (M. Li et al., 2017). To solve such problems, a new strategy has been developed which consists in adding ionic liquids within mixed matrix membranes. Hudiono et al. (Hudiono et al., 2011) showed in their work that the addition of IL ([Emim] [Tf₂]) to the MMMs enhanced the interfacial adhesion between the polymer matrix (Styrene-based poly(RTIL) and Vinyl-based poly(RTIL)) and inorganic fillers (SAPO-34) as well as CO₂ adsorption.

For the first polymer, their results showed that the addition of the zeolite and the ionic liquid (12 wt% RTIL and 40 wt% SAPO-34) increases the overall permeability (CO₂ permeability for example increases from 9.2 to 66.2 Barrer) and CO₂/CH₄ selectivity. However, the addition of the filler and the IL does not have a significant effect on the CO₂/N₂ selectivity (around 34.7).

Results for the second polymer showed high CO₂ permeability values ranging between 67.3 and 527.2 Barrer which is attributed to the longer alkyls substituents in this polymer. Furthermore, the addition of the IL and fillers (36 wt% RTIL and 40 wt% SAPO-34) to the polymer has increased CO₂/CH₄ selectivity by almost 81%.

Mohshim and his team (Mohshim, Mukhtar, & Man, 2014) also showed that incorporating ionic liquid into mixed matrix membranes is a good way to improve the compatibility between fillers and polymer matrix by reducing the agglomeration of fillers. They have incorporated 20 wt% of [Emim] [Tf2] into a polyethersulfone-SAPO-34 mixed matrix membrane containing a filler amount of 20 wt% and showed that the ideal CO₂/CH₄ selectivity reached 62.6 which is high compared to the pure mixed matrix membrane (20.7).

Recently, metal-organic frameworks (MOFs) have been used in such systems thanks to their various functionalities and high porosity compared to zeolites and carbon molecular sieves (H. Li et al., 2016). Several researchers have focused their work on those systems (Hao et al., 2013; H. Li et al., 2016). Coterillo et al. (Casado-Coterillo et al., 2015) have prepared three-component MMMs based on chitosan, [Emim] [Ac] and ZIF-8. They showed that the thermal stability of the prepared membrane was enhanced by the combined effect of the IL and MOFs particles. Moreover, interesting gas separation properties have been obtained for the studied membranes with respect to the amounts of each additive. The best properties have been obtained for 10 wt% ZIF-8-IL-chitosan membranes where CO₂ permeability was as high as 5413 Barrer while CO₂/N₂ selectivity was around 11.5. Besides, Hao et al. (Hao et al., 2013) have shown that CO₂ permeability of membranes consisting in Poly(RTIL) combined with RTIL and ZIF-8 particles (P[vbim] [NTf2]/[Emim] [NTf2]/ZIF-8) can reach over $1000 \times 3.348 \times 10^{-19}$ kmol m/(m²s pa). For a membrane containing 25.8 wt% ZIF-8 (the weight ratio of poly(RTIL) and RTIL was fixed to 2), an impressive performance of CO₂/N₂ separation was recorded where CO₂ permeability is around 906.4 Barrer and CO₂/N₂ selectivity was 21. It must be added here that the obtained enhancement of the permeability was in agreement with the Maxwell law. Li et al. (M. Li et al., 2017) have combined three components (Pebax, ZIF-8 and IL) to develop a membrane with good gas separation properties. Their results have highlighted the important role of the ionic liquid in determining the gas permeability and more particularly in the improvement of the compatibility between ZIF-8 particles and the polymer matrix. The CO₂ permeability of the Pebax/15 wt% ZIF-8 /80 wt% IL membranes was 4.3 times that of the pure Pebax membrane without sacrificing the CO₂/N₂ selectivity. It was concluded that a three-component approach could be a promising

way for the efficient separation of CO₂. To the best of our knowledge, Polyetherimide was not used as matrix in such three-component systems. Additionally, all of the cited three component membranes are made of important amounts of IL (beyond 20 wt%) which led us to develop three-component membranes for gas separation applications based on Ultem polymer with the incorporation of low amounts of [Emim] [BF₄] (below 10 wt%) and ZIF-8 particles.

1.2 Modeling of gas transport properties

Concurrently to the experimental development of MMMs, an increasing interest has been paid to the modeling of their gas transport properties. This section focuses on reviewing the analytical and numerical models available in literature for describing mass transfer in MMMs for gas separation applications.

1.2.1 Analytical modeling

1.2.1.1 Models for gas transport in MMMs

Several models have been developed in order to predict the relationship between MMMs physical properties and their transport properties.

1.2.1.1.1 Models for gas transport in ideal MMMs

In these models, MMMs are assumed to be ideal binary systems meaning that they don't present any defect. The calculation of the permeability of MMMs requires a prior knowledge of the permeability of gas through the continuous phase (the polymer matrix) and the dispersed phase (fillers), respectively (Keskin & Sholl, 2010). One of the most classic and known models which was adapted from electrical models is the Maxwell and Bruggeman model (Banhegyi, 1986; Basu, Cano-Odena, & Vankelecom, 2010; Bouma et al., 1997; Chung et al., 2007; Keskin & Sholl, 2010).

The Maxwell model is basically dedicated to the study of the electrical conductivity of composite materials. It has also been used to predict Mixed Matrix Membranes effective permeability (P_{eff}) according to the following equation:

$$\frac{P_0}{P_{eff}} = \frac{P_d + 2P_0 + f(P_0 - P_d)}{P_d + 2P_0 - 2f(P_0 - P_d)} \quad (\text{B.1.3})$$

assuming that P_0 and P_d are the permeability coefficients of the neat polymer and the dispersed phase, respectively, and f is the dispersed phase volume fraction. The validity of

this model is limited to low filler volume fractions since it assumes that mass transport around fillers is not affected by the presence of nearby particles (Bouma et al., 1997).

Increasing filler volume fraction in the polymer matrix requires the use of another model, which was developed first, as the Maxwell model, to predict dielectric properties of composite materials. Bruggeman model has been applied to predict gas transport properties of mixed matrix membranes for higher filler volume fractions and the corresponding equation can be written as follows:

$$\frac{P_0}{P_{eff}} = \frac{(1-f)^3 \left(1 - \frac{P_d}{P_0}\right)^3}{\left(\frac{P_{eff}}{P_0} - \frac{P_d}{P_0}\right)^3} \quad (\text{B.1.4})$$

Despite its use to predict gas transport properties for relatively high filler volume fractions, Bruggeman equation has some limitations (Dong et al., 2013):

- it cannot be applied for very high filler volume fractions (>0.2);
- it does not take into account the filler shape and dimensions which are very important parameters that could affect MMMs transport properties
- it requires numerical solution (Aroon et al., 2010; Nielsen, 1967).

Nielsen (Lewis & Nielsen, 1970; Nielsen, 1967) developed a model which can be applied for high filler volume fractions. It was initially dedicated to predict the elastic modulus in composite materials. The developed equation can be written as follow:

$$\frac{P_0}{P_{eff}} = \frac{1 - f\rho \frac{\left(\frac{P_d}{P_0}\right) - 1}{\left(\frac{P_d}{P_0}\right) + 2}}{1 + 2f \frac{\left(\frac{P_d}{P_0}\right) - 1}{\left(\frac{P_d}{P_0}\right) + 2}} \quad (\text{B.1.5})$$

assuming that $\rho = 1 + f\left(\frac{1-f_{max}}{f_{max}^2}\right)$ where f_{max} is the maximum value of filler volume fraction.

Moreover, Cussler and coworkers (Monsalve-Bravo & Bhatia, 2018; Pal, 2007) developed a model in which the membrane was modeled as a superposition of layers: one containing only polymer and the other containing both polymer and fillers. The model is called an “idealized resistance model” through which the ideal selectivity of two gases i and j was derived and written as:

$$\alpha_{ij} = \frac{1 + \frac{\alpha^2 f^2 / (1-f)^2}{1 + (\frac{\alpha^2 f}{\omega(1-f)})}}{1 + \frac{\alpha^2 f^2 / (1-f)^2}{1 + (\frac{\psi \alpha^2 f}{\omega(1-f)})}} \quad (\text{B.1.6})$$

where ω is the ratio between polymer and fillers diffusion coefficients respectively, f is the filler volume fraction, α is their aspect ratio and ψ is the selectivity of the fillers.

Additionally, Pal and coworkers (Pal, 2007) developed a model dedicated at first to thermal conductivity in composite materials which can also be applied for the prediction of gas separation properties of MMMs. It is given by the following equation:

$$\left(\frac{P_0}{P_{eff}}\right)^{-1/3} \times \left(\frac{\left(\frac{P_d}{P_0}\right) - \left(\frac{P_{eff}}{P_0}\right)}{\left(\frac{P_d}{P_0}\right) - 1}\right) = \left(1 - \frac{f}{f_{max}}\right)^{f_{max}} \quad (\text{B.1.7})$$

It must be noticed here that if $f_{max} = 1$ (f_{max} being the maximum filler volume fraction), Pal model reduces to Bruggemann model. The Pal model is able to calculate the permeance in MMMs systems taking into account the effect of the morphology on permeability through the parameter f_{max} , which is sensitive to morphology.

1.2.1.1.2 Models for gas transport in non-ideal MMMs

As previously discussed, in real MMMs, the contact between polymer matrix and fillers is not perfect, which means that the models cited above don't fit exactly with the actual properties of the so-called "non-ideal mixed matrix membranes". Koros et al. (Mahajan et al., 2002) modified the Maxwell model in order to take into account non-ideal interfaces between the polymer and filler phases (i.e. more specifically to account for the formation of voids at the interface). Accordingly, the Maxwell equation was modified as follows:

$$\frac{P_0}{P_{eff}} = \frac{P_{eff} + 2P_0 + (f + f_v)(P_0 - P_{eff})}{P_{eff} + 2P_0 - 2(f + f_v)(P_0 - P_{eff})} \quad (\text{B.1.8})$$

assuming that P_{eff} is the composite permeability and f_v is the voids volume fraction.

Li and coworkers (Y. Li, Guan, Chung, & Kulprathipanja, 2006) developed an analytical model describing mass transport in zeolite-A mixed matrix membranes by considering the mixed matrix membrane as a pseudo three-phase composite where a partial pore blockage of zeolites and polymer chain rigidification is occurring. The derived equation is the following:

$$\frac{P_0}{P_{eff}} = \frac{P_{eff} + 2P_0 + (f + f_v + f_{bl})(P_0 - P_{eff})}{P_{eff} + 2P_0 - 2(f + f_v + f_{bl})(P_0 - P_{eff})} \quad (\text{B.1.9})$$

assuming that f_{bl} is blocked pores volume fraction.

1.2.1.2 Models for gas transport in Polymer/IL membranes

The general mechanism of gas transport through such membranes is described by a solution-diffusion model (Wijmans & Baker, 1995). To design an efficient gas separation membrane, it is necessary to model the effect of IL on those properties. The simplest mathematical models existing in literature (Mannan et al., 2017) are the logarithmic, series and parallel models which were dedicated to estimate the permeability of gases in a blend of two components:

Table B.1.6 Mathematical models for permeability prediction in two component systems

<i>Model</i>	<i>Equation</i>
Logarithmic model	$\ln P_{eff} = f_1 \ln P_1 + f_2 \ln P_2$
Series model	$P_{eff} = f_1 P_1 + f_2 P_2$
Parallel model	$P_{eff} = \frac{P_1 P_2}{(f_1 P_2 + f_2 P_1)}$

Those mathematical models have been applied for Polymer/IL membranes but they have some drawbacks such as considering the polymer and ionic liquid as a single phase which is not actually true for most of the ionic liquid-polymeric membranes (Mannan et al., 2017). Mannan et al. (Mannan et al., 2017) have used the modified Maxwell model to predict gas transport properties through their systems which is given by the following equation:

$$\frac{P_0}{P_{eff}} = \frac{P_d + 2P_0 + \beta_{eff} f (P_0 - P_d)}{P_d + 2P_0 - 2\beta_{eff} f (P_0 - P_d)} \quad (\text{B.1.10})$$

It can be noticed that equation (B.1.10) is very similar to equation (B.1.1) except the presence of the factor β_{eff} which is a model parameter for the effectiveness of volume fraction of the dispersed phase. β_{eff} was defined by the authors as follows:

$$\beta_{eff} = \frac{f_{optim}}{f} \quad (\text{B.1.11})$$

assuming that f_{optim} is the optimized value of the dispersed phase volume fraction ($0 < \beta_{eff} < \infty$).

1.2.1.3 Models for gas transport in MMMs/IL membranes

Modeling of gas transport through MMMs/IL membranes was studied by Mohshim et al. (Mohshim et al., 2014). The functional properties were estimated by the Maxwell-Wagner-Sillar (MWS) model, which was modified in order to fit the experimental results. The developed equation is given as follow:

$$\frac{P_0}{P_{eff}} = \frac{\alpha_c P_d + (1 - n_i)P_0 + \alpha_c f_w (P_0 - P_d)}{\alpha_c P_d + (1 - n_i)P_0 + (1 - \alpha_c) f_w (P_0 - P_d)} \quad (\text{B.1.12})$$

where α_c is the corrected shape factor and f_w is the volume fraction of wetted dispersed phase through the three-component membranes. f_w is given by:

$$f_w = f + f_{IL} \quad (\text{B.1.13})$$

The model showed good prediction of CO₂ relative permeability compared to existing experimental data.

In conclusion, almost all the models found in literature to predict gas separation properties of two-component and three-component systems are derived from the Maxwell model which can be modified depending on the studied systems and the corresponding conditions. The different equations are summarized in **Table B.1.7**.

Table B.1.7 A sum-up of the theoretical models for gas transport properties in composite systems

<i>System</i>	<i>Model</i>	<i>Equation</i>
Ideal MMMs	Maxwell(Maxwell, 1873)	$\frac{P_0}{P_{eff}} = \frac{P_d + 2P_0 + f(P_0 - P_d)}{P_d + 2P_0 - 2f(P_0 - P_d)}$
	Bruggemann(Bruggeman, 1935)	$\frac{P_0}{P_{eff}} = \frac{(1 - f)^3 \left(1 - \frac{P_d}{P_0}\right)^3}{\left(\frac{P_{eff}}{P_0} - \frac{P_d}{P_0}\right)^3}$
	Nielsen(Lewis & Nielsen, 1970)	$\frac{P_0}{P_{eff}} = \frac{1 - f\rho \frac{\left(\frac{P_d}{P_0}\right) - 1}{\left(\frac{P_d}{P_0}\right) + 2}}{1 + 2f \frac{\left(\frac{P_d}{P_0}\right) - 1}{\left(\frac{P_d}{P_0}\right) + 2}}$

	Cussler(Monsalve-Bravo & Bhatia, 2018)	$\frac{P_0}{P_{eff}} = (1 - f) + \left(\frac{1}{\left(\frac{1}{\omega f} - \frac{1 - f}{\alpha^2 \phi^2} \right)^3} \right)$
	Pal(Pal, 2007)	$\left(\frac{P_0}{P_{eff}} \right)^{-1/3} \times \left(\frac{\left(\frac{P_d}{P_0} \right) - \left(\frac{P_{eff}}{P_0} \right)}{\left(\frac{P_d}{P_0} \right) - 1} \right) = \left(1 - \frac{f}{f_{max}} \right)^{f_{max}}$
Non-ideal MMMs	Modified Maxwell(Mahajan & Koros, 2002b)	$\frac{P_0}{P_{eff}} = \frac{P_{eff} + 2P_0 + (f + f_v)(P_0 - P_{eff})}{P_{eff} + 2P_0 - 2(f_d + f_v)(P_0 - P_{eff})}$
	Li(Y. Li et al., 2006)	$\frac{P_0}{P_{eff}} = \frac{P_{eff} + 2P_0 + (f + f_v + f_{bl})(P_0 - P_{eff})}{P_{eff} + 2P_0 - 2(f_d + f_v + f_{bl})(P_0 - P_{eff})}$
Polymer/IL	Mannan(Mannan et al., 2017)	$\frac{P_0}{P_{eff}} = \frac{P_d + 2P_0 + \beta_{eff}f(P_0 - P_d)}{P_d + 2P_0 - 2\beta_{eff}f(P_0 - P_d)}$
MMMs/IL	MWS(Mohshim et al., 2014)	$\frac{P_0}{P_{eff}} = \frac{\alpha_c P_d + (1 - n_i)P_0 + \alpha_c f_w(P_0 - P_d)}{\alpha_c P_d + (1 - \alpha_c)P_0 + (1 - \alpha_c)f_w(P_0 - P_d)}$

1.2.2 Numerical modeling

This section is devoted to the numerical analysis of transport properties of mixed matrix membranes. Although various analytical models exist in literature to describe mass transport through these membranes, they present some limitations such as not considering the effect of the adsorption equilibrium at the polymer/filler interface (Singh, Kang, & Nair, 2013). Moreover, most of analytical models do not consider the non-idealities of the MMMs such as the presence of interfacial voids or rigidified regions in the polymers. Including those complexities in models usually leads to mathematical formulations that can only be solved numerically.

A 2D numerical model has been developed by Boom and coworkers (Boom et al., 1998) considering a single filler placed in a matrix to predict the permeation behavior of zeolite/polymer MMMs. The mass transport was considered as Fickian and the obtained

results showed that the interfacial adsorption equilibrium is an important factor to predict the permeation behavior in the MMMs.

Later, Singh et al. (Singh et al., 2013) expanded the previous model to a 3D geometry considering dispersed spherical fillers in the polymer matrix. Their model was based on the Finite Element Method and mass transfer was described by Fick's law. The objective of their simulations was to calculate the effective diffusivity in the MMM.

The predicted relative effective diffusivity was shown to increase when the filler volume fraction increased. These results were in agreement with the analytical models when the interface equilibrium constant was set to unity. However, it was shown through the model that the interface equilibrium and the ratio of the filler diffusivity to the matrix diffusivity are the factors that govern MMMs permeability.

Moreover, the developed model takes into account the effect of filler size and no important effect of this parameter on the MMM permeability was demonstrated. These calculations showed also that the non-idealities of MMMs (such as the presence of interfacial voids or rigidified polymeric regions at the interface with the filler) must be taken into account in order to describe transport and adsorption behavior through MMMs.

Wang and coworkers have reported a method to estimate the effective diffusivity through MMMs where fillers had a tubular shape (T. P. Wang & Kang, 2015).

The considered geometry in their work is the following:

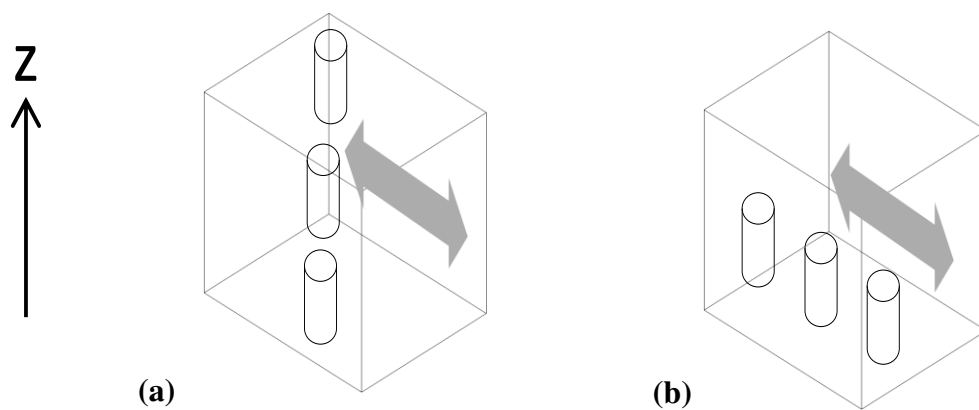


Figure B.1.6 The geometry used in Wang et al. work (a) fillers parallel to z-axis (mass flux direction) (b) fillers normal to z-axis (mass flux direction) (T. P. Wang & Kang, 2015)

The numerical solutions were obtained by solving Fick's diffusion equation using the FEM method. Several morphological parameters were taken into consideration in their model such

as fillers distribution, aspect ratio, orientation, etc. It has been shown that diffusivity strongly depends on filler spatial distribution, which was preferred to be normal to the mass transfer direction (the z-axis direction) in order to maximize the effective diffusivity. Furthermore, it has been shown through the developed model that filler aspect ratio does not have a significant effect when fillers are randomly oriented in the MMM. However, a high aspect ratio is beneficial when fillers are normally oriented to the flux direction. In addition, it has been demonstrated that MMM diffusivity is improved when fillers are very highly diffusive.

The same authors studied later the effective diffusivity and selectivity of mixed matrix membranes with layered fillers (T. P. Wang & Kang, 2016). The objective of the built model was to investigate the effects of fillers aspect ratio, shape, and orientation on the transport properties taking into account anisotropic diffusivity of the fillers.

Mass transfer in MMMs was described by Fick's law, which was solved numerically using the finite element method. It has been shown through the obtained results that when diffusivity is anisotropic in the fillers (meaning that the in-plane diffusivity is different from the out-of-plane diffusivity (**Figure B.1.7**)), the resulting effective diffusivity is governed by the out-of-plane diffusivity. Moreover, it has been concluded that high MMMs selectivity could be obtained using fillers with isotropic diffusivity.

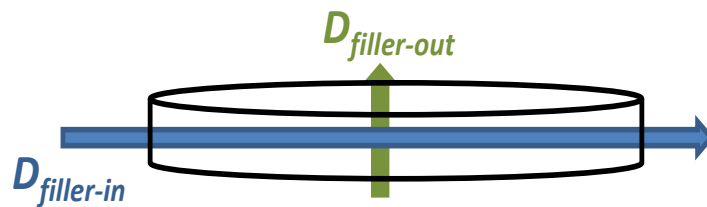


Figure B.1.7 Schematic illustration of in-plane and out-of-plane diffusivity of the filler

The estimation of the effective diffusivity in the mixed matrix membranes was also studied by Yang and coworkers (A. C. Yang, Liu, & Kang, 2015). The specificity of their work is the consideration of hollow fibers made from mixed matrix membranes, which had not been reported in literature before. The relative effective diffusivity variation as a function of the filler volume fraction has been investigated and compared to Maxwell model. The simulation results highlighted the effect of the filler diffusivity and solubility on the enhancement of the overall transport in the mixed matrix membranes hollow fiber. Moreover, the team evidenced that filler size can affect the diffusivity (the smaller the filler, the higher the MMMs diffusivity). The dimensions of the MMMs are also factors that influence the overall

diffusivity. Indeed, it has been shown that increasing the thickness of the skin layer, which can lead to a reduction of fillers size, enhances the overall diffusivity. Moreover, decreasing its interior diameter could also increase the relative effective diffusivity values. Finally, the built model suggests that the diffusivity calculated for the hollow fiber MMMs is higher than for the respective dense MMMs (A. C. Yang et al., 2015).

The impact of fillers structural parameters on MMMs was studied also by Azimi et al. (Azimi, Tezel, & Thibault, 2018) who built a 3D numerical model based on finite difference method by solving Fick's equation of diffusion. They have considered a uniform distribution of cubical, cylindrical and spherical fillers in the membrane. Their results showed that fillers volume fraction had an impact on the overall permeability. As in previous works, they have shown that fillers dimensions do not have a significant effect on the transport properties. Moreover, results also showed that the relative effective permeability of MMMs was higher for cylindrical fillers having a vertical orientation to the flux direction compared to horizontal cylinders under identical conditions.

To conclude, it must be noticed that only few numerical models investigating the transport properties in mixed matrix membranes can be found in the literature. Moreover, most of analytical cited models are mainly interested in permeability while numerical models do not take into account the aggregation effect of fillers in the MMMs. In this work, we will propose a 3D numerical approach based on finite element method to investigate filler effect on gas diffusion properties of the different studied mixed matrix membranes. Indeed, this factor will be identified as the governing parameter of the transport in our materials series. In our modeling approach, the formation of filler aggregates will be considered and the predictions will be compared to our experimental results in order to evaluate the effectiveness of the proposed model and to highlight the structural parameters that influence significantly the transport properties of our mixed matrix membranes.

1.3 Conclusion

This chapter has reviewed the parameters governing gas transport through multiphase polymer-based systems for gas separation applications and has presented the available analytical and numerical models dealing with this phenomenon.

Those systems are basically made of a polymer matrix and various fillers which can be liquids such as the Ionic Liquid or permeable organic/inorganic fillers. It has been shown through this

chapter that gas transport properties are related to different parameters including the polymer and fillers properties as well as morphological and interfacial parameters. Moreover, a literature survey of the analytical and numerical models predicting the transport properties of the studied systems has been presented. In the next chapter, we will focus on the investigation of gas transport in two- and three-component systems based on PEI, ZIF and IL through an experimental study in order to expand the works cited previously and develop new conclusions concerning the governing parameters of gas diffusion. In addition, a modeling approach will be proposed in order to validate the experimental results and highlight the effects of various parameters on the transport properties of multiphase polymer systems.

Chapter 2 Gas transport properties of membranes based on polyetherimide, metal organic framework and ionic liquid: Influence of the composition and morphology

An overview of the chapter

This last chapter aims to study the gas separation properties of three particular types of multiphase polymer systems selected from those presented in the previous chapter.

Mixed matrix membranes based on polyetherimide as continuous phase and ZIF-8 as dispersed phase are considered and their transport properties are investigated. A second system consisting of polyetherimide matrix with ionic liquid ([Emim] [BF₄]) is prepared and its separation properties are characterized. Finally, a system of mixed matrix membrane with ionic liquid is presented and its transport properties are compared to those obtained for the previous systems. The results are assessed in relation to existing experimental and theoretical data from the literature.

Furthermore, this chapter includes a numerical analysis of the transport properties of mixed matrix membranes using the finite element method according to the approach developed in Part A of this thesis.

2.1 Introduction

Global warming is recognized by almost all atmospheric scientists as a significant environmental problem caused by an increase in levels of certain trace gases in earth's atmosphere since the beginning of the Industrial Revolution in the mid-18th century. These gases, collectively called greenhouse gases, include carbon dioxide (CO₂) (Jacobson, 2009; Smithson, 2002; Tollefson & Weiss, 2015). Removing CO₂ from gas mixtures emitted by human activity is of crucial importance to cut down its atmospheric concentration increase (Metz, Davidson, De Coninck, Loos, & Meyer, 2005). Different strategies have been developed for that purpose including sorbents/solutions methods, cryogenic distillation methods and membranes separation methods (Bredesen, Jordal, & Bolland, 2004; Favre, 2011; Hägg & Lindbråthen, 2005; Ho, Allinson, & Wiley, 2008; Oyenekan & Rochelle, 2006; Powell & Qiao, 2006; Rochelle, 2009; Tuinier, van Sint Annaland, Kramer, & Kuipers, 2010; M. Wang, Lawal, Stephenson, Sidders, & Ramshaw, 2011). The latter is a promising technique because of its advantages concerning energy savings, small footprint and environmental sustainability (Baker, 2002; Baker & Lokhandwala, 2008; Koros, 2002). More particularly, polymeric membranes are the most widely used for separation applications (Freeman & Pinnau, 1999; Maier, 1998; Stern, 1994). However, the challenge of enhancing both gas permeability and selectivity of polymeric membranes suggests the incorporation of selective and highly permeable fillers into the polymer matrix to form mixed matrix membranes (MMMs) (Hibshman, Cornelius, & Marand, 2003; Joly, Smaïhi, Porcar, & Noble, 1999; J. H. Kim & Lee, 2001; Merkel et al., 2002; Moaddeb & Koros, 1997; Suzuki & Yamada, 2005). Zeolitic imidazolate frameworks (ZIFs) are a new class of inorganic materials that have been extensively mixed with polymer matrix for gas separation applications in the last decade (Banerjee et al., 2008; Dai et al., 2012; H. Li, Eddaoudi, O'Keeffe, & Yaghi, 1999; Yaghi et al., 2003). They are characterized by their exceptional thermal and chemical stability (X.-C. Huang, Lin, Zhang, & Chen, 2006; K. S. Park et al., 2006), high sorption capacity and their high surface areas and pore volumes (Bux et al., 2009; Ordonez et al., 2010). Haldoupis et al. (Haldoupis, Watanabe, Nair, & Sholl, 2012) showed that those fillers could have important membrane selectivity for CO₂/CH₄ mixture. Several authors focused on MMMs based on polymeric membranes and zeolitic imidazolate frameworks (ZIF-8) particles. Nafisi et al. (Nafisi & Hägg, 2014) incorporated ZIF-8 within a commercial polyamide-block-ether copolymer (Pebax 2533). The initially good CO₂ permeability of the semi-crystalline and rubbery matrix was further improved: the

permeability increased from 351 to 1287 Barrer for a membrane containing 35 wt% of ZIF-8. Xu et al. even showed a higher enhancement in CO₂ permeation performance by inserting ZIF-8 particles in Pebax 1657 matrix (Xu et al., 2017). The membrane containing 18 wt% ZIF-8 exhibited as high as 300 % increase in CO₂ permeability in comparison with the neat polymer membrane. More recently, some researchers used glassy polymers such as polyetherimide (PEI-Ultem1000) to prepare mixed matrix membranes for gas separation applications. This amorphous polymer has already been shown as particularly interesting for membrane applications. It is a thermally stable material from which it is possible to easily form dense or porous membranes (Clémenson, Espuche, David, & Léonard, 2010; Kurdi & Tremblay, 1999; López-González, Compan, Saiz, Riande, & Guzman, 2005; Qariouh, Schué, Schué, & Bailly, 1999; Ripoche, Menut, Dupuy, Caquineau, & Deratani, 2002; Uriarte, Alfageme, & Iruin, 1998). Eiras et al. (Eiras et al., 2016) prepared MMMs from PEI, with the aim to improve its gas separation properties. They showed that the addition of ZIF-8 could increase CO₂ permeability without detrimental effects on CO₂/CH₄ and CO₂/N₂ selectivities. Moreover, Dai and coworkers (Dai et al., 2012), reported the development of PEI/ZIF-8 mixed matrix hollow fiber membranes which was dedicated to the improvement of CO₂/N₂ selectivity. However, some authors showed that the incorporation of ZIF-8 particles in polymeric membranes could lead to the formation of interfacial defects due to poor adhesion between both components (Song et al., 2012). To face those issues, filler surface modification through alkoxysilane grafting is often performed (N. N. R. Ahmad, Mukhtar, Mohshim, Nasir, & Man, 2016). In this context, one original route could be to add a third component in the medium with the aim to favor the accessibility to the porous fillers while avoiding defects and maintaining specific interactions towards CO₂ (M. Li et al., 2017). Ionic liquids (ILs) are being a new alternative to prepare membranes for CO₂ removal applications (Gao et al., 2018; Hasib-ur-Rahman, Siaj, & Larachi, 2010; Tomé, Patinha, Freire, Rebelo, & Marrucho, 2013). Their distinct properties such as negligible vapor pressure and their affinity to capture the CO₂ molecules make them very useful today. Blanchard et al. (L. A. Blanchard, Gu, & Brennecke, 2001) showed that CO₂ has a very high solubility in 1-Butyl-3-methylimidazolium hexafluorophosphate ([bmim] [PF₆]). Different other ILs such as 1-Ethyl-3-methylimidazolium tetrafluoroborate ([Emim] [BF₄]) are also recognized for their interesting CO₂ sorption ability (Magana et al., 2016). Moreover, a recent work performed on a system composed of poly(Room Temperature IL)s, Room Temperature ILs and SAPO-34 particles showed an improvement of the filler/matrix compatibility, as well as an enhancement of the CO₂ absorption (Hudiono et al., 2011).

In the current work, two component and three component membranes have been prepared and characterized and their gas transport properties are reported. The studied systems are composed essentially of Polyetherimide (PEI), ZIF-8 particles and [Emim] [BF₄] ionic liquid. The specificity of this work consists in the investigation of the gas separation properties of such systems through experimental analysis and finite element modeling.

2.2 Experimental

2.2.1 Materials

Polyetherimide (Ultem 1000) with bulk density of 1.27 g/cm³ was purchased from GE Plastics. Basolite Z1200 (ZIF-8) with bulk density 0.35 g/cm³ and methylene chloride (CH₂Cl₂, boiling temperature T_b=40°C) were purchased from Sigma-Aldrich. 1-ethyl-methylimidazolium tetrafluoroborate ionic liquid (purity > 98%; degradation temperature T_d=450°C) with density 1.387 g/cm³ was purchased from Io-Li-Tech.

2.2.2 Membranes preparation

Four film series were prepared: PEI reference films, PEI films containing increasing amounts of IL (from 2.5 to 20 wt%), mixed matrix films composed of PEI and ZIF-8 in which ZIF-8 content was varied between 10 and 25 wt% and mixed matrix films combining IL and ZIF-8.

2.2.2.1 PEI/IL membranes

In all series, PEI was dried at 120°C in a vacuum oven for 6 hours prior to be used. Then, it was dissolved in CH₂Cl₂ for almost 1 hour at ambient temperature under stirring to prepare 80 g/L PEI solution.

For reference PEI film, the prepared solution was cast onto a glass plate which was covered with a holey box and kept overnight in order to evaporate the solvent.

For PEI/IL films, defined amounts of IL were dissolved in the same solvent as that used to prepare the PEI solution. The mixture was mechanically stirred for 30 min. Then, PEI granules (pre-dried) were added to the solution and further stirred for 1 h to ensure complete mixing. The solutions were cast onto glass plate and dried under ambient conditions overnight. The obtained films are named: PEI/x IL, where x corresponds to the weight amount of IL contained in the membranes.

2.2.2.2 *PEI/ZIF-8 membranes*

Appropriate amounts of ZIF-8 were dispersed in CH_2Cl_2 for 1 h by using a sonication bath. 20% of the PEI solution was added to the ZIF-8 dispersion and the blend was sonicated for 1h. In the last step, the rest of the polymer solution was added gradually to the ZIF-8 mixture and the resulting mixture was kept under mechanical stirring for almost 2h. The solutions were cast on glass plates and dried at room temperature. The obtained films are denoted by: PEI/y ZIF-8, where y represents the weight amount of ZIF-8 within the membrane (increased up to 25 wt%).

2.2.2.3 *PEI/ZIF-8/IL membranes*

The protocol used to prepare the three-component membranes was as follows: first, the appropriate amount of IL was added to the polymer solution to reach a final IL content of 2.5 or 7 wt% within the membrane. The solution was kept under stirring for almost 1 h. Then, a dispersion of ZIF-8 particles was prepared as described before and sonicated for 1 h. 20 vol% of the polymer/IL solution was added to ZIF-8 dispersion and kept in the ultrasonic bath for 1h. Subsequently, the rest of PEI/IL solution was added to the mixture and sonicated for another 1h. The obtained solutions were poured onto glass plate and dried under ambient temperature overnight in order to obtain finally two defined membrane compositions. The membranes were denoted by: PEI/2.5 IL/10 ZIF-8 and PEI/7 IL/10 ZIF-8.

2.2.3 *Membrane characterization*

The thermal degradation behavior of the prepared membranes was investigated using thermogravimetric analyzer TGA Q500 (TA Instruments) in order to measure the mass change versus temperature under air (60 mL/min) and helium (40 mL/min) with a heating rate of $10^\circ\text{C}/\text{min}$ in a temperature range from 25°C to 650°C . Differential scanning calorimeter (DSC) Q200 1854 (TA Instruments) was used to determine the glass transition temperature (T_g) of the polymer matrix by heating samples from 25°C to 250°C at a heating rate of $10^\circ\text{C}/\text{min}$ under helium atmosphere. Two heating cycles were recorded and glass transition temperature T_g values were determined as usually done for high T_g systems (Grigoryeva et al., 2006) on the thermo-gram corresponding to the second cycle using the midpoint method.

The morphology of PEI/IL, PEI/ZIF-8 and PEI/IL/ZIF-8 membranes was analyzed by Scanning Electron Microscopy (SEM) using a Quanta 250 from FEI. SEM images were taken on the membrane cross section. The samples were prepared by ultra-microtomy at room

temperatures using a diamond knife to obtain smooth surfaces. They were metallized with carbon.

Energy-dispersive X-ray (EDX) analysis was conducted in order to complete SEM observations with information about the chemical composition of the different domains evidenced by SEM.

Surface energy of the membranes was calculated thanks to the measurement of contact angles. The contact angles (θ_c) were measured with an optical contact angle meter (DSA 100 equipped with CDD2/3 camera, Krüss) via the sessile drop technique. Water ($\gamma_L^d=21.8$ mN/m; $\gamma_L^p=51$ mN/m) and diiodomethane ($\gamma_L^d=48.5$ mN/m; $\gamma_L^p=2.3$ mN/m) were used as liquid probes. Fowkes model (Fowkes, 1964) (equation (B.2.1)) was applied in order to determine both dispersive (γ_s^d) and polar (γ_s^p) components of the surface energy.

$$\gamma_L(1 + \cos\theta_c) = 2\sqrt{\gamma_s^d\gamma_L^d} + 2\sqrt{\gamma_s^p\gamma_L^p} \quad (\text{B.2.1})$$

where θ_c is the contact angle, γ_L is the liquid surface energy, γ_L^d and γ_s^d are the dispersive components of the surface energy of the liquid and the film, respectively and γ_L^p and γ_s^p are the polar components of the surface energy of the liquid and the film, respectively.

2.2.4 Gas permeation analysis

Gas permeation experiments were carried out at 20°C for He, CO₂ and H₂. The permeation cell, consisting of two compartments separated by the membrane, was desorbed under secondary vacuum before each experiment. A 2 bar gas pressure was then applied to the upstream compartment of the cell. The pressure variations in the downstream compartment were measured over time allowing to determine the flux (J) of gas diffusing through the membrane. The permeability coefficient, P_i , expressed in Barrer (1 Barrer = 10^{-10} cm_{STP}³.cm.cm⁻².s⁻¹.cm_{Hg}⁻¹ = 3.36×10^{-16} mol.m.m⁻².s⁻¹.Pa⁻¹) was calculated thanks to the flux J in the steady state.

However, the diffusion coefficient D_i is determined by the time-lag method:

$$D_i = \frac{e^2}{6 \cdot \theta_{lg}} \quad (\text{B.2.2})$$

where θ_{lg} is the time lag determined through the intersection of the extrapolated steady state linear part with the time axis.

The solubility and selectivity are calculated as explained before in this manuscript through equation (A.1.1) and (B.1.1).

2.3 Results

2.3.1 PEI/IL membranes

2.3.1.1 Membrane bulk and surface characterization

The thermal properties of the studied membranes were determined by thermo-gravimetric analysis (TGA) and differential scanning calorimetry (DSC). **Figure B.2.1** (a) and (b) show mass loss curves and DSC thermo-grams for reference PEI membranes and PEI/IL membranes.

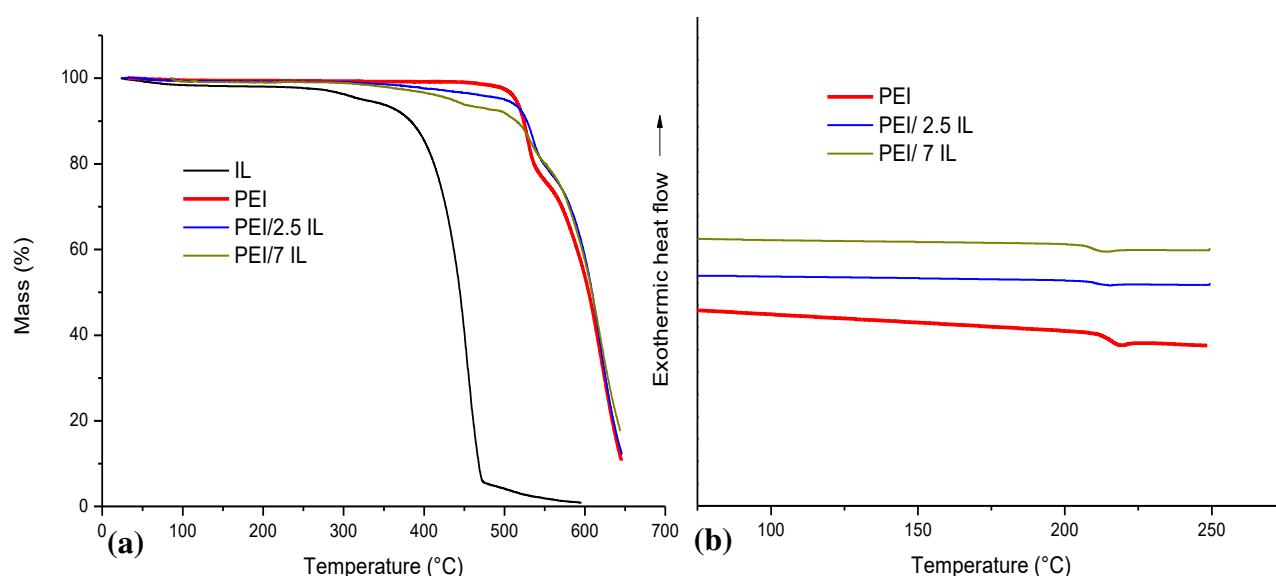


Figure B.2.1 (a) TGA mass loss curves and (b) DSC thermograms for PEI/x IL (x=0; 2.5; 7)

It can be observed from figure 1a that IL degradation begins at lower temperature in comparison with PEI (around 300°C for IL and 530° for PEI). The small weight loss observed at low temperature for IL could be assigned to the presence of water. For PEI/IL membranes, a first mass loss is observed in the range between 350°C and 530°C, which corresponds to the content of IL within the film. At higher temperature, the mass loss curves of PEI/IL are similar to that obtained for PEI. Moreover, it has to be noticed that no significant weight loss is observed on the studied membranes below 250°C meaning that the membranes do not contain any residual solvent. This is important to check as the presence of residual solvent, even in low amount, can significantly modify the transport properties of glassy polymers (Clémenson et al., 2010).

The DSC thermograms of PEI/IL membranes are presented in **Figure B.2.1** (b). The PEI reference membrane exhibits a glass transition temperature of 216°C which is in agreement with T_g values reported in literature (Clémenson et al., 2010; Eiras et al., 2016). The glass transition temperature is very slightly shifted to lower values when IL is added to the polymer matrix ($T_{g_{PEI/2.5\text{ IL}}}$ and $T_{g_{PEI/7\text{ IL}}}$ values are around 211°C). Since T_g value of the IL is around -99 °C (Magana et al., 2015), the observed decrease of T_g value for PEI/IL membranes could be assigned to a miscibility phenomenon between the ionic liquid and the polymer matrix. Fox law was used in order to determine the amount of IL dissolved within the PEI matrix.

$$\frac{1}{T_g} = \frac{w_i}{T_{g_i}} + \frac{w_j}{T_{g_j}} \quad (\text{B.2.3})$$

where w_i and w_j are the weight fractions of the components i and j , T_g , T_{g_i} and T_{g_j} are the glass transition temperatures of the blend, the component i and j respectively.

The content of IL dissolved in the PEI matrix was found to be 0.57 wt% for both PEI/2.5 IL and PEI/7 IL which is far from the amount of IL that was mixed with the PEI matrix. Thus a low miscibility degree between the PEI matrix and the ionic liquid was evidenced in our membranes.

Cross sectional SEM images of neat PEI, PEI/ 2.5 IL and PEI/ 7 IL membranes are presented in **Figure B.2.2** a to d.

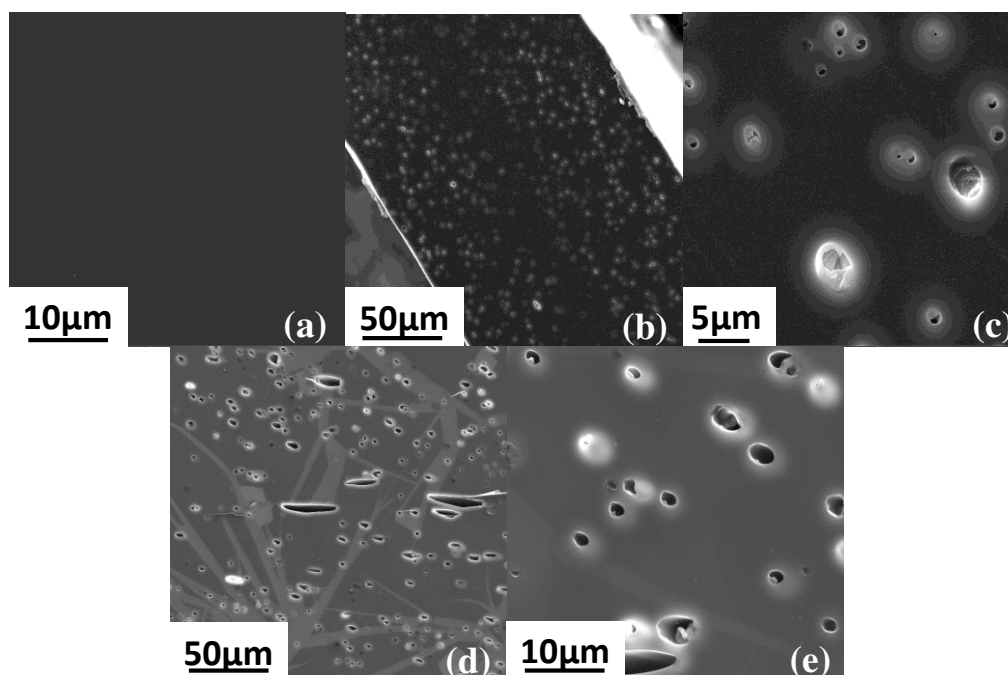


Figure B.2.2 SEM images for the cross-section morphologies of (a) neat PEI (b) and (c) PEI/2.5 IL membranes (d) and (e) PEI/7 IL membranes

Figure B.2.2 (a) reveals a homogenous smooth cross section for neat PEI membrane. Introducing ionic liquid in the polymer matrix leads to the formation of micrometer size domains that are uniformly dispersed in the polymer matrix (**Figure B.2.2** b to d). The EDX spectra performed on the matrix and on the dispersed domains confirm that the dispersed domains are composed of IL. Indeed the presence of a signal relative to Fluorine is observed on the EDX spectrum of the dispersed domains whereas this signal is logically not observed for the PEI matrix (**Figure B.2.3**).

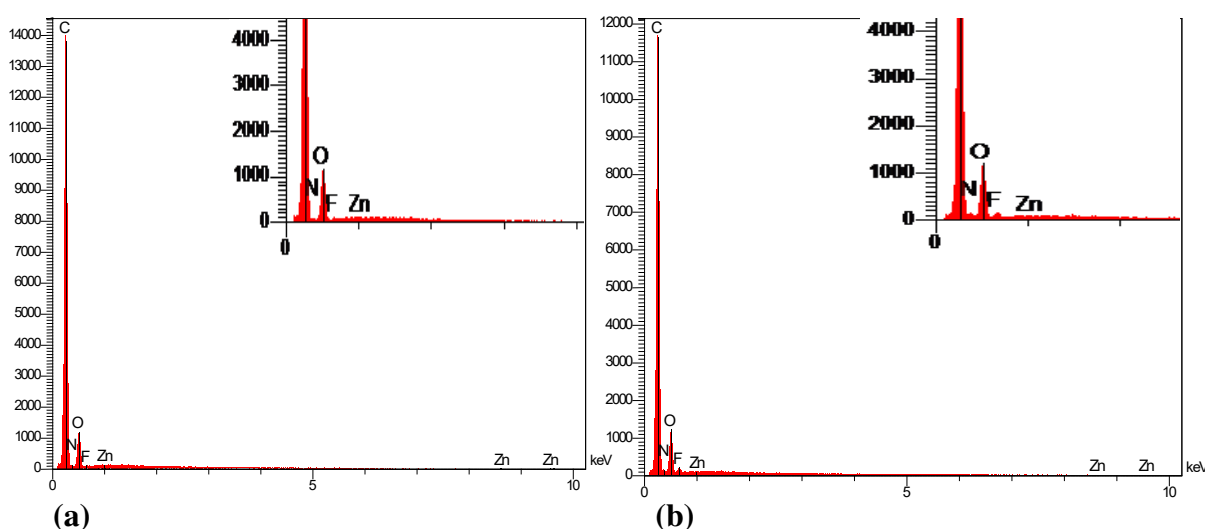


Figure B.2.3 EDX spectra of (a) PEI matrix and (b) IL

From SEM images, it can also be observed that the more IL content is increasing, the more the dispersed domains corresponding to IL are numerous and large-sized. Thus, the phase separation observed for PEI/IL systems is in agreement with the low miscibility degree between IL and PEI that was evidenced by the low decrease of the glass temperature of PEI in the PEI/IL systems.

The wettability of the membranes was analyzed through water and diiodomethane contact angle measurements and surface energy calculations (**Table B.2.1**).

Table B.2.1 Contact angle and surface energy measurements of the studied films

Film	Contact angle (°)		Surface energy (mN/m)		
	H ₂ O	CH ₂ I ₂	γ_d	γ_p	γ_s
PEI	88.8±3.0	48.9±6.5	36.5±3.8	1.6±0.2	38.1±2.0
PEI/2.5 IL	87.0±1.8	47.2±4.6	37.5±2.7	2.9±0.1	40.4±0.5
PEI/7 IL	83.2±0.8	47.7±1.7	37.2±1.0	1.8±0.04	39.1±1.4
PEI/10 ZIF-8	78.8±4.7	58.8±4.2	30.7±2.5	6.1±1.3	36.7±1.9
PEI/15 ZIF-8	79.1±3.5	65.6±2.7	26.6±1.6	7.2±1.1	33.8±1.4
PEI/20 ZIF-8	77.2±2.9	63.5±2.0	27.8±1.2	7.7±1.0	35.5±1.1
PEI/25 ZIF-8	83.5±3.7	57.1±2.6	31.7±1.6	4.0 ±0.9	35.7±1.3
PEI/2.5 IL/10 ZIF-8	79.0±5.8	49.0±4.3	36.5±2.5	4.5±1.6	41.0±2.0
PEI/7 IL/10 ZIF-8	71.3±4.5	44.0±4.1	39.3±2.3	6.9±1.4	46.2±1.8

The water contact angle value obtained for the neat PEI membrane is $88.8^\circ \pm 3.0$ as reported in literature (Kaba, Raklaoui, Guimon, & Mas, 2005). Moreover, its surface energy is also in the same range as values reported in several publications (45.3 mN/m as reported by Kaba et al. (Kaba et al., 2005) and 41.5 mN/m by Gleich et al. (Gleich, Criens, Mosle, & Leute, 1989)). It can be seen from **Table B.2.1** that diiodomethane contact angle does not depend on the presence of IL. Thus, the dispersive component of the surface energy of the membranes is not modified by the introduction of IL. On the other hand, the water contact angle decreases from 89° to 83° when IL weight fraction is raised to 7%, leading then to an increase of the polar component of the surface energy from 1.6 to 2.9 mN/m. As a consequence, the membrane surface energy increases slightly due to a higher polarity related to the introduction of IL.

2.3.1.2 Gas transport properties

This section presents and discusses the influence of IL on PEI gas transport properties. The gas transport properties are summarized in **Table B.2.2**.

Table B.2.2 Gas transport properties of PEI/IL membranes (the uncertainty is about 5% for P and D_{CO_2} and 10% for S_{CO_2})

	P_{He} (Barrer)	P_{CO_2} (Barrer)	P_{H_2} (Barrer)	$D_{CO_2} \times 10^{-9}$ (cm^2/s)	S_{CO_2} ($cc_{STP}/cm^3 \cdot cm_{Hg}$)	α_{H_2/CO_2}
PEI	9.2	1.83	7.9	1.6	0.11	4.32
PEI/2.5 IL	8.6	1.15	7.4	1.9	0.06	6.43
PEI/7 IL	9.1	1.49	10	2	0.07	6.71

It can be seen that whatever the gases, the permeability coefficients of PEI/IL are similar to those obtained for reference PEI. The same trend is observed concerning the CO_2 diffusion and solubility coefficients. This behavior is in agreement with the trends already observed on other polymer/IL systems that contain low IL amounts (Magana et al., 2016; Sood et al., 2015). As IL forms dispersed domains and is in a relatively low amount, it can be assumed that the gas transport properties are mainly governed by the continuous PEI matrix. As a consequence, H_2/CO_2 selectivity values determined for the reference PEI and PEI/IL membranes are similar.

2.3.2 Polymer/ZIF-8 membranes

In this section, we focused on PEI/ZIF-8 membranes with ZIF-8 amounts ranging between 10 and 25 wt%.

2.3.2.1 Membranes bulk and surface properties

Thermo-gravimetric analyses (TGA) were used to evaluate the thermal stability of the prepared membranes. **Figure B.2.4** compares the mass loss curves of the PEI/ZIF-8 membranes to that of neat PEI.

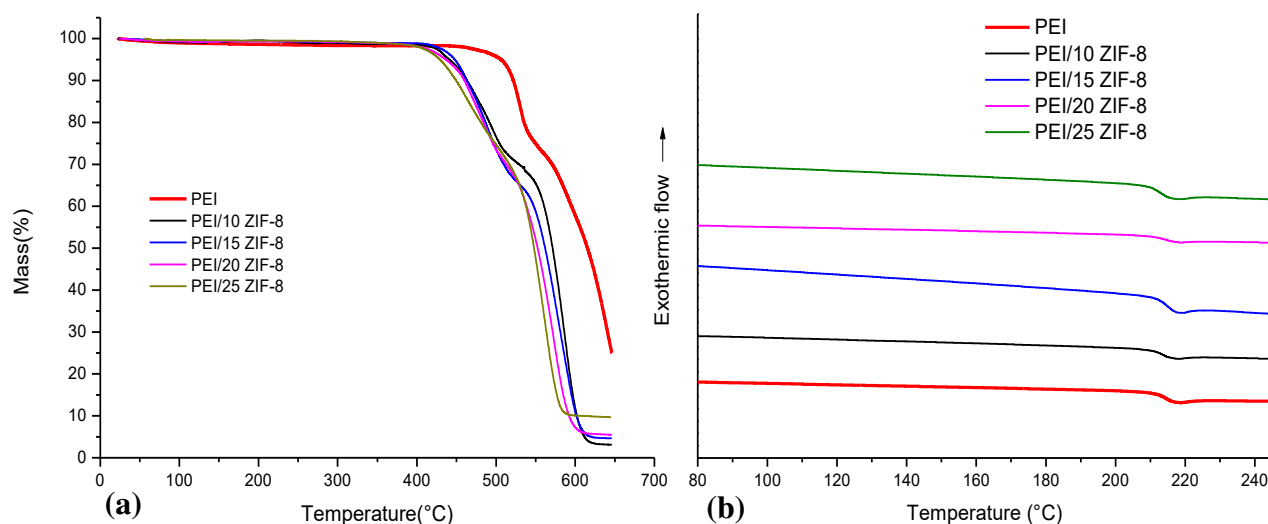


Figure B.2.4 (a) TGA mass loss curves and (b) DSC thermograms of the mixed matrix membranes

The mass loss curve is shifted towards lower temperatures after the introduction of 10 wt% ZIF-8 fillers within the PEI matrix. All PEI/ZIF-8 samples start to degrade at around 421°C. Increasing the ZIF-8 amount does not lead to significant modification of the mass loss curves except for the value of the residue at high temperature which increases when the filler content increases.

It can be seen from **Figure B.2.4 b** that the glass transition temperature measured on the mixed matrix membranes is slightly lower than the value corresponding to the neat PEI membrane. It decreases from 216°C to 212°C for 25 wt% of ZIF-8. An increase of T_g value is often associated with strong filler/matrix interactions (Ordoñez, Balkus, Ferraris, & Musselman, 2010). It is not the case here as no modification of the filler surface has been performed.

SEM analysis was performed to investigate the filler dispersion within the PEI matrix. The images of the membranes cross sections are reported in **Figure B.2.5**.

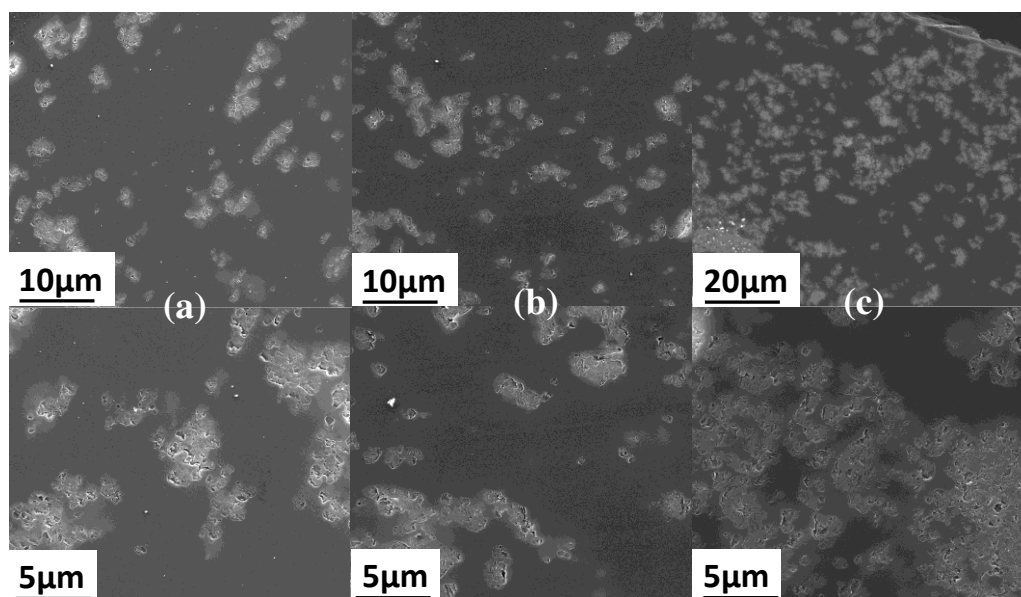


Figure B.2.5 SEM images of (a) PEI/10 wt% ZIF-8 (b) PEI/15 wt% ZIF-8 and (c) PEI/20 wt% ZIF-8

The SEM images show that ZIF-8 particles are homogeneously dispersed within the polymer matrix under the form of small aggregates of few micrometer sizes. Besides the EDX analysis performed on the dispersed domains (**Figure B.2.6**) clearly shows the presence of an intense peak of characteristic of Zn species. This result is in agreement with the chemical composition of the fillers. Looking more precisely at the filler dispersion, one can observe that the ZIF-8 domains form percolation paths at high filler content **Figure B.2.5 c**. It is then expected to observe a specific gas transport behavior for filler content equal or above 20 wt%.

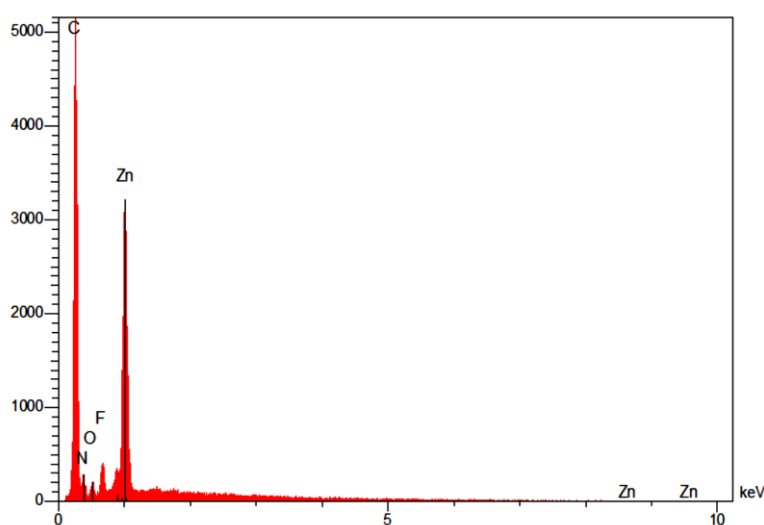


Figure B.2.6 EDX spectra of a filler aggregate in PEI/10 wt% ZIF-8

Concerning the membrane surface properties, **Table B.2.1** shows that the introduction of ZIF-8 fillers within PEI matrix has a significant impact on the value of the contact angles for both liquid probes (H_2O and CH_2I_2). The contact angle increases for diiodomethane whereas it decreases for water. Finally, the dispersive surface tension γ_s^d decreases whereas the polar surface tension γ_s^p increases, leading to global surface energy value close to that determined for reference PEI.

2.3.2.2 Gas transport properties

Table B.2.3 summarizes the permeability coefficients measured for He, H_2 and CO_2 as well as the CO_2 diffusion and solubility coefficients. The H_2/CO_2 selectivity values are also reported in the table.

Table B.2.3 Gas transport properties of the prepared membranes

	P_{He} (Barrer)	P_{CO_2} (Barrer)	P_{H_2} (Barrer)	$D_{\text{CO}_2} \times 10^{-9}$ (cm^2/s)	S_{CO_2} ($\text{cc}_{\text{STP}}/\text{cm}^3 \cdot \text{cm}_{\text{Hg}}$)	$\alpha_{\text{H}_2/\text{CO}_2}$
PEI	9.2	1.8	7.9	1.6	0.11	4.4
PEI/10 ZIF-8	18,3	3,6	17,1	2.7	0.13	4.8
PEI/15 ZIF-8	19,7	3,7	18,3	2.9	0.12	5.0
PEI/20 ZIF-8	27,8	5,5	25,6	4.8	0.11	4.7
PEI/25 ZIF-8	36,2	6,8	30,0	6.7	0.10	4.4

As the ZIF-8 loading increases up to 25 wt%, the permeability to all gases increases to four times the neat PEI membrane's value. Moreover, it can be observed that the evolution of the CO_2 diffusion coefficients follows the same trend as that observed for the permeability whereas the solubility coefficient is not significantly modified by the presence of fillers. Thus the diffusion coefficient is the governing factor in this membrane series of membranes. The percolation paths formed through the ZIF-8 domains at high filler content seem to facilitate gas permeation. This is clearly evidenced in **Figure B.2.7** where the dotted lines reported as guides for eyes show a higher increase of relative permeability in the range of filler content between 17 and 25 wt% than in the range below 17 wt%. The relative permeability is defined as the permeability of the PEI/ZIF-8 membranes ratioed by the permeability of the neat PEI. The data of **Figure B.2.7** also suggests that the formation of continuous paths begins for filler amounts between 15 and 20 wt% increasing is accelerated at this fillers content range.

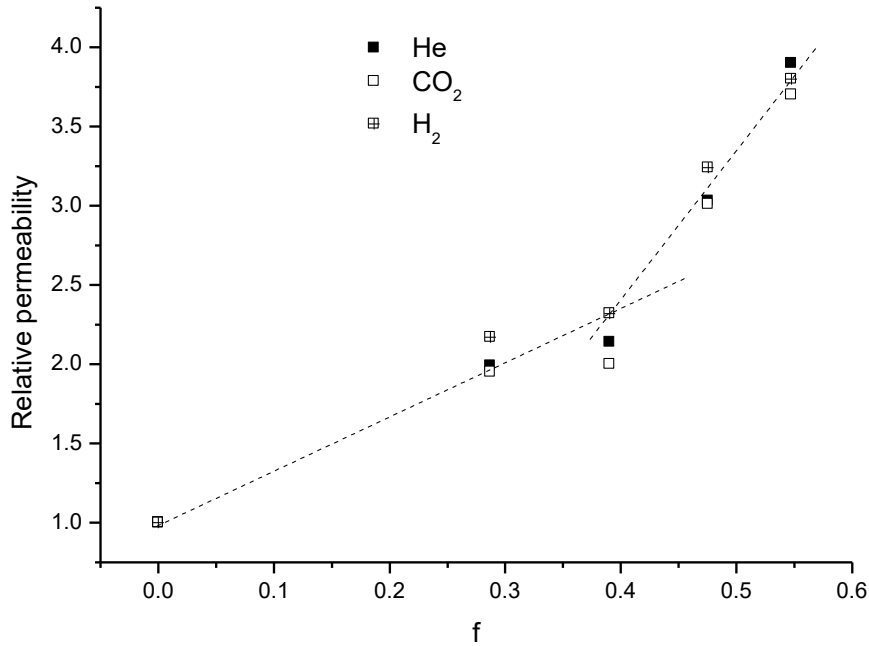


Figure B.2.7 Relative permeability variation as a function of ZIF-8 content for the three studied gases

In order to further understand the permeation behavior of the prepared membranes, a comparison between CO₂ permeability experimental values and the Maxwell model was made. It should be noted that Maxwell model is often used to predict the gas permeation behavior of mixed matrix membranes containing spherical fillers (Cong, Radosz, Towler, & Shen, 2007; Song et al., 2012) (Eq. (B.1.3)).

The CO₂ permeability of the fillers was taken equal to 3300 Barrer as reported by Xu et al. (Xu et al., 2017). It has to be noticed that other values of ZIF-8 permeability can be found in the literature (2819.6 Barrer in (Hao et al., 2013)). However, they remain in the same range and it was checked that the small deviation observed between them (around 10%) has no significant impact on the calculated values of the permeability.

The dotted line in **Figure B.2.8** represents the permeability predicted by Maxwell model. It can be observed that the experimental points are lying below this theoretical curve. However, the difference remains low (around 20%). Maxwell law considers ideal binary systems in which each component keeps its initial properties. It can then be suspected that when the ZIF-8 fillers are embedded in the polymer matrix, they do not behave exactly as they would do if they were alone. However, as previously said, what could be called the matrix effect remains low.

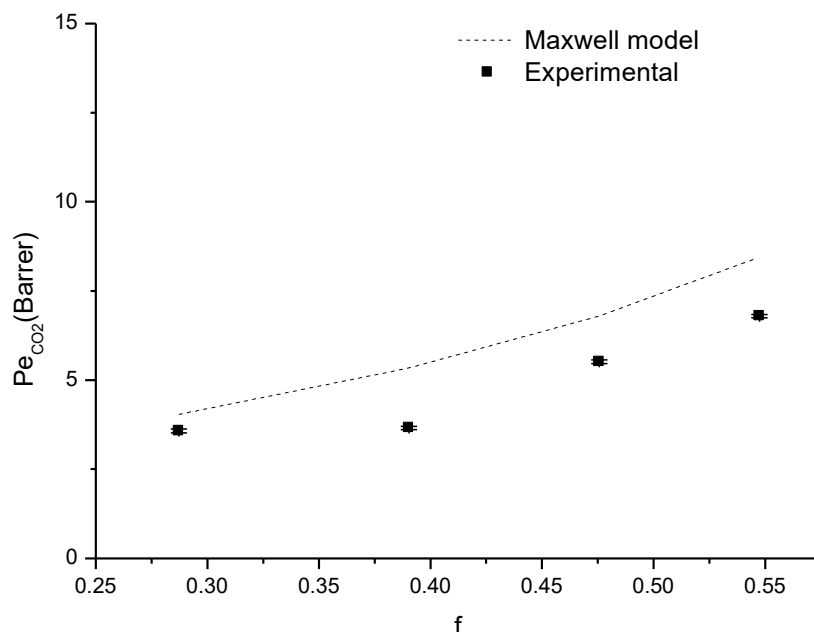


Figure B.2.8 Comparison between Maxwell model and experimental CO₂ permeability coefficients for the studied membranes

To complete the analysis, the CO₂ relative permeability values of our systems were compared to literature data relative to mixed matrix membranes containing ZIF-8 particles (**Figure B.2.9**).

For all systems, the evolution of relative permeability as a function of the filler volume fraction exhibits an increasing trend. It is noteworthy that the relative permeability values obtained in this work are slightly higher than those reported in the literature for similar systems (Deniz, 2012; Eiras et al., 2016). Moreover, considering an extended range of mixed matrix membranes based on ZIF-8, we can conclude from **Figure B.2.9** that the performances of our membranes are interesting.

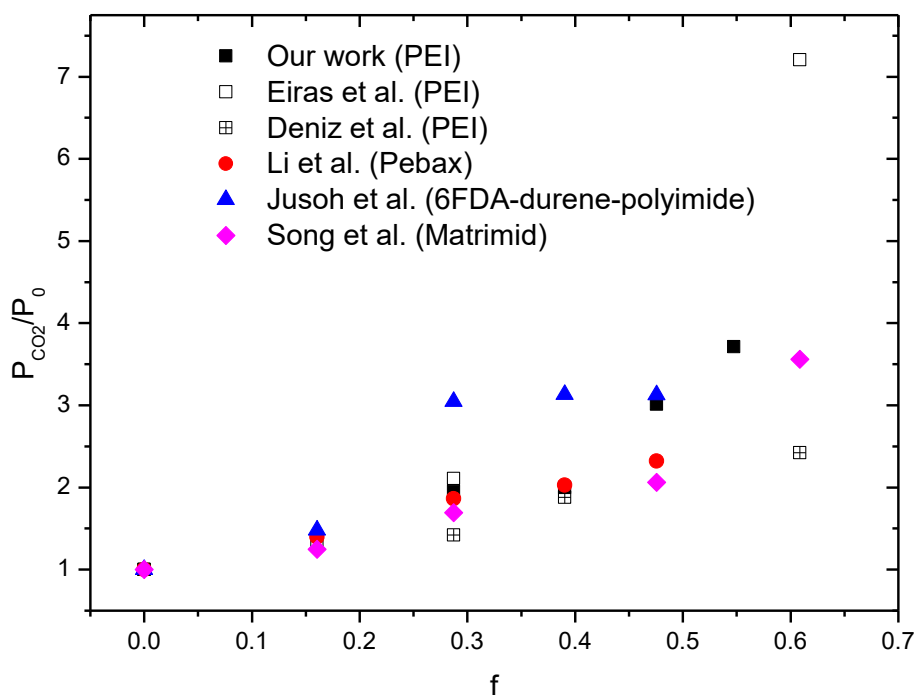


Figure B.2.9 Comparison of the experimental data of this work with several systems based on ZIF-8 from literature (Deniz, 2012; Eiras et al., 2016; Jusoh, Yeong, Lau, & Shariff, 2016; M. Li et al., 2017; Song et al., 2012)

Looking now at the H_2/CO_2 selectivity of our PEI/ZIF-8 membranes, we can see through the values reported in **Table B.2.3** that there is no significant change in the gas selectivity as a function of ZIF-8 content. Although the gas selectivity value of the PEI/ZIF-8 membranes remains close to that of the reference PEI, the increase in H_2 permeability with the filler amount without any impact on the gas selectivity is a beneficial feature for gas separation application. It can be noticed that the same trend was observed by Eiras et al. (Eiras et al., 2016) for CO_2/N_2 gas separation considering the same PEI/ZIF-8 system and Li et al. (M. Li et al., 2017) for CO_2/N_2 separation considering the Pebax/ZIF-8 system.

2.3.3 PEI/IL/ZIF-8 membranes

The aim of this part was to investigate whether a synergistic effect could be obtained by using both IL and ZIF-8 within the PEI matrix. The ZIF-8 particle amount was fixed at 10 wt% in order to avoid the formation of percolation paths through that could make difficult the observation of the IL effect. Two amounts of IL, 2.5 wt% and 7 wt% respectively were considered.

2.3.3.1 Membrane bulk and surface characterization

Figure B.2.10 compares the TGA and DSC plots of the three component membranes to that of the corresponding two component membranes. The thermograms of the neat PEI film have also been included in the figures as reference.

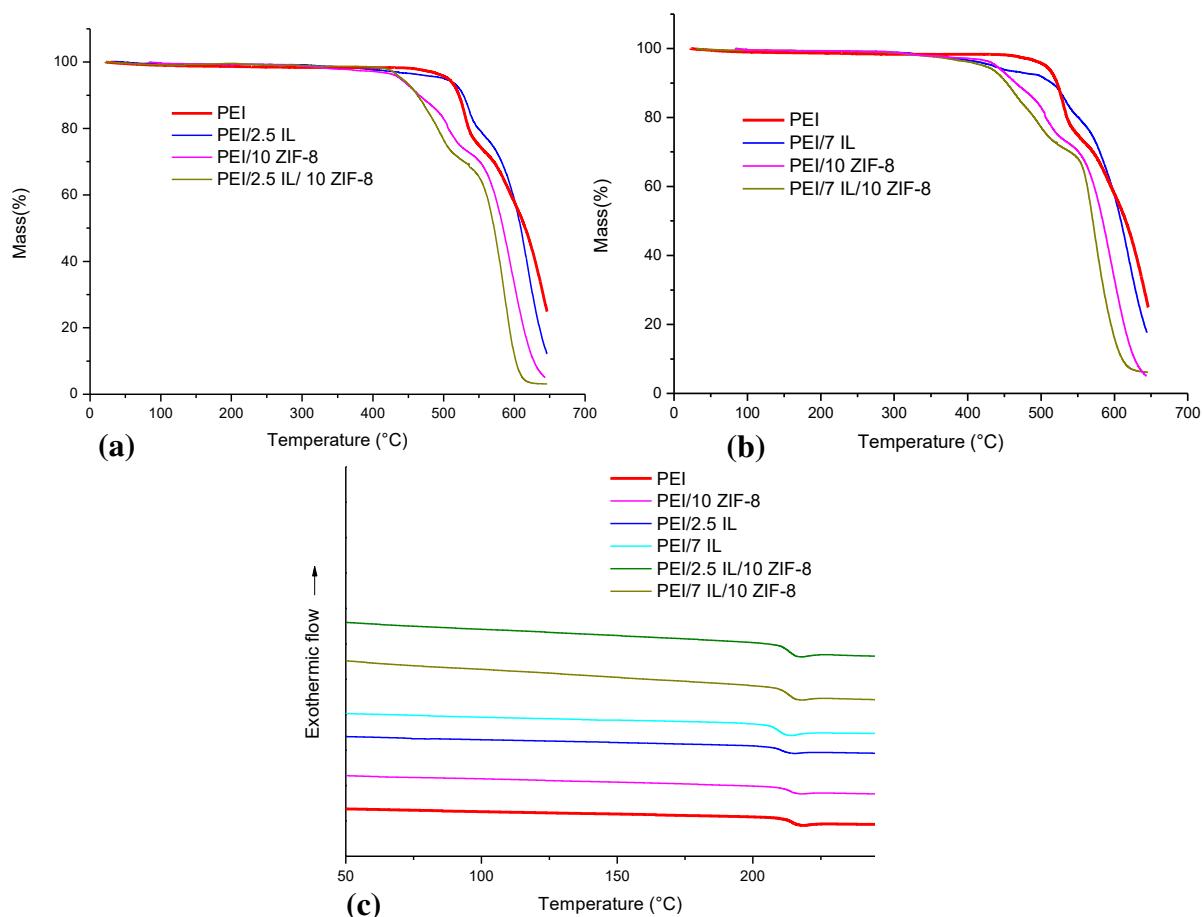


Figure B.2.10 (a), (b) TGA and (c) DSC plots of the studied membranes

The TGA results reported in **Figure B.2.10** (a) evidence that, in the studied range of compositions, all the thermal degradation behavior of the three component systems is close to that of the corresponding PEI/ZIF-8 systems, whereas neat PEI and PEI/IL systems exhibit similar degradation curves. It can then be concluded that the shift of the membrane degradation curve towards lower temperature observed in the three component membrane series is mainly due to the presence of ZIF-8.

The DSC thermograms (**Figure B.2.10** (c)) show that the T_g of the three-component membranes is around 213°C which is similar to that measured on the two-component systems and slightly lower than that corresponding to the neat PEI membrane (216°C). Thus, it can be

concluded from thermal analysis that all the studied membranes exhibit good thermal stability and glassy behavior over an extended range of temperature.

SEM images of the cross sections of the three-component MMMs and that of the corresponding two-component systems are presented in **Figure B.2.11**.

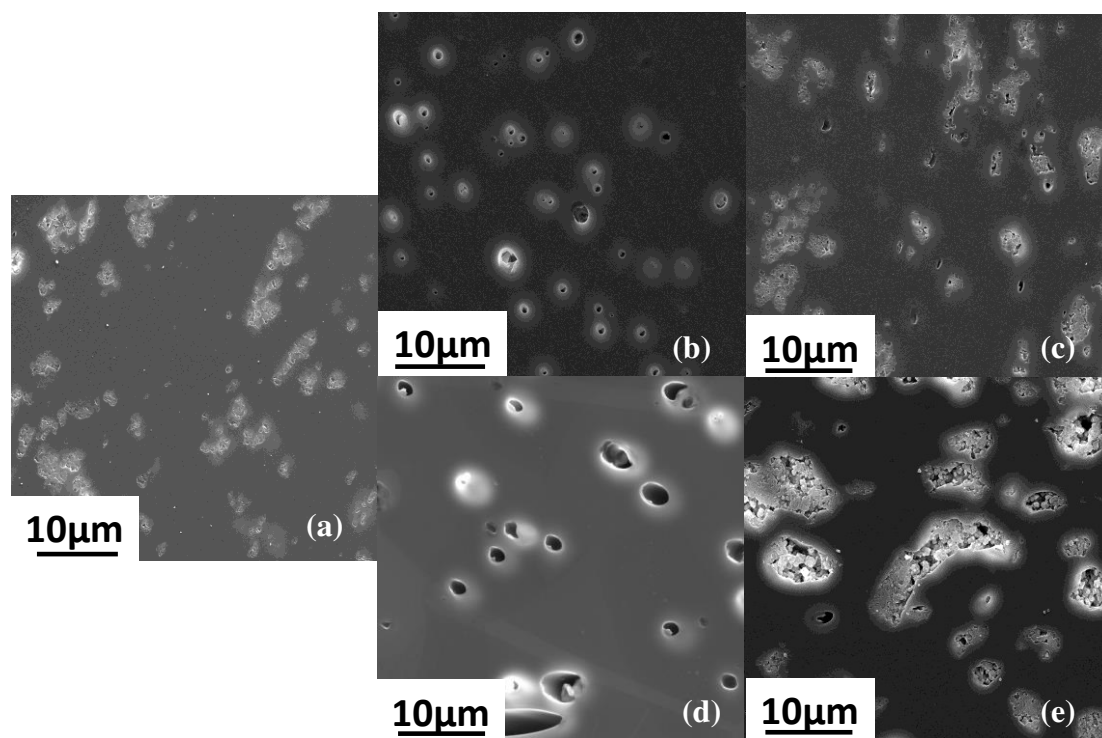


Figure B.2.11 SEM images of the prepared membranes (a) PEI/10 ZIF-8 (b) PEI/2.5 IL (c) PEI/2.5 IL/10 ZIF-8 (d) PEI/7 IL (e) PEI/7 IL/10 ZIF-8

Surprisingly, IL domains cannot be distinguished on the SEM images of PEI/IL/ZIF-8 membranes (**Figure B.2.11** c and e). Moreover, by comparing the SEM images of PEI/ZIF-8, it can be observed that ZIF-8 aggregates are less compact when the membrane contains IL. It seems difficult to assert that the IL is dissolved in the PEI matrix in view of the results previously discussed concerning the PEI/IL systems. One might then assume that IL is located in the domains including the ZIF, which would explain why these aggregates are less compact. EDX analyses were then performed to check if the presence of IL in the domains containing the fillers could be confirmed.

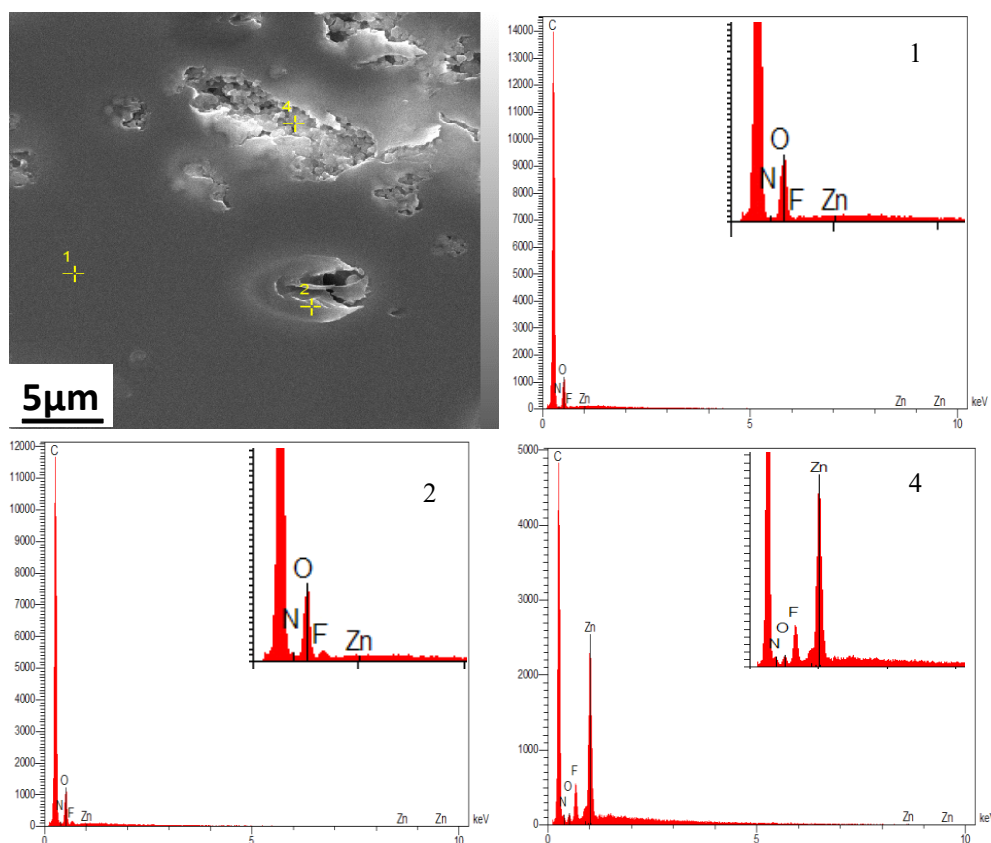


Figure B.2.12 EDX spectra characterizing the different domains observed on SEM of PEI/7 IL/ 10 ZIF-8

It can be seen in **Figure B.2.12** that, at point 1 in SEM image, no characteristic signature of IL is found confirming the absence of IL in the polymer matrix. On the other hand, at point 2 a small peak related to the presence of F species is detected evidencing the presence of IL around ZIF-8 particles. Moreover, at point 4, IL and ZIF-8 signatures (F peak and Zn peak, respectively) are observed confirming the presence of both fillers and IL in the aggregates.

The dispersive and polar components of the surface energy of the PEI/IL/ZIF-8 membranes are reported in **Table B.2.1**. One can see that each component (IL and ZIF-8) plays a role on the membrane surface properties. Indeed, the value of the dispersive component of the surface energy is close to that measured for the respective PEI/IL systems whereas the polar component of the surface energy is similar to that measured on PEI/10 ZIF-8.

2.3.3.2 Gas transport properties

The effect of both IL and ZIF-8 on the MMMs gas transport properties was investigated. The measured values are presented in **Table B.2.4**.

Table B.2.4 Gas permeability, diffusivity and selectivity of the prepared membranes

	P_{He} (Barrer)	P_{CO_2} (Barrer)	P_{H_2} (Barrer)	D_{CO_2} $\times 10^{-9}$ (cm^2/s)	S_{CO_2} ($cc_{STP}/cm^3.cm_{Hg}$)	α_{H_2/CO_2}
PEI/2.5 IL/10 ZIF-8	20	8.5	18	6.1	0.14	2.1
PEI/7 IL/10 ZIF-8	28.3	14	36.6	25	0.056	2.6

Comparing the permeability values of the PEI/IL/ZIF-8 membranes to those of PEI/IL and PEI/ZIF-8 membranes (**Table B.2.2** and **Table B.2.3**, respectively), one can evidence the drastic increase of gas flux by adding both IL and ZIF-8 in the PEI matrix. CO₂ diffusion coefficient increases by a factor around 10 when adding 7 wt% of IL to PEI/ZIF-8 membranes whereas CO₂ solubility coefficient decreases by a factor around 2 which confirms the prevailing role of the diffusion coefficient in the gas transport mechanism. Moreover, one can see thanks to the SEM observations made at larger scale on PEI/7 IL/10 ZIF-8 (**Figure B.2.13**) that the introduction of IL in a high enough amount allows obtaining less dense ZIF-8 aggregates and percolation paths that finally act as diffusion paths.

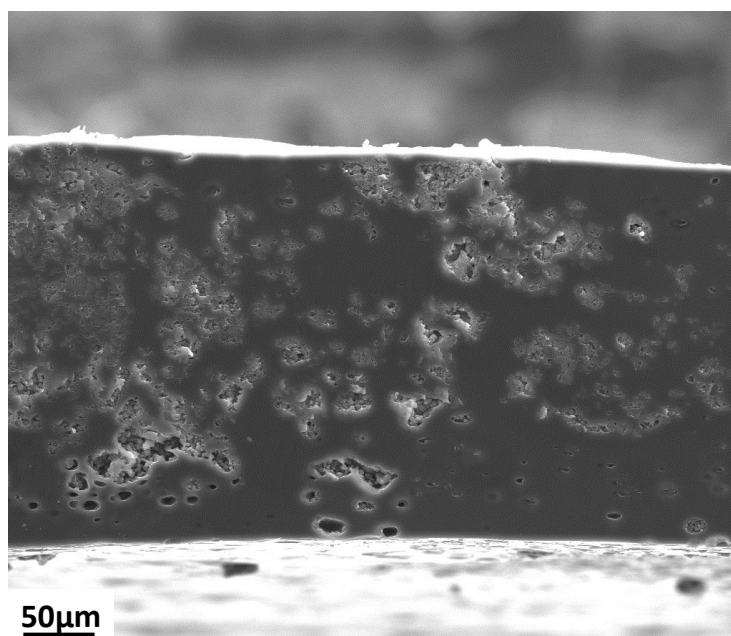
**Figure B.2.13** SEM image of the cross section of PEI/7 IL/10 ZIF-8

Figure B.2.14 presents a plot of H₂/CO₂ selectivity versus H₂ permeability for the membranes studied in this work. The data is compared to the upper bound line determined by Robeson

(Robeson, 2008) as well as to results of PEI/ZIF-8 systems from literature (Deniz, 2012; E. Y. Kim, Kim, Kim, Kim, & Lee, 2019).

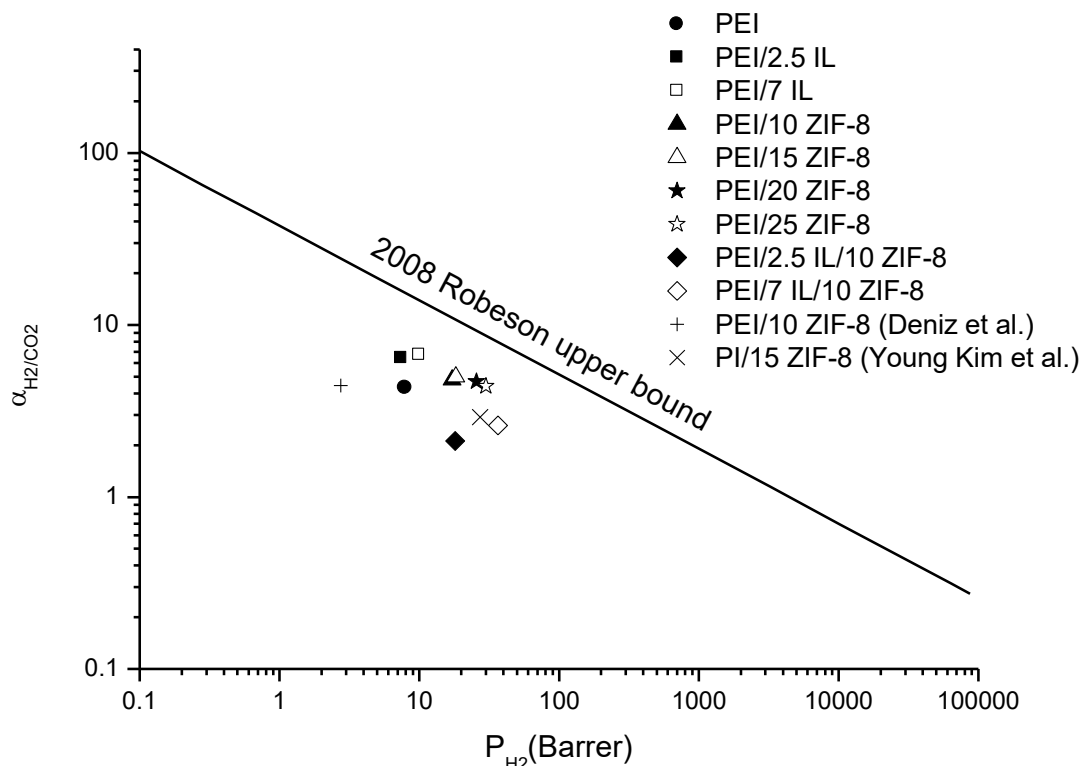


Figure B.2.14 H_2/CO_2 selectivity of the prepared membranes versus H_2 permeability compared to literature data (Deniz, 2012; E. Y. Kim et al., 2019)

It can be observed that our membranes exhibit good separation properties with experimental points lying near the upper bound line. It can also be observed that the data relative to PEI/7 IL/10 ZIF-8 is located in the vicinity of those relative to PEI/20 ZIF-8 and PEI/25 ZIF-8 for which filler percolation was evidenced. This confirms our assumption concerning the gas transport mechanism in the three component membranes and the interest of creating percolation paths through the PEI matrix.

2.3.4 Numerical modeling of gas diffusion in 2- and 3-component systems

For the purpose of predicting the gas transport properties of mixed matrix membranes, various analytical approaches have been proposed in the literature to estimate the effective permeability as a function of several parameters such as filler volume fraction, size and permeability of the components (Bruggeman, 1935; Maxwell, 1873; Pal, 2007). We have compared in section 2.3.2.2 our experimental permeability values to the predictions of the widely used Maxwell model and found fair agreement. However, Maxwell model is limited as

it does not take into account the filler dispersion state. Indeed, our experimental analysis has shown that this factor could play a significant role on the gas transport properties, especially when percolation paths are formed. Hence, for overcoming the limitations of the analytical models, it appears necessary to consider numerical approaches. We have also demonstrated that in the whole range of membranes series studied in this work, the transport properties were mainly governed by the diffusion mechanism. We have thus developed a numerical approach based on 3D finite element simulation of diffusion in these systems in order to predict the effective transport properties of PEI/ZIF-8 and PEI/IL/ZIF-8 membranes.

The morphological analysis of the filled matrix has shown that small aggregates of few micrometer sizes were present in our systems and that depending on the filler amount, percolation paths could be formed. To take into account these different morphologies, two configurations were modeled: the first one corresponds to a dispersion of single permeable spheres (diameter $D = 5 \mu\text{m}$), randomly positioned in the polymer matrix (**Figure B.2.15 (a)**). This choice of filler shape and dimension was based on SEM images and aimed at representing the discrete aggregates observed within the materials. The simulation domain is a cubic representative volume element (RVE) with $50 \mu\text{m}$ edge length. The random positioning of fillers in the computational domain was generated using a JAVA algorithm coupled with the finite element package COMSOL Multiphysics. This algorithm contains conditions that ensure non-overlapping of the spheres. The second configuration corresponds to a dispersion of stacks composed of three permeable spheres, randomly positioned in the polymer matrix using the same generation algorithm (**Figure B.2.15 (b)**).

The numerical analysis was based on solving Fick's diffusion equation in the absence of mass source and in stationary regime. Diffusivity in the neat matrix was fixed to $D_0 = 1.6 \cdot 10^{-9} \text{ cm}^2/\text{s}$ (which is the experimental value corresponding to the reference PEI film). The diffusion coefficient assigned to the aggregates domains was estimated thanks to equation (A.1.1) using ZIF-8 permeability and solubility coefficients from the literature (Eiras et al., 2016; Xu et al., 2017). The calculation led to $D_{\text{ZIF-8}} = 1.902 \times 10^{-6} \text{ cm}^2/\text{s}$ assuming $S_{\text{ZIF-8}} = 13.34 \text{ cc}_{\text{STP}}/\text{cm}^3 \cdot \text{atm}$ and $P_{\text{ZIF-8}} = 3300 \text{ Barrer}$, which is in agreement with another value reported in literature (D. Liu et al., 2014). Thus the theoretical $D_{\text{ZIF-8}}/D_0$ value was around 10^3 . In the simulations, a range of $D_{\text{ZIF-8}}/D_0$ values between 10 and 10^5 was considered. Indeed, the diffusivity in a stack of fillers may not be equal to that of single filler.

Concentration boundary conditions were imposed on the upper and lower sides of the simulation domain: $c_1 = 1000 \text{ mol} \cdot \text{m}^{-3}$, $c_2 = 500 \text{ mol} \cdot \text{m}^{-3}$. The matrix diffusivity is considered

constant and not concentration-dependent, meaning that boundary concentration values have rigorously no effect on the calculated effective diffusivity. For symmetry reasons, no-flux boundary conditions were applied on the lateral sides of the simulation domain. More details about the numerical approach used here can be found in sections 3.2 and 4.2 .

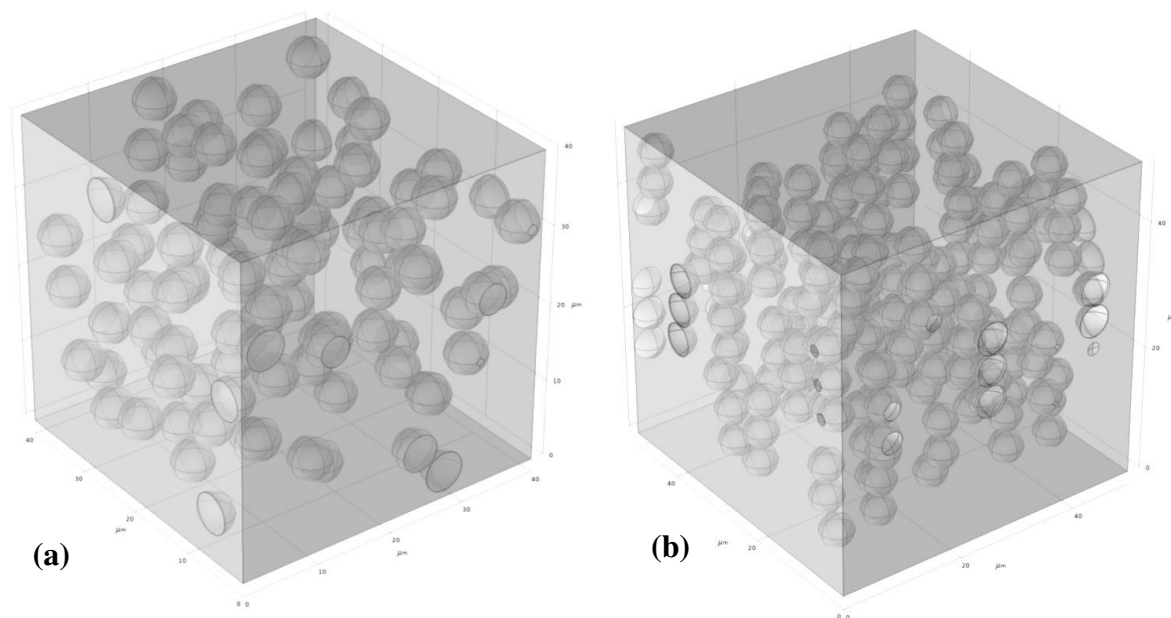


Figure B.2.15 Simulation domain containing (a) discrete spherical filler aggregates (b) stacks composed of three aggregates

The predicted effective diffusivity values obtained by considering PEI as the continuous phase and ZIF-8 as the dispersed phase are plotted in **Figure B.2.16** and compared to the experimental data.

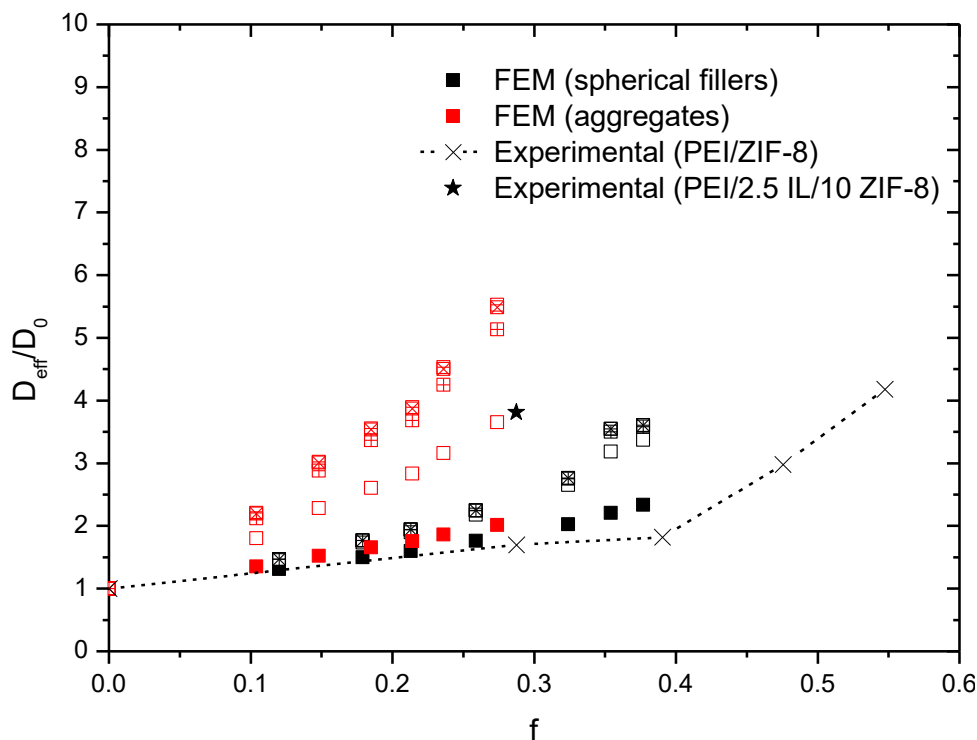


Figure B.2.16 Comparison of the experimental relative effective diffusivity (\times : PEI/ZIF-8; \star : PEI/2.5 IL/7 ZIF-8) and numerical results obtained for several D_{ZIF-8}/D_0 values: (\blacksquare : 10; \square : 10^2 ; \boxplus : 10^3 ; \boxtimes : 10^4 and \boxminus : 10^5)

Two general trends are observed in **Figure B.2.16**: First, the relative diffusivity increases with the filler volume fraction whatever the considered system. Moreover, the simulated relative effective diffusivity values are higher when considering stacks of aggregates, which is consistent with the trend generally reported in literature (Greco et al., 2016). Indeed, for a given value of filler volume fraction, the presence of stacks of permeable fillers increases the probability of obtaining continuous diffusion paths, which leads to higher D_{eff}/D_0 values. It has also to be noticed that, in our simulations, it was not possible to expand the filler volume fractions beyond 38 % due to geometrical constraints. SEM analysis have shown that for filler volume content below 38 %, the PEI/ZIF-8 membranes featured single filler aggregates homogenously dispersed within the PEI matrix. The results of **Figure B.2.16** show that the simulated configurations leading to the best fitting of the experimental data correspond to such morphology with aggregates diffusivity value equal to 10 times the diffusivity of the PEI matrix. Thus, the actual D_{ZIF-8}/D_0 value is probably lower than one (10^3). This result could be explained by the fact that the matrix surrounding the fillers may lead to actual dispersed phase diffusivity values different from intrinsic diffusivity of neat fillers. Considering now the three component system PEI/2.5 IL/10 ZIF-8, it can be noticed that the experimental D_{eff}/D_0 point is lying close to that of the simulation corresponding to stacks of aggregates having diffusivity

higher than the PEI matrix by a factor 100. This result confirms the prevailing role of IL surrounding the fillers which facilitates the accessibility of the gases to the fillers and contributes to obtain less compact aggregates allowing then to form more easily diffusion paths through percolation of filler/IL domains.

2.4 Conclusion

In this study, a step-by-step methodology was applied to develop and characterize series of composite materials with enhanced gas transport properties. It was shown that IL incorporation in PEI matrix enhances H_2/CO_2 selectivity without significant modification of CO_2 permeability. On the other hand, the addition of ZIF-8 particles to PEI membranes is a good alternative to enhance the CO_2 permeability without sacrificing H_2/CO_2 selectivity. Then three-component systems (PEI/IL/ZIF-8) were developed, leading to an enhancement of both CO_2 permeability and CO_2/H_2 selectivity compared to that of neat polymer matrix. It was shown that in the three-component systems, IL was located around the fillers and allowed the formation of less compact fillers aggregates making them more easily accessible for the gases. Specific diffusion paths through filler-IL percolated domains could be obtained at lower filler content than for the two-component PEI/ZIF-8 systems. Finally, a numerical model has been built in order to predict gas diffusivity through PEI/ZIF-8 and PEI/IL/ZIF-8 systems. The model confirmed the interest of the three-component system and showed the beneficial effect of having percolated fillers domains rather than homogeneously dispersed discrete filler domains.

Conclusion and perspectives

This thesis has focused on the investigation of gas transport properties of two different multiphase material families: nanocomposite systems based on impermeable fillers and membranes containing permeable inorganic fillers and ionic liquid for two different applications, e.g. barrier properties and gas selectivity, respectively. Our approach included the development of 3D numerical models for the prediction of the relationships between the systems structures and their mass transfer properties, especially diffusion properties. It was also essential to validate our modeling approach by comparison to results from previous works and to experimental data generated during this PhD project.

A step-by-step approach was carried out in this work. We have presented in the first part of the thesis a detailed bibliographical review of existing analytical and numerical models, which aimed at giving a comprehensive understanding of the impact of nanocomposites structure on gas barrier properties. It has been shown through our study that despite their usefulness for representing the major trends of the phenomena, analytical models suffer from limitations when the structure of the system is becoming more complex. In the meantime, numerical approaches based on various computational methods have been developed and appeared as very good alternatives to predict gas transport through complex nanocomposite systems. The Finite Element Method (FEM), which has been massively used recently, is considered as one of the most efficient approaches for the prediction of complex nanocomposites barrier properties, especially in three-dimensional systems. However, some parameters have not yet been studied in detail. For this purpose, a 3D FEM model was developed in this work to analyze the effects of various parameters on gas diffusion in nanocomposites based on the dispersion of disk-shaped impermeable nanofillers. This simple, yet 3D filler shape is considered as representative of platelet-like fillers and has already been considered in literature to investigate the gas transport properties of nanocomposites, allowing us to compare our results to existing data.

First, we have shown that for disk-shaped fillers regularly distributed in the polymer matrix, the improvement of barrier properties is almost observed for high filler volume fraction and aspect ratio values. Moreover, in such 3D geometry, a parameter named the projected area ratio -reflecting the area available for straight path diffusion- was defined as the ratio of the projected area of the matrix phase to the total projected area of the unit cell, respectively. It was proven that this factor is governing gas diffusivity, i.e. the higher the projected area ratio, the higher the diffusivity values. a new analytical equation has been derived from our

calculations and showed very good agreement with FEM results on a wide range of structural parameter values. It was also consistent with other existing analytical models serving the same purpose.

The developed model was incremented to analyze systems with more complex structural configurations: random dispersion of the fillers, filler size polydispersity, intercalated structures, etc. We have shown that for both exfoliated and intercalated structures, fillers with polydisperse sizes were found to be more efficient in the enhancement of barrier properties than monodisperse ones. Moreover, it must be noticed that intercalated systems were found to be less efficient than the exfoliated systems in the same context.

It is noteworthy that fully exfoliated structures are often difficult to obtain in real nanocomposite systems. That is why a detailed study of the intercalated structure has been conducted in our work. Besides, stacks of fillers are generally considered in literature as impermeable media and only few studies, including work from our laboratory, have shown that diffusing molecules can penetrate through the intra-stack space. Therefore, the main objective of this part of our work was to see whether the intra-stack diffusivity has a governing effect on the overall properties of the nanocomposite system in function of fillers dimensions and interplatelet spacing. We have shown through our calculations that gas diffusion is strongly dependent on interplatelet spacing within stacks. Thus, when the intrastack relative diffusivity (which was varied between 10^{-4} and 10^5) is relatively small compared to the matrix diffusivity, the contribution is considered as limited. However, when fillers diameter is relatively small, the contribution of the interplatelet spacing to the overall diffusivity becomes significant.

To extend this approach, a numerical study of the effect of the interphase layer has been carried out. Indeed, the existence of an interphase with specific properties has been evidenced in several experimental works in literature and its impact (either positive or negative) on the overall barrier properties has been demonstrated. We have validated through the current work that barrier properties can be widely affected by the presence of this phase for different filler volume fractions and orientation angle values. In addition, we were able to consider a large range of values for the interphase properties: its relative diffusivity was varied between 10^{-4} and 10^6 (with respect to the matrix diffusivity) while its thickness was varied between 0.25 nm and 1.5 nm. Consequently, it has been shown that the contribution of the interphase to the overall diffusivity could be assumed negligible when it is weakly diffusive and a plateau-shaped curve has been obtained in the corresponding range of diffusivity values.

Moreover, it has been highlighted the effect of the “continuous path” which could exist due to the interconnection between interphase layers for high thickness and volume fraction values. This parameter can affect dramatically the gas barrier properties by promoting the diffusion of penetrating species and thus yielding higher diffusivity values, which occurs when the interphase is highly diffusive. The random distribution of fillers in the polymer matrix is the most realistic configuration and we showed that the continuous path might occur more easily in that case than in the ordered case.

Regarding the problematic of the relationship between the gas transport properties of multiphase polymer-based systems and the structural parameters of the dispersed phase, the developed numerical approach can also be used to model gas diffusion in other systems such as mixed matrix membranes by considering permeable dispersed fillers in the polymer matrix. Hence, the second part of this work focused on two main objectives: first, developing through an experimental approach original polymeric membranes with interesting permeation and separation properties and secondly, implementing a numerical model able to predict the gas transport properties in such systems.

For this purpose, our membranes were composed essentially of a glassy polymer (PEI) with the addition of other components to form two-component systems: the PEI/ZIF-8 and PEI/IL systems. The choice of the ionic liquid and the ZIF-8 particles was based on their excellent separation properties, especially for CO₂ removal purposes. Results showed that mixed matrix membranes made of ZIF-8 particles had excellent permeability values, whereas polymer/ionic liquid membranes exhibited good gas selectivity. It has been noticed that important ZIF-8 volume fraction values are required to obtain percolation paths, whereas for polymer/IL systems, the dispersion of the ionic liquid in the polymer matrix was almost homogenous. The main objective of this work was to obtain membranes with excellent thermal and morphological properties as well as enhanced CO₂ permeability and selectivity. A route to achieve the latter properties was developed, consisting in combining ZIF-8 particles and the ionic liquid. Filler content was chosen to be around 10 wt% in order to avoid the formation of percolation paths that could prevent the observation of the IL effect, while the IL amount was also fixed to lower values, unlike what was reported in the literature. As a result, it has been shown that IL was located in the domains including ZIF-8 particles, leading to less compact aggregates. This allowed obtaining percolation paths that act as gas diffusion paths and thus good separation properties were obtained (a high increase in H₂ and CO₂ permeability values

has been observed) compared to the neat polymer properties. This makes the three-component membranes a promising approach for efficient separation of CO₂.

On the other hand, the SEM characterization of the prepared membranes showed that fillers had small spherical shapes, which motivated the choice of the filler geometry in our finite element model. Since it has been shown that the diffusivity is a governing factor in the mass transport process, a model based on the diffusion mechanism can be considered as a solid first approach for simulating gas transport in multiphase polymer-based membranes. This model accounts for the effects of filler volume fraction, stacking and diffusivity. As a result, it has been shown that relative effective diffusivity increased when filler volume fraction increased for a fixed filler diffusivity value. Moreover, a comparison between structures containing aggregates and dispersed fillers, respectively, has shown that higher diffusivity values are obtained in the first case. This is expected, as when permeable fillers are interconnected, penetrating species can diffuse more easily through the percolation paths.

Finally, our numerical results confirmed the interest of the three-component system and showed an acceptable agreement with experimental results for the considered range of filler volume fraction values. Furthermore, it showed the beneficial effect of having percolated fillers rather than homogeneously dispersed discrete fillers.

Perspectives

- Modeling

For the nanocomposite systems, a perspective of this work could consist in modeling structures with both exfoliated and intercalated structures in order to represent more realistically the actual systems. Moreover, substantial experimental work has been developed in the laboratory evidencing the importance of semi-crystalline matrix-based nanocomposites. Thus, an interesting continuation of the present modeling work could consist in simulating mass transfer in such systems by considering crystal lamellae as fillers and studying their orientation effect on the overall gas transport properties. One must realize that modeling water transport through nanocomposite systems is an interesting issue today, so a further development of the current model could be to consider concentration-dependent diffusivity instead of constant diffusivity.

For the modeling of MMMs, the developed approach in this work can be refined taking into account the variation of spheres size which was modeled here as monodisperse filler

aggregates. This study can be enriched by considering aggregates of polydisperse-sized spheres. Moreover, the orientation angle of the dispersed stacks could be varied and its effect on the transport properties could be investigated consequently. As in the case of the nanocomposites, the effect of the filler-matrix interphase layer could be considered in the case of mixed matrix membranes.

The lack of modeling approaches taking into account the effect of solubility constitutes a reason to develop new models for both considered systems. Furthermore, the active transport effect (i.e. trapping of diffusing molecules, etc.) has been widely studied in our laboratory thanks to the development of dedicated materials and specific experimental methodologies. It deserves now to be analyzed through numerical approaches.

- Experimental

The performance of mixed matrix membranes depends on various parameters such as the nature of the polymer matrix. A further development of the current study could consist in the consideration of other polymer matrices presenting nice potentials for gas separation as well as good mechanical stability such as copolymers (Pebax or others). Obtaining specific location of the fillers by using well defined copolymers could also be an interesting way to achieve promising properties.

Another perspective of the current work is to graft specific functions to the filler surface in order to modify the polymer/filler interfaces and study its effect on gas separation properties, as a first step before developing specific modeling approaches.

References

- Adams, R. T., Lee, J. S., Bae, T. H., Ward, J. K., Johnson, J. R., Jones, C. W., ... Koros, W. J. (2011). CO₂–CH₄ permeation in high zeolite 4A loading mixed matrix membranes. *Journal of Membrane Science*, 367(1), 197–203.
<https://doi.org/10.1016/j.memsci.2010.10.059>
- Ahmad, J., & Hägg, M. B. (2013a). Polyvinyl acetate/titanium dioxide nanocomposite membranes for gas separation. *Journal of Membrane Science*, 445, 200–210.
<https://doi.org/10.1016/j.memsci.2013.04.052>
- Ahmad, J., & Hägg, M. B. (2013b). Preparation and characterization of polyvinyl acetate/zeolite 4A mixed matrix membrane for gas separation. *Journal of Membrane Science*, 427, 73–84. <https://doi.org/10.1016/j.memsci.2012.09.036>
- Ahmad, N. N. R., Mukhtar, H., Mohshim, D. F., Nasir, R., & Man, Z. (2016). Surface modification in inorganic filler of mixed matrix membrane for enhancing the gas separation performance. *Reviews in Chemical Engineering*, 32(2), 181–200.
- Aitken, C. L., Koros, W. J., & Paul, D. R. (1992). Gas transport properties of biphenol polysulfones. *Macromolecules*, 25(14), 3651–3658.
<https://doi.org/10.1021/ma00040a008>
- Alexandre, B., Langevin, D., Médéric, P., Aubry, T., Couderc, H., Nguyen, Q. T., ... Marais, S. (2009). Water barrier properties of polyamide 12/montmorillonite nanocomposite membranes : Structure and volume fraction effects. *Journal of Membrane Science*, 328(1), 186–204. <https://doi.org/10.1016/j.memsci.2008.12.004>
- Alix, S., Follain, N., Tenn, N., Alexandre, B., Bourbigot, S., Soulestin, J., & Marais, S. (2012). Effect of Highly Exfoliated and Oriented Organoclays on the Barrier Properties of Polyamide 6 Based Nanocomposites. *The Journal of Physical Chemistry C*, 116(8), 4937–4947. <https://doi.org/10.1021/jp2052344>
- Amnuaypanich, S., Naowanon, T., Wongthep, W., & Phinyocheep, P. (2012). Highly water-selective mixed matrix membranes from natural rubber-blend-poly(acrylic acid) (NR-blend-PAA) incorporated with zeolite 4A for the dehydration of water–ethanol mixtures through pervaporation. *Journal of Applied Polymer Science*, 124(S1), E319–E329. <https://doi.org/10.1002/app.34722>

- Aris, R. (1985). On the permeability of membranes with parallel, but interconnected, pathways. *Mathematical Biosciences*, 77(1-2), 5-16. [https://doi.org/10.1016/0025-5564\(85\)90089-6](https://doi.org/10.1016/0025-5564(85)90089-6)
- Aris, R. (1986). On a problem in hindered diffusion. *Archive for Rational Mechanics and Analysis*, 95(2), 83-91. <https://doi.org/10.1007/BF00281082>
- Aroon, M. A., Ismail, A. F., Matsuura, T., & Montazer-Rahmati, M. M. (2010). Performance studies of mixed matrix membranes for gas separation : A review. *Separation and Purification Technology*, 75(3), 229-242. <https://doi.org/10.1016/j.seppur.2010.08.023>
- Attaran, S. A., Hassan, A., & Wahit, M. U. (2017). Materials for food packaging applications based on bio-based polymer nanocomposites : A review. *Journal of Thermoplastic Composite Materials*, 30(2), 143-173. <https://doi.org/10.1177/0892705715588801>
- Azimi, H., Tezel, H. F., & Thibault, J. (2018). On the Effective Permeability of Mixed Matrix Membranes. *Journal of Membrane Science and Research*, 4(3), 158-166.
- Bae, T. H., Lee, J. S., Qiu, W., Koros, W. J., Jones, C. W., & Nair, S. (2010). A High-Performance Gas-Separation Membrane Containing Submicrometer-Sized Metal–Organic Framework Crystals. *Angewandte Chemie International Edition*, 49(51), 9863-9866. <https://doi.org/10.1002/anie.201006141>
- Baker, R. W. (2002). Future directions of membrane gas separation technology. *Industrial & engineering chemistry research*, 41(6), 1393-1411.
- Baker, R. W., & Lokhandwala, K. (2008). Natural Gas Processing with Membranes : An Overview. *Industrial & Engineering Chemistry Research*, 47(7), 2109-2121. <https://doi.org/10.1021/ie071083w>
- Baker, R. W., & Low, B. T. (2014). Gas separation membrane materials : A perspective. *Macromolecules*, 47(20), 6999-7013.
- Banerjee, R., Phan, A., Wang, B., Knobler, C., Furukawa, H., O’Keeffe, M., & Yaghi, O. M. (2008). High-Throughput Synthesis of Zeolitic Imidazolate Frameworks and Application to CO₂ Capture. *Science*, 319(5865), 939-943. <https://doi.org/10.1126/science.1152516>
- Banhegyi, G. (1986). Comparison of electrical mixture rules for composites. *Colloid and polymer science*, 264(12), 1030-1050.
- Bara, J. E., Hatakeyama, E. S., Gin, D. L., & Noble, R. D. (2008). Improving CO₂ permeability in polymerized room-temperature ionic liquid gas separation membranes

- through the formation of a solid composite with a room-temperature ionic liquid.
Polymers for Advanced Technologies, 19(10), 1415-1420.
<https://doi.org/10.1002/pat.1209>
- Barrer, R. M. (1968). Diffusion and permeation in heterogeneous media. *Diffusion in Polymers*, 165-217.
- Basu, S., Cano-Odena, A., & Vankelecom, I. FJ. (2010). Asymmetric Matrimid®/[Cu₃ (BTC)₂] mixed-matrix membranes for gas separations. *Journal of membrane science*, 362(1-2), 478-487.
- Bernardo, P., Drioli, E., & Golemme, G. (2009). Membrane Gas Separation : A Review/State of the Art. *Industrial & Engineering Chemistry Research*, 48(10), 4638-4663.
<https://doi.org/10.1021/ie8019032>
- Bernardo, P., Jansen, J. C., Bazzarelli, F., Tasselli, F., Fuoco, A., Friess, K., ... Clarizia, G. (2012). Gas transport properties of Pebax®/room temperature ionic liquid gel membranes. *Separation and Purification Technology*, 97, 73-82.
- Bertelle, S., Gupta, T., Roizard, D., Vallières, C., & Favre, E. (2006). Study of polymer-carbon mixed matrix membranes for CO₂ separation from flue gas. *Desalination*, 199(1), 401-402. <https://doi.org/10.1016/j.desal.2006.03.207>
- Bharadwaj, R. K. (2001). Modeling the Barrier Properties of Polymer-Layered Silicate Nanocomposites. *Macromolecules*, 34(26), 9189-9192.
<https://doi.org/10.1021/ma010780b>
- Bharadwaj, R. K., Mehrabi, A. R., Hamilton, C., Trujillo, C., Murga, M., Fan, R., ... Thompson, A. K. (2002). Structure-property relationships in cross-linked polyester-clay nanocomposites. *Polymer*, 43(13), 3699-3705. [https://doi.org/10.1016/S0032-3861\(02\)00187-8](https://doi.org/10.1016/S0032-3861(02)00187-8)
- Bhunja, K., Dhawan, S., & Sablani, S. S. (2012). Modeling the Oxygen Diffusion of Nanocomposite-based Food Packaging Films. *Journal of Food Science*, 77(7), N29-N38. <https://doi.org/10.1111/j.1750-3841.2012.02768.x>
- Bitinis, N., Verdejo, R., Maya, E. M., Espuche, E., Cassagnau, P., & Lopez-Manchado, M. A. (2012). Physicochemical properties of organoclay filled polylactic acid/natural rubber blend bionanocomposites. *Composites Science and Technology*, 72(2), 305-313.
<https://doi.org/10.1016/j.compscitech.2011.11.018>

- Blanchard, A., Gouanvé, F., & Espuche, E. (2017). Effect of humidity on mechanical, thermal and barrier properties of EVOH films. *Journal of Membrane Science*, 540, 1-9. <https://doi.org/10.1016/j.memsci.2017.06.031>
- Blanchard, L. A., Gu, Z., & Brennecke, J. F. (2001). High-Pressure Phase Behavior of Ionic Liquid/CO₂ Systems. *The Journal of Physical Chemistry B*, 105(12), 2437-2444. <https://doi.org/10.1021/jp003309d>
- Boom, J. P., Pünt, I. G. M., Zwijnenberg, H., de Boer, R., Bargeman, D., Smolders, C. A., & Strathmann, H. (1998). Transport through zeolite filled polymeric membranes. *Journal of Membrane Science*, 138(2), 237-258. [https://doi.org/10.1016/S0376-7388\(97\)00228-7](https://doi.org/10.1016/S0376-7388(97)00228-7)
- Boucif, N., Favre, E., & Roizard, D. (2008). CO₂ capture in HFMM contactor with typical amine solutions : A numerical analysis. *Chemical Engineering Science*, 63(22), 5375-5385. <https://doi.org/10.1016/j.ces.2008.07.015>
- Bouma, R. H. B., Checchetti, A., Chidichimo, G., & Drioli, E. (1997). Permeation through a heterogeneous membrane : The effect of the dispersed phase. *Journal of Membrane Science*, 128(2), 141-149. [https://doi.org/10.1016/S0376-7388\(96\)00303-1](https://doi.org/10.1016/S0376-7388(96)00303-1)
- Breck, D. W. (1974). Zeolite Molecular Sieves : Structure, Chemistry and Use, John Wiley and Sons. Inc., New York, Malabar, Florida.
- Bredesen, R., Jordal, K., & Bolland, O. (2004). High-temperature membranes in power generation with CO₂ capture. *Chemical Engineering and Processing: Process Intensification*, 43(9), 1129-1158.
- Bruggeman, D. A. G. (1935). Berechnung verschiedener physikalischer Konstanten von heterogenen Substanzen. I. Dielektrizitätskonstanten und Leitfähigkeiten der Mischkörper aus isotropen Substanzen. *Annalen der physik*, 416(7), 636-664.
- Bugatti, V., Costantino, U., Gorrasi, G., Nocchetti, M., Tammaro, L., & Vittoria, V. (2010). Nano-hybrids incorporation into poly(ϵ -caprolactone) for multifunctional applications : Mechanical and barrier properties. *European Polymer Journal*, 46(3), 418-427. <https://doi.org/10.1016/j.eurpolymj.2009.11.003>
- Bux, H., Liang, F., Li, Y., Cravillon, J., Wiebcke, M., & Caro, J. (2009). Zeolitic Imidazolate Framework Membrane with Molecular Sieving Properties by Microwave-Assisted Solvothermal Synthesis. *Journal of the American Chemical Society*, 131(44), 16000-16001. <https://doi.org/10.1021/ja907359t>

- Camargo, P. H., Satyanarayana, K. G., & Wypych, F. (2009). Nanocomposites : Synthesis, structure, properties and new application opportunities. *Materials Research*, 12(1), 1-39.
- Car, A., Stropnik, C., & Peinemann, K. V. (2006). Hybrid membrane materials with different metal–organic frameworks (MOFs) for gas separation. *Desalination*, 200(1), 424-426. <https://doi.org/10.1016/j.desal.2006.03.390>
- Carlisle, T. K., Nicodemus, G. D., Gin, D. L., & Noble, R. D. (2012). CO₂/light gas separation performance of cross-linked poly(vinylimidazolium) gel membranes as a function of ionic liquid loading and cross-linker content. *Journal of Membrane Science*, 397-398, 24-37. <https://doi.org/10.1016/j.memsci.2012.01.006>
- Carreon, M., Dahe, G., Feng, J., & Venna, S. R. (2017). Mixed Matrix Membranes for Gas Separation Applications. *Membranes for Gas Separations; World Scientific Series in Membrane Science and Technology: Biological and Biomimetic Applications, Energy and the Environment*, 1-57.
- Casado-Coterillo, C., Fernández-Barquín, A., Zornoza, B., Téllez, C., Coronas, J., & Irabien, Á. (2015). Synthesis and characterisation of MOF/ionic liquid/chitosan mixed matrix membranes for CO₂/N₂ separation. *RSC Advances*, 5(124), 102350-102361. <https://doi.org/10.1039/C5RA19331A>
- Cerisuelo, J. P., Gavara, R., & Hernández-Muñoz, P. (2015). Diffusion modeling in polymer–clay nanocomposites for food packaging applications through finite element analysis of TEM images. *Journal of Membrane Science*, 482, 92-102. <https://doi.org/10.1016/j.memsci.2015.02.031>
- Charifou, R., Espuche, E., Gouanvé, F., Dubost, L., & Monaco, B. (2016). SiO_x and SiO_xCzHw mono- and multi-layer deposits for improved polymer oxygen and water vapor barrier properties. *Journal of Membrane Science*, 500, 245-254. <https://doi.org/10.1016/j.memsci.2015.11.040>
- Charifou, R., Gouanvé, F., Fulchiron, R., & Espuche, E. (2015). Polypropylene/layered double hydroxide nanocomposites : Synergistic effect of designed filler modification and compatibilizing agent on the morphology, thermal, and mechanical properties. *Journal of Polymer Science Part B: Polymer Physics*, 53(11), 782-794. <https://doi.org/10.1002/polb.23695>

- Chen, H. Z., Li, P., & Chung, T. S. (2012). PVDF/ionic liquid polymer blends with superior separation performance for removing CO₂ from hydrogen and flue gas. *International journal of hydrogen energy*, 37(16), 11796-11804.
- Chen, X., & Papathanasiou, T. D. (2007). Barrier Properties of Flake-Filled Membranes : Review and Numerical Evaluation. *Journal of Plastic Film & Sheeting*, 23(4), 319-346. <https://doi.org/10.1177/8756087907088437>
- Cheviron, P., Gouanvé, F., & Espuche, E. (2016). Preparation, characterization and barrier properties of silver/montmorillonite/starch nanocomposite films. *Journal of Membrane Science*, 497, 162-171.
- Choudalakis, G., & Gotsis, A. D. (2009). Permeability of polymer/clay nanocomposites : A review. *European Polymer Journal*, 45(4), 967-984. <https://doi.org/10.1016/j.eurpolymj.2009.01.027>
- Chung, T. S., Jiang, L. Y., Li, Y., & Kulprathipanja, S. (2007). Mixed matrix membranes (MMMs) comprising organic polymers with dispersed inorganic fillers for gas separation. *Progress in Polymer Science*, 32(4), 483-507. <https://doi.org/10.1016/j.progpolymsci.2007.01.008>
- Clémenson, S., Espuche, E., David, L., & Léonard, D. (2010). Nanocomposite membranes of polyetherimide nanostructured with palladium particles : Processing route, morphology and functional properties. *Journal of Membrane Science*, 361(1-2), 167-175.
- Clémenson, S., Léonard, D., Sage, D., David, L., & Espuche, E. (2008). Metal nanocomposite films prepared in situ from PVA and silver nitrate. Study of the nanostructuration process and morphology as a function of the in situ routes. *Journal of Polymer Science Part A: Polymer Chemistry*, 46(6), 2062-2071. <https://doi.org/10.1002/pola.22541>
- Close, J. J., Farmer, K., Moganty, S. S., & Baltus, R. E. (2012). CO₂/N₂ separations using nanoporous alumina-supported ionic liquid membranes : Effect of the support on separation performance. *Journal of Membrane Science*, 390-391, 201-210. <https://doi.org/10.1016/j.memsci.2011.11.037>
- Compton, J., Thompson, D., Kranbuehl, D., Ohl, S., Gain, O., David, L., & Espuche, E. (2006). Hybrid films of polyimide containing in situ generated silver or palladium nanoparticles : Effect of the particle precursor and of the processing conditions on the morphology and the gas permeability. *Polymer*, 47(15), 5303-5313. <https://doi.org/10.1016/j.polymer.2006.05.048>

- Compton, O. C., Kim, S., Pierre, C., Torkelson, J. M., & Nguyen, S. T. (2010). Crumpled Graphene Nanosheets as Highly Effective Barrier Property Enhancers. *Advanced Materials*, 22(42), 4759-4763. <https://doi.org/10.1002/adma.201000960>
- Cong, H., Radosz, M., Towler, B. F., & Shen, Y. (2007). Polymer–inorganic nanocomposite membranes for gas separation. *Separation and purification technology*, 55(3), 281-291.
- Corcione, C. E., Freuli, F., & Maffezzoli, A. (2013). The aspect ratio of epoxy matrix nanocomposites reinforced with graphene stacks. *Polymer Engineering & Science*, 53(3), 531-539. <https://doi.org/10.1002/pen.23292>
- Cornelius, C. J., & Marand, E. (2002). Hybrid silica-polyimide composite membranes : Gas transport properties. *Journal of Membrane Science*, 202(1), 97-118. [https://doi.org/10.1016/S0376-7388\(01\)00734-7](https://doi.org/10.1016/S0376-7388(01)00734-7)
- Crank, J., & Park, G. S. (1968). *Diffusion in polymers*,. London; New York: Academic Press.
- Crétois, R., Follain, N., Dargent, E., Soulestin, J., Bourbigot, S., Marais, S., & Lebrun, L. (2014). Microstructure and barrier properties of PHBV/organoclay bionanocomposites. *Journal of Membrane Science*, 467, 56-66. <https://doi.org/10.1016/j.memsci.2014.05.015>
- Cserjési, P., Nemestóthy, N., & Bélafi-Bakó, K. (2010). Gas separation properties of supported liquid membranes prepared with unconventional ionic liquids. *Journal of Membrane Science*, 349(1), 6-11. <https://doi.org/10.1016/j.memsci.2009.10.044>
- Cui, Y., Kumar, S., Rao Kona, B., & van Houcke, D. (2015). Gas barrier properties of polymer/clay nanocomposites. *RSC Advances*, 5(78), 63669-63690. <https://doi.org/10.1039/C5RA10333A>
- Cui, Y., Kundalwal, S. I., & Kumar, S. (2016). Gas barrier performance of graphene/polymer nanocomposites. *Carbon*, 98, 313-333. <https://doi.org/10.1016/j.carbon.2015.11.018>
- Cussler, E. L., Hughes, S. E., Ward, W. J., & Aris, R. (1988). Barrier membranes. *Journal of Membrane Science*, 38(2), 161-174. [https://doi.org/10.1016/S0376-7388\(00\)80877-7](https://doi.org/10.1016/S0376-7388(00)80877-7)
- Dai, Y., Johnson, J. R., Karvan, O., Sholl, D. S., & Koros, W. J. (2012). Ultem®/ZIF-8 mixed matrix hollow fiber membranes for CO₂/N₂ separations. *Journal of Membrane Science*, 401-402, 76-82. <https://doi.org/10.1016/j.memsci.2012.01.044>
- Dal Pont, K. (2011). *Nanocomposites à matrice élastomère à base de charges lamellaires synthétiques alpha-ZrP : Influence de la modification des charges sur les propriétés*

- mécaniques et barrière aux gaz* (Phdthesis, Université Claude Bernard - Lyon I).
Consulté à l'adresse <https://tel.archives-ouvertes.fr/tel-00845462/document>
- Dal Pont, K., Gérard, J. F., & Espuche, E. (2012). Modification of α -ZrP nanofillers by amines of different chain length : Consequences on the morphology and mechanical properties of styrene butadiene rubber based nanocomposites. *European Polymer Journal*, 48(1), 217-227. <https://doi.org/10.1016/j.eurpolymj.2011.11.006>
- Dal Pont, K., Gérard, J.-F., & Espuche, E. (2013). Microstructure and properties of styrene-butadiene rubber based nanocomposites prepared from an aminosilane modified synthetic lamellar nanofiller. *Journal of Polymer Science Part B: Polymer Physics*, 51(13), 1051-1059. <https://doi.org/10.1002/polb.23307>
- Darrin, A., & O'Leary, B. L. (2009). *Handbook of space engineering, archaeology, and heritage*. CRC Press.
- Das, M., Perry, J. D., & Koros, W. J. (2010). Gas-Transport-Property Performance of Hybrid Carbon Molecular Sieve-Polymer Materials. *Industrial & Engineering Chemistry Research*, 49(19), 9310-9321. <https://doi.org/10.1021/ie100843r>
- de los Ríos, A. P., Irabien, A., Hollmann, F., & Fernández, F. J. (2013). Ionic liquids : Green solvents for chemical processing. *Journal of Chemistry*, 2013.
- Deniz, S. (2012). Characterization and Gas permeation properties of Polyetherimide/Zeolitic Imidazolate Framework-8 (PEI/ZIF-8) Mixed Matrix Membranes. *Vol.*, 12(01), 11.
- Deveci, S., Oksuz, Y., Birtane, T., & Oner, M. (2016). Application of constant volume – variable pressure (time-lag) method to measure oxygen gas diffusion through polypropylene pipes. *Polymer Testing*, 55, 287-296.
<https://doi.org/10.1016/j.polymertesting.2016.08.026>
- Di Maio, F. P., Santaniello, A., Di Renzo, A., & Golemme, G. (2017). Description of gas transport in perfluoropolymer/SAPO-34 mixed matrix membranes using four-resistance model. *Separation and Purification Technology*, 185, 160-174.
<https://doi.org/10.1016/j.seppur.2017.05.024>
- Díaz, K., Garrido, L., López-González, M., Del Castillo, L. F., & Riande, E. (2009). CO₂ transport in polysulfone membranes containing zeolitic imidazolate frameworks as determined by permeation and PFG NMR techniques. *Macromolecules*, 43(1), 316-325.
- Dondero, M., Tomba, J. P., & Cisilino, A. P. (2016). The effect of flake orientational order on the permeability of barrier membranes : Numerical simulations and predictive models.

- Journal of Membrane Science*, 514, 95-104.
<https://doi.org/10.1016/j.memsci.2016.04.064>
- Dong, G., Li, H., & Chen, V. (2013). Challenges and opportunities for mixed-matrix membranes for gas separation. *Journal of Materials Chemistry A*, 1(15), 4610-4630.
<https://doi.org/10.1039/C3TA00927K>
- Duval, J.-M., Folkers, B., Mulder, M. H. V., Desgrandchamps, G., & Smolders, C. A. (1993). Adsorbent filled membranes for gas separation. Part 1. Improvement of the gas separation properties of polymeric membranes by incorporation of microporous adsorbents. *Journal of Membrane Science*, 80(1), 189-198.
[https://doi.org/10.1016/0376-7388\(93\)85143-K](https://doi.org/10.1016/0376-7388(93)85143-K)
- Duval, J.-M., Kemperman, A. J. B., Folkers, B., Mulder, M. H. V., Desgrandchamps, G., & Smolders, C. A. (1994). Preparation of zeolite filled glassy polymer membranes. *Journal of Applied Polymer Science*, 54(4), 409-418.
<https://doi.org/10.1002/app.1994.070540401>
- Eiras, D., Labreche, Y., & Pessan, L. A. (2016). Ultem®/ZIF-8 mixed matrix membranes for gas separation : Transport and physical properties. *Materials Research*, 19(1), 220-228.
- Eitzman, D. M., Melkote, R. R., & Cussler, E. L. (1996). Barrier membranes with tipped impermeable flakes. *AIChE Journal*, 42(1), 2-9.
<https://doi.org/10.1002/aic.690420103>
- Erdni-Goryaev, E. M., Alent'ev, A. Y., Belov, N. A., Ponkratov, D. O., Shaplov, A. S., Lozinskaya, E. I., & Vygodskii, Y. S. (2012). Gas separation characteristics of new membrane materials based on poly (ethylene glycol)-crosslinked polymers and ionic liquids. *Petroleum Chemistry*, 52(7), 494-498.
- Espuche, E. (2011). Gas Diffusion in Multiphase Polymer Systems. In *Handbook of Multiphase Polymer Systems* (p. 749-775).
<https://doi.org/10.1002/9781119972020.ch19>
- Espuche, E., David, L., Rochas, C., Afeld, J. L., Compton, J. M., Thompson, D. W., ... Kranbuehl, D. E. (2005). In situ generation of nanoparticulate lanthanum(III) oxide-polyimide films : Characterization of nanoparticle formation and resulting polymer properties. *Polymer*, 46(17), 6657-6665.
<https://doi.org/10.1016/j.polymer.2005.05.020>

- Falla, W. R., Mulski, M., & Cussler, E. L. (1996). Estimating diffusion through flake-filled membranes. *Journal of Membrane Science*, 119(1), 129-138.
- Favre, E. (2011). Membrane processes and postcombustion carbon dioxide capture : Challenges and prospects. *Chemical Engineering Journal*, 171(3), 782-793.
- Follain, N., Alexandre, B., Chappey, C., Colasse, L., Médéric, P., & Marais, S. (2016). Barrier properties of polyamide 12/montmorillonite nanocomposites : Effect of clay structure and mixing conditions. *Composites Science and Technology*, 136, 18-28. <https://doi.org/10.1016/j.compscitech.2016.09.023>
- Fortunato, R., González-Muñoz, M. J., Kubasiewicz, M., Luque, S., Alvarez, J. R., Afonso, C. A. M., ... Crespo, J. G. (2005). Liquid membranes using ionic liquids : The influence of water on solute transport. *Journal of Membrane Science*, 249(1), 153-162. <https://doi.org/10.1016/j.memsci.2004.10.007>
- Fowkes, F. M. (1964). *Dispersion force contributions to surface and interfacial tensions, contact angles, and heats of immersion*. ACS Publications.
- Fredrickson, G. H., & Bicerano, J. (1999). Barrier properties of oriented disk composites. *The Journal of chemical physics*, 110(4), 2181-2188.
- Freeman, B. D., & Pinnau, I. (1999). Polymeric Materials for Gas Separations. In ACS *Symposium Series: Vol. 733. Polymer Membranes for Gas and Vapor Separation* (Vol. 733, p. 1-27). <https://doi.org/10.1021/bk-1999-0733.ch001>
- Fried, J. R. (2006). Gas Diffusion and Solubility in Poly(organophosphazenes) : Results of Molecular Simulation Studies. *Journal of Inorganic and Organometallic Polymers and Materials*, 16(4), 407. <https://doi.org/10.1007/s10904-006-9059-2>
- Friess, K., Jansen, J. C., Bazzarelli, F., Izák, P., Jarmarová, V., Kačírková, M., ... Bernardo, P. (2012). High ionic liquid content polymeric gel membranes : Correlation of membrane structure with gas and vapour transport properties. *Journal of membrane science*, 415, 801-809.
- Gain, O., Espuche, E., Pollet, E., Alexandre, M., & Dubois, P. (2005). Gas barrier properties of poly(ϵ -caprolactone)/clay nanocomposites : Influence of the morphology and polymer/clay interactions. *Journal of Polymer Science Part B: Polymer Physics*, 43(2), 205-214. <https://doi.org/10.1002/polb.20316>
- Galizia, M., Chi, W. S., Smith, Z. P., Merkel, T. C., Baker, R. W., & Freeman, B. D. (2017). 50th anniversary perspective : Polymers and mixed matrix membranes for gas and

- vapor separation : A review and prospective opportunities. *Macromolecules*, 50(20), 7809-7843.
- Gao, H., Bai, L., Han, J., Yang, B., Zhang, S., & Zhang, X. (2018). Functionalized ionic liquid membranes for CO₂ separation. *Chemical Communications*, 54(90), 12671 - 12685. <https://doi.org/10.1039/C8CC07348A>
- Ge, C., & Popham, J. (2016). A Review and Evaluation of Prediction Models of Gas Permeation for a Blended Flexible Packaging Film : C.GE. Prediction Models of Gas Permeation. *Packaging Technology and Science*, 29(4-5), 247-262. <https://doi.org/10.1002/pts.2200>
- Geyer, R., Jambeck, J. R., & Law, K. L. (2017). Production, use, and fate of all plastics ever made. *Science advances*, 3(7), e1700782.
- Giannelis, E. P. (1996). Polymer Layered Silicate Nanocomposites. *Advanced Materials*, 8(1), 29-35. <https://doi.org/10.1002/adma.19960080104>
- Gleich, H., Criens, R. M., Mosle, H. G., & Leute, U. (1989). The influence of plasma treatment on the surface properties of high-performance thermoplastic. *International journal of adhesion and adhesives*, 9(2), 88-94.
- Goh, P. S., Ismail, A. F., Sanip, S. M., Ng, B. C., & Aziz, M. (2011). Recent advances of inorganic fillers in mixed matrix membrane for gas separation. *Separation and Purification Technology*, 81(3), 243-264. <https://doi.org/10.1016/j.seppur.2011.07.042>
- Goodyer, C. E., & Bunge, A. L. (2007). Numerical simulations compared against experimental results for barrier membranes with lithographically printed flakes. *Journal of Membrane Science*, 306(1), 196-208. <https://doi.org/10.1016/j.memsci.2007.08.046>
- Graham, T. (1866). The solution-diffusion model. *London Edinburgh Dublin Phil. Mag. Sci. Serie*, 32, 401-425.
- Greco, A. (2014a). Numerical simulation and mathematical modeling of 2D multi-scale diffusion in lamellar nanocomposite. *Computational Materials Science*, 90, 203-209. <https://doi.org/10.1016/j.commatsci.2014.04.017>
- Greco, A. (2014b). Simulation and modeling of diffusion in oriented lamellar nanocomposites. *Computational Materials Science*, 83, 164-170. <https://doi.org/10.1016/j.commatsci.2013.11.019>

- Greco, A., Corcione, C. E., & Maffezzoli, A. (2016). Effect of multi-scale diffusion on the permeability behavior of intercalated nanocomposites. *Journal of Membrane Science*, 505, 92-99. <https://doi.org/10.1016/j.memsci.2016.01.029>
- Greco, A., & Maffezzoli, A. (2013). Two-dimensional and three-dimensional simulation of diffusion in nanocomposite with arbitrarily oriented lamellae. *Journal of Membrane Science*, 442, 238-244. <https://doi.org/10.1016/j.memsci.2013.04.038>
- Greco, A., & Maffezzoli, A. (2015a). Finite Element Modeling of Multiscale Diffusion in Intercalated Nanocomposites. *Journal of Nanomaterials*, 2015, 1-11. <https://doi.org/10.1155/2015/482698>
- Greco, A., & Maffezzoli, A. (2015b). Finite element simulation and analytical modeling of 3D multi scale diffusion in nanocomposites with permeable stacks. *Modelling and Simulation in Materials Science and Engineering*, 24(1), 015003. <https://doi.org/10.1088/0965-0393/24/1/015003>
- Green, O., Grubjesic, S., Lee, S., & Firestone, M. A. (2009). The Design of Polymeric Ionic Liquids for the Preparation of Functional Materials. *Polymer Reviews*, 49(4), 339-360. <https://doi.org/10.1080/15583720903291116>
- Grigoryeva, O., Fainleib, A., Tolstov, A., Pissis, P., Spanoudaki, A., Vatalis, A., & Delides, C. (2006). Thermal analysis of thermoplastic elastomers based on recycled polyethylenes and ground tyre rubber. *Journal of thermal analysis and calorimetry*, 86(1), 229-233.
- Grossi, N., Espuche, E., & Escoubes, M. (2001). Transport properties of Nafion®/cyclodextrin membranes. *Separation and Purification Technology*, 22-23, 255-267. [https://doi.org/10.1016/S1383-5866\(00\)00126-X](https://doi.org/10.1016/S1383-5866(00)00126-X)
- Guan, Y., Meyers, K. P., Mendon, S. K., Hao, G., Douglas, J. R., Trigwell, S., ... Rawlins, J. W. (2016). Ecofriendly Fabrication of Modified Graphene Oxide Latex Nanocomposites with High Oxygen Barrier Performance. *ACS Applied Materials & Interfaces*, 8(48), 33210-33220. <https://doi.org/10.1021/acsami.6b11554>
- Gusev, A. A., & Lusti, H. R. (2001). Rational Design of Nanocomposites for Barrier Applications. *Advanced Materials*, 13(21), 1641-1643. [https://doi.org/10.1002/1521-4095\(200111\)13:21<1641::AID-ADMA1641>3.0.CO;2-P](https://doi.org/10.1002/1521-4095(200111)13:21<1641::AID-ADMA1641>3.0.CO;2-P)
- Ha, H., Park, J., Ando, S., Kim, C. B., Nagai, K., Freeman, B. D., & Ellison, C. J. (2016). Gas permeation and selectivity of poly(dimethylsiloxane)/graphene oxide composite

- elastomer membranes. *Journal of Membrane Science*, 518, 131-140.
<https://doi.org/10.1016/j.memsci.2016.06.028>
- Hägg, M.-B., & Lindbråthen, A. (2005). CO₂ capture from natural gas fired power plants by using membrane technology. *Industrial & engineering chemistry research*, 44(20), 7668-7675.
- Haldoupis, E., Watanabe, T., Nair, S., & Sholl, D. S. (2012). Quantifying Large Effects of Framework Flexibility on Diffusion in MOFs : CH₄ and CO₂ in ZIF-8. *ChemPhysChem*, 13(15), 3449-3452. <https://doi.org/10.1002/cphc.201200529>
- Hao, L., Li, P., Yang, T., & Chung, T. S. (2013). Room temperature ionic liquid/ZIF-8 mixed-matrix membranes for natural gas sweetening and post-combustion CO₂ capture. *Journal of membrane science*, 436, 221-231.
- Hasib-ur-Rahman, M., Siaj, M., & Larachi, F. (2010). Ionic liquids for CO₂ capture—Development and progress. *Chemical Engineering and Processing: Process Intensification*, 49(4), 313-322. <https://doi.org/10.1016/j.cep.2010.03.008>
- He, X. (2018). *The Latest Development on Membrane Materials and Processes for Post-combustion CO₂ Capture : A Review. 1*, 9.
- Hellums, M. W., Koros, W. J., Husk, G. R., & Paul, D. R. (1989). Fluorinated polycarbonates for gas separation applications. *Journal of Membrane Science*, 46(1), 93-112.
[https://doi.org/10.1016/S0376-7388\(00\)81173-4](https://doi.org/10.1016/S0376-7388(00)81173-4)
- Hernández-Fernández, F. J., de los Ríos, A. P., Tomás-Alonso, F., Palacios, J. M., & Villora, G. (2009). Preparation of supported ionic liquid membranes : Influence of the ionic liquid immobilization method on their operational stability. *Journal of Membrane Science*, 341(1), 172-177. <https://doi.org/10.1016/j.memsci.2009.06.003>
- Hibshman, C., Cornelius, C. J., & Marand, E. (2003). The gas separation effects of annealing polyimide–organosilicate hybrid membranes. *Journal of Membrane Science*, 211(1), 25-40. [https://doi.org/10.1016/S0376-7388\(02\)00306-X](https://doi.org/10.1016/S0376-7388(02)00306-X)
- Higuchi, W. I. (1958). A New Relationship for the Dielectric Properties of Two Phase Mixtures. *The Journal of Physical Chemistry*, 62(6), 649-653.
<https://doi.org/10.1021/j150564a003>
- Higuchi, W. I., & Higuchi, T. (1960). Theoretical analysis of diffusional movement through heterogeneous barriers. *Journal of the American Pharmaceutical Association*, 49(9), 598-606.

- Ho, M. T., Allinson, G. W., & Wiley, D. E. (2008). Reducing the cost of CO₂ capture from flue gases using pressure swing adsorption. *Industrial & Engineering Chemistry Research*, 47(14), 4883-4890.
- Hojniak, S. (2014). *Ionic Liquids for Carbon Dioxide Separation on Membranes*. Consulté à l'adresse <https://lirias.kuleuven.be/1723864?limo=0>
- Hong, S. U., Park, D., Ko, Y., & Baek, I. (2009). Polymer-ionic liquid gels for enhanced gas transport. *Chemical Communications*, (46), 7227-7229.
<https://doi.org/10.1039/B913746G>
- Hotta, S., & Paul, D. R. (2004). Nanocomposites formed from linear low density polyethylene and organoclays. *Polymer*, 45(22), 7639-7654.
<https://doi.org/10.1016/j.polymer.2004.08.059>
- Huang, H. D., Ren, P. G., Xu, J. Z., Xu, L., Zhong, G. J., Hsiao, B. S., & Li, Z. M. (2014). Improved barrier properties of poly(lactic acid) with randomly dispersed graphene oxide nanosheets. *Journal of Membrane Science*, 464, 110-118.
<https://doi.org/10.1016/j.memsci.2014.04.009>
- Huang, X.-C., Lin, Y.-Y., Zhang, J.-P., & Chen, X.-M. (2006). Ligand-Directed Strategy for Zeolite-Type Metal–Organic Frameworks : Zinc(II) Imidazoles with Unusual Zeolitic Topologies. *Angewandte Chemie International Edition*, 45(10), 1557-1559.
<https://doi.org/10.1002/anie.200503778>
- Hudiono, Y. C., Carlisle, T. K., LaFrate, A. L., Gin, D. L., & Noble, R. D. (2011). Novel mixed matrix membranes based on polymerizable room-temperature ionic liquids and SAPO-34 particles to improve CO₂ separation. *Journal of Membrane Science*, 370(1), 141-148. <https://doi.org/10.1016/j.memsci.2011.01.012>
- Husain, S., & Koros, W. J. (2007). Mixed matrix hollow fiber membranes made with modified HSSZ-13 zeolite in polyetherimide polymer matrix for gas separation. *Journal of Membrane Science*, 288(1), 195-207.
<https://doi.org/10.1016/j.memsci.2006.11.016>
- Idris, A., Man, Z. B., Maulud, A., & Ahmed, I. (2016). Modified Higuchi Model Applied to Permeation Prediction of Nanocomposite Membranes. *Procedia Engineering*, 148, 208-214. <https://doi.org/10.1016/j.proeng.2016.06.574>
- Ilconich, J., Myers, C., Pennline, H., & Luebke, D. (2007). Experimental investigation of the permeability and selectivity of supported ionic liquid membranes for CO₂/He

- separation at temperatures up to 125°C. *Journal of Membrane Science*, 298(1), 41-47.
<https://doi.org/10.1016/j.memsci.2007.03.056>
- Ismail, A. F., Khulbe, K. C., & Matsuura, T. (2015). Gas Separation Membrane Materials and Structures. In A. F. Ismail, K. Chandra Khulbe, & T. Matsuura (Éd.), *Gas Separation Membranes : Polymeric and Inorganic* (p. 37-192). https://doi.org/10.1007/978-3-319-01095-3_3
- Jacobson, M. Z. (2009). Review of Solutions to Global Warming. *Air Pollution, and Energy*, 28, 14.
- Jacquelot, E., Espuche, E., Gérard, J.-F., Duchet, J., & Mazabraud, P. (2006). Morphology and gas barrier properties of polyethylene-based nanocomposites. *Journal of Polymer Science Part B: Polymer Physics*, 44(2), 431-440. <https://doi.org/10.1002/polb.20707>
- Jalali Dil, E., Ben Dhieb, F., & Ajji, A. (2019). Modeling the effect of nanoplatelets orientation on gas permeability of polymer nanocomposites. *Polymer*, 168, 126-130.
<https://doi.org/10.1016/j.polymer.2019.02.024>
- Jansen, J. C., Friess, K., Clarizia, G., Schauer, J., & Izak, P. (2010). High ionic liquid content polymeric gel membranes : Preparation and performance. *Macromolecules*, 44(1), 39-45.
- Jeazet, H. B. T., Staudt, C., & Janiak, C. (2012). Metal–organic frameworks in mixed-matrix membranes for gas separation. *Dalton Transactions*, 41(46), 14003-14027.
<https://doi.org/10.1039/C2DT31550E>
- Jia, L., Ma, J., Gao, D., & Lv, B. (2018). Layered Double Hydroxides/Polymer Nanocomposites. *PROGRESS IN CHEMISTRY*, 30(2-3), 295-303.
- Jindaratamee, P., Shimoyama, Y., Morizaki, H., & Ito, A. (2011). Effects of temperature and anion species on CO₂ permeability and CO₂/N₂ separation coefficient through ionic liquid membranes. *The Journal of Chemical Thermodynamics*, 43(3), 311-314.
- Joly, C., Smaïhi, M., Porcar, L., & Noble, R. D. (1999). Polyimide–Silica Composite Materials : How Does Silica Influence Their Microstructure and Gas Permeation Properties? *Chemistry of Materials*, 11(9), 2331-2338.
<https://doi.org/10.1021/cm9805018>
- Jourdain, A., Antoniuk, I., Serghei, A., Espuche, E., & Drockenmuller, E. (2017). 1,2,3-Triazolium-based linear ionic polyurethanes. *Polymer Chemistry*, 8(34), 5148-5156.
<https://doi.org/10.1039/C7PY00406K>

- Jr, D. L. S., & Gupta, R. K. (2007). *A Finite Element Analysis of the Influence of Morphology on Barrier Properties of Polymer-Clay Nanocomposites*. 6.
- Jusoh, N., Yeong, Y. F., Lau, K. K., & Shariff, A. M. (2016). Mixed Matrix Membranes Comprising of ZIF-8 Nanofillers for Enhanced Gas Transport Properties. *Procedia Engineering*, 148, 1259-1265. <https://doi.org/10.1016/j.proeng.2016.06.499>
- Kaba, M., Raklaoui, N., Guimon, M.-F., & Mas, A. (2005). Improvement of the water selectivity of ULTEM poly(ether imide) pervaporation films by an allylamine-plasma-polymerized layer. *Journal of Applied Polymer Science*, 97(5), 2088-2096. <https://doi.org/10.1002/app.21684>
- Kato, M., Okamoto, H., Hasegawa, N., Tsukigase, A., & Usuki, A. (2003). Preparation and properties of polyethylene-clay hybrids. *Polymer Engineering & Science*, 43(6), 1312-1316. <https://doi.org/10.1002/pen.10111>
- Kausar, A. (2018). Polymer coating technology for high performance applications : Fundamentals and advances. *Journal of Macromolecular Science, Part A*, 55(5), 440-448. <https://doi.org/10.1080/10601325.2018.1453266>
- Keskin, S., & Sholl, D. S. (2010). Selecting metal organic frameworks as enabling materials in mixed matrix membranes for high efficiency natural gas purification. *Energy & Environmental Science*, 3(3), 343-351.
- Kim, D., & Kim, S. W. (2003). Barrier property and morphology of polypropylene/polyamide blend film. *Korean Journal of Chemical Engineering*, 20(4), 776-782. <https://doi.org/10.1007/BF02706923>
- Kim, E. Y., Kim, H. S., Kim, D., Kim, J., & Lee, P. S. (2019). Preparation of Mixed Matrix Membranes Containing ZIF-8 and UiO-66 for Multicomponent Light Gas Separation. *Crystals*, 9(1), 15. <https://doi.org/10.3390/cryst9010015>
- Kim, H., Abdala, A. A., & Macosko, C. W. (2010). Graphene/Polymer Nanocomposites. *Macromolecules*, 43(16), 6515-6530. <https://doi.org/10.1021/ma100572e>
- Kim, J. H., & Lee, Y. M. (2001). Gas permeation properties of poly(amide-6-b-ethylene oxide)-silica hybrid membranes. *Journal of Membrane Science*, 193(2), 209-225. [https://doi.org/10.1016/S0376-7388\(01\)00514-2](https://doi.org/10.1016/S0376-7388(01)00514-2)
- Klopffer, M. H., Berne, P., & Espuche, E. (2015). Development of Innovating Materials for Distributing Mixtures of Hydrogen and Natural Gas. Study of the Barrier Properties and Durability of Polymer Pipes. *Oil & Gas Science and Technology – Revue d'IFP Energies nouvelles*, 70(2), 305-315. <https://doi.org/10.2516/ogst/2014008>

- Kong, C., Shintani, T., & Tsuru, T. (2010). "Pre-seeding"-assisted synthesis of a high performance polyamide-zeolite nanocomposite membrane for water purification. *New Journal of Chemistry*, 34(10), 2101-2104. <https://doi.org/10.1039/C0NJ00581A>
- Koresh, J. E., & Soffer, A. (1987). The Carbon Molecular Sieve Membranes. General Properties and the Permeability of CH₄/H₂ Mixture. *Separation Science and Technology*, 22(2-3), 973-982. <https://doi.org/10.1080/01496398708068993>
- Koros, W. J. (2002). Gas separation membranes : Needs for combined materials science and processing approaches. *Macromolecular Symposia*, 188(1), 13-22. [https://doi.org/10.1002/1521-3900\(200211\)188:1<13::AID-MASY13>3.0.CO;2-W](https://doi.org/10.1002/1521-3900(200211)188:1<13::AID-MASY13>3.0.CO;2-W)
- Koros, W. J., & Mahajan, R. (2000). Pushing the limits on possibilities for large scale gas separation : Which strategies? *Journal of Membrane Science*, 175(2), 181-196. [https://doi.org/10.1016/S0376-7388\(00\)00418-X](https://doi.org/10.1016/S0376-7388(00)00418-X)
- Kurdi, J., & Tremblay, A. Y. (1999). Preparation of defect-free asymmetric membranes for gas separations. *Journal of applied polymer science*, 73(8), 1471-1482.
- Kwon, K., & Chang, J. H. (2015). Comparison of the properties of polyimide nanocomposites containing three different nanofillers : Organoclay, functionalized graphene, and organoclay/functionalized graphene complex. *Journal of Composite Materials*, 49(24), 3031-3044. <https://doi.org/10.1177/0021998314559277>
- Lape, N. K., Nuxoll, E. E., & Cussler, E. L. (2004). Polydisperse flakes in barrier films. *Journal of Membrane Science*, 236(1-2), 29-37. <https://doi.org/10.1016/j.memsci.2003.12.026>
- Le, N. L., & Nunes, S. P. (2016). Materials and membrane technologies for water and energy sustainability. *Sustainable Materials and Technologies*, 7, 1-28.
- Lee, S. H., Kim, B. S., Lee, E. W., Park, Y. I., & Lee, J. M. (2006). The removal of acid gases from crude natural gas by using novel supported liquid membranes. *Desalination*, 200(1), 21-22. <https://doi.org/10.1016/j.desal.2006.03.227>
- Lewis, T. B., & Nielsen, L. E. (1970). Dynamic mechanical properties of particulate-filled composites. *Journal of Applied Polymer Science*, 14(6), 1449-1471.
- Li, H., Eddaoudi, M., O'Keeffe, M., & Yaghi, O. M. (1999). Design and synthesis of an exceptionally stable and highly porous metal-organic framework. *Nature*, 402(6759), 276-279. <https://doi.org/10.1038/46248>

- Li, H., Tuo, L., Yang, K., Jeong, H. K., Dai, Y., He, G., & Zhao, W. (2016). Simultaneous enhancement of mechanical properties and CO₂ selectivity of ZIF-8 mixed matrix membranes : Interfacial toughening effect of ionic liquid. *Journal of Membrane Science*, 511, 130-142. <https://doi.org/10.1016/j.memsci.2016.03.050>
- Li, M., Zhang, X., Zeng, S., Bai, L., Gao, H., Deng, J., ... Zhang, S. (2017). Pebax-based composite membranes with high gas transport properties enhanced by ionic liquids for CO₂ separation. *RSC Advances*, 7(11), 6422-6431. <https://doi.org/10.1039/C6RA27221E>
- Li, P., Pramoda, K. P., & Chung, T. S. (2011). CO₂ Separation from Flue Gas Using Polyvinyl-(Room Temperature Ionic Liquid)-Room Temperature Ionic Liquid Composite Membranes. *Industrial & Engineering Chemistry Research*, 50(15), 9344-9353. <https://doi.org/10.1021/ie2005884>
- Li, X., Bandyopadhyay, P., Nguyen, T. T., Park, O., & Lee, J. H. (2018). Fabrication of functionalized graphene oxide/maleic anhydride grafted polypropylene composite film with excellent gas barrier and anticorrosion properties. *Journal of Membrane Science*, 547, 80-92. <https://doi.org/10.1016/j.memsci.2017.10.031>
- Li, X., Li, L., Song, Y., Li, H., Zhu, Z., & Chai, Y. (2016). A permeation cup method for screening packaging materials for fragrance preservation in Chinese medicine. *Analytical Methods*, 8(40), 7387-7395. <https://doi.org/10.1039/C6AY01620K>
- Li, Y., Chung, T. S., Cao, C., & Kulprathipanja, S. (2005). The effects of polymer chain rigidification, zeolite pore size and pore blockage on polyethersulfone (PES)-zeolite A mixed matrix membranes. *Journal of Membrane Science*, 260(1-2), 45-55.
- Li, Y., Guan, H. M., Chung, T. S., & Kulprathipanja, S. (2006). Effects of novel silane modification of zeolite surface on polymer chain rigidification and partial pore blockage in polyethersulfone (PES)-zeolite A mixed matrix membranes. *Journal of Membrane Science*, 275(1-2), 17-28.
- Liang, C. Y., Uchytel, P., Petrychkovych, R., Lai, Y. C., Friess, K., Sipek, M., ... Suen, S. Y. (2012). A comparison on gas separation between PES (polyethersulfone)/MMT (Na-montmorillonite) and PES/TiO₂ mixed matrix membranes. *Separation and Purification Technology*, 92, 57-63. <https://doi.org/10.1016/j.seppur.2012.03.016>
- Liang, L., Gan, Q., & Nancarrow, P. (2014). Composite ionic liquid and polymer membranes for gas separation at elevated temperatures. *Journal of membrane science*, 450, 407-417.

- Liu, C., Greer, D. W., & O'Leary, B. W. (2016). Advanced Materials and Membranes for Gas Separations : The UOP Approach. In *ACS Symposium Series: Vol. 1224. Nanotechnology : Delivering on the Promise Volume 2* (Vol. 1224, p. 119-135).
<https://doi.org/10.1021/bk-2016-1224.ch007>
- Liu, D., Ma, X., Xi, H., & Lin, Y. S. (2014). Gas transport properties and propylene/propane separation characteristics of ZIF-8 membranes. *Journal of membrane science*, 451, 85-93.
- Liu, J., Bae, T. H., Qiu, W., Husain, S., Nair, S., Jones, C. W., ... Koros, W. J. (2009). Butane isomer transport properties of 6FDA-DAM and MFI-6FDA-DAM mixed matrix membranes. *Journal of Membrane Science*, 343(1), 157-163.
<https://doi.org/10.1016/j.memsci.2009.07.018>
- Liu, Q., & Cussler, E. L. (2006). Barrier membranes made with lithographically printed flakes. *Journal of Membrane Science*, 285(1), 56-67.
<https://doi.org/10.1016/j.memsci.2006.07.018>
- Lizundia, E., Vilas, J. L., Sangroniz, A., & Etxeberria, A. (2017). Light and gas barrier properties of PLLA/metallic nanoparticles composite films. *European Polymer Journal*, 91, 10-20. <https://doi.org/10.1016/j.eurpolymj.2017.03.043>
- López-González, M. M., Compan, V., Saiz, E., Riande, E., & Guzman, J. (2005). Effect of the upstream pressure on gas transport in poly (ether-imide) films. *Journal of membrane science*, 253(1-2), 175-181.
- Lu, C., & Mai, Y. W. (2007). Permeability modelling of polymer-layered silicate nanocomposites. *Composites Science and Technology*, 67(14), 2895-2902.
<https://doi.org/10.1016/j.compscitech.2007.05.008>
- Magalhães, T. O., Aquino, A. S., Vecchia, F. D., Bernard, F. L., Seferin, M., Menezes, S. C., ... Einloft, S. (2014). Syntheses and characterization of new poly(ionic liquid)s designed for CO₂ capture. *RSC Advances*, 4(35), 18164-18170.
<https://doi.org/10.1039/C4RA00071D>
- Magana, S., Festin, N., Fumagalli, M., Chikh, L., Gouanvé, F., Mareau, V. H., ... Espuche, E. (2015). Hydrophobic networks for advanced proton conducting membrane : Synthesis, transport properties and chemical stability. *Journal of Membrane Science*, 494, 161-173. <https://doi.org/10.1016/j.memsci.2015.07.036>
- Magana, S., Gain, O., Gouanvé, F., & Espuche, E. (2016). Influence of different alkyl-methylimidazolium tetrafluoroborate ionic liquids on the structure of pebax® films.

- Consequences on thermal, mechanical, and water sorption and diffusion properties. *Journal of Polymer Science Part B: Polymer Physics*, 54(8), 811-824.
<https://doi.org/10.1002/polb.23977>
- Mahajan, R., Burns, R., Schaeffer, M., & Koros, W. J. (2002). Challenges in forming successful mixed matrix membranes with rigid polymeric materials. *Journal of Applied Polymer Science*, 86(4), 881-890. <https://doi.org/10.1002/app.10998>
- Mahajan, R., & Koros, W. J. (2000). Factors Controlling Successful Formation of Mixed-Matrix Gas Separation Materials. *Industrial & Engineering Chemistry Research*, 39(8), 2692-2696. <https://doi.org/10.1021/ie990799r>
- Mahajan, R., & Koros, W. J. (2002a). Mixed matrix membrane materials with glassy polymers. Part 1. *Polymer Engineering & Science*, 42(7), 1420-1431.
<https://doi.org/10.1002/pen.11041>
- Mahajan, R., & Koros, W. J. (2002b). Mixed matrix membrane materials with glassy polymers. Part 2. *Polymer Engineering & Science*, 42(7), 1432-1441.
<https://doi.org/10.1002/pen.11042>
- Mahurin, S. M., Hillesheim, P. C., Yeary, J. S., Jiang, D., & Dai, S. (2012). High CO₂ solubility, permeability and selectivity in ionic liquids with the tetracyanoborate anion. *RSC Advances*, 2(31), 11813-11819. <https://doi.org/10.1039/C2RA22342B>
- Maier, G. (1998). Gas Separation with Polymer Membranes. *Angewandte Chemie International Edition*, 37(21), 2960-2974. [https://doi.org/10.1002/\(SICI\)1521-3773\(19981116\)37:21<2960::AID-ANIE2960>3.0.CO;2-5](https://doi.org/10.1002/(SICI)1521-3773(19981116)37:21<2960::AID-ANIE2960>3.0.CO;2-5)
- Makinouchi, T., Tanaka, M., & Kawakami, H. (2017). Improvement in characteristics of a Nafion membrane by proton conductive nanofibers for fuel cell applications. *Journal of Membrane Science*, 530, 65-72. <https://doi.org/10.1016/j.memsci.2017.02.018>
- Mannan, H. A., Mukhtar, H., Murugesan, T., Man, Z., Bustam, M. A., Shaharun, M. S., & Abu Bakar, M. Z. (2017). Prediction of CO₂ gas permeability behavior of ionic liquid-polymer membranes (ILPM). *Journal of Applied Polymer Science*, 134(17).
- Marcilla, R., Alcaide, F., Sardon, H., Pomposo, J. A., Pozo-Gonzalo, C., & Mecerreyes, D. (2006). Tailor-made polymer electrolytes based upon ionic liquids and their application in all-plastic electrochromic devices. *Electrochemistry Communications*, 8(3), 482-488. <https://doi.org/10.1016/j.elecom.2006.01.013>

- Mariano, D. M., Freitas, D. F., Mendes, L. C., Carvalho, A. L. F., & Ramos, F. J. H. (2019). Investigation on Structural, Morphological and Relaxometric Properties of Lamellar Zrp Modified with Long Chain Amine. *Materials Research*, 22(2).
- Martínez-Palou, R., Likhanova, N. V., & Olivares-Xometl, O. (2014). Supported ionic liquid membranes for separations of gases and liquids : An overview. *Petroleum Chemistry*, 54(8), 595-607. <https://doi.org/10.1134/S0965544114080106>
- Masclaux, C., Gouanvé, F., & Espuche, E. (2010). Experimental and modelling studies of transport in starch nanocomposite films as affected by relative humidity. *Journal of Membrane Science*, 363(1), 221-231. <https://doi.org/10.1016/j.memsci.2010.07.032>
- Mattioli, S., Peltzer, M., Fortunati, E., Armentano, I., Jiménez, A., & Kenny, J. M. (2013). Structure, gas-barrier properties and overall migration of poly (lactic acid) films coated with hydrogenated amorphous carbon layers. *Carbon*, 63, 274-282.
- Maxwell, J. C. (1873). *A treatise on electricity and magnetism* (Vol. 1). Oxford: Clarendon Press.
- Mecerreyes, D. (2011). Polymeric ionic liquids : Broadening the properties and applications of polyelectrolytes. *Progress in Polymer Science*, 36(12), 1629-1648. <https://doi.org/10.1016/j.progpolymsci.2011.05.007>
- Meneghetti, P., Shaikh, S., Qutubuddin, S., & Nazarenko, S. (2008). Synthesis and Characterization of Styrene-Butadiene Rubber-Clay Nanocomposites with Enhanced Mechanical and Gas Barrier Properties. *Rubber Chemistry and Technology*, 81(5), 821-841. <https://doi.org/10.5254/1.3548234>
- Merkel, T. C., Freeman, B. D., Spontak, R. J., He, Z., Pinnau, I., Meakin, P., & Hill, A. J. (2002). Ultrapervious, Reverse-Selective Nanocomposite Membranes. *Science*, 296(5567), 519-522. <https://doi.org/10.1126/science.1069580>
- Metz, B., Davidson, O., De Coninck, H., Loos, M., & Meyer, L. (2005). *IPCC special report on carbon dioxide capture and storage*. Intergovernmental Panel on Climate Change, Geneva (Switzerland). Working
- Minelli, M. (2009). *Characterization and modeling of the barrier properties in nanostructured systems* (Thesis). Consulté à l'adresse <http://amsdottorato.unibo.it/1477/>
- Minelli, M., Baschetti, M. G., & Doghieri, F. (2009). Analysis of modeling results for barrier properties in ordered nanocomposite systems. *Journal of Membrane Science*, 327(1), 208-215. <https://doi.org/10.1016/j.memsci.2008.11.021>

- Minelli, M., Baschetti, M. G., & Doghieri, F. (2011). A comprehensive model for mass transport properties in nanocomposites. *Journal of Membrane Science*, 381(1), 10-20. <https://doi.org/10.1016/j.memsci.2011.06.036>
- Mittal, V. (2008). Epoxy—Vermiculite Nanocomposites as Gas Permeation Barrier. *Journal of Composite Materials*, 42(26), 2829-2839. <https://doi.org/10.1177/0021998308096954>
- Moaddeb, M., & Koros, W. J. (1997). Gas transport properties of thin polymeric membranes in the presence of silicon dioxide particles. *Journal of Membrane Science*, 125(1), 143-163. [https://doi.org/10.1016/S0376-7388\(96\)00251-7](https://doi.org/10.1016/S0376-7388(96)00251-7)
- Moggridge, G. D., Lape, N. K., Yang, C., & Cussler, E. L. (2003). Barrier films using flakes and reactive additives. *Progress in Organic Coatings*, 46(4), 231-240. [https://doi.org/10.1016/S0300-9440\(02\)00180-7](https://doi.org/10.1016/S0300-9440(02)00180-7)
- Mohshim, D. F., Mukhtar, H., & Man, Z. (2014). The effect of incorporating ionic liquid into polyethersulfone-SAPO34 based mixed matrix membrane on CO₂ gas separation performance. *Separation and Purification Technology*, 135, 252-258. <https://doi.org/10.1016/j.seppur.2014.08.019>
- Mokwena, K. K., & Tang, J. (2012). Ethylene vinyl alcohol : A review of barrier properties for packaging shelf stable foods. *Critical reviews in food science and nutrition*, 52(7), 640-650.
- Mokwena, K. K., Tang, J., Dunne, C. P., Yang, T. C. S., & Chow, E. (2009). Oxygen transmission of multilayer EVOH films after microwave sterilization. *Journal of Food Engineering*, 92(3), 291-296.
- Monsalve-Bravo, G. M., & Bhatia, S. K. (2018). Modeling Permeation through Mixed-Matrix Membranes : A Review. *Processes*, 6(9), 172. <https://doi.org/10.3390/pr6090172>
- Monteiro, B., Nabais, A., Casimiro, M., Martins, A., Francisco, R., Neves, L., & Pereira, C. (2018). Impact on CO₂/N₂ and CO₂/CH₄ Separation Performance Using Cu-BTC with Supported Ionic Liquids-Based Mixed Matrix Membranes. *Membranes*, 8(4), 93.
- Moore, T. T., & Koros, W. J. (2005). Non-ideal effects in organic–inorganic materials for gas separation membranes. *Journal of Molecular Structure*, 739(1-3), 87-98.
- Moore, T. T., Mahajan, R., Vu, D. Q., & Koros, W. J. (2004). Hybrid membrane materials comprising organic polymers with rigid dispersed phases. *AIChE Journal*, 50(2), 311-321. <https://doi.org/10.1002/aic.10029>

- Morel, F., Bounor-Legaré, V., Espuche, E., Persyn, O., & Lacroix, M. (2012). Surface modification of calcium carbonate nanofillers by fluoro- and alkyl-alkoxysilane : Consequences on the morphology, thermal stability and gas barrier properties of polyvinylidene fluoride nanocomposites. *European Polymer Journal*, 48(5), 919-929. <https://doi.org/10.1016/j.eurpolymj.2012.03.004>
- Morel, F., Espuche, E., Bounor-Legaré, V., Persynn, O., & Lacroix, M. (2016). Impact of coated calcium carbonate nanofillers and annealing treatments on the microstructure and gas barrier properties of poly(lactide) based nanocomposite films. *Journal of Polymer Science Part B: Polymer Physics*, 54(6), 649-658. <https://doi.org/10.1002/polb.23957>
- Morgan, D., Ferguson, L., & Scovazzo, P. (2005). Diffusivities of Gases in Room-Temperature Ionic Liquids : Data and Correlations Obtained Using a Lag-Time Technique. *Industrial & Engineering Chemistry Research*, 44(13), 4815-4823. <https://doi.org/10.1021/ie048825v>
- Müller, K., Bugnicourt, E., Latorre, M., Jorda, M., Echegoyen Sanz, Y., Lagaron, J., ... Schmid, M. (2017). Review on the Processing and Properties of Polymer Nanocomposites and Nanocoatings and Their Applications in the Packaging, Automotive and Solar Energy Fields. *Nanomaterials*, 7(4), 74. <https://doi.org/10.3390/nano7040074>
- Nafisi, V., & Hägg, M. B. (2014). Development of dual layer of ZIF-8/PEBAX-2533 mixed matrix membrane for CO₂ capture. *Journal of Membrane Science*, 459, 244-255. <https://doi.org/10.1016/j.memsci.2014.02.002>
- Nagy, T. F., & Duxbury, P. M. (2002). Permeability and conductivity of platelet-reinforced membranes and composites. *Physical Review E*, 66(2), 020802. <https://doi.org/10.1103/PhysRevE.66.020802>
- Nazarenko, S., Meneghetti, P., Julmon, P., Olson, B. G., & Qutubuddin, S. (2007). Gas barrier of polystyrene montmorillonite clay nanocomposites : Effect of mineral layer aggregation. *Journal of Polymer Science Part B: Polymer Physics*, 45(13), 1733-1753. <https://doi.org/10.1002/polb.21181>
- Nielsen, L. E. (1967). Models for the Permeability of Filled Polymer Systems. *Journal of Macromolecular Science: Part A - Chemistry*, 1(5), 929-942. <https://doi.org/10.1080/10601326708053745>

- Okada, A., & Usuki, A. (1995). The chemistry of polymer-clay hybrids. *Materials Science and Engineering: C*, 3(2), 109-115.
- Ordonez, M. J. C., Balkus Jr, K. J., Ferraris, J. P., & Musselman, I. H. (2010). Molecular sieving realized with ZIF-8/Matrimid® mixed-matrix membranes. *Journal of Membrane Science*, 361(1-2), 28-37.
- Ordoñez, M. J. C., Balkus, K. J., Ferraris, J. P., & Musselman, I. H. (2010). Molecular sieving realized with ZIF-8/Matrimid® mixed-matrix membranes. *Journal of Membrane Science*, 361(1), 28-37. <https://doi.org/10.1016/j.memsci.2010.06.017>
- Osman, M. A., Mittal, V., Morbidelli, M., & Suter, U. W. (2003). Polyurethane Adhesive Nanocomposites as Gas Permeation Barrier. *Macromolecules*, 36(26), 9851-9858. <https://doi.org/10.1021/ma035077x>
- Oyenekan, B. A., & Rochelle, G. T. (2006). Energy performance of stripper configurations for CO₂ capture by aqueous amines. *Industrial & Engineering Chemistry Research*, 45(8), 2457-2464.
- Pal, R. (2007). New models for thermal conductivity of particulate composites. *Journal of reinforced plastics and composites*, 26(7), 643-651.
- Pandey, P., & Chauhan, R. S. (2001). Membranes for gas separation. *Progress in Polymer Science*, 26(6), 853-893. [https://doi.org/10.1016/S0079-6700\(01\)00009-0](https://doi.org/10.1016/S0079-6700(01)00009-0)
- Park, H. B., Kamcev, J., Robeson, L. M., Elimelech, M., & Freeman, B. D. (2017). Maximizing the right stuff : The trade-off between membrane permeability and selectivity. *Science*, 356(6343), eaab0530. <https://doi.org/10.1126/science.aab0530>
- Park, K. S., Ni, Z., Côté, A. P., Choi, J. Y., Huang, R., Uribe-Romo, F. J., ... Yaghi, O. M. (2006). Exceptional chemical and thermal stability of zeolitic imidazolate frameworks. *Proceedings of the National Academy of Sciences*, 103(27), 10186-10191. <https://doi.org/10.1073/pnas.0602439103>
- Park, Y. T., Qian, Y., Lindsay, C. I., Nijs, C., Camargo, R. E., Stein, A., & Macosko, C. W. (2013). Polyol-Assisted Vermiculite Dispersion in Polyurethane Nanocomposites. *ACS Applied Materials & Interfaces*, 5(8), 3054-3062. <https://doi.org/10.1021/am303244j>
- Paul, D. R., & Robeson, L. M. (2008). Polymer nanotechnology : Nanocomposites. *Polymer*, 49(15), 3187-3204. <https://doi.org/10.1016/j.polymer.2008.04.017>

- Pechar, T. W., Kim, S., Vaughan, B., Marand, E., Baranauskas, V., Riffle, J., ... Tsapatsis, M. (2006). Preparation and characterization of a poly (imide siloxane) and zeolite L mixed matrix membrane. *Journal of Membrane Science*, 277(1-2), 210-218.
- Perez, E. V., Balkus, K. J., Ferraris, J. P., & Musselman, I. H. (2009). Mixed-matrix membranes containing MOF-5 for gas separations. *Journal of Membrane Science*, 328(1), 165-173. <https://doi.org/10.1016/j.memsci.2008.12.006>
- Picard, E., Espuche, E., & Fulchiron, R. (2011). Effect of an organo-modified montmorillonite on PLA crystallization and gas barrier properties. *Applied Clay Science*, 53(1), 58-65.
- Picard, E., Gauthier, H., Gérard, J.-F., & Espuche, E. (2007). Influence of the intercalated cations on the surface energy of montmorillonites : Consequences for the morphology and gas barrier properties of polyethylene/montmorillonites nanocomposites. *Journal of Colloid and Interface Science*, 307(2), 364-376. <https://doi.org/10.1016/j.jcis.2006.12.006>
- Picard, E., Gérard, J.-F., & Espuche, E. (2008). Water transport properties of polyamide 6 based nanocomposites prepared by melt blending : On the importance of the clay dispersion state on the water transport properties at high water activity. *Journal of Membrane Science*, 313(1), 284-295. <https://doi.org/10.1016/j.memsci.2008.01.011>
- Picard, E., Gérard, J.-F., & Espuche, E. (2015). Reinforcement of the Gas Barrier Properties of Polyethylene and Polyamide Through the Nanocomposite Approach : Key Factors and Limitations. *Oil & Gas Science and Technology – Revue d'IFP Energies Nouvelles*, 70(2), 237-249. <https://doi.org/10.2516/ogst/2013145>
- Picard, E., Vermogen, A., Gérard, J.-F., & Espuche, E. (2007). Barrier properties of nylon 6-montmorillonite nanocomposite membranes prepared by melt blending : Influence of the clay content and dispersion state: Consequences on modelling. *Journal of Membrane Science*, 292(1), 133-144. <https://doi.org/10.1016/j.memsci.2007.01.030>
- Pinnavaia, T. J. (1983). Intercalated clay catalysts. *Science*, 220(4595), 365-371.
- Powell, C. E., & Qiao, G. G. (2006). Polymeric CO₂/N₂ gas separation membranes for the capture of carbon dioxide from power plant flue gases. *Journal of Membrane Science*, 279(1-2), 1-49.

- Qariouh, H., Schué, R., Schué, F., & Bailly, C. (1999). Sorption, diffusion and pervaporation of water/ethanol mixtures in polyetherimide membranes. *Polymer international*, 48(3), 171-180.
- Rabiee, H., Ghadimi, A., & Mohammadi, T. (2015). Gas transport properties of reverse-selective poly (ether-b-amide6)/[Emim][BF₄] gel membranes for CO₂/light gases separation. *Journal of membrane science*, 476, 286-302.
- Rafiq, S., Maulud, A. S., Man, Z., & Muhammad, N. (2014). Gas Permeation Models in Mixed Matrix Membranes for Gas Separation. *Advanced Materials Research*, 917, 317-324. Trans Tech Publ.
- Rayleigh, L. (1892). LVI. On the influence of obstacles arranged in rectangular order upon the properties of a medium. *The London, Edinburgh, and Dublin Philosophical Magazine and Journal of Science*, 34(211), 481-502.
- Rayleigh, Lord. (1892). LVI. *On the influence of obstacles arranged in rectangular order upon the properties of a medium. The London, Edinburgh, and Dublin Philosophical Magazine and Journal of Science*, 34(211), 481-502.
<https://doi.org/10.1080/14786449208620364>
- Ripoche, A., Menut, P., Dupuy, C., Caquineau, H., & Deratani, A. (2002). Poly (ether imide) membrane formation by water vapour induced phase inversion. *Macromolecular symposia*, 188, 37-48. Wiley Online Library.
- Robeson, L. M. (1991). Correlation of separation factor versus permeability for polymeric membranes. *Journal of Membrane Science*, 62(2), 165-185.
[https://doi.org/10.1016/0376-7388\(91\)80060-J](https://doi.org/10.1016/0376-7388(91)80060-J)
- Robeson, L. M. (1999). Polymer membranes for gas separation. *Current Opinion in Solid State and Materials Science*, 4(6), 549-552. [https://doi.org/10.1016/S1359-0286\(00\)00014-0](https://doi.org/10.1016/S1359-0286(00)00014-0)
- Robeson, L. M. (2008). The upper bound revisited. *Journal of Membrane Science*, 320(1), 390-400. <https://doi.org/10.1016/j.memsci.2008.04.030>
- Rochelle, G. T. (2009). Amine Scrubbing for CO₂ Capture. *Science*, 325(5948), 1652-1654.
<https://doi.org/10.1126/science.1176731>
- Rosi, N. L., Eckert, J., Eddaoudi, M., Vodak, D. T., Kim, J., O'Keeffe, M., & Yaghi, O. M. (2003). Hydrogen storage in microporous metal-organic frameworks. *Science*, 300(5622), 1127-1129.

- Sabard, M., Gouanvé, F., Espuche, E., Fulchiron, R., Fillot, L.-A., & Trouillet-Fonti, L. (2014a). Erasure of the processing effects in polyamide 6 based cast films by the introduction of montmorillonite : Effect on water and oxygen transport properties. *Journal of membrane science*, 456, 11-20.
- Sabard, M., Gouanvé, F., Espuche, E., Fulchiron, R., Fillot, L.-A., & Trouillet-Fonti, L. (2014b). Erasure of the processing effects in polyamide 6 based cast films by the introduction of montmorillonite : Effect on water and oxygen transport properties. *Journal of Membrane Science*, 456, 11-20.
<https://doi.org/10.1016/j.memsci.2014.01.018>
- Sabard, M., Gouanvé, F., Espuche, E., Fulchiron, R., Seytre, G., Fillot, L.-A., & Trouillet-Fonti, L. (2014). Influence of montmorillonite and film processing conditions on the morphology of polyamide 6 : Effect on ethanol and toluene barrier properties. *Journal of membrane science*, 450, 487-498.
- Sadeghi, M., Semsarzadeh, M., & Moadel, H. (2009). Enhancement of the gas separation properties of polybenzimidazole (PBI) membrane by incorporation of silica nano particles. *Journal of Membrane Science*, 331(1-2), 21-30.
<https://doi.org/10.1016/j.memsci.2008.12.073>
- Sánchez-Laínez, J., Gracia-Guillén, I., Zornoza, B., Téllez, C., & Coronas, J. (2018). Thin supported MOF based mixed matrix membranes of Pebax® 1657 for biogas upgrade. *New Journal of Chemistry*, 43(1), 312-319. <https://doi.org/10.1039/C8NJ04769C>
- Sanders, D. F., Smith, Z. P., Guo, R., Robeson, L. M., McGrath, J. E., Paul, D. R., & Freeman, B. . D. (2013). Energy-efficient polymeric gas separation membranes for a sustainable future : A review. *Polymer*, 54(18), 4729-4761.
- Santos, E., Albo, J., & Irabien, A. (2014). Acetate based Supported Ionic Liquid Membranes (SILMs) for CO₂ separation : Influence of the temperature. *Journal of Membrane Science*, 452, 277-283. <https://doi.org/10.1016/j.memsci.2013.10.024>
- Saufi, S. M., & Ismail, A. F. (2004). Fabrication of carbon membranes for gas separation—a review. *Carbon*, 42(2), 241-259. <https://doi.org/10.1016/j.carbon.2003.10.022>
- Scovazzo, P., Havard, D., McShea, M., Mixon, S., & Morgan, D. (2009). Long-term, continuous mixed-gas dry fed CO₂/CH₄ and CO₂/N₂ separation performance and selectivities for room temperature ionic liquid membranes. *Journal of Membrane Science*, 327(1), 41-48. <https://doi.org/10.1016/j.memsci.2008.10.056>

- Scovazzo, P., Kieft, J., Finan, D. A., Koval, C., DuBois, D., & Noble, R. (2004). Gas separations using non-hexafluorophosphate [PF₆]⁻ anion supported ionic liquid membranes. *Journal of Membrane Science*, 238(1), 57-63.
<https://doi.org/10.1016/j.memsci.2004.02.033>
- Scovazzo, P., Visser, A. E., Davis, J. H., Rogers, R. D., Koval, C. A., DuBois, D. L., & Noble, R. D. (2002). Supported Ionic Liquid Membranes and Facilitated Ionic Liquid Membranes. In *ACS Symposium Series: Vol. 818. Ionic Liquids* (Vol. 818, p. 69-87).
<https://doi.org/10.1021/bk-2002-0818.ch006>
- Semsarzadeh, M., & Ghalei, B. (2013). Preparation, characterization and gas permeation properties of polyurethane-silica/polyvinyl alcohol mixed matrix membranes. *Journal of membrane science*, 432, 115-125.
- Shah, R. K., Krishnaswamy, R., Takahashi, S., & Paul, D. R. (2006). Blown films of nanocomposites prepared from low density polyethylene and a sodium ionomer of poly(ethylene-co-methacrylic acid). *Polymer*, 47(17), 6187-6201.
<https://doi.org/10.1016/j.polymer.2006.06.051>
- Shen, Y., & Lua, A. C. (2012). Preparation and characterization of mixed matrix membranes based on PVDF and three inorganic fillers (fumed nonporous silica, zeolite 4A and mesoporous MCM-41) for gas separation. *Chemical Engineering Journal*, 192, 201-210. <https://doi.org/10.1016/j.cej.2012.03.066>
- Shindo, R., & Nagai, K. (2013). Gas Separation Membranes. In S. Kobayashi & K. Müllen (Éd.), *Encyclopedia of Polymeric Nanomaterials* (p. 1-8). https://doi.org/10.1007/978-3-642-36199-9_134-1
- Simon, S., Alcouffe, P., & Espuche, E. (2014). Hybrid films of polyetherimide containing in situ grown Ag, Pd, and AgPd alloy nanoparticles : Synthesis route, morphology, and gas transport properties. *Journal of Polymer Science Part B: Polymer Physics*, 52(18), 1211-1220. <https://doi.org/10.1002/polb.23545>
- Singh, T., Kang, D.-Y., & Nair, S. (2013). Wan. *Journal of membrane science*, 448, 160-169.
- Smithson, P. A. (2002). IPCC, 2001 : Climate change 2001 : The scientific basis. Contribution of Working Group 1 to the Third Assessment Report of the Intergovernmental Panel on Climate Change, edited by JT Houghton, Y. Ding, DJ Griggs, M. Noguer, PJ van der Linden, X. Dai, K. Maskell and CA Johnson (eds). Cambridge University Press, Cambridge, UK, and New York, USA, 2001. No. Of pages : 881. Price£ 34.95, US 49.95, ISBN0-521-01495-6(paperback).£90.00,US 130.00, ISBN 0-521-80767-0

- (hardback). *International Journal of Climatology: A Journal of the Royal Meteorological Society*, 22(9), 1144-1144.
- Song, Q., Nataraj, S. K., Roussanova, M. V., Tan, J. C., Hughes, D. J., Li, W., ... Sivaniah, E. (2012). Zeolitic imidazolate framework (ZIF-8) based polymer nanocomposite membranes for gas separation. *Energy & Environmental Science*, 5(8), 8359-8369. <https://doi.org/10.1039/C2EE21996D>
- Sood, R., Iojoiu, C., Espuche, E., Gouanvé, F., Mendil-Jakani, H., & Lyonard, S. (2015). Influence of different perfluorinated anion based Ionic liquids on the intrinsic properties of Nafion®. *Journal of membrane science*, 495, 445-456.
- Sorrentino, A., Tortora, M., & Vittoria, V. (2006). Diffusion behavior in polymer-clay nanocomposites. *Journal of Polymer Science Part B: Polymer Physics*, 44(2), 265-274.
- Sridhar, L. N., Gupta, R. K., & Bhardwaj, M. (2006). Barrier Properties of Polymer Nanocomposites. *Industrial & Engineering Chemistry Research*, 45(25), 8282-8289. <https://doi.org/10.1021/ie0510223>
- Sridhar, S., Bee, S., & Bhargava, S. (2014). Membrane-based Gas Separation : Principle. *Applications and Future Potential. chemical industry digest*.
- Stern, A. (1994). Polymers for gas separations : The next decade. *Journal of Membrane Science*, 94(1), 1-65. [https://doi.org/10.1016/0376-7388\(94\)00141-3](https://doi.org/10.1016/0376-7388(94)00141-3)
- Su, N. C., Buss, H. G., McCloskey, B. D., & Urban, J. J. (2015). Enhancing Separation and Mechanical Performance of Hybrid Membranes through Nanoparticle Surface Modification. *ACS Macro Letters*, 4(11), 1239-1243. <https://doi.org/10.1021/acsmacrolett.5b00681>
- Süer, M. G., Baç, N., & Yilmaz, L. (1994). Gas permeation characteristics of polymer-zeolite mixed matrix membranes. *Journal of Membrane Science*, 91(1), 77-86. [https://doi.org/10.1016/0376-7388\(94\)00018-2](https://doi.org/10.1016/0376-7388(94)00018-2)
- Sun, L., Boo, W.-J., Clearfield, A., Sue, H.-J., & Pham, H. Q. (2008). Barrier properties of model epoxy nanocomposites. *Journal of Membrane Science*, 318(1), 129-136. <https://doi.org/10.1016/j.memsci.2008.02.041>
- Suzuki, T., & Yamada, Y. (2005). Physical and Gas Transport Properties of Novel Hyperbranched Polyimide – Silica Hybrid Membranes. *Polymer Bulletin*, 53(2), 139-146. <https://doi.org/10.1007/s00289-004-0322-9>

- Swannack, C., Cox, C., Liakos, A., & Hirt, D. (2005). A three-dimensional simulation of barrier properties of nanocomposite films. *Journal of Membrane Science*, 263(1), 47-56. <https://doi.org/10.1016/j.memsci.2005.04.023>
- Szymczyk, A., Paszkiewicz, S., Pawelec, I., Lisiecki, S., Jotko, M., Špitalský, Z., ... Rosłaniec, Z. (2015). Oxygen Barrier Properties and Melt Crystallization Behavior of Poly(ethylene terephthalate)/Graphene Oxide Nanocomposites. *Journal of Nanomaterials*, 2015, 1-10. <https://doi.org/10.1155/2015/382610>
- Takahashi, S., Goldberg, H. A., Feeney, C. A., Karim, D. P., Farrell, M., O'Leary, K., & Paul, D. R. (2006). Gas barrier properties of butyl rubber/vermiculite nanocomposite coatings. *Polymer*, 47(9), 3083-3093. <https://doi.org/10.1016/j.polymer.2006.02.077>
- Tanaka, K., & Okamoto, L.-I. (2006). Structure and Transport Properties of Polyimides as Materials for Gas and Vapor Membrane Separation. In *Materials Science of Membranes for Gas and Vapor Separation* (p. 271-291). <https://doi.org/10.1002/047002903X.ch10>
- Tang, J., Sun, W., Tang, H., Radosz, M., & Shen, Y. (2005). Enhanced CO₂ absorption of poly (ionic liquid) s. *Macromolecules*, 38(6), 2037-2039.
- Tenn, N., Follain, N., Soulestin, J., Crétois, R., Bourbigot, S., & Marais, S. (2013). Effect of Nanoclay Hydration on Barrier Properties of PLA/Montmorillonite Based Nanocomposites. *The Journal of Physical Chemistry C*, 117(23), 12117-12135. <https://doi.org/10.1021/jp401546t>
- Thomas P, S., & Thomas, S. (2012). Effect of organoclay on the gas barrier properties of natural rubber nanocomposites. *Polymer Composites*, 33(4), 524-531.
- Tollefson, J., & Weiss, K. R. (2015). Nations approve historic global climate accord. *Nature News*, 528(7582), 315.
- Tomé, L. C. (2014). *Development of new membranes based on ionic liquid materials for gas separation*. 381.
- Tomé, L. C., & Marrucho, I. M. (2015). Poly(ionic liquid)s : Designing CO₂ Separation Membranes. In D. Mecerreyes (Éd.), *Applications of Ionic Liquids in Polymer Science and Technology* (p. 267-295). https://doi.org/10.1007/978-3-662-44903-5_10
- Tomé, L. C., Patinha, D. J. S., Freire, C. S. R., Rebelo, L. P. N., & Marrucho, I. M. (2013). CO₂ separation applying ionic liquid mixtures : The effect of mixing different anions on gas permeation through supported ionic liquid membranes. *RSC Advances*, 3(30), 12220-12229. <https://doi.org/10.1039/C3RA41269E>

- Tsiantis, A., & Papathanasiou, T. D. (2017). The Barrier Properties of Flake-Filled Composites with Precise Control of Flake Orientation. *Materials Sciences and Applications*, 08(03), 234-246. <https://doi.org/10.4236/msa.2017.83016>
- Tsiantis, A., & Papathanasiou, T. D. (2019). A closed-form solution for the barrier properties of randomly oriented high aspect ratio flake composites. *Journal of Composite Materials*, 53(16), 2239-2247. <https://doi.org/10.1177/0021998318825295>
- Tuinier, M. J., van Sint Annaland, M., Kramer, G. J., & Kuipers, J. A. M. (2010). Cryogenic CO₂ capture using dynamically operated packed beds. *Chemical Engineering Science*, 65(1), 114-119.
- Uchytel, P., Schauer, J., Petrychkovych, R., Setnickova, K., & Suen, S. Y. (2011). Ionic liquid membranes for carbon dioxide-methane separation. *Journal of membrane science*, 383(1-2), 262-271.
- Uriarte, C., Alfageme, J., & Iruin, J. J. (1998). Carbon dioxide transport properties of composite membranes of a polyetherimide and a liquid crystal polymer. *European polymer journal*, 34(10), 1405-1413.
- Van Rooyen, L. J., Bissett, H., Khoathane, M. C., & Karger-Kocsis, J. (2016). Gas barrier properties of oxyfluorinated graphene filled polytetrafluoroethylene nanocomposites. *Carbon*, 109, 30-39. <https://doi.org/10.1016/j.carbon.2016.07.063>
- Vandewijngaarden, J., Murariu, M., Dubois, P., Carleer, R., Yperman, J., Adriaenssens, P., ... Buntinx, M. (2014). Gas Permeability Properties of Poly (3-hydroxybutyrate-co-3-hydroxyhexanoate). *Journal of Polymers and the Environment*, 22(4), 501-507.
- Versteeg, H. K., & Malalasekera, W. (2007). *An Introduction to Computational Fluid Dynamics : The Finite Volume Method*. Pearson Education.
- V. Plechkova, N., & R. Seddon, K. (2008). Applications of ionic liquids in the chemical industry. *Chemical Society Reviews*, 37(1), 123-150. <https://doi.org/10.1039/B006677J>
- Vu, D. Q., Koros, W. J., & Miller, S. J. (2003). Mixed matrix membranes using carbon molecular sieves : II. Modeling permeation behavior. *Journal of Membrane Science*, 211(2), 335-348. [https://doi.org/10.1016/S0376-7388\(02\)00425-8](https://doi.org/10.1016/S0376-7388(02)00425-8)
- Waché, R. (2004). *Formulation et caractérisation de polyéthylènes chargés avec des argiles : Propriétés barrière des nanocomposites obtenus* (PhD Thesis). Consulté à l'adresse <http://www.theses.fr/2004BRES2035>

- Waché, R., Klopffer, M. H., & Gonzalez, S. (2015). Characterization of Polymer Layered Silicate Nanocomposites by Rheology and Permeability Methods : Impact of the Interface Quality. *Oil & Gas Science and Technology – Revue d'IFP Energies Nouvelles*, 70(2), 267-277. <https://doi.org/10.2516/ogst/2013196>
- Wakeham, W. A., & Mason, E. A. (1979). Diffusion through multiperforate laminae. *Industrial & Engineering Chemistry Fundamentals*, 18(4), 301-305.
- Wang, M., Lawal, A., Stephenson, P., Sidders, J., & Ramshaw, C. (2011). Post-combustion CO₂ capture with chemical absorption : A state-of-the-art review. *Chemical engineering research and design*, 89(9), 1609-1624.
- Wang, T. P., & Kang, D. Y. (2015). Predictions of effective diffusivity of mixed matrix membranes with tubular fillers. *Journal of Membrane Science*, 485, 123-131. <https://doi.org/10.1016/j.memsci.2015.03.028>
- Wang, T. P., & Kang, D. Y. (2016). Highly selective mixed-matrix membranes with layered fillers for molecular separation. *Journal of Membrane Science*, 497, 394-401. <https://doi.org/10.1016/j.memsci.2015.09.057>
- Wijmans, J. G., & Baker, R. W. (1995). The solution-diffusion model : A review. *Journal of membrane science*, 107(1-2), 1-21.
- Wolf, C., Angellier-Coussy, H., Gontard, N., Doghieri, F., & Guillard, V. (2018). How the shape of fillers affects the barrier properties of polymer/non-porous particles nanocomposites : A review. *Journal of Membrane Science*, 556, 393-418. <https://doi.org/10.1016/j.memsci.2018.03.085>
- Wrobel, L. C. (2002). *The Boundary Element Method, Applications in Thermo-Fluids and Acoustics*. John Wiley & Sons.
- Xu, L., Xiang, L., Wang, C., Yu, J., Zhang, L., & Pan, Y. (2017). Enhanced permeation performance of polyether-polyamide block copolymer membranes through incorporating ZIF-8 nanocrystals. *Chinese Journal of Chemical Engineering*, 25(7), 882-891. <https://doi.org/10.1016/j.cjche.2016.11.007>
- Yaghi, O. M., O'Keeffe, M., Ockwig, N. W., Chae, H. K., Eddaoudi, M., & Kim, J. (2003). Reticular synthesis and the design of new materials. *Nature*, 423(6941), 705-714. <https://doi.org/10.1038/nature01650>

- Yamazaki, K., & Kawakami, H. (2010). High Proton Conductive and Low Gas Permeable Sulfonated Graft Copolyimide Membrane. *Macromolecules*, 43(17), 7185-7191. <https://doi.org/10.1021/ma101288w>
- Yang, A. C., Liu, C. H., & Kang, D. Y. (2015). Estimations of effective diffusivity of hollow fiber mixed matrix membranes. *Journal of Membrane Science*, 495, 269-275. <https://doi.org/10.1016/j.memsci.2015.08.030>
- Yang, C., Smyrl, W. H., & Cussler, E. L. (2004). Flake alignment in composite coatings. *Journal of Membrane Science*, 231(1-2), 1-12.
- Yano, K., Usuki, A., Okada, A., Kurauchi, T., & Kamigaito, O. (1993). Synthesis and properties of polyimide-clay hybrid. *Journal of Polymer Science Part A: Polymer Chemistry*, 31(10), 2493-2498. <https://doi.org/10.1002/pola.1993.080311009>
- Yong, H. H., Park, H. C., Kang, Y. S., Won, J., & Kim, W. N. (2001). Zeolite-filled polyimide membrane containing 2,4,6-triaminopyrimidine. *Journal of Membrane Science*, 188(2), 151-163. [https://doi.org/10.1016/S0376-7388\(00\)00659-1](https://doi.org/10.1016/S0376-7388(00)00659-1)
- Yu, D., Yang, Y. Q., Chen, Z., Tao, Y., & Liu, Y. F. (2016). Recent progress on thin-film encapsulation technologies for organic electronic devices. *Optics Communications*, 362, 43-49. <https://doi.org/10.1016/j.optcom.2015.08.021>
- Yuan, J., & Antonietti, M. (2011). Poly(ionic liquid)s : Polymers expanding classical property profiles. *Polymer*, 52(7), 1469-1482. <https://doi.org/10.1016/j.polymer.2011.01.043>
- Yuan, J., Mecerreyes, D., & Antonietti, M. (2013). Poly(ionic liquid)s : An update. *Progress in Polymer Science*, 38(7), 1009-1036. <https://doi.org/10.1016/j.progpolymsci.2013.04.002>
- Zhang, C., Dai, Y., Johnson, J. R., Karvan, O., & Koros, W. J. (2012). High performance ZIF-8/6FDA-DAM mixed matrix membrane for propylene/propane separations. *Journal of Membrane Science*, 389, 34-42. <https://doi.org/10.1016/j.memsci.2011.10.003>
- Zhang, X., Tu, Z., Li, H., Huang, K., Hu, X., Wu, Y., & MacFarlane, D. R. (2017). Selective separation of H₂S and CO₂ from CH₄ by supported ionic liquid membranes. *Journal of Membrane Science*, 543, 282-287. <https://doi.org/10.1016/j.memsci.2017.08.033>
- Zid, S., Zinet, M., & Espuche, E. (2018). Modeling diffusion mass transport in multiphase polymer systems for gas barrier applications : A review. *Journal of Polymer Science Part B: Polymer Physics*, 56(8), 621-639. <https://doi.org/10.1002/polb.24574>

- Zid, S., Zinet, M., & Espuche, E. (2019a). 3D Mass diffusion in ordered nanocomposite systems : Finite element simulation and phenomenological modeling. *Journal of Polymer Science Part B: Polymer Physics*, 57(1), 51-61.
<https://doi.org/10.1002/polb.24758>
- Zid, S., Zinet, M., & Espuche, E. (2019b). Numerical analysis of 3D mass diffusion in random (nano) composite systems : Effects of polydispersity and intercalation on barrier properties. *Journal of Membrane Science*, 117301.